



TECHNISCHE UNIVERSITÄT MÜNCHEN

FAKULTÄT FÜR MEDIZIN

**ROLE OF LYMPHOTOXIN/NON-CANONICAL NF- $\kappa$ B SIGNALING IN  
GASTRIC CARCINOGENESIS**

Karin Taxauer

Vollständiger Abdruck der Fakultät der Medizin der Technischen Universität München zur Erlangung des akademischen Grades einer

**Doktorin der Naturwissenschaften (Dr. rer. nat.)**

genehmigten Dissertation.

Vorsitz: apl. Prof. Dr. Gisela Keller

Prüfende/-r der Dissertation:

1. Prof. Dr. Markus Gerhard

2. Prof. Dr. Dietmar Zehn

Die Dissertation wurde am 15.07.2021 bei der Technischen Universität München eingereicht und durch die Fakultät für Medizin am 04.01.2022 angenommen.



Diese Arbeit wurde in der Zeit von November 2016 bis Juli 2021 im Institut für Medizinische Mikrobiologie, Immunologie und Hygiene der Technischen Universität München unter Anleitung von Herrn Prof. Dr. Markus Gerhard durchgeführt.

München, Juli 2021



*„Gehe nicht, wohin der Weg führen mag,  
sondern dorthin, wo kein Weg ist,  
und hinterlasse eine Spur.“*

Jean Paul, dt. Schriftsteller  
(1763-1825)



## List of abbreviations

2D	two-dimensional
3D	three-dimensional
A antigen	blood group A
A20	tumor necrosis factor, alpha-induced protein 3
Abl kinase	Abelson murine leukemia viral oncogene homolog 1 kinase, tyrosine kinase
ACH6	murine lymphotoxin-receptor agonizing antibody
Akt	v-akt murine thymoma viral oncogene homolog 1, serine/threonine kinase
ANK	ankyrin-repeat domain
AP-1	activator protein 1, transcription factor
APC	adenomatosis polyposis coli; APC regulator of WNT signaling pathway
APS	Ammonium Persulfate
ARHGAP26	rho GTPase activating protein 26
ARID1A	AT-rich interactive domain-containing protein 1A
ARS	age-standardized incidence rate
ATCC	American Type Culture Collection
ATR	Ataxia telangiectasia and Rad3 related protein kinase
B antigen	blood group B
B220	= CD45, a pan B-cell marker in mice
BabA	blood group antigen-binding
BAFFR	B-cell activation factor receptor
BAX	bcl-2-associated X protein, apoptosis regulator
BGH	bovine growth hormone
BHI	brain heart infusion
BSA	bovine serum albumin
CagA	cytotoxin-associated gene A
CagE	cytotoxin-associated gene E
cagPAI	cag pathogenicity island
CAPE	caffeic acid phenethyl ester
Cas9n	CRISPR associated protein 9 nickase
CC	coiled-coil domain
CCK8	cell counting kit 8
CCL2	C-C motif chemokine ligand 2
CCL20	C-C motif chemokine ligand 20
CCND1	cyclin D1
CCNE1	cyclin E1
CD27	= tumor necrosis factor receptor superfamily, member 7
CD3	cluster of differentiation 3, T cell co-receptor
CD4	cluster of differentiation 4; on T helper cells, monocytes, macrophages, and dendritic cells

CD40	cluster of differentiation 40 = tumor necrosis factor receptor superfamily, member 5
CDH1	cadherin 1
CDK6	cyclin-dependent kinase 6
CDKN2A	cyclin-dependent kinase inhibitor 2A
CEACAM	carcinoembryonic antigen-related cell adhesion molecule
CFSE	carboxyfluorescein succinimidyl ester
CFU	colony-forming unit
clAP	cellular inhibitors of apoptosis
CIN	chromosomal instable tumors
CLDN18	claudin 18
cmyc	MYC proto-oncogene, bHLH transcription factor
CO <sub>2</sub>	carbon dioxide
CXCL10	C-X-C motif chemokine ligand 10
CXCL13	chemokine (C-X-C motif) ligand 13 = B lymphocyte chemoattractant (BLC) or BCA-1
CXCL9	chemokine (C-X-C motif) ligand 9
DAB	3,3'-Diaminobenzidine
DCs	dendritic cells
DD	death domain
DENT	Oxoid™ Helicobacter Pylori Selektiv-Supplement
DMEM	Dulbecco's Modified Eagle's Medium
DMSO	dimethyl sulfoxide
DNA	deoxyribonucleic acid
DOC	deoxycholic acid
DTT	DL-Dithiothreitol
<i>E. coli</i>	<i>Escherichia coli</i>
E2F4	transcription factor E2F4
EBV	Epstein-Barr virus
EDTA	ethylenediaminetetraacetic acid
EGF	epidermal growth factor
EGFR	epidermal growth factor receptor
EGTA	ethylene glycol-bis(β-aminoethyl ether)-N,N,N',N'-Tetra acetic acid
ELISA	enzyme-linked immunosorbent assay
EMSA	electrophoretic mobility shift assay
EMT	epithelial-to-mesenchymal transition
EPHB2	ephrin type-B receptor 2
ERBB2	erb-b2 receptor tyrosine kinase 2
F480	EGF-like module-containing mucin-like hormone receptor-like 1; macrophage marker
FCS	fetal calf serum
FGF-10	fibroblast growth factor 10

FN14	fibroblast growth factor-inducible 14
Foxp3	forkhead box P3
GAPDH	glyceraldehyde 3-phosphate dehydrogenase
GC	gastric cancer
GEJ	gastroesophageal junction
GERD	gastro esophageal reflux disease
gRNA	guide ribonucleic acid
GRR	glycine-rich region
<i>H. felis</i>	<i>Helicobacter felis</i>
<i>H. pylori</i>	<i>Helicobacter pylori</i>
H1 antigen	= substance H; is a precursor to each of the ABO blood group antigens
H <sub>2</sub> O	water
H <sub>2</sub> O <sub>2</sub>	hydrogen peroxide
HE	Hematoxylin and eosin stain
HER2	human epidermal growth factor receptor 2 = ERBB2
HEV	high endothelial venule
HLH	helix-loop-helix domain
Hop	<i>H. pylori</i> outer membrane protein
HopQ	<i>H. pylori</i> outer membrane protein Q
HopZ	<i>H. pylori</i> outer membrane protein Z
HPF	high power field
HRP	enzyme horseradish peroxidase
HVEM	herpesvirus entry mediator
ICAM	intercellular adhesion molecules
Ifng	interferon gamma
Ig	immunoglobulin
IKK	IκB kinase
IL	interleukin
IL-1R	interleukin-1 receptor
IL-1β	interleukin-1β
IL-8	interleukin-8
ILCs	innate lymphoid cells
IMEM	Iscove's Modified Dulbecco's Media
IκB	inhibitor of NF-κ proteins
JAK2	Janus kinase 2
JBRC	Japanese Collection of Research Bioresources
KC	= chemokine (C-X-C motif) ligand 1 (CXCL1); keratinocytes-derived chemokine (KC) in mice
KH <sub>2</sub> PO <sub>4</sub>	potassium dihydrogen phosphate
Ki67	marker of proliferation Ki-67

KRAS	kirsten ras oncogene homolog from the mammalian ras gene family
LB media	Luria-Bertani media
LN	lymph nodes
LPS	lipopolysaccharides
LT	lymphotoxin
LTβR	lymphotoxin β receptor
LZ	leucine-zipper domain
MALT	mucosa-associated lymphoid tissue
MAPK	mitogen-activated protein kinase
MET	tyrosine-protein kinase Met or hepatocyte growth factor receptor
MLH1	MutL homolog 1
MMP	matrix metalloproteinase or matrix metalloproteinases
MOD/UBD	minimal oligomerization domain/ubiquitin-binding domain
MOI	multiplicity of infection
MRE1	metal response element 1
mRNA	messenger ribonucleic acid
MSI	microsatellite instable tumors
MSI-H	microsatellite instable high
MSI-L	microsatellite instable low
MSS	microsatellite stable
mTOR	mechanistic target of rapamycin kinase
MTT	3-(4,5-dimethylthiazol-2-yl)-2,5-diphenyltetrazolium bromide
MyD88	myeloid differentiation primary response 88
Na <sub>2</sub> HPO <sub>4</sub>	disodium phosphate
NaCl	sodium chloride
NaOH	sodium hydroxide
NBD	NEMO-binding domain
NEMO	NF-κB essential modulator
<i>Nfkb1</i> <sup>-/-</sup>	mouse strain deficient in NF-κB1 (p105/p50)
<i>Nfkb2</i> <sup>-/-</sup>	mouse strain deficient in NF-κB2 (p100/p52)
NF-κB	nuclear factor kappa-light-chain-enhancer of activated B cells
NIK	NF-κB inducing kinase
NK cells	natural killer cells
NP-40	nonyl phenoxypolyethoxyethanol
OipA	outer inflammatory protein A
P/S	penicillin/streptomycin
p16 <sup>INK4A</sup>	= CDKN2A - cyclin dependent kinase inhibitor 2A
PAM	protospacer adjacent motif
PBS	phosphate-buffered saline

PBS-T	phosphate-buffered saline with Tween
PCR	polymerase chain reaction
PD-L1 (CD274)	Programmed death-ligand 1 (=cluster of differentiation 274)
PD-L2 (PDCD1LG2)	Programmed cell death 1 ligand 2
PEST	proline, glutamic acid, serine, and threonine rich
PFA	paraformaldehyde
PI3K	phosphoinositide 3-kinases
PIK3CA	phosphatidylinositol-4,5-bisphosphate 3-kinase, catalytic subunit alpha
PNI	pronuclear injections
PP	Peyer's patches
PTEN	phosphatase and tensin homolog
qPCR	quantitative polymerase chain reaction
RANK	receptor activator for nuclear factor kappa B
RAS	rat sarcoma
RHD	Rel homology domain
RHOA	ras homolog family member A
RIPA	Radio immunoprecipitation assay
RNA	ribonucleic acid
RNAi	RNA interference
RNF43	ring finger protein 43
RTK	receptor tyrosine kinase
SabA	sialic acid-binding
SD	standard deviation
SDS	Sodium Dodecyl Sulfate
SDS	sodium dodecyl sulfate
SDS-page	sodium dodecyl sulfate-polyacrylamide gel electrophoresis
shRNA	short/small hairpin RNA
siRNA	small interfering RNA
siSCR	scramble siRNA, negative control
SLO	secondary lymphoid organs
SMAD4	mothers against decapentaplegic homolog 4
Src (c- <u>Src</u> )	proto-oncogene tyrosine-protein kinase Src ( <u>c</u> ellular <u>sar</u> coma)
STAT	signal transducer and activator of transcription
T4SS	type IV secretion system
TAD	transactivation domain
TANK	TRAF family member associated NFKB activator
TBK1	TANK-binding kinase 1
TBS	tris buffered saline
TBS-T	tris buffered saline with Tween

TCGA	the Cancer Genome Atlas
Temed	tetramethylethylenediamine
TGFBR2	transforming growth factor, beta receptor II
TGFβ <sub>i</sub>	transforming growth factor β inhibitor
TGFβ	transforming growth factor beta
TLO	tertiary lymphoid organs
TLRs	Toll-like receptors
TMB	3,3',5,5'-Tetramethylbenzidine
TNFR	tumor necrosis factor receptor
TNFR2	tumor necrosis factor receptor 2
TNFSF14/LIGHT	tumor necrosis factor superfamily member 14 = homologous to lymphotoxin, exhibits inducible expression, and competes with HSV glycoprotein D for binding to herpesvirus entry mediator, a receptor expressed on T lymphocytes
TNFα	tumor necrosis factor α
TP53	tumor suppressor protein 53
TPCA-1	[5-(p-Fluorophenyl)-2-ureido] thiophene-3-carboxamide; inhibitor of human IKK-2
TRAF	TNF-receptor associated factor
TWEAK	tumor necrosis factor-like weak inducer of apoptosis
VacA	vacuolating toxin A
VEGF	vascular endothelial growth factor
VEGFR	vascular endothelial growth factor receptor
WB	western blot
WC	Wilkins-Chalgren
WC-DENT	Wilkins-Chalgren-DENT blood agar plates
WT	wild type
Z	zinc-finger domain



## Table of Contents

<b>1</b>	<b>INTRODUCTION .....</b>	<b>17</b>
1.1	GASTRIC CANCER .....	17
1.1.1	<i>Epidemiology .....</i>	<i>17</i>
1.1.2	<i>GC development.....</i>	<i>18</i>
1.1.3	<i>Helicobacter pylori.....</i>	<i>20</i>
1.1.3.1	<i>Virulence factors of H. pylori .....</i>	<i>20</i>
1.2	NF- $\kappa$ B SIGNALING PATHWAY .....	22
1.2.1	<i>The canonical (classical) NF-<math>\kappa</math>B signaling pathway .....</i>	<i>24</i>
1.2.2	<i>The non-canonical (alternative) NF-<math>\kappa</math>B signaling pathway .....</i>	<i>25</i>
1.2.3	<i>GC and the canonical NF-<math>\kappa</math>B signaling .....</i>	<i>27</i>
1.2.4	<i>The non-canonical NF-<math>\kappa</math>B and NIK in GC .....</i>	<i>29</i>
1.3	AIM OF THE STUDY .....	31
<b>2</b>	<b>MATERIAL AND METHODS .....</b>	<b>32</b>
2.1	APPLIED LABORATORY EQUIPMENT, REAGENTS, SOLUTIONS, SUBSTANCES, AND CELL CULTURE MEDIA/SUPPLEMENTS. ....	32
2.2	CELL CULTURE .....	39
2.2.1	<i>Cell lines and their cultivation.....</i>	<i>39</i>
2.2.2	<i>Propagation of cell lines .....</i>	<i>39</i>
2.2.3	<i>Cell counting .....</i>	<i>39</i>
2.2.4	<i>Cell Freezing.....</i>	<i>40</i>
2.2.5	<i>Cell thawing .....</i>	<i>40</i>
2.3	DOWN MODULATION OF NF- $\kappa$ B INDUCING KINASE (NIK).....	40
2.3.1	<i>CRISPR/Cas9n knockdown of NIK .....</i>	<i>40</i>
2.3.1.1	<i>Generation of NIK knock down cells.....</i>	<i>43</i>
2.3.2	<i>siRNA based down-regulation of NIK.....</i>	<i>44</i>
2.3.3	<i>shRNA based down-modulation of NIK by lentiviruses.....</i>	<i>44</i>
2.3.3.1	<i>Generation of NIK knock down cells by using lentiviruses .....</i>	<i>46</i>
2.4	EXPRESSION ANALYSIS.....	46
2.4.1	<i>Determination of mRNA expression level .....</i>	<i>46</i>
2.4.2	<i>Determination of protein expression level.....</i>	<i>50</i>
2.5	ASSAYS AND TECHNIQUES .....	52

2.5.1	<i>Killing Assay</i> .....	52
2.5.2	<i>Proliferation Assay</i> .....	52
2.5.3	<i>Clonogenicity Assay</i> .....	53
2.5.4	<i>Soft agar Assay</i> .....	53
2.6	<i>HELICOBACTER PYLORI</i> .....	54
2.6.1	<i>H. pylori strains</i> .....	54
2.6.2	<i>H. pylori cultivation and propagation</i> .....	54
2.6.3	<i>Cell infection experiments</i> .....	54
2.6.4	<i>Enzyme-linked immunosorbent Assay</i> .....	55
2.6.5	<i>H. pylori binding assay by flow cytometry</i> .....	55
2.7	<i>GENERATION OF A NOVEL ATP4B-LT<sup>TG</sup> MOUSE MODEL</i> .....	55
2.7.1	<i>Generation of plasmid construct and mouse line</i> .....	56
2.7.2	<i>Genotyping of mice</i> .....	58
2.7.3	<i>Mouse infection experiments</i> .....	58
2.7.3.1	<i>Mouse strains and housing</i> .....	58
2.7.3.2	<i>Experimental infection with H. pylori PMSS1</i> .....	59
2.7.3.3	<i>Analysis of infected mice</i> .....	59
2.8	<i>MOLECULAR CLONING TECHNIQUES</i> .....	60
2.8.1	<i>Transformation of plasmid DNA in competent cells</i> .....	60
2.8.2	<i>Bacterial o/n culture</i> .....	60
2.8.3	<i>Plasmid Miniprep and Midiprep System</i> .....	60
2.9	<i>GASTRIC ORGANIDS</i> .....	61
2.9.1	<i>Preparation and cultivation of gastric organoids</i> .....	61
2.9.2	<i>Stimulation of human gastric organoids with ligands of the non-canonical NF-κB pathway</i> .....	63
2.9.3	<i>Generation of a two-dimensional culture of organoids</i> .....	63
2.10	<i>IMMUNOHISTOCHEMISTRY</i> .....	64
2.11	<i>HEMATOXYLIN-EOSIN STAINING</i> .....	65
2.12	<i>IMMUNOFLUORESCENCE</i> .....	66
2.13	<i>STATISTICS</i> .....	66
<b>3</b>	<b>RESULTS</b> .....	<b>67</b>
3.1	<b>HOPQ–CEACAM INTERACTION INFLUENCES THE ACTIVATION OF THE NON-CANONICAL NF-KB</b>	

PATHWAY .....	67
<b>3.2 NIK DEPLETION DECREASES THE TUMORIGENIC POTENTIAL OF GC CELLS .....</b>	<b>77</b>
3.2.1 <i>NIK knock out by CRISPR/Cas9n technology was not effective .....</i>	<i>78</i>
3.2.2 <i>NIK down regulation by siRNA reduced proliferation of GC cells .....</i>	<i>79</i>
3.2.3 <i>Down regulation of NIK by shRNA resulted in reduced proliferation, and fewer formed clones in AGS shNIK cells.....</i>	<i>81</i>
<b>3.3 L<math>\text{T}\alpha\text{B}^{\text{TG}}</math> TRANSGENIC MICE SHOWED ACTIVATION OF THE NON-CANONICAL NF-<math>\kappa</math>B PATHWAY IN THE STOMACH OF MICE OLDER THAN ONE YEAR .....</b>	<b>85</b>
3.3.1 <i>Characterization of L<math>\text{T}\alpha\text{B}^{\text{TG}}</math> transgenic mouse model at basal conditions.</i>	<i>86</i>
3.3.2 <i>Constitutive activation of non-canonical NF-<math>\kappa</math>B pathway in combination with H. pylori infection results in an increased T cell infiltration in the stomach. ....</i>	<i>94</i>
<b>3.4 STIMULATION OF HUMAN GASTRIC ORGANIDS WITH LIGANDS ACTIVATING THE NON-CANONICAL NF-<math>\kappa</math>B PATHWAY RESULTS IN ENHANCED GROWTH OF CORPUS AS WELL AS ANTRUM ORGANIDS. .</b>	<b>99</b>
<b>4 DISCUSSION AND CONCLUSION .....</b>	<b>103</b>
<b>5 SUMMARY.....</b>	<b>114</b>
<b>6 ZUSAMMENFASSUNG .....</b>	<b>115</b>
<b>7 PUBLICATION BIBLIOGRAPHY .....</b>	<b>117</b>
<b>8 PUBLICATION .....</b>	<b>136</b>
<b>9 APPENDIX .....</b>	<b>137</b>
9.1 LIST OF FIGURES .....	137
9.2 LIST OF TABLES.....	139
<b>10 DECLARATION.....</b>	<b>141</b>
<b>11 ACKNOWLEDGEMENT .....</b>	<b>142</b>
<b>12 CURRICULUM VITAE .....</b>	<b>FEHLER! TEXTMARKE NICHT DEFINIERT.</b>

# 1 Introduction

## 1.1 Gastric Cancer

### 1.1.1 Epidemiology

In 2020, gastric cancer (GC) accounted for 15,322 new cancer cases diagnosed and 9,196 deaths in Germany (Sung et al. 2021; Ferlay et al. 2019). Globally, GC is the fifth most common cancer type, with about 1 million new cancer cases and 780,000 cancer-related deaths per year (GLOBOCAN 2018; Rawla and Barsouk 2019). Different factors predispose to GC development (Rawla and Barsouk 2019). For instance, men are more often affected than women (Rawla and Barsouk 2019). In developed countries, males are 2.2 times (1.83 in developing countries) more predisposed to be diagnosed with GC than females (Rawla and Barsouk 2019). In Figure 1, the age-standardized incidence rates (ARS) of both sexes are shown, representing a very heterogeneous distribution of GC cases worldwide (GLOBOCAN 2018; Rawla and Barsouk 2019). GC has the highest incidence rate in developing countries such as Central/South-East Asia, East Europe, and South America (GLOBOCAN 2018; Rawla and Barsouk 2019; Balakrishnan et al. 2017).

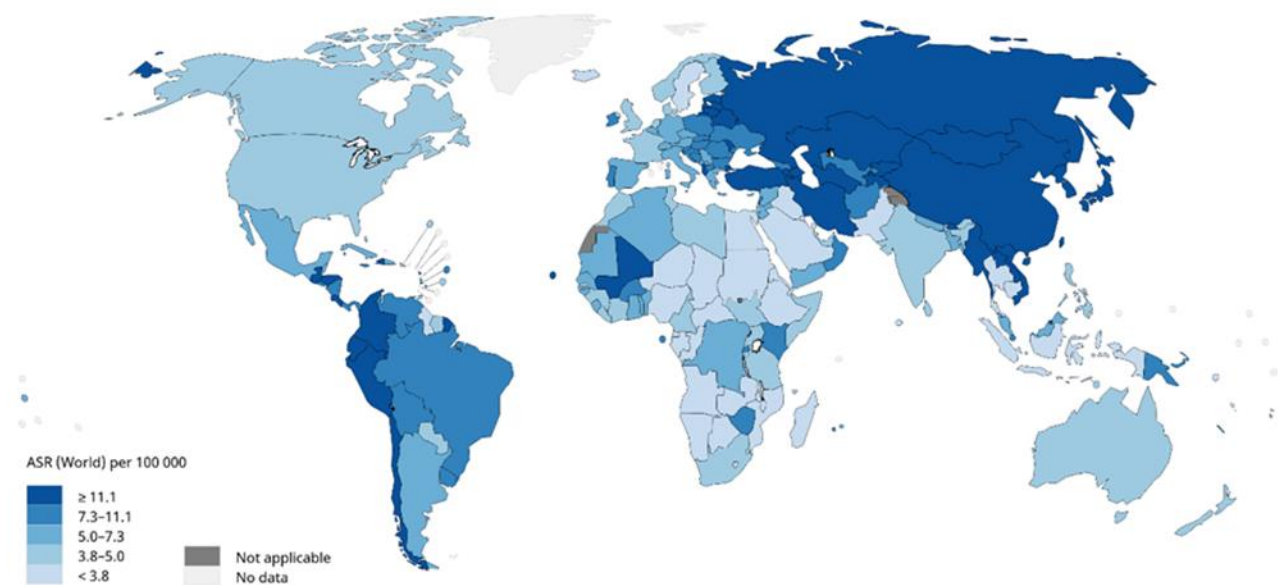


**Figure 1: Map of age-standardized incidence rates (ASR) of both sexes on stomach cancer cases/100.000 citizens in 2018 (GLOBOCAN 2018).**

© International Agency for Research on Cancer (available from: <https://gco.iarc.fr/today/online-analysis-map>, 04.06.2021)

The different incidence rates between Asia and Western countries are attributed to various risk factors such as *Helicobacter pylori* infection, diet, culture (ethnic), or host genetics (Rawla and Barsouk 2019; GLOBOCAN 2018; Balakrishnan et al. 2017). For instance, in North America, Latinos are more prone to develop GC than the non-Hispanic white population (Siegel et al. 2018). Up to

the mid-1990s, GC was the most common cancer-related death cause (Rawla and Barsouk 2019; Balakrishnan et al. 2017). This decline is attributed to the successful reduction of *H. pylori* infection due to better treatment and prevention (Rawla and Barsouk 2019). However, also modifications in food preservation like less pickling of vegetables, smoking or processing of meat, and higher availability of fresh fruit/vegetables improved the outcome (Rawla and Barsouk 2019; Roder 2002). Nonetheless, the 5-year survival rate of GC is still very poor, only 20 percent globally, except for Japan, where it is at 70 percent (Balakrishnan et al. 2017; Bollschweiler et al. 1993). In Japan, mass screening programs started in the 1960s. Thus, already early-stage GC is detected (Bollschweiler et al. 1993; Isobe et al. 2011). The low average survival rate is related to a late diagnosis (metastatic GC) (Rawla and Barsouk 2019). Hence, the 5-year survival rate for pre-metastatic GC is about 67 percent (Rawla and Barsouk 2019; Karimi et al. 2014). The early stages of GC are mainly asymptomatic, thus hard to identify (Correa 2013).

### **1.1.2 GC development**

GC is a very heterogeneous disease, and both environmental and genetic factors are involved in the malignant transformation of a healthy gastric epithelial cell (Karimi et al. 2014). GC can develop sporadically (Smith et al. 2006). About 90 percent of GC are adenocarcinomas arising from glands of the most superficial layer of the stomach (Karimi et al. 2014; Smith et al. 2006). To a lesser extent, other cancers arising in the stomach are mucosa-associated lymphoid tissue (MALT) lymphomas coming from lymphoid tissue of the stomach, and leiomyosarcomas that arise from muscles surrounding the mucosa (Karimi et al. 2014). A general classification of GC is the Lauren classification which divides GC into two distinct histology types: diffuse (undifferentiated) and intestinal-type (differentiated) gastric carcinoma (Lauren 1965; Karimi et al. 2014). The step-wise progression describes the intestinal type of GC development via the Correa's pathway initiating with chronic gastritis, atrophic gastritis, intestinal metaplasia, dysplasia, and finally terminating in intestinal type of GC (Figure 2) (Correa 2003; Correa 1992).

*H. pylori* infection can induce an inflammatory response favouring cancer development as shown in Figure 2 (Hatakeyama 2009). *H. pylori* is one of the best-studied risk factors for gastric carcinogenesis (Smith et al. 2006; Peek and Crabtree 2006). It colonizes the stomach of half of the world's population, and persistent infection results in GC development in around two percent of infected individuals (Smith et al. 2006; Peek and Crabtree 2006).

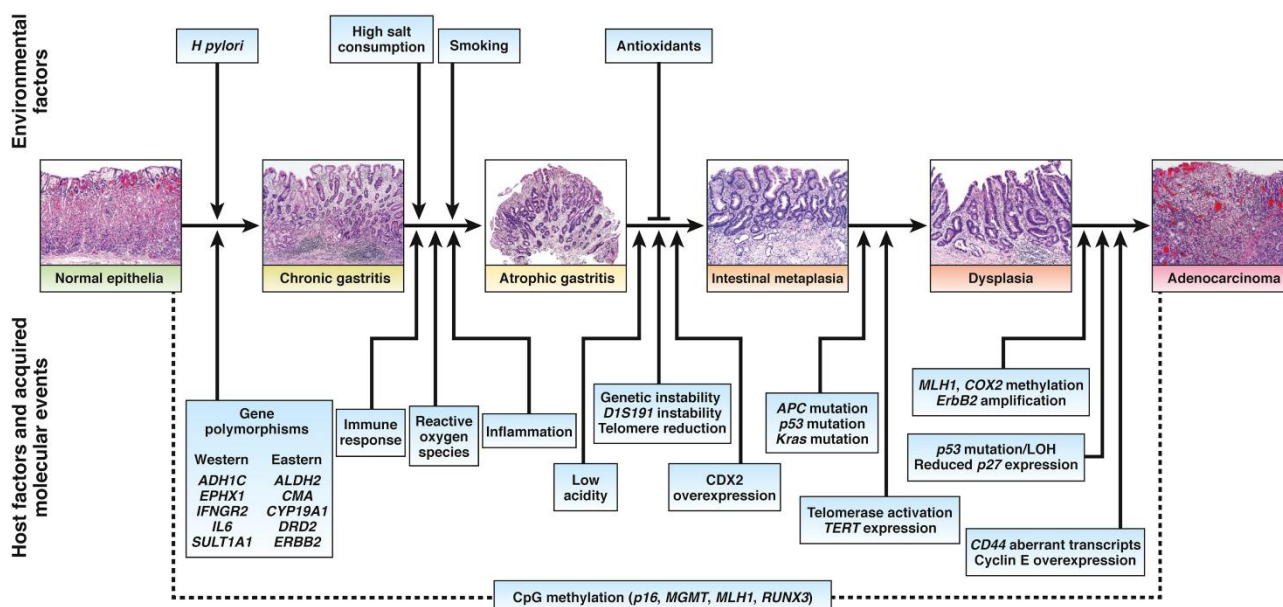


**Figure 2: Environmental and host factors contributing to the development of intestinal-type of GC (Tan and Yeoh 2015).**

Reprinted with permission from Elsevier: [Gastroenterology] (Gastroenterology (2015); 149:1153–1162; Tan and Yeoh) copyright (2015). (License: Creative Commons CC BY-NC-ND 4.0)

In 2014, the Cancer Genome Atlas (TCGA) project evaluated 295 primary gastric adenocarcinomas to establish a molecular classification and thereby separated GC into four subtypes (Figure 3): Epstein-Barr virus (EBV) positive tumors, microsatellite unstable (MSI) tumors, genomically stable (GS) tumors and chromosomal unstable (CIN) tumors (Cancer Genome Atlas Research Network 2014). For the molecular classification, primary tumor tissues were analysed using six molecular platforms such as array-based somatic copy number analysis, array-based DNA methylation profiling, whole-exome sequencing, mRNA sequencing, microRNA (miRNA) sequencing, and reverse-phase protein array (RPPA) (Cancer Genome Atlas Research Network 2014). The TCGA project aimed to detect deregulated signaling pathways and key drivers for each distinct subtype of GCs (Cancer Genome Atlas Research Network 2014). This new classification should help clinical trials to identify therapies for each GC subtype in order to improve the survival of cancer patients (Cancer Genome Atlas Research Network 2014).

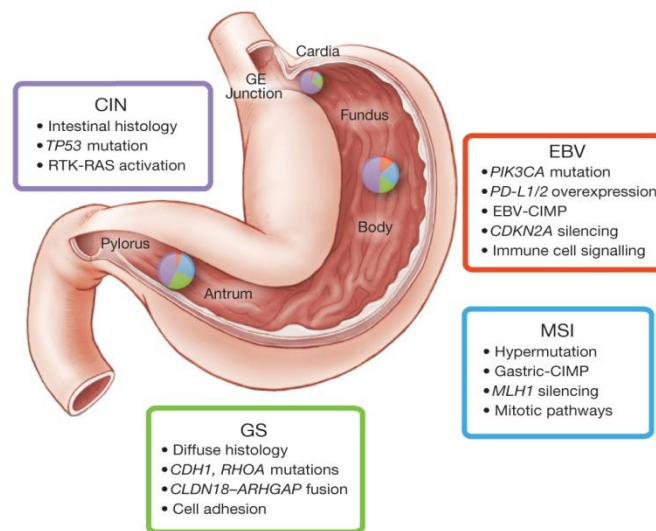


**Figure 3: Key features of the different molecular subtypes of GC (Cancer Genome Atlas Research Network 2014).**

Reprinted with permission from Springer Nature: [Nature] (Nature 513, 202–209; The Cancer Genome Atlas Research Network, Analysis Working Group: Dana-Farber Cancer Institute., Bass, A. et al.) copyright (2014). (License: Creative Commons CC-BY-NC-SA).

### 1.1.3 *Helicobacter pylori*

*H. pylori*, former *Campylobacter pylori*, is a gram-negative bacterium that was found to be causative for antral gastritis and peptic ulceration by Barry J. Marshall and J. Robin Warren in 1984 (Marshall and Warren 1984). In 1985, a self-experiment by Marshall and other volunteers showed that oral intake of *H. pylori* could induce acute gastritis in the stomach, confirming Koch's 3<sup>rd</sup> postulate (Marshall et al. 1985; Morris and Nicholson 1987; Morris et al. 1991; Kidd and Modlin 1998). In 2005, Marshall and Warren were awarded with the Nobel Prize in medicine for the discovery of *H. pylori* (Pincock 2005). *H. pylori* infection is established already in childhood and persists for a lifetime if left untreated (Banatvala et al. 1993; Smith et al. 2006). The exact transmission route is not clear yet; however, the most plausible transmission routes may be oral-oral, fecal-oral, or gastro-oral exposure, as food exposed to contaminated water or soil seems to increase risk of *H. pylori* infection (Brown 2000; Yang et al. 2014). The high infection rate is often in line with high GC rates, for instance in Asia (Figure 1) (Amieva and Peek 2016). In 1994, *H. pylori* was classified as class I carcinogen due to its causal relationship to GC development (International Agency for Research on Cancer and International Agency for Research on Cancer 1994).

#### 1.1.3.1 Virulence factors of *H. pylori*

*H. pylori* has inhabited the human stomach for thousands of years, which has allowed the pathogen to develop various mechanisms to adapt to the hostile environment of the stomach and to evade the human immune response (Falush et al. 2003; Linz et al. 2007; Suerbaum and Josenhans 2007; Moodley et al. 2012; Kalali et al. 2014; Tegtmeyer et al. 2016). The outcome of the infection

is shaped by the interaction of the gastric microbe and the host (strain-specific bacterial factors and/or inflammatory immune response determined by host genetic diversity) (Kuipers et al. 1995; Peek and Crabtree 2006).

*H. pylori* possesses several factors to survive in the stomach, such as urease, or flagella mediated motility (Ansari and Yamaoka 2019). Urease helps to neutralize the acid in the stomach, bacterial shape, as well as flagella number, enable to penetrate as well as to move within the mucous to finally colonize the stomach (Ansari and Yamaoka 2019). Thereby, *H. pylori* interacts with the host epithelium, which protects it from the harsh acidic environment and supplies the microbe with nutrients (Tegtmeyer and Backert 2017). Moreover, the adhesion of the *H. pylori* to gastric epithelial cells is essential to deliver bacterial virulence factors to and into the host cells (Wroblewski et al. 2010).

#### **1.1.3.1.1 Adhesion molecules of *H. pylori***

Bacterial cell-surface proteins, so-called adhesins, allow the adherence of the microbe to the host cells enabling colonization, persistence of infection, and delivery of virulence factors (Kalali et al. 2014; Ansari and Yamaoka 2019; Wroblewski et al. 2010). Approximately four percent of the *H. pylori* genome is encoding for outer membrane proteins (OMPs) (Wroblewski et al. 2010). OMPs are, for instance, blood group antigen-binding adhesin (BabA), sialic acid-binding adhesion (SabA), outer inflammatory protein (OipA), *H. pylori* outer membrane protein Z (HopZ), *H. pylori* outer membrane protein Q (HopQ), or other adhesins (Kalali et al. 2014; Javaheri et al. 2016; Ansari and Yamaoka 2019). OMPs are interacting with receptors expressed on host epithelial cells such as the di-fucosylated Lewis<sup>b</sup> and mono-fucosylated glycan found on H1-, A-, B-antigen of blood groups O, A, and B respectively for BabA, sialyl-dimeric-Lewis x antigen for SabA or carcinoembryonic antigen-related cell adhesion molecule (CEACAM) for HopQ (Kalali et al. 2014; Javaheri et al. 2016; Ansari and Yamaoka 2019). OMP expression is associated with gastroduodenal diseases and may enhance the risk of GC development (Wroblewski et al. 2010).

#### **1.1.3.1.2 The *cag* pathogenicity island (*cagPAI*)**

The best-studied virulence factors of *H. pylori*, contributing to the inflammatory response, are the *cag* pathogenicity island (*cagPAI*), cytotoxin-associated gene A (CagA), and vacuolating toxin A (VacA) (Kalali et al. 2014; Kuipers et al. 1995).

CagPAI, a 40 kb region, encodes proteins for the type IV secretion system (T4SS) (Censini et al. 1996; Kalali et al. 2014). T4SS is a multiprotein machinery forming a syringe-like structure to bind to the host epithelium and translocate effector proteins such as CagA, peptidoglycan, or soluble LPS metabolite (heptose intermediate metabolite HBP) into the host cell (Ansari and Yamaoka 2019;

Stein et al. 2017). CagPAI positive (*cagPAI*<sup>+</sup>) *H. pylori* strains are linked to develop severe gastritis, atrophic gastritis, and distal GC compared to *cagPAI* negative (*cagPAI*<sup>-</sup>) *H. pylori* strains (Wroblewski et al. 2010).

#### **1.1.3.1.3 Type IV secretion system (T4SS) of *H. pylori***

*H. pylori* utilizes its T4SS, encoded by *cagPAI*, to deliver protein across the bacterial membrane into host cells (Wroblewski and Peek 2013). The core complex of the T4SS, located in the membrane of *H. pylori*, is composed of Cag3, CagM, CagT, CagX, and CagY proteins and it is connected to the extracellular pilus, and produced upon contact with the host cells (Backert and Tegtmeyer 2017). Thereby, different T4SS proteins, such as CagL, CagY, CagI, and CagA, are exposed at the pilus surface, interacting with the integrin  $\alpha_5\beta_1$  host receptor allowing CagA translocation into the host cells (Backert and Tegtmeyer 2017). An important factor for the T4SS functionality is CagE (Shariq et al. 2015), since CagE deficient *H. pylori* strains induced very low levels of IL-8 secretion resulting in highly diminished NF- $\kappa$ B activity compared to wild type *H. pylori* strains (Belogolova et al. 2013; Mejías-Luque et al. 2017).

#### **1.1.3.1.4 CagA protein of *H. pylori***

The CagA protein, a 120-140 kDa protein, is translocated into the host cell via the T4SS (Wroblewski et al. 2010). About 60-70 percent of Western *H. pylori* strains and almost 100 percent of East Asian *H. pylori* strains express the CagA protein (Wroblewski et al. 2010). After translocation, CagA is phosphorylated by Src family kinases such as c-Src or Abl kinase, resulting in cytoskeleton rearrangement inducing the so-called hummingbird phenotype, or in activation of diverse signaling pathways involved in inflammation (AP-1, NF- $\kappa$ B, IL8) (Backert and Meyer 2006; Selbach et al. 2002; Fischer et al. 2001; Hatakeyama 2009; Hoesel and Schmid 2013).

## **1.2 NF- $\kappa$ B signaling pathway**

Chronic gastric inflammation induced by *H. pylori* virulence factors or adhesion molecules fuels the production of transcription factors and cytokines (Ito et al. 2020). Thereby, a prominent pathway involved in the host response to fight microbial infections is the NF- $\kappa$ B pathway regulating the first line of defense activated by the innate immune system (Peng et al. 2020).

NF- $\kappa$ B is a transcription factor regulating a vast number of genes involved in various biological processes such as inflammation, proliferation, immunity, cell death, and cancer, as seen in Figure 4 (Sen and Baltimore 1986; Hoesel and Schmid 2013; Zinatizadeh et al. 2021).

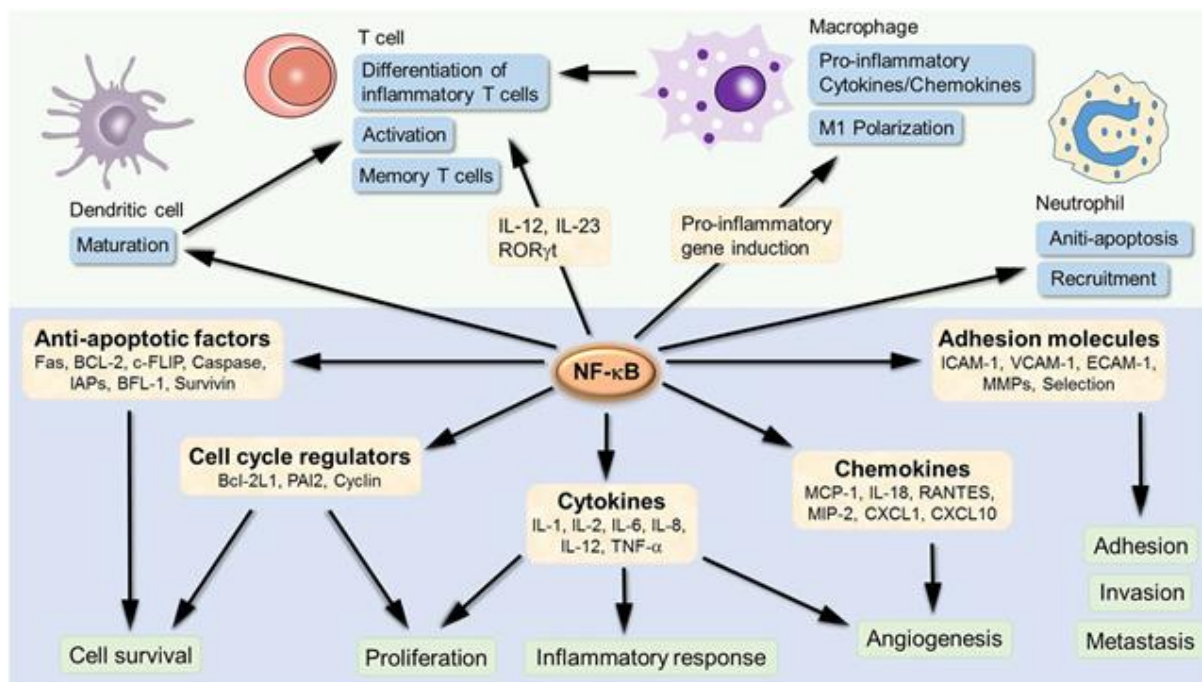


**Figure 4: Target genes of the NF- $\kappa$ B pathway induced upon inflammation development and progression (Liu et al. 2017).**

Reprinted with permission from Springer Nature: [Nature (*Sig Transduct Target Ther*)] (*Signal Transduction and Target Therapy* 2, 17023; Ting Liu et al.) copyright (2017). (License: Creative Commons CC BY)

The NF- $\kappa$ B protein family comprises two distinct proteins, the NF- $\kappa$ B proteins and the REL family, sharing a Rel homology domain (RHD), a highly conserved DNA-binding/dimerization domain to form homo- or heterodimers (Figure 5) (Gilmore 2006; Hayden and Ghosh 2011). The NF- $\kappa$ B/REL family is composed of five different members: RelA (p65), RelB, c-Rel, NF- $\kappa$ B1 (p105/p50), and NF- $\kappa$ B2 (p100/p52) (Figure 5) (Oeckinghaus and Ghosh 2009; Sun 2011). As the NF- $\kappa$ B pathway is involved in numerous pathways, its activity is tightly regulated at different levels (Oeckinghaus and Ghosh 2009). Primarily, its activity is regulated by the so-called inhibitor of NF- $\kappa$ B proteins (I $\kappa$ B) and I $\kappa$ B kinase (IKK) complex, which phosphorylates I $\kappa$ Bs (Oeckinghaus and Ghosh 2009). NF- $\kappa$ B is present in all cells as inactive form and thereby mainly located in the cytoplasm bound by I $\kappa$ B proteins (Shishodia and Aggarwal 2004; Hayden and Ghosh 2011).

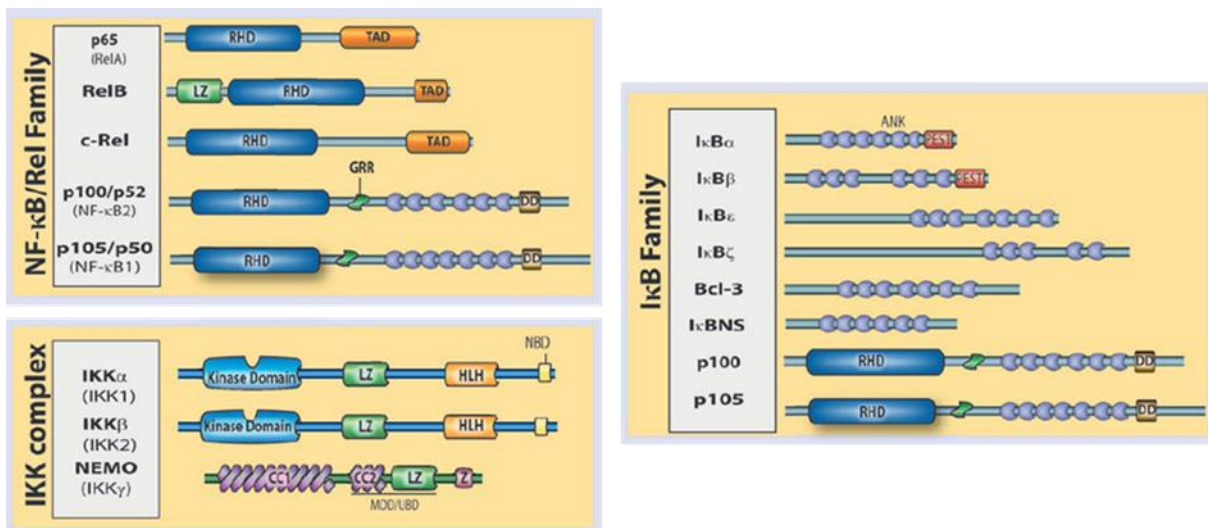


**Figure 5: Members of NF- $\kappa$ B/Rel family, I $\kappa$ B family, and the IKK complex family (Hayden and Ghosh 2011).**

Different domains of each protein family: RHD, REL homology domain; TAD, transactivation domain; LZ, leucine-zipper domain; GRR, glycine-rich region; DD, death domain; ANK, ankyrin-repeat domain; PEST, proline, glutamic acid, serine, and threonine rich; HLH, helix-loop-helix domain; NBD, NEMO-binding domain; CC1, coiled-coil domain 1; CC2, coiled-coil domain 2; Z, zinc-finger domain; MOD/UBD, minimal oligomerization domain/ubiquitin-binding domain. Alternative names of the proteins are provided in brackets. Adapted by permission from RightsLink: Springer Nature [Cell Research (Review)] [Cell Research (2011) 21:223-244, Hayden and Ghosh] copyright (2011). (License Number: 5073100890680, 20.05.21)

The NF- $\kappa$ B signaling pathway is divided into two main signaling arms: the canonical and the non-canonical NF- $\kappa$ B signaling, regulated by different ligands and receptors (Oeckinghaus and Ghosh 2009).

### 1.2.1 The canonical (classical) NF- $\kappa$ B signaling pathway

The **canonical or classical signaling** activation is mediated via Toll-like receptors (TLRs), interleukin-1 receptor (IL-1R), antigen receptors, and tumor necrosis factor receptor (TNFR) stimulated through bacterial cell wall components like lipopolysaccharides (LPS), interleukin-1  $\beta$  (IL-1 $\beta$ ), and tumor necrosis factor  $\alpha$  (TNF $\alpha$ ) (Hoesel and Schmid 2013). The main mechanism for activation of classical NF- $\kappa$ B signaling is the proteasomal degradation of I $\kappa$ B $\alpha$  that is provoked by site-specific phosphorylation via the IKK complex resulting in the prompt and transient translocation of heterodimers (p50/RelA, p50/c-Rel) into the nucleus to induce target gene expression (Gilmore 2006; Liu et al. 2017). The IKK complex is composed of IKK $\alpha$  and IKK $\beta$  (two catalytic subunits) and a regulatory part called NF- $\kappa$ B essential modulator (NEMO or IKK $\gamma$ ) (Gilmore 2006; Liu et al. 2017). The classical NF- $\kappa$ B pathway plays an essential role in regulating genes involved in inflammation, cell proliferation/survival, epithelial-to-mesenchymal transition (EMT), invasion, angiogenesis, and metastasis (Taniguchi and Karin 2018).

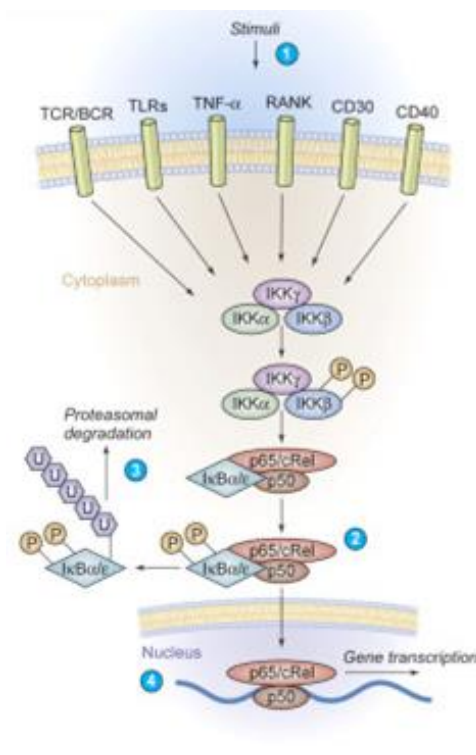


**Figure 6: Activation of canonical/classical NF-κB pathway upon stimulation (Jost and Ruland 2007).**

Different stimuli activate the canonical NF-κB pathway. Ligand-receptor interaction leads to the activation of IKK. Thus, IKK phosphorylates IκB proteins resulting in its proteasomal degradation. The cytoplasmic NF-κB dimer is released and translocates into the nucleus to induce gene expression. Adapted by permission from RightsLink: Elsevier [Blood (Review in translational hematology)] (Blood Vol. 109, No. 7, 2700-2707; Philipp J. Jost, Jürgen Ruland) copyright (2007). (License Number: 5082041476659, 04.06.21)

### 1.2.2 The non-canonical (alternative) NF-κB signaling pathway

The **non-canonical or alternative** signaling pathway is activated by a defined subset of TNFR superfamily members such as B-cell activation factor receptor (BAFFR), tumor necrosis factor receptor 2 (TNFR2), FN14/TWEAK receptor, CD40, lymphotoxin β-receptor (LTβR), CD27, and receptor activator for nuclear factor kappa B (RANK) (Hoesel and Schmid 2013; Sun 2011; Pflug and Sitcheran 2020). Upon pathway activation, the processing of p100, NF-κB2 precursor protein, is induced via IKKα (Liu et al. 2017). A central protein of this pathway is the NF-κB inducing kinase (NIK) that is kept at low levels under unstimulated conditions via proteasomal degradation (Tegowski and Baldwin 2018). TNF-receptor-associated factor 3 (TRAF3) is important for keeping NIK at low basal levels (Tegowski and Baldwin 2018). TRAF3 has no ubiquitinase activity itself and couples NIK to a degradation complex consisting of TRAF2 and cellular inhibitors of apoptosis 1 (cIAP1) and cIAP2 (Zarnegar et al. 2008; Tegowski and Baldwin 2018). Upon complex building, NIK gets marked with K48-linked ubiquitin chains for proteasomal degradation (Tegowski and Baldwin 2018). However, upon pathway activation, TRAF2/TRAF3/cIAP1/cIAP2-NIK complex is recruited to the active receptor (Tegowski and Baldwin 2018). cIAP1/2 marks TRAF2 and TRAF3 with ubiquitin chains resulting in their proteasomal degradation (Tegowski and Baldwin 2018). Without the degradation complex, NIK

is quickly accumulating and stabilized, inducing the phosphorylation of the IKK $\alpha$  homodimer, which subsequently facilitates the phosphorylation of p100, resulting in its proteasomal degradation to form the mature form p52 (Bauer et al. 2012; Paul et al. 2018; Tegowski and Baldwin 2018). p52 predominantly forms a heterodimer with RelB and translocates into the cell nucleus to induce target gene expression (Bauer et al. 2012). The non-canonical NF- $\kappa$ B pathway plays a key role in induction of inflammation and development of secondary lymphoid organs (SLO), thymus, TLO, and B cell survival, as well as maturation of follicular dendritic cells (Weih and Caamaño 2003; Zhu and Fu 2011; Bauer et al. 2012).

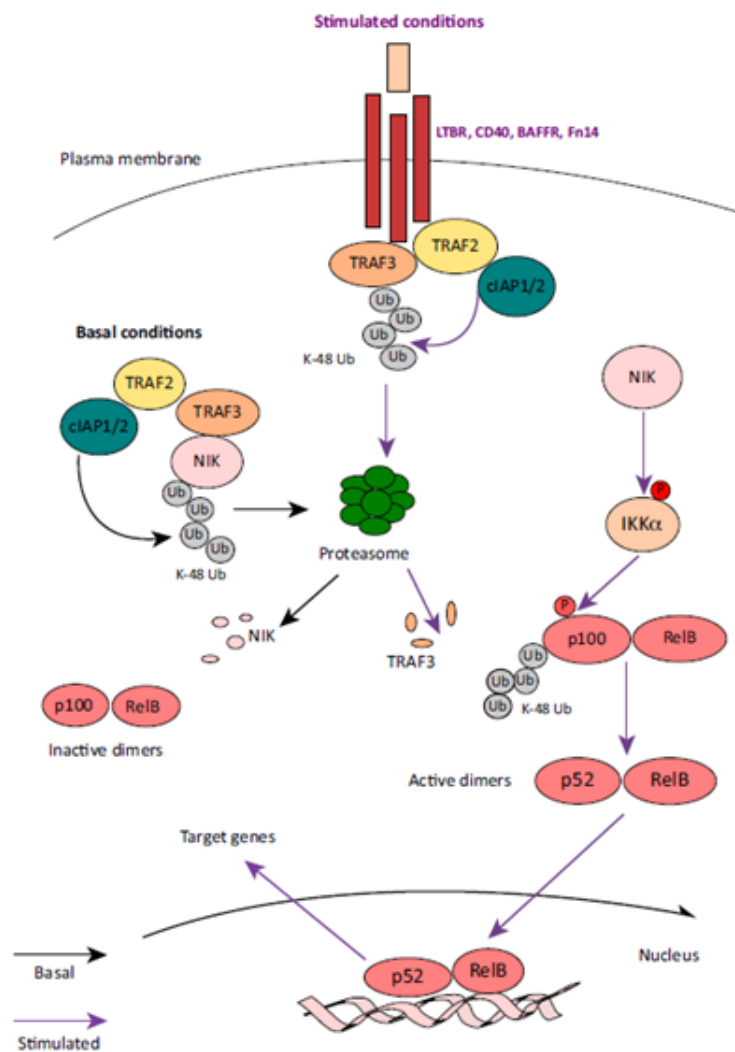


**Figure 7: Activation of non-canonical NF- $\kappa$ B pathway at basal conditions and upon stimulation (Cildir et al. 2016).**

NIK is bound by the TRAF2/3/cIAP1/2 complex at basal conditions, leading to its ubiquitination followed by proteasomal degradation to keep the levels low. At ligand-receptor interaction, this complex is recruited to the receptor. NIK is released to activate IKK $\alpha$  by phosphorylation that phosphorylates p100 resulting in its proteasomal degradation forming the mature form p52. p52 forms a heterodimer with RelB and translocates into the nucleus to initiate target gene expression. (Cildir et al. 2016) Reprinted by permission from RightsLink: Elsevier [CellPress (Trends in Molecular Medicine)] (Trends in Molecular Medicine, Vol. 22, No. 5, 414-429; Gökhan Cildir, Kee Chung Low, Vinay Tergaonkar) copyright (2016). (License Number: 5082040902688, 04.06.21)

### The LT-LT $\beta$ R signaling axis

The activation of the non-canonical NF- $\kappa$ B pathway via LT has been linked to the development of different types of inflammation-driven tumors (Wolf et al. 2010; Bauer et al. 2012; Fernandes et al. 2016). *H. pylori* has been shown to induce non-canonical NF- $\kappa$ B signaling in the stomach via LT $\beta$ R in a T4SS-dependent manner (Mejías-Luque et al. 2017). In human gastritis samples, activation of the non-canonical NF- $\kappa$ B pathway was observed by elevated LT $\beta$  and nuclear p52 staining (Mejías-Luque et al. 2017) as well as by increased NIK levels (Feige et al. 2018). Still, it is not clear whether activation of the non-canonical NF- $\kappa$ B is involved in gastric carcinogenesis.

The cytokine lymphotoxin (LT)  $\alpha$ ,  $\beta$ , and the receptor LT $\beta$ R are members of the tumor necrosis factor superfamily, which have a plethora of functions, including lymphoid organ development and signal via activating the canonical as well as non-canonical NF- $\kappa$ B pathway (Wolf et al. 2010). LT $\beta$  is a type II transmembrane protein anchored in the cell membrane, while LT $\alpha$  can be secreted as a soluble LT $\alpha_3$  homotrimer (Wolf et al. 2010). LT $\alpha_3$  can bind to TNFR1 or 2, thereby activating the canonical NF- $\kappa$ B pathway (Wolf et al. 2010). LT $\alpha$  and LT $\beta$  form membrane-anchored heterotrimers like LT $\alpha_2\beta_1$  that binds TNFR1 and 2 representing a minor form of LT expressed by T cells and LT $\alpha_1\beta_2$  that binds to LT $\beta$ R (Wolf et al. 2010). LT $\beta$ , but not LT $\alpha$ , is constitutively expressed in lymphocytes (Fernandes et al. 2016). An alternative ligand for LT $\beta$ R is LIGHT, or also called TNFSF14, which also binds to the herpesvirus entry mediator (HVEM) (Ware 2009; Wolf et al. 2010). LT $\alpha_1\beta_2$  and LIGHT are expressed by lymphocytes such as T cells, B cells, natural killer (NK) cells, innate lymphoid cells (ILCs), and dendritic cells (DCs) (Ruddle 2014; Mejías-Luque et al. 2017). In contrast, its receptor, LT $\beta$ R, is predominantly expressed by non-lymphocyte populations such as epithelial cells, stromal cells, DCs, and macrophages, enabling the communication between lymphocytes and stromal cells and thereby influencing a variety of biological processes (Wolf et al. 2010; Koroleva et al. 2018; Fernandes et al. 2016). Mice deficient in *Ita*, *Itb*, or *Itbr* genes show no lymph nodes (LN) and Peyer's patches (PP), demonstrating disrupted architecture of spleen, thymus, and other lymphoid organs (Koroleva et al. 2018). Moreover, LT $\beta$ R signaling is also involved in liver regeneration, lipid homeostasis, high endothelial venule (HEV) differentiation as well as in protection against atherosclerosis (Fernandes et al. 2016). Thus, the deregulation of the LT $\beta$ R/LT axis is involved in autoimmune and inflammatory diseases like rheumatoid arthritis, Sjögren's syndrome, autoimmune pancreatitis, hepatitis, colitis, and cancer (Fernandes et al. 2016).

### 1.2.3 GC and the canonical NF- $\kappa$ B signaling

As mentioned above, the NF- $\kappa$ B pathway is involved in cell proliferation and apoptosis and is mainly activated during inflammation and cancer (Shishodia and Aggarwal 2004). Sasaki et al.

showed constitutive activity of the canonical NF- $\kappa$ B signaling in GC tissue by detecting increased nuclear RelA and/or NF- $\kappa$ B1 translocation via EMSA and immunohistochemical analysis (Sasaki et al. 2001). Similar results could be observed in the human GC cells, HTB-135 cells, stimulated with IL-1 $\beta$  (Sasaki et al. 2001). The NF- $\kappa$ B activity showed an association with the size of the tumor, lymphatic invasion, invasion depth, and peritoneal metastasis in GC patients analysed (Sasaki et al. 2001). This may indicate that NF- $\kappa$ B activity is associated with the aggressiveness of GC (Sasaki et al. 2001).

In contrast, Lee et al. indicated that the NF- $\kappa$ B activation via nuclear RelA expression was more enhanced in early-stage GC and negatively correlated with lymphatic invasion (Lee et al. 2005). In their study, GC patients positive for NF- $\kappa$ B activation demonstrated a better prognosis than patients showing no NF- $\kappa$ B activation (Lee et al. 2005). Additionally, NF- $\kappa$ B activity was positively linked to Akt protein expression in gastric tumor samples, which is involved in apoptosis and cell cycle progression (Lee et al. 2005). Similar results were reported by Wu et al. that NF- $\kappa$ B activity was linked to tumor invasion and induced expression of MMP-9 and pro-inflammatory cytokines, which were even more elevated upon *H. pylori* infection resulting in the expression of IL-1 $\beta$  as well as IL-8 secretion (Wu et al. 2007). In this study, the application of an NF- $\kappa$ B inhibitor, caffeic acid phenethyl ester (CAPE), an active anti-inflammatory component of propolis, diminished the MMP-9 expression and IL-8 secretion by blocking NF- $\kappa$ B activity and reducing the invasive phenotype of AGS cells (Wu et al. 2007). Huang et al. showed that NF- $\kappa$ B1 is a direct target of miR-508-3p which was downregulated in GC (Huang et al. 2016). Overexpression of miR-508-3p in GC cells reduced the expression of NF- $\kappa$ B1 and RelA, lowering the proliferative and invasive capacities by inhibiting MMP-9 expression *in vitro* (Huang et al. 2016). Li et al. illustrated that polymorphisms in *NFKB1* encoding p50 (rs3755867 locus) and *NFKBIA* coding for I $\kappa$ B gene (rs696 locus, rs2233406 locus) showed an association with increased GC susceptibility (Li et al. 2017). In line with this observation, O'Reilly et al. showed that NF- $\kappa$ B1 acts as a tumor suppressor in GC, as loss of NF- $\kappa$ B1-dependent STAT1 upregulation induced inflammation as well as elevated expression of immune checkpoint regulators (O'Reilly et al. 2018). Thus, mice deficient in p50/p105-NF- $\kappa$ B1 (*Nfkb1*<sup>-/-</sup>) showed pathologies in the stomach at the age of six months that initially showed diffuse gastritis in antrum and corpus of the stomach; one-year-old *Nfkb1*<sup>-/-</sup> mice showed lymphocytic infiltrates, chronic mucosal damage/repair, elongated/branched gastric pits and elevated gastric epithelial proliferation (O'Reilly et al. 2018). Interestingly, 95 percent of 18 months old mice deficient in NF- $\kappa$ B1 developed macroscopic gastric adenocarcinomas (O'Reilly et al. 2018). RNAseq data showed that the lack of NF- $\kappa$ B1 led to abnormal JAK-STAT signaling resulting in a sterile inflammation, increased antigen presentation and immune checkpoint expression linked to aberrant STAT1 activity (O'Reilly et al. 2018). Similar results were described by Burkitt et al. using *Nfkb1*<sup>-/-</sup> mice which developed

spontaneous gastric atrophy by housing them for 12 months in a conventional animal facility or after short-term *H. felis* infection (Burkitt et al. 2013). This may indicate that NF- $\kappa$ B1 is protective against gastric pathologies by preventing aberrant JAK-STAT signaling (O'Reilly et al. 2018; Burkitt et al. 2013). As mentioned previously, *H. pylori* infection can induce chronic gastric inflammation and thereby increases GC development (Peek and Crabtree 2006). The bacteria-induced inflammation leads to the secretion of IL-8 via activation of the NF- $\kappa$ B pathway dependent on the presence of certain virulence factors such as cagPAI island but independent of CagA (Peek and Crabtree 2006).

#### 1.2.4 The non-canonical NF- $\kappa$ B and NIK in GC

The activation of the canonical NF- $\kappa$ B pathway in *H. pylori*-induced gastric pathologies is already well established; however, only a few data focusing on the contribution of the non-canonical NF- $\kappa$ B pathway during *H. pylori*-induced inflammation are available (Mejías-Luque et al. 2017). The expression of LT $\beta$ , a specific ligand activating the alternative NF- $\kappa$ B pathway by binding to LT $\beta$ R, was found to be increased in *H. pylori*-induced gastritis as well as in gastric tumor samples compared to healthy stomach tissue specimens (Mejías-Luque et al. 2017). *H. pylori* infection upregulated the mRNA expression levels of LT $\beta$  as well as p100 to p52 processing in infected mice and GC cells (Mejías-Luque et al. 2017). This induction was T4SS-dependent but CagA-independent, since *H. pylori* CagE mutants, lacking a functional T4SS, were unable to induce LT $\beta$  expression or activate the pathway (Mejías-Luque et al. 2017). Blockage of LT $\beta$ R signaling by treating infected animals with LT $\beta$ R-Ig resulted in a higher gastric bacterial load leading to a reduced gastric inflammation accompanied by a lower number of infiltrating T/B cells, diminished nuclear RelB translocation as well as reduced expression levels of *KC*, *CXCL10*, *CCL20*, and *CCL2* in the stomach (Mejías-Luque et al. 2017). In line with these observations, Burkitt et al. showed in *Nfkb2*<sup>-/-</sup> mice infected with *H. felis* high bacterial load accompanied with low parietal cell loss, no change in mucosal thickness, and reduced gastric inflammation compared to WT infected mice (Burkitt et al. 2013). The activation of the pathway by applying an LT $\beta$ R agonist (ACH6) in *H. pylori*-infected mice reduced the gastric bacterial load leading to a higher gastric inflammation (slightly lower CD3<sup>+</sup> cells, no change in CD4<sup>+</sup> or F480<sup>+</sup> cells, more B cells, higher expression of *CXCL13*, *LIGHT*, *ICAM*, and *CCL2*) compared to infected control mice (Mejías-Luque et al. 2017). Along with these results, Ishikawa et al. showed in a mouse model lacking the COOH-terminal ankyrin domain of NF- $\kappa$ B (p100<sup>-/-</sup>) but still having the functional domain p52 present, increased proliferation as well as gastric hyperplasia leading to early postnatal death (Ishikawa et al. 1997; Merga et al. 2016).

The canonical and non-canonical NF- $\kappa$ B pathways have many cross regulatory mechanisms (Basak and Hoffmann 2008). For instance, TNF $\alpha$  stimulation in GC cells resulted in an increased LT $\beta$

expression, and the application of a human IKK2 inhibitor (TPCA-1) lowered A20 as well as LT $\beta$  expression levels and reduced the p100 expression levels while processing levels were unchanged due to increased LIGHT expression (Mejías-Luque et al. 2017). The absence of the adaptor molecule myeloid differentiation primary response 88 (MyD88), which is a crucial molecule in the inflammatory pathways in IL-1/IL-18/TLR signaling, led to enhanced gastric pathology upon *H. felis* infection in mice (*Myd88*<sup>-/-</sup>) (Banerjee et al. 2014; Mejías-Luque et al. 2019). *H. felis* infected *Myd88*<sup>-/-</sup> mice showed increased LIGHT expression activating the non-canonical NF- $\kappa$ B pathway resulting in increased *Cxcl9* and *Icam1* expression, increased Stat3 signaling, and a higher T cell infiltration developing augmented gastric pathologies compared to WT infected mice (Mejías-Luque et al. 2019).

NIK, a key protein of the non-canonical NF- $\kappa$ B pathway, is important for activating the pathway (Sun 2012; Pflug and Sitcheran 2020). NIK, which can interact with the canonical NF- $\kappa$ B pathway, is indispensable for activating the alternative NF- $\kappa$ B pathway as shown in a NIK deficient mouse model (NIK<sup>-/-</sup>) (Shinkura et al. 1999; Yin et al. 2001). NIK<sup>-/-</sup> mice showed abnormal lymphorgan development, as these mice were lacking in all lymph nodes, and did not establish Peyer's patches, indicating its importance in lymphorganogenesis and architecture of the spleen and thymus (Yin et al. 2001). Regarding its role in cancer, different studies already highlighted the involvement of NIK in carcinogenesis (Paul et al. 2018). In solid tumors, like head and neck cancer, breast cancer, pancreatic cancer or ovarian cancer, NIK dysregulation or aberrant non-canonical NF- $\kappa$ B signaling activation can induce increased cell proliferation, invasiveness, stemness, and tumorigenicity favouring cancer progression (Das et al. 2018; Vazquez-Santillan et al. 2016; Wharry et al. 2009; Uno et al. 2014; Pflug and Sitcheran 2020). In GC cells, transfection with kinase-deficient NIK led to inhibition of the NF- $\kappa$ B pathway upon infection with *H. pylori* (Maeda et al. 2000). TRAF2 and TRAF6 were needed to activate NIK in GC cells (Maeda et al. 2000). These studies indicate the importance of NIK in activating the non-canonical NF- $\kappa$ B upon infection (Maeda et al. 2000). Similar results have been postulated by Feige et al., showing higher non-canonical NF- $\kappa$ B signaling activity (increased expression of the key protein of the pathway, NIK) in patient samples with *H. pylori*-induces gastritis compared to healthy controls (Feige et al. 2018).

The NF- $\kappa$ B signaling is a very complex network in carcinogenesis, and hence it is essential to elucidate different aspects of NF- $\kappa$ B signaling, its interaction partner, and upstream regulators (Brücher et al. 2019) in order to shed more light on the role of this signaling axis, especially in terms of GC.

### 1.3 Aim of the study

In the present study, the aim was to decipher the role of the non-canonical NF- $\kappa$ B pathway, more precisely, the LT/LT $\beta$ R signaling axis during gastric carcinogenesis.

Previous data have shown that different *H. pylori* virulence factors are involved in activating the non-canonical NF- $\kappa$ B pathway (Mejías-Luque et al. 2017). So far, the adhesion molecule, HopQ, which binds to CEACAM receptors expressed on gastric epithelial cells and is involved in the T4SS-dependent CagA translocation as well as in IL-8 secretion (Javaheri et al. 2016), was not investigated regarding its impact on the non-canonical NF- $\kappa$ B pathway upon *H. pylori* infection. **Therefore, the first objective was to determine whether the adhesin HopQ influences the activation of the non-canonical NF- $\kappa$ B signaling.**

The activation of the LT/LT $\beta$ R signaling axis has been linked to carcinogenesis in different organs (Fernandes et al. 2016). However, its impact on GC development has not been completely shown. **To investigate whether stomach-specific lymphotoxin overexpression and hence, activation of the non-canonical NF- $\kappa$ B pathway via the LT $\beta$ R signaling is sufficient to induce gastric carcinogenesis,** a new mouse model expressing lymphotoxin under the control of the H<sup>+</sup>/K<sup>+</sup>-ATPase promotor was generated and analysed at different time points. Moreover, a three-dimensional (3D) cell cultivation system from adult stem cells of primary human stomach tissue was established, representing an emerging approach to more closely mimic the *in vivo* situation (Bartfeld 2016; Alzeeb et al. 2020). **This approach was used to verify whether stimulation of human gastric organoids with ligands, LT $\alpha_1\beta_2$  or LIGHT, activating the non-canonical NF- $\kappa$ B pathway induces changes in growth.**

NIK kinase is a key protein of the non-canonical NF- $\kappa$ B pathway (Sun 2011), which has been shown to be upregulated in gastric tumors. However, no data on the role of NIK in GC are available. **By depleting NIK expression in GC cells, the impact on the tumorigenic potential of GC cells was explored.**

## 2 Material and Methods

### 2.1 Applied laboratory equipment, reagents, solutions, substances, and cell culture media/supplements.

Table 1: List laboratory equipment used.

APPARATUS	COMPANY
Agarose Gel chamber	Bio-Rad Laboratories
C100 Touch thermal cycler	Bio-Rad Laboratories
Centrifuge 5415D	Eppendorf
CERO 3D cell incubator	OMNI Life Science (OLS)
CFX384 Real-Time System	Bio-Rad Laboratories
Cooling Plate COP30	medite Medizintechnik
Fine Balance (max: 120g, d~0.0001g)	ScalTec
Forma Series II Water Jacket CO <sub>2</sub> incubator, bacteria incubator	Thermo scientific
Freezer -20, Premium	Liebherr
Freezer -80 Hera Freeze basic	Thermo fisher
Fridge, Premium	Liebherr
Gel-Blotting Paper 580x600mm, 195g/m <sup>2</sup> (100Bg.)	A. Hartenstein (#GB58)
Heating plate/magnetic stirrer	ARE VELP Scientifica
Hemocytometer, Neubauer improved (0.100 mm, 0.025 mm <sup>2</sup> )	Marienfeld superior Germany
Hera cells 240 incubator, cell culture incubator	Thermo electorn corporation
Hera Safe Bio-Flow cell culture	Hera Instruments
Heraeus Biofuge Primo centrifuge	Thermo Electron corporation
Heraeus Megafuge 40R centrifuge	Thermo Fisher Scientific
Homogenizer ultra-Turrax IKA T10 basic	IKA
Ice machine CoolNat (S-No. 174279)	Ziegra Eismaschinen
MaxWell RSC48	Promega
Microtome RM2245	Leica
Microwave	iCES
Mini Gel Tank	LifeTechnologie
Mini shaking oven, hybridization open; OV3	Biometra
Molecular Imager Gel Dox XR+ (Eagle Eye)	Bio-Rad Laboratories
NIKON eclipse TS-100 microscope	NIKON
pH-meter, FIVEeasy	Mettler Toledo
PowerPac (WB)	Bio-Rad Laboratories
PowerPac 200 (Agarose Gel)	Bio-Rad Laboratories
Precellys 24, lysis & homogenization	Peqlab Biotechnologie GmbH
Rocker-shaker MR-12	BioSan
Slide scanner Olympus BX61VS OVK-S5-00036FL	Olympus
Sunrise plate reader	Tecan
Thermomixer compact (block heater)	Eppendorf

Tissue Flotation Bath TFB35	medite Medizintechnik
Trans-Blot Semi-Dry Transfer Cell	Bio-Rad Laboratories
Ultrasonic water bath, SONOREX DIGITEC	Bandelin
water bath	GFL
WB detection machine	INTAS Science Imaging
XcitaBlue Conversion Screen	Bio-Rad Laboratories

Table 2: List of consumables used.

CONSUMABLES	ORDER NUMBER	COMPANY
10 cm culture dish	430293	Corning
10 cm petri dish, not treated	10720052	Falcon
12-well plate	353043	Falcon
15 mL falcon	188271	Greiner Bio-one GmbH
25 cm <sup>2</sup> flask	7696781	Labsolute – Th. Geyer GmbH & Co. KG
48-well plate	353047	Falcon
50 mL falcon	210261	Greiner Bio-one GmbH
6-well plate	353046	Falcon
75 cm <sup>2</sup> flask	7696782	Labsolute – Th. Geyer GmbH & Co. KG
96-well plate (flat bottom)	351172	Falcon
96-well plate (round bottom)	353077	Falcon
96-well plate (V bottom)	9-22	Kuhnle
96-well plate, block, clear bottom	3603	Costar Corning
96-well plate, flat bottom, maxi sorb	260836	Thermo Fisher
Ab diluent SignalStain	8112L	Cell Signaling Technology
CCK8 (cell counting kit)	96992-100TESTS-F	Sigma
Cell scraper M, L=30 cm	99003	TPP Techno Plastic Products AG
Clarity™ Western ECL substrate	170-5061	Bio-Rad Laboratories
Cotton Buds ROTILABO wood, 5 mm	EH11.1	Carl Roth GmbH & Co. KG
DNA-free™ KitDNase Treatment and Removal Reagents (10x DNase I buffer, rDNase I (2 units/μL), DNase Inactivation Reagent)	AM1906	Ambion by Life Technologies
dNTP mix (each dA/dC/dG/dT TP, 10 mM in water)	U1515	Promega
GenElute™ Mammalian Total RNA Miniprep Kit	RNT350-1KT	Sigma-Aldrich
GoTaq® qPCR Master Mix	A6002	Promega
Hydrogen peroxidase solution (30 percent) in H <sub>2</sub> O, contains stabilizer	H1009-100 mL	Sigma
Inoculation loop, 10 μL	612-9358	VWR
Lipofectamine 2000 Reagent	11668-019	Invitrogen
L-shaped spreaders	612-1561	VWR
MaxWell RSC simply RNA tissue kit	AS1340	Promega
M-MLV Reverse Transcriptase, RNase H Minus, Point Mutant (50.000 units) includes M-MLV RT 5x buffer	M3683	Promega
M-MLV RT 5x buffer (5x 1 mL)	M531A	Promega

PCR tube stripes with lid (8 tubes)	G003-SF	Kisker Biotech GmbH & Co. KG
Pierce ECL Western Blotting substrate	32106	Thermo Scientific
Plastic pipettes (10 mL, sterile)	607180	Greiner Bio-one GmbH
Plastic pipettes (25 mL, sterile)	760180	Greiner Bio-one GmbH
Plastic pipettes (5 mL, sterile)	606180	Greiner Bio-one GmbH
Polybrene Infection/transfection Reagent [final conc. 8 µg/mL]	TR-1003-G	Sigma-Aldrich
PureYield™ Plasmid Midiprep System	A2495	Promega
PureYield™ Plasmid Miniprep System	A1222	Promega
Recombinant Human LIGHT (TNFSF14)	664-LI-025	R&D Systems
Recombinant Human Lymphotoxin (LTα <sub>1</sub> β <sub>2</sub> )	678-LY	R&D Systems
Restore PLUS Western Blot Stripping buffer	46430	Thermo Scientific
SignalStain DAB-Substrate Kit	8059S	Cell signaling Technology
Wizard® SV Gel and PCR Clean-Up System	A9281	Promega
40 percent Acrylamide/Bis Solution 37.5:1	1610148	Bio-Rad Laboratories
Combitips advanced, 0.1 mL	0030.089.405	Eppendorf AG
2.0 mL microtubes, CapLock	96.10834.9.01	TreffLab – Nolato Treff AG
0.5 mL microtubes, CapLock	96.10833.9.01	TreffLab – Nolato Treff AG
Albumin (BSA) Fraction V (pH 7.0)	A1391,0500	AppliChem
1.2 mL cryo tube	7696651	Labsolute – Th. Geyer GmbH & Co. KG
Amersham Protean 0.45 NC nitrocellulose Western blotting membranes (300mm x 4m)	10600002	GE Healthcare Life Science
1.5 mL microtubes, CapLock	96.08668.9.01	TreffLab – Nolato Treff AG
3.5 cm dishes	430165	Corning

Table 3: List of buffers

BUFFERS	AMOUNT OF INGREDIENTS
Chelation buffer	<p>For 1 L:</p> <ul style="list-style-type: none"> <li>➤ 5.6 mM Na<sub>2</sub>HPO<sub>4</sub> (0.795 g)</li> <li>➤ 8.0 mM KH<sub>2</sub>PO<sub>4</sub> (1.089 g)</li> <li>➤ 96.2 mM NaCl (5.622 g)</li> <li>➤ 1.6 mM KCl (0.1193 g)</li> <li>➤ 43.4 mM Sucrose (14.86 g)</li> <li>➤ 54.9 mM D-sorbitol (9.998 g)</li> <li>➤ 0.5 mM DL-Dithiothreitol (0.0771 g)</li> </ul> <p>dissolved in 800 mL dH<sub>2</sub>O, adjust pH at 7.0 and filled up to 1 L; stored at 4°C</p>
10x TBS	<p>For 1 L:</p> <ul style="list-style-type: none"> <li>➤ 500 mM Tris ultra-pure (60.5 g)</li> <li>➤ 1.5 M NaCl (87.6 g)</li> </ul> <p>dissolved Tris/NaCl in about 800 mL dH<sub>2</sub>O and adjusted pH at 7.5 with HCl; filled up to 1 L, stored at RT</p>
1x TBS-T	<p>For 1 L:</p> <ul style="list-style-type: none"> <li>➤ 100 mL TBS 10x</li> </ul> <p>diluted with 900 mL dH<sub>2</sub>O and added 1 mL (0.1 percent) Tween20; stored at RT</p>
10x PBS	<p>For 1 L:</p> <ul style="list-style-type: none"> <li>➤ 137 mM NaCl</li> </ul>

	<ul style="list-style-type: none"> <li>➤ 2.7 mM KCl</li> <li>➤ 100 mM Na<sub>2</sub>HPO<sub>4</sub>*2H<sub>2</sub>O</li> <li>➤ 2 mM KH<sub>2</sub>PO<sub>4</sub></li> </ul> <p>dissolved in 800 mL dH<sub>2</sub>O and adjusted pH at 7.4 with HCl; filled up to 1 L, stored at RT</p>
<b>1x PBS-T</b>	<p>For 1 L:</p> <ul style="list-style-type: none"> <li>➤ 100 mL PBS 10x</li> </ul> <p>diluted with 900 mL dH<sub>2</sub>O and added 1 mL (0.1 percent) Tween20; stored at RT</p>
<b>five percent milk in TBS-T</b>	<p>For 250 mL:</p> <ul style="list-style-type: none"> <li>➤ 12.5 g milk powder</li> </ul> <p>dissolved filled with TBS-T to 250 mL, stirred and stored at 4°C.</p>
<b>five percent BSA in TBS-T</b>	<p>For 50 mL:</p> <ul style="list-style-type: none"> <li>➤ 2.5 g BSA</li> </ul> <p>Dissolved with TBS-T, stirred and stored at 4°C; only use for max. 1 week.</p>
<b>1.5 M Tris pH 8.8</b>	<p>For 1 L:</p> <ul style="list-style-type: none"> <li>➤ 181,71 g</li> </ul> <p>dissolved with 800 mL dH<sub>2</sub>O, pH adjusted at 8.8, filled up to 1 L, stirred, and stored at RT</p>
<b>0.5 M Tris pH 6.5</b>	<p>For 1 L:</p> <ul style="list-style-type: none"> <li>➤ 60.57 g</li> </ul> <p>dissolved with 800 mL dH<sub>2</sub>O, pH adjusted at 6.5, filled up to 1 L, stirred, and stored at RT</p>
<b>1 M Tris pH 7.4</b>	<p>For 1 L:</p> <ul style="list-style-type: none"> <li>➤ 121.14 g</li> </ul> <p>dissolved with 800 mL dH<sub>2</sub>O, pH adjusted at 7.4, filled up to 1 L, stirred, and stored at RT</p>
<b>Separating gel buffer</b>	<p>For 0.5 L:</p> <ul style="list-style-type: none"> <li>➤ 1.5 M Tris ultra-pure; pH 8.8</li> <li>➤ 0.4 percent of SDS</li> </ul> <p>filled up with dH<sub>2</sub>O to 0.5 L; stored at RT</p>
<b>Stacking gel buffer</b>	<p>For 0.5 L:</p> <ul style="list-style-type: none"> <li>➤ 0.5 M Tris ultra-pure; pH 6.5</li> <li>➤ 0.4 percent of SDS</li> </ul> <p>filled up with dH<sub>2</sub>O to 0.5 L; stored at RT</p>
<b>SDS lysis buffer stock</b>	<p>For 50 mL:</p> <ul style="list-style-type: none"> <li>➤ 250 mM TRIS pH 6.8 (12.5 mL of 1 M TRIS)</li> <li>➤ 6 percent SDS (3 g)</li> <li>➤ 10 percent of glycerol (5 mL)</li> <li>➤ 0.01 percent of bromophenol blue</li> </ul> <p>filled up with dH<sub>2</sub>O to 50 mL</p>
<b>1x SDS lysis buffer, ready to use</b>	Add 0.5 mL 1 M DTT to 9.5 mL lysis buffer before use.
<b>Ripa buffer stock</b>	<p>For 250 mL:</p> <ul style="list-style-type: none"> <li>➤ 50 mM TRIS ultra-pure; pH 7.4</li> <li>➤ 1 percent of NP-40 (Igepal = NP-40 substitute)</li> <li>➤ 150 mM NaCl</li> <li>➤ 0.25 percent DOC</li> <li>➤ 1 mM EGTA</li> </ul> <p>mixed well and filled up to 250 mL with dH<sub>2</sub>O.</p>
<b>Ripa buffer, ready to use</b>	<ul style="list-style-type: none"> <li>➤ 10 mL of Ripa buffer</li> </ul>

	<ul style="list-style-type: none"> <li>➤ 1 tablet of protease + phosphatase inhibitor mixed well, aliquoted, and stored at -20°C until usage.</li> </ul>
<b>4x SDS lysis buffer</b>	<p>For 100 mL:</p> <ul style="list-style-type: none"> <li>➤ 250 mM Tris ultrapure (pH 6.8)</li> <li>➤ 8 percent (w/v) of SDS</li> <li>➤ 40 percent (v/v) of glycerol</li> <li>➤ 20 percent (v/v) of β-mercaptoethanol</li> <li>➤ 0.2 percent (w/v) of bromophenol blue</li> </ul> <p>mixed well and filled up to 100 mL with dH<sub>2</sub>O</p>
<b>ten percent APS</b>	<p>For 100 mL:</p> <ul style="list-style-type: none"> <li>➤ 10g ammonium persulfate</li> </ul> <p>dissolved in dH<sub>2</sub>O, prepared 0.5 mL aliquots, and stored at -20°C.</p>
<b>1M DTT</b>	<p>For 100 mL:</p> <ul style="list-style-type: none"> <li>➤ 15,43 g</li> </ul> <p>dissolved in dH<sub>2</sub>O, prepared 0.5 mL aliquots, and stored at -20°C.</p>

Table 4: List of used substances.

SUBSTANCES	ORDER NUMBER	COMPANY
<b>Agarose, BioReagent for molec. Biology</b>	A9539-500G	Sigma
<b>Ammonium Persulfate (APS)</b>	A3678-25G	Sigma
<b>BenchTop 100 bp DNA ladder</b>	G829B	Promega
<b>BenchTop 1kb DNA ladder</b>	G754A	Promega
<b>Bromophenol Blue Sodium Salt</b>	B8026-5G	Sigma
<b>Cell titre glo 3D reagent, cell viability assay</b>	G968A	Promega
<b>Chloroform</b>	288306-100mL	Sigma
<b>cOmplete Tablets, Mini EDTA-free, EASYpack protease Inhibitor cocktail</b>	04 693 159 001	Roche
<b>Dimethyl Sulfoxide (DMSO) for cell culture</b>	A3672,0250	AppliChem
<b>DL-Dithiothreitol (DTT)</b>	D9779	Sigma
<b>Doxycycline, Hyclate</b>	342385-1GM	Millipore
<b>D-sorbitol</b>	S6021	Sigma
<b>Ethanol absolute, molecular biology grade</b>	A3678,1000	AppliChem
<b>Ethylenediaminetetraacetic acid (EDTA)</b>	E9884-100G	Sigma
<b>Glycerol</b>	3783.2	Roth
<b>Glycine</b>	0079.4 (2,5 kg)	Roth
<b>KCl</b>	6781.1	Roth
<b>KH<sub>2</sub>PO<sub>4</sub></b>	P018.1	Roth
<b>Methanol</b>	106002	Merck
<b>MG132 proteasome inhibitor, Ready-made solution</b>	M7449-200UL	Sigma
<b>Na<sub>2</sub>HPO<sub>4</sub></b>	T876.1	Roth
<b>NaCl</b>	3957.4	Roth
<b>NaOH</b>	9356.1	Roth
<b>PhosSTOP EASYpack phosphatase Inhibitor Cocktail</b>	04 906 837 001	Roche
<b>Powdered milk, blotting grade</b>	T145.3	Roth
<b>Precision Plus Protein Dual Color Standards</b>	161-0374	Bio-Rad Laboratories

ROTI-GelStain	3865.2 (5x1mL)	Roth
Sodium Dodecyl Sulfate (SDS), pellets	CN30.2	Roth
Staurosporine, from Streptomyces sp.	S4400-1MG	Sigma
Sucrose	1076875000	Millipore
Temed (N, N, N', N'-Tetramethylethylenediamine)	T9281-100ML	Sigma
Thiazolyl Blue Tetrazolium Bromide, approx. 98 percent TLC (MTT)	M2128-1G	Sigma
TPCA-1	T1452-1MG	Sigma
TRIS ultra-pure	A1086,1000	AppliChem
Trypan Blue Stain (0.4 percent)	15250-061	Gibco
TWEEN® 20 Molecular biology grade	A4974,0500	AppliChem
β-Mercaptoethanol (cell culture grade)	M3148	Sigma

Table 5: List of applied media and supplements.

MEDIA AND SUPPLEMENTS	ORDER NUMBER	COMPANY
[Leu-15] Gastrin-I (human)	G9145	Sigma
0.05 percent Trypsin-EDTA (1x)	25300-054 (100 mL)	Gibco
Advanced DMEM/F12 cell culture medium (DMEM/F12 advanced)	12634 -010 (500 mL)	Gibco
B27 supplement (50x)	17504-044	Gibco
Collagen I, Bovine 5mg/mL	A10644-01 (10 mL)	Gibco
Corning® Matrigel Basalmembranematrix with reduced growth factors	734-0269	VWR
Dulbecco's Modified Eagle Medium (DMEM)	41965-039 (500 mL)	Gibco
EGF (recombinant, murine)	PMG8043	Gibco
Foetal Bovine Serum (FCS) heat inactivated	12133C-500 mL	Sigma
Glutamax	35050-079	Gibco
HEPES	15630-056	Gibco
Human FGF-10	100-26-100UG	PEPROTech
Iscove`s Modified Dulbecco`s Medium (IMEM) Medium	21056-023	Gibco
N2 supplement (100x)	17502-048	Gibco
N-Acetyl-L-cysteine	A9165-5G	Sigma
Nicotinamide	N3376-100G	Sigma
Normocin	ant-nr-1 (10x 1 mL)	InvivoGen
Opti-Mem I (1x) Reduced Serum Medium	31985-070 (500 mL)	Gibco
p38i (SB 202190)	S1077	Selleckchem
Penicillin (5000 units/mL)/Streptomycin (5000 µg/mL) (P/S)	15070-063 (100 mL)	Gibco
Phosphate Buffered Saline (PBS) pH 7.4 (1x)	10010-015 (500 mL)	Gibco
Plasmocure	ant-pc (100 mg; 1 mL)	InvivoGen
TGFβ <sub>i</sub> (A83-01), 10 mg	2939	Tocris
TrypLE™ Express Trypsin for organoids	12605028	Thermo Scientific
Y-27632 dihydrochloride (Rho Kinase Inhibitor)	Y0503	Sigma

Table 6: List of bacterial culture media.

<b>BACTERIAL CULTURE MEDIA</b>	
<b>Luria-bertani (LB) media</b>	20 g/L Lennox-L-Broth (Gibco), autoclaved
<b>Dent supplement</b>	Vancomycin, Amphotericin B, Cefsulodin, Trimethopimlactat (OXOID)
<b>Horse Serum</b>	Invitrogen
<b>Brain Heart Infusion (BHI) media</b>	36 g BHI (MP Biomedicals), 0.25 percent (w/v) yeast extract, five percent (v/v) FCS, 1 L acqua
<b>Wilkins-Chalgren (WC)-Dent blood agar plates</b>	21.5 g WC-agar, 50 mL inactivated horse serum, 0.4 g potassium nitrate, Dent
<b>WC-Dent special blood agar plates</b>	WC-Dent blood agar plates were supplemented with one percent (v/v) of "special" supplement comprising further antibiotics (200 g/ml bacitracin, 10 g/ml nalidixic acid, 3 g/ml polymycin B)
<b><i>H. pylori</i> Freezing media</b>	20 percent glycerol, BHI media plus 20 percent FCS

## 2.2 Cell culture

### 2.2.1 Cell lines and their cultivation

GC cells were purchased from ATCC or JBRC (Table 7) and cultivated in DMEM supplemented with ten percent (v/v) FCS, one percent (v/v) penicillin/streptomycin (P/S), and Normocin (InvivoGen, #ant-1) under humidified conditions at 37°Celsius (°C) and five percent (v/v) CO<sub>2</sub> (Hera cells 240 incubator). All GC cells were tested for mycoplasma contamination. Cells were splitted once per week in a ratio of 1:4 - 10 depending on their growth behaviour (Table 7).

**Table 7: List of GC cells used (American Type Culture Collection; Swiss Institute of Bioinformatics).**

CELL LINES	COMPANY/NUMBER	ESTABLISHED BY	SPLIT RATIO
<b>AGS</b>	ATCC CRL-1739	Barranco, SC.; in 1979	1:10
<b>Kato III</b>	ATCC HTB-103	Sekiguchi, M.; in 1978	1:10
<b>MKN7*</b>	JCRB1025	Hojo, H.; in 1989	1:5
<b>MKN28*</b>	JCRB0253	Hojo, H.; in 1989	1:10
<b>MKN45</b>	JCRB0254	Hojo, H.; in 1989	1:10
<b>NCI-N87</b>	ATCC CRL-5822	Park, J.; in 1976	1:4-8
<b>NUGC-4</b>	JCRB0834	Akiyama, S.: in 1993	1:6-10
<b>SNU1</b>	ATCC CRL-5971	Park, J.; in 1984	1:5-8
<b>St2957*</b>	CVCL_9557	Vollmers, HP et al.; in 1993	1:10
<b>St3051*</b>	CVCL_9558	Vollmers, HP et al.; in 1993	1:10

\*cells are contaminated with different cells.

### 2.2.2 Propagation of cell lines

Cells were split at least once a week to keep them in the exponential growth phase. To do so, cell culture medium was discarded, washed once with PBS, and cells were incubated with trypsin (two mL) for three to five minutes at 37°C to detach them from the flask bottom. The enzymatic activity of trypsin was stopped by using six mL of medium containing ten percent (v/v) FCS. The cell suspension was transferred to a 15 mL centrifugation tube and centrifuged (five minutes at 1000 rpm). The pellet was resuspended in 1 mL medium and seeded in a new T75 cell culture flask (split ratio Table 7).

### 2.2.3 Cell counting

To determine the cell number, cells were processed as described in 2.2.2. Ten µL of the cell suspension is mixed with 90 µL of trypan blue. Ten µL of the cell-trypan blue mixture is transferred to a hemocytometer. The cell number is determined by counting four big squares. The cell number per mL is calculated by using the following equation:

$$\frac{\text{cell number}}{\text{mL}} = \frac{\text{counted cell number}}{4} \times 10^4 \times 10^1 (\text{dilution factor})$$

## 2.2.4 Cell Freezing

For cell freezing, cells were grown to full confluency (80 to 90 percent) in a T75 flask. Cells were processed as described in 2.2.2. The pellet was resuspended in an appropriate volume of media to achieve a concentration of one million cells/mL. 100  $\mu$ L of DMSO were filled in a 1.5 mL cryotube. Next, 900  $\mu$ L of the cell suspension was added to the cryotube and immediately stored at  $-80^{\circ}\text{C}$ . For long-term storage, cryotubes were transferred into liquid nitrogen tanks.

## 2.2.5 Cell thawing

For cell thawing, a cryotube was taken from the  $-80^{\circ}\text{C}$  freezer or liquid nitrogen tank and thawed quickly until only a small lump of ice was left over. Meanwhile, a 15 mL tube was filled with 5 mL of fresh culture medium ( $4^{\circ}\text{C}$ ) containing FCS. Thawed cells (1 mL) were transferred to a 15 mL tube and centrifuged (five minutes/1.000 rpm). The pellet was resuspended in one mL medium and transferred into a T25 flask containing five mL culture medium. Twenty-four hours later, the medium was exchanged to remove residual DMSO. Cells were propagated and split as described in 2.2.2.

## 2.3 Down modulation of NF- $\kappa$ B inducing kinase (NIK)

### 2.3.1 CRISPR/Cas9n knockdown of NIK

We used the CRISPR/Cas9 nickase (Cas9n) technology to knockdown endogenous NIK in GC cells. Cas9n is a D10A mutant of SpCas9 that introduces a single-strand break in the target DNA (Loureiro and da Silva 2019; Valenti et al. 2019); however, by applying two Cas9 nickases, the specificity of the genome editing can be increased, and off-targets are less (Valenti et al. 2019).

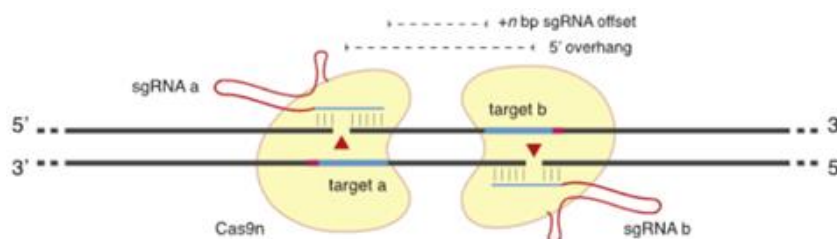


**Figure 8: CRISPR/Cas9n strategy (Ran et al. 2013)**

Adapted by permission from RightsLink: Elsevier [Cell] (Cell, 154, 1380–1389, F. Ann Ran, Patrick D. Hsu, Chie-Yu Lin, Jonathan S. Gootenberg, Silvana Konermann, Alexandro E. Trevino, David A. Scott, Azusa Inoue, Shogo Matoba, Yi Zhang, Feng Zhang) copyright (2013). (License Number: 5082050612287, 04.06.21)

For this purpose, two guide RNAs (gRNAs) were synthesized to target the functional region of NIK, which is located in exon 7 (Table 8). The gRNA sequence starts at 5' CACC-GNNNNNNNNNNNNNNNNNNNNNN (19) and the reverse at 5' AAAC-NNNNNNNNNNNNNNNNNNNNN(19)C. Both were generated by using the Benchling website. The gRNA needs an additional 5'G (marked in grey in Table 8), if not already present in the sequence for the RNA polIII transcription, and is located next to a protospacer adjacent motif (PAM) sequence (Gokcezade et al. 2014). gRNAs are inserted via two *BbsI* restriction enzyme sites, which are located after the U6 promotor region and before the sgRNA scaffold (Gokcezade et al. 2014).

**Table 8: List of guide RNAs and sequencing primers.**

GUIDE RNAs (gRNAs)	FORWARD SEQUENCE	REVERSE SEQUENCE
nickNIKex7aA	CACC GGCCTGGCCAGGTAGTACA	AAAC TGTACTACCTGGGCCAGGCC
nickNIKex7aB	CACC GTCGTGAGTGGAGGTATTCCA	AAAC TGGAATACCTCCACTCACGAC
nickNIKex7bA	CACC GCATGCAGAATCCTTCGTGAG	AAAC CTCACGAAGGATTCTGCATGC
nickNIKex7bB	CACC GGGCCTTACCTTTGACGTCC	AAAC GGACGTCAAAGGTAAGGCC
nickNIKex7cA	CACC GAGTACAGGGCCCGTCTCT	AAAC AGAGGACCGGGCCCTGTACTC
nickNIKex7cB	CACC GTCGTGAGTGGAGGTATTCCA	AAAC TGGAATACCTCCACTCACGAC
U6 primer	ACT ATC ATA TGC TTA CCG TAA C	-
Sequencing primer	GTG ACC CTG CTT TCC ACT G	AGA GGA GATCAG ACA GGA TGG
VECTOR	CATALOG #	COMPANY
pX335-U6-Chimeric_BB-CBh-hSpCas9n(D10A) (Le Cong et al. 2013)	42335	Addgene

Designed gRNAs were first annealed (Table 9) by incubating for 30 minutes at 37°C, five minutes at 95°C, and ramp down to 25°C at 1.5°C/minute. Oligos were stored at -20°C or further used to insert them into the *BbsI* digested pX335-U6-Chimeric vector. Before ligation, the pX335 vector was digested by incubating *BbsI* for one hour at 37°C (Table 10). Afterward, the digested vector was purified using the Promega Wizard SV gel & PCR clean-up kit according to the manufacturer's instructions. Next, the annealed oligos were ligated into the digested vector and incubated for two to three hours at RT (Table 11).

**Table 9: Oligo annealing reaction for gRNAs.**

REAGENTS	VOLUME [ $\mu$ L]
100 $\mu$ M Oligo1 (for example, aA fwd.)	1
100 $\mu$ M Oligo2 (for example, aA rev.)	1
adenosine triphosphate (ATP)	1
10x T4 ligation buffer (NEB, #B0202S)	1
H <sub>2</sub> O	6
total	10

Table 10: Vector digestion with *BbsI*.

REAGENTS	VOLUME [ $\mu\text{L}$ ]
1 $\mu\text{g}$ pX335-U6-chimeric vector	x
<i>BbsI</i> (NEB, #R0539)	1
10x Buffer 2.1 (NEB, #B7202)	2
H <sub>2</sub> O	x
<b>Total</b>	20

Table 11: Ligation reaction for inserting annealed gRNA in digested pX335 vector.

REAGENTS	VOLUME [ $\mu\text{L}$ ]
digested pX335-U6-chimeric vector	1
annealed gRNA (1:10 diluted, for example: aA)	6
ATP	1
T4 DNA Ligase (NEB, #M0202)	1
10x T4 ligation buffer (NEB, #B0202)	1
<b>Total</b>	10

Subsequently, two  $\mu\text{L}$  of the ligated vector were transformed into competent DH5alpha *Escherichia coli* (*E. coli*) as described in section 2.8.1. The next day, single colonies were picked to perform a U6 screening by PCR (using U6 forward primer and reverse primer of used oligo). For PCR, only a bit of the bacterial colony was taken up with a tip and dipped into the master mix (Table 12 and Table 13). The PCR product was separated on a two percent agarose gel. A band at around 250 bp was expected for the successful insertion of the gRNA into the vector.

Table 12: Master mix for screening for PCR.

REAGENTS	VOLUME [ $\mu\text{L}$ ]
Green Taq polymerase	12.5
U6 fwd. (1:10 diluted)	1
Oligo rev. (1:10 diluted)	1
H <sub>2</sub> O	10.5
<b>Total</b>	25

Table 13: Thermal cycle program for screening PCR.

THERMOCYCLER STEPS	TEMPERATURE [ $^{\circ}\text{C}$ ]	TIME [min:sec]
Initiation	95	05:00
Denaturation	95	00:30
Annealing	50	00:30
Elongation	72	01:40
Final elongation	72	05:00
Hold	12	$\infty$

Positive colonies were inoculated in 5 mL LB medium with antibiotics for a bacterial o/n culture as described in section 2.8.2 and cleaned up as in section 2.8.3. 1  $\mu\text{g}$  of cleaned-up plasmid DNA

supplemented with two  $\mu\text{L}$  of U6 forward primer (1:10 diluted) in a final volume of 17  $\mu\text{L}$  was sent for sequencing. One mL of bacterial suspension was transferred into a 1.5 ml Eppendorf tube and centrifuged at 4000 rpm for five minutes, and the supernatant was discarded. The pellet was resuspended in 500  $\mu\text{L}$  LB medium and transferred into a cryo tube. 500  $\mu\text{L}$  of glycerol were added, mixed well, and glycerol stocks were stored at  $-80^{\circ}\text{C}$  as a backup.

### **2.3.1.1 Generation of NIK knock down cells**

After successful insertion of the gRNA into the pX335 vector, NIK knockdown cells could be generated. Before transfection,  $3 \times 10^5$  cells/well were seeded in a 6-well plate. The next day, cells were transfected with a lipid-based reagent. Therefore, four  $\mu\text{L}$  lipofectamine (diluted 1:50) were added to 200  $\mu\text{L}$  OptiMEM media per well, mixed gently, and incubated for five minutes at RT. Meanwhile, the DNA mix was prepared, and 500 ng of each nickase plasmid (for example, pX335+nickNIKex7aA and pX335+ nickNIKex7aB) were prepared in 200  $\mu\text{L}$  OptiMEM. Then, 200  $\mu\text{L}$  of the lipofectamine mix was added to the DNA mix, mixed gently, and incubated for 20 minutes at RT. The media was aspirated from the preplated cells and washed once with PBS. 400  $\mu\text{L}$  of the lipofectamine/DNA mix were added per well and incubated for two to three hours. The plate was moved every 30 minutes to prevent dehydration of the cells. Two mL of OptiMEM were added and incubated again for three to four hours to increase transfection efficiency. Afterward, two mL of complete DMEM medium was added, and cells were grown for 48 hours.

Since the pX335 plasmid contains a GFP (cloned by Martina Grandl), successfully transfected cells can be selected by cell sorting. To do so, transfected cells and an untransfected control (used to adjust the forward/sideward scatter) were trypsinized as described in section 2.2.2. The cell pellet was resuspended in 500  $\mu\text{L}$  PBS, filtered (22  $\mu\text{m}$  filter) to obtain single cells, and transferred into a FACS tube. GFP<sup>+</sup> cells were collected in FACS tubes containing 500  $\mu\text{L}$  FCS and cells were seeded in a 96-/48- or 12-well plate depending on the number of gained GFP<sup>+</sup> cells. Expanded cells were then either directly screened or seeded in a lower density to grow single-cell colonies. Single colonies were scratched off with a pipette tip and put into a 96-well plate containing 20  $\mu\text{L}$  PBS per well. Next, 30  $\mu\text{L}$  of trypsin was added and incubated for ten minutes at  $37^{\circ}\text{C}$ . Finally, 90  $\mu\text{L}$  of media was added, and half of the cells were transferred to a second 96-well plate. Therefore, one plate was used to cultivate the single-cell colonies, and the second one was used for PCR-based screening of the single colonies. After grown confluent, cells were detached, resuspended in 25  $\mu\text{L}$  H<sub>2</sub>O, transferred to a PCR tube, and lysed by adding five  $\mu\text{L}$  proteinase K (1:5 diluted). Cells were incubated at  $56^{\circ}\text{C}$  for one hour and heated to  $95^{\circ}\text{C}$  for ten minutes. DNA lysates were used as templates for screening PCR and selecting knockdown cells by sequencing (see section 2.3.1).

### 2.3.2 siRNA based down-regulation of NIK

To down-modulate endogenous NIK expression, a small interfering RNA (siRNA) targeting NIK was used. RNA interference (RNAi) is a biological process that induces gene inactivation by degrading the target mRNA through double-stranded RNAs (Lodish 2008). This process can be used experimentally by synthesizing synthetic siRNA that target mRNA of interest. To do so,  $5 \times 10^5$  cells/well were seeded in a six-well plate the day before. Next, lipofectamine was mixed with 200  $\mu$ L OptiMEM for each treatment/sample (see section 2.3.1.1). Ten nM of siNIK or siSCR (Table 14) were mixed with 200  $\mu$ L OptiMEM each. The 200  $\mu$ L of the lipofectamine mix was added to the siSCR or siNIK and incubated for 20 minutes. Cells were washed with PBS, and 400  $\mu$ L of the lipofectamine-siRNA mix was added. The cells were incubated for two to three hours, and every 30 minutes, the plate was moved to avoid drying out of the cells. Next, two mL OptiMEM was added, incubated for three to four hours, and finally, two mL of complete culture media were added, and the cells were incubated for 48 hours.

Table 14: List of used siRNAs.

SIRNA	ORDER NUMBER	COMPANY
Accell Control siRNA Red non-targeting (siSCR)	D-001960-01-05	Dharmacon
Accell SMART pool human MAP3K14 (siNIK)	E-003580-00 5 nmol	

48 hours later, transfected cells were reseeded for a proliferation assay (see section 2.5.2), or RNA and/or protein were extracted from transfected cells to check for successful down-modulation of NIK by qPCR (see section 2.4.1) or western blot (see section 2.4.2)

### 2.3.3 shRNA based down-modulation of NIK by lentiviruses

To down-modulate the endogenous NIK protein levels, short hairpin RNAs (shRNAs) were used, which are delivered into the host cell and can be continuously synthesized by the host cell machinery to enable a more prolonged gene knockdown effect compared to siRNAs that are degraded in the cell and hence almost gone after 48 hours (Rao et al. 2009).

Table 15: List of plasmids for shRNA-based down-modulation.

PLASMIDS		COMPANY
pLKO.1 puro (#8453) (Stewart et al. 2003)	order: 373891	Addgene
RESTRICTION ENZYME		COMPANY
<i>AgeI</i>	#R3552	NEB
<i>EcoRI</i>	#R0101	

First, the used plasmid (Table 15) had to be digested to insert the shRNAs of interest. Therefore, the pLKO.1 plasmid was digested with *AgeI* and *EcoRI* restriction enzymes. The successful digestion was confirmed by electrophoresis and cleaned up from the agarose gel with Promega wizard SV gel & PCR clean-up kit according to manufacturer's instructions. Next, shRNAs targeting NIK were designed by using the GENETIC PERTURBATION PLATFORM (GPP) Web Portal of the Broad Institute (<https://portals.broadinstitute.org/gpp/public/gene/details?genelid=9020> (26/01/18)). With the help of this platform, a list of shRNAs were generated, and four different shRNAs were selected (Table 16).

**Table 16: List of selected shRNA sequences.**

SHRNA	SHRNA SEQUENCES	
shNIK1	forward	5'- CCGGCTCAGGACTCACGTAGCATTACTCGAGTAATGCTACGTGAGTCCTGAGTTTTTG -3'
	reverse	5'- AATTCAAAAACCTCAGGACTCACGTAGCATTACTCGAGTAATGCTACGTGAGTCCTGAG -3'
shNIK2	forward	5'- CCGGCCAGGCTGAGTGTGAGAATAGCTCGAGCTATTCTCACACTCAGCCTGGTTTTTG -3'
	reverse	5'- AATTCAAAAACCTCAGGCTGAGTGTGAGAATAGCTCGAGCTATTCTCACACTCAGCCTGG -3'
shNIK3	forward	5'- CCGGCCTCGATCAGAACTCCACAACTCGAGTTTGTGGAGTTCTGATCGAGGTTTTTG -3'
	reverse	5'- AATTCAAAAACCTCGATCAGAACTCCACAACTCGAGTTTGTGGAGTTCTGATCGAGG -3'
shNIK4	forward	5'- CCGGGTGTGAGAATAGCCAAGAGTTCTCGAGAACTCTGGCTATTCTCACACTTTTTG -3'
	reverse	5'- AATTCAAAAAGTGTGAGAATAGCCAAGAGTTCTCGAGAACTCTGGCTATTCTCACAC -3'
shcontrol	forward	5'- CCGGAAGTACAGCCGCCTCAATTCTCTCGAGAGAATTGAGGCGGCTGTACTTTTTTTG -3'
	reverse	5'- AATTCAAAAAGTACAGCCGCCTCAATTCTCTCGAGAGAATTGAGGCGGCTGTACTT -3'

shRNA oligos were first reconstituted to 20  $\mu$ M by adding the appropriate amount of dH<sub>2</sub>O. Oligos were annealed (Table 17) by incubating four minutes at 95°C, ten minutes at 70°C, and ramp down to 22°C at 1.5°C/minute.

**Table 17: Master mix for annealing oligos.**

Reagents	Volume [ $\mu$ L]
Forward oligo (20 $\mu$ M)	5
Reverse oligo (20 $\mu$ M)	5
10x NEB buffer 2	5
H <sub>2</sub> O	35
<b>Total</b>	<b>50</b>

Subsequently, the annealed oligos were ligated into the digested vector (Table 18) by incubating for four hours at room temperature or o/n at four°C. Two  $\mu$ L of the ligation were transformed into *Stab13* bacteria and grown on LB agar plates containing 100  $\mu$ g/mL ampicillin. Grown clones were picked and screened for correct insertion of the shRNAs by sequencing (see section 2.3.1).

**Table 18: Master mix for ligation reaction.**

REAGENTS	VOLUME [ $\mu$ L]
annealed oligo	2

20 ng of digested pLKO.1 or Tet-pLKO vector	x
ATP	1
10x T4 DNA ligase buffer (Promega)	2
T4 DNA ligase (Promega)	1
H <sub>2</sub> O	x
Total	20

### 2.3.3.1 Generation of NIK knock down cells by using lentiviruses

The positive selected clones containing shRNA or shco in the pLKO.1 vector were packaged in lentivirus particles by the group of Prof. Martina Anton. To generate stable NIK knockdown cells,  $3 \times 10^5$  cells/well were seeded in a 6-well plate. The next day, the generated virus particles (one vial = one mL) and eight  $\mu\text{g/mL}$  polybrene were added to the cells to increase the efficiency of the infection. Twenty-four hours later, the media was exchanged to a fresh culture medium. The following day, puromycin (concentration selected by killing assay of non-transfected cells) was added to the media to select positive infected cells. Knock down was investigated by harvesting RNA for qPCR or protein for western blot.

## 2.4 Expression Analysis

### 2.4.1 Determination of mRNA expression level

Two different methods were used to isolate total RNA from cells or tissue by using either the **GenElute™ Mammalian Total RNA Miniprep Kit** from Sigma using a column-based RNA isolation approach or the **Maxwell® RSC simply RNA Tissue Kit** from Promega, an automated nucleic acid purification platform with prefilled cartridges.

#### **Isolation of total RNA from cells or tissue (GenElute™ Mammalian Total RNA Miniprep Kit, Sigma) and subsequent DNase Treatment**

For RNA isolation from **cells**, cells were seeded in a 6-well plate at a density of  $5,5 - 6 \times 10^5$  cells per well, depending on cells used. Forty-eight hours later, cells were washed once with PBS, and 300  $\mu\text{L}$  of lysis buffer supplemented with 2-mercaptoethanol (10  $\mu\text{L/mL}$  lysis buffer) was added to the cells that were scratched off by using a cell scraper. Lysed cells were transferred to 1.5 mL micro tubes and put on ice.

For RNA isolation from **tissue**, 10-20 mg of tissue were transferred into a 2 mL Precellys tube containing ceramic beads. Next, the tissue was homogenized by adding 500  $\mu\text{L}$  of lysis buffer supplemented with 2-mercaptoethanol (10 $\mu\text{L/mL}$  lysis buffer) and run on the homogenizer

Precellys24 at 5.500 G (two times) 30 seconds and five seconds pause.

According to the manufacturer's instructions, RNA from cells or tissue was isolated by using the GenElute™ Mammalian Total RNA Miniprep Kit. To do so, cell lysate or tissue homogenate was spun through a filtration column to eliminate cell debris. Next, an equal amount of 70 percent ethanol (300 or 500 µL) was added to the filtrate, and the mixture was applied to a high-capacity silica column to bind total RNA. RNA was washed three times and eluted in 30 µL elution buffer or nuclease-free water. Finally, RNA concentration was measured with a spectrophotometer, nanodrop, and as blank elution buffer or nuclease-free water was used.

For removing “contaminating” DNA in RNA samples, a DNase treatment and removal kit (Invitrogen Ambion, DNA free) was applied. Therefore, 25 µL RNA/water sample (15 µL RNA sample + 10 µL nuclease-free water; max. 50 µg RNA in 25 µL) was transferred into a fresh 0.5 mL tube, 0.1 volume 10x DNase I buffer, one µL rDNase I were added and mixed gently. The mixture was incubated at 37°C for 20 - 30 minutes. Next, DNase was inactivated by adding a 0.1 volume DNase inactivation reagent and incubated at RT for two minutes by mixing occasionally. The micro tubes were centrifuged at 10.000 rpm for 1.5 minutes. DNA was present as a cloudy pellet, and the supernatant containing RNA was transferred to a fresh 0.5 mL micro tube. The concentration was measured, and cDNA synthesis was started, or RNA was stored at - 80°C.

### **Isolation of RNA from cells or tissue, including DNase treatment**

#### **(Maxwell® RSC simply RNA Tissue Kit, Promega)**

For RNA isolation from cells, cells were seeded at a density of  $5,5 - 6 \times 10^5$  cells/well in a 6-well plate depending on the used cell line. Forty-eight hours later, cells were washed once with PBS and trypsinized. The cell pellet was resuspended in 200 µL chilled 1- Thioglycerol/homogenization solution (20 µL of 1-Thioglycerol is added per mL homogenization solution) and vortexed until the pellet was lysed.

For RNA isolation from tissue, 10-20 µg of tissue were used. The tissue was thawed on ice and transferred into a two mL Precellys tube, and 200 µL chilled 1-Thioglycerol/Homogenization solution was added. Next, tissue was processed by Precellys24 homogenizer at 5.500 rpm for 30 seconds (two times) and five seconds pause.

Homogenates were stored on ice until further processing. Before using the Maxwell machine, the cartridges for automated RNA isolation had to be prepared. For this purpose, the Maxwell machine was started, and the cartridges were placed on the deck tray. In well #4, a blue DNase I solution was added (five µL for cell lysate, ten µL for tissue lysate), and in well #8, one plunger was added. 60 µL of nuclease-free water was added to each elution tube and placed into the elution

tube position. Next, 200  $\mu\text{L}$  lysis buffer was added to chilled homogenate (cell or tissue), vortexed vigorously for 15 seconds, and 400  $\mu\text{L}$  of lysate were transferred to well #1 in the cartridge. Finally, the Maxwell instrument was started. After the run was finished, RNA concentration was measured, and cDNA synthesis was started, or RNA was stored at  $-80^{\circ}\text{C}$ .

### **Complementary DNA (cDNA) synthesis using reverse transcriptase polymerase chain reaction (rt-PCR)**

The following steps had to be performed on ice: DNase treated RNA samples were thawed on ice and diluted to a final concentration of 1  $\mu\text{g}$  RNA in a volume of 14  $\mu\text{L}$  RNA/nuclease-free water mixture. Samples were prepared in duplicates. 1  $\mu\text{L}$  of random hexamer primers (stock conc.: 150  $\text{ng}/\mu\text{L}$ ) was added and incubated for five minutes at  $70^{\circ}\text{C}$ . Next, samples were cooled on ice for a few minutes. Meanwhile, two master mixes (MM) were prepared, as seen in Table 19. MM A contained reverse transcriptase, whereas MM B did not contain the reverse transcriptase and served as a control to exclude any DNA contaminations in the processed RNA samples. 11  $\mu\text{L}$  of MM A or B was added to each sample. Samples were incubated ten minutes at RT, 50 minutes at  $50^{\circ}\text{C}$ , and to stop the reaction, samples were heated for 15 minutes at  $70^{\circ}\text{C}$ . cDNA was diluted 1:10 (cells) or 1:5 (tissue) with nuclease-free water and stored at  $-20^{\circ}\text{C}$ .

**Table 19: Master mix components for rt-PCR.**

Master mix (MM) reagents	MM A - VOLUME [ $\mu\text{L}$ ]	MM B – volume [ $\mu\text{L}$ ]
M-MLV RT 5x Buffer	5	5
dNTPs mix (10 mM)	1.25	1.25
M-MLV Reverse Transcriptase	1	-
Nuclease-free water	3.75	4.75
Total volume	<b>11</b>	<b>11</b>

### **Quantitative real time-PCR (qPCR)**

GoTaq<sup>®</sup> qPCR system comprised of a ready-to-use 2x master mixes supplemented with BRYT green dye, a fluorescent DNA binding dye with minimal PCR inhibition and maximal amplification efficiency, was used to evaluate the gene expression profile. For this purpose, the GoTaq qPCR master mix and forward/reverse primer of genes of interest were added to the cDNAs in duplicates or triplicates (Table 20). For the qPCR, the Bio-Rad CFX384 system was applied (program: Table 21).

**Table 20: Master mix components for qPCR**

MASTER MIX REAGENTS	VOLUME [ $\mu\text{L}$ ]
2x GoTaq <sup>®</sup> qPCR master mix	5
10 $\mu\text{M}$ Primer forward	0.5
10 $\mu\text{M}$ Primer reverse	0.5
cDNA template (1:5 or 1:10 diluted)	4

Table 21: Thermal cycle profile for qPCR.

STAGES	TEMP [°C]	TIME [min:sec]
Enzyme activation	95	03:00
Denaturation	95	00:45
Annealing and elongation	60	00:15
Melting Curve	60-95	Increment of 0.5°C/s
Final Hold	12	∞

As a negative control, a template-free and a reverse transcriptase-free control were included in each run. *GAPDH/Gapdh* served as a housekeeping gene.

Table 22: List of used human primers.

GENE (HUMAN)	PRIMER FORWARD	PRIMER REVERSE
<i>GAPDH</i>	GAA GGT GAA GGT CGG AGT	GAA GAT GGT GAT GGG ATT TC
<i>LTA</i>	CCA CCC TAC ACC TCC TT	AGT CTG GGC AGC TGA AGG T
<i>LTB</i>	GAG GAC TGG TAA CGG AGA CG	GGG CTG AGA TCT GTT TCT GG
<i>A20</i>	TCC TCA GGC TTT GTA TTT GAG C	TCT CCC GTA TCT TCA CAG CTT
<i>CXCL13</i> <sup>1</sup>	GAG GCA GAT GGA ACT TGA GC	CTG GGG ATC TTC GAA TGC TA
<i>CXCL10</i>	TAT TCC TGC AAG CCA ATT TTG TC	TCT TGA TGG CCT TCG ATT CTG
<i>CCL2</i>	CTT CGG AGT TTG GGT TTG CTT	CAT TGT GGC CAA GGA GAT CTG
<i>NIK</i>	AGT ACA GCC AGT CCG AGA GT	GAC TCA TCC TGC ACT GG
<i>CEACAM1</i>	GCA ACA GGA CCA CAG TCA AG	CCA GGG CTA CTG CTA TCA G
<i>CEACAM5</i>	AGG CCA ATA ACT CAG CCA GT <sup>2</sup>	GGC TTG GGC AGC TCC GC
<i>CEACAM6</i> <sup>3</sup>	CGT CGG CAT CAC GAT TGG	TGG GAT TGG AGG AGC TAG AAG
<i>CEACAM3</i>	CAG CTC TGC CTT CTC GAT G	CTC ATA GAT GGA AGC TGC TG

Table 23: List of used mouse primers.

GENE (MOUSE)	PRIMER FORWARD	PRIMER REVERSE
<i>Gapdh</i>	GCC TTC TCC ATG GTG GTG AA	GCA CAG TCA AGG CCG AGA AT
<i>Lta</i>	TCC ACT CCC TCA GAA GCA CT	AGA GAA GCC ATG TCG GAG AA
<i>Ltb</i>	TAC ACC AGA TCC AGG GGT TC	ACT CAT CCA AGC GCC TAT GA
<i>A20</i>	AGT GTC CAG GCT TCC CTG G	GGC AGT TTC CAT CAC CAT TGG
<i>Cxcl13</i>	ATA TGT GTG AAT CCT CGT GCC A	GGG AGT TGA AGA CAG ACT TTT GC
<i>Cxcl10</i>	AAG TGC TGC CGT CAT TTT CT	CCT ATG GCC CTC ATT CTC AC
<i>Infg</i>	TCA AGT GGC ATA GAT GTG GAA GAA	TGG CTC TGC AGG ATT TTC ATG
<i>Ccl2</i>	TTA AAA AAC CTG GAT CGG AAC CAA	GCA TTA GCT TCA GAT TTA CGG GT
<i>KC (Cxcl1)</i>	TGC ACC CAA ACC GAA GTC AT	TTG TCA GAA GCC AGC GTT CAC
<i>cmyc</i>	TTC TCT TCC TCG TCG CAG AT	TGA AGG CTG GAT TTC CTT TG
<i>Il-17a</i>	GCT CCA GAA GGC CCT CAG A	AGC TTT CCC TCC GCA TTG A
<i>Foxp3</i>	AGG AGC CGC AAG CTA AAA GC	TGC CTT CGT GCC CAC TGT

<sup>1</sup> Panse et al. 2008: *CXCL13* primer sequence

<sup>2</sup> Klaile et al. 2013: *Ceacam5* FWD primer sequence

<sup>3</sup> Bednarek et al. 2018: *Cecam6* primer sequence

For quantification of the gene expression levels, results were analysed by using the CFX manager program. The mRNA levels were normalized to the housekeeping gene and calculated using the  $\Delta C_T$ -method for relative expression or  $\Delta\Delta C_T$ -method for fold control expression.

## **2.4.2 Determination of protein expression level**

### **Isolation of total protein from cells using SDS lysis buffer**

Cells were seeded in a 24-well plate at a density of  $1 \times 10^5$  cells/well. Cells were grown for 48 hours. The medium was removed, and the cells were washed once with PBS. Depending on the cell line used, 80 to 100  $\mu\text{L}$  of SDS lysis buffer were added to each well. Cells were scratched off with the help of a pipette tip and transferred into a 1.5 mL micro tube. Lysed cells were sonicated for five to ten minutes in a water bath to disrupt the cell membrane and were boiled ( $99^\circ\text{C}$ ) for five to ten minutes. Cell lysates were centrifuged five minutes at maximum speed and frozen at  $-20^\circ\text{C}$  or immediately used for western blotting.

### **Isolation of total protein from cells using RIPA-buffer to detect NIK**

Cells were seeded at a density of  $1 \times 10^5$  cells/well in a 24-well plate and grown for 48 hours. For NIK protein levels detection, cells had to be treated with ten  $\mu\text{M}$  of MG132 for four hours (proteasome inhibitor) to prevent proteasomal degradation of NIK. The medium was removed, and the cells were washed once with PBS. Depending on the cell line used, 80 to 100  $\mu\text{L}$  of RIPA buffer containing phosphoStop and protease inhibitors were added per well. Next, the plate was incubated on ice for 15 to 30 minutes until cells started to detach. Cells were scratched off with a pipette tip and transferred into a 1.5 mL micro tube. Samples were sonicated for ten minutes in a water bath and centrifuged for few minutes. The supernatant was transferred into a fresh 1.5 mL micro tube, and 20 to 30  $\mu\text{L}$  of 4x SDS lysis buffer was added. Samples were boiled for ten minutes at  $99^\circ\text{C}$ . Cell lysates were centrifuged for five minutes at maximum speed and frozen at  $-20^\circ\text{C}$  or immediately used for western blotting.

### **Sodium Dodecyl Sulphate Polyacrylamide Gel Electrophoresis (SDS-Page) according to Laemmli**

Proteins were separated according to their molecular weight and charge by sodium dodecyl sulphate (SDS)-polyacrylamide gel electrophoresis (page). SDS is a negatively charged detergent that binds to hydrophobic regions of proteins, causing them to unfold into their native structure/extended polypeptide chains and masks the protein's intrinsic charge (Alberts 2008).  $\beta$ -mercaptoethanol serves as a reducing agent that breaks up any disulfate bonds, and all multimeric proteins can be analysed in their subunits (Alberts 2008). The polyacrylamide gel serves as a

molecular sieve, and large proteins are migrating slower than small proteins (Lodish 2008). The pore size can be adjusted by altering the acrylamide to bisacrylamide ratio to reach the optimal separation of proteins of interest.

Two different gel types were needed for the electrophoresis: a stacking and a separating gel (Table 24 and Table 25). At first, the separating gel (percentage of six or eight) was cast, covered with isopropanol to remove bubbles and achieve a smooth surface. Forty-five minutes later, the separating gel was polymerized. Next, the stacking gel was prepared and added after removing isopropanol with filter paper. The stacking gel was cast, and a comb was inserted. Forty-five minutes later, prepared gels could be used for electrophoresis or were wrapped in wet paper tissue and stored at four°C until usage.

**Table 24: Reagents for the separating gel.**

SEPARATING GEL	percentage of six	percentage of eight
dH <sub>2</sub> O	3.564 mL	3,264 mL
40 percent Acrylamide (37.5:1)	0.9 mL	1.2 mL
1.5 M Tris pH 8.8	1.5 ml	
10 percent APS	30 µL	
TEMED	6 µL	
<b>Total</b>	6 mL	

**Table 25: Reagents for the stacking gel.**

STACKING GEL	VOLUME
dH <sub>2</sub> O	1.288 mL
0.5 M Tris pH 6.5 0.4 percent SDS	0.5 mL
40 percent Acrylamide (37.5:1)	0.2 mL
10 percent APS	10 µL
TEMED	2 µL
<b>Total</b>	2 mL

For protein separation, about six to ten µL of protein lysate was loaded depending on cells or samples used. As molecular standard, six µL of the precision plus protein dual colour standards were loaded. The gel was fixed in a Mini Gel Tank and filled with 1x SDS running buffer for electrophoresis. Samples were loaded, and electrophoresis was started by applying 150 V for one hour or until the separation of protein of interest was achieved.

### Western blotting

After electrophoresis, the proteins were transferred on a nitrocellulose membrane using a semi-dry transfer cell at 90 mA/membrane for 100 minutes in transfer buffer. The successful transfer was examined by staining with reversible Ponceau S solution, which was destained by washing with dH<sub>2</sub>O and TBS-T. The membrane was blocked in five percent (w/v) milk TBS-T for one hour at RT. After

blocking, the membrane was rinsed once in TBS-T and incubated o/n in primary antibody against human or mouse proteins (see Table 26) diluted in five percent BSA in TBS-T. GAPDH was used as a loading control. The next day, the membrane was washed three times ten minutes with TBS-T and incubated for one hour with secondary HRP labelled anti-mouse, or anti-rabbit antibody diluted 1:3000 in five percent (w/v) milk in TBS-T at RT. The membrane was washed six times ten minutes with TBS-T and developed using Pierce ECL Western Blotting substrate (Thermo Scientific) or Clarity™ Western ECL substrate (Bio-Rad). Detection of the membrane was performed using INTAS Science Imaging, and the signal intensities were quantified by densitometry using ImageLab software.

**Table 26: List of antibodies**

PRIMARY ANTIBODY	DILUTION	MOLECULAR WEIGHT	COMPANY
GAPDH (14C10, rabbit Ab)	1:1000	37 kDa	Cell signaling
NIK (rabbit Ab) #ab137671	1:800	120-130 kDa	Abcam
pCagA (rabbit Ab)	1:500	150 kDa	BioGene GmbH
CagA (serum, mouse Ab)	1:3000	150 kDa	provided by Vogelmann
NF-κB2 (rabbit Ab) #3017	1:1000	100 + 52 kDa	Cell signaling
SAB3 Ab anti Ceacam 1/3/5 (rabbit Ab)	2.5 µg/mL	150 + 75 kDa	from B. B. Singer
SECONDARY ANTIBODY	DILUTION	COMPANY	
Anti-Rabbit HRP	1:3000	Promega	
Anti-mouse-HRP	1:3000	Promega	

## 2.5 Assays and Techniques

### 2.5.1 Killing Assay

A killing assay was performed to figure out the appropriate concentration of puromycin necessary for selection of positive clones. Therefore,  $1.5 \times 10^5$  cells were seeded in quadruplets in a 12-well plate. Twenty-four hours later, one well was counted and set as a starting number of cells, and different concentrations (15, 25, 30, 40, 45, 50, 60, 75, 90 µg/mL) of puromycin were added to seeded cells. Every other day, cells were counted until day four, and a growth curve was plotted with counted number of cells.

### 2.5.2 Proliferation Assay

To check for the proliferative capacity, cells were seeded in a 96-well plate (flat bottom). In brief,  $2 \times 10^3$  cells in 100 µL complete growth medium (AGS, NUGC-4, NCI-N87, MKN28, MKN45, MKN7 cells) were seeded and incubated at 37°C and five percent (v/v) CO<sub>2</sub>. Cells were left to attach o/n, and the next day, staurosporine, a proliferation inhibitor, was added to some extra wells and used

as an internal control. The plate was incubated for further 48 hours. The proliferative capacity was evaluated by using the cell counting kit (CCK8) that determines the number of viable cells proportional to the produced formazan. For this purpose, ten  $\mu\text{L}$  of CCK8 solution was added to each well, and each treatment was prepared in quintuplicates. After incubating the plate at  $37^\circ\text{C}$  and five percent (v/v)  $\text{CO}_2$  in a humidified incubator for two hours (AGS, NUGC-4) or three hours (NCI-N87, MKN28, MKN45, MKN7), the absorbance was measured at 570 nm and as reference measurement at 670 nm. The measured values were corrected by subtracting the absorbance of medium-only wells. Then, the mean of each treatment/cell line was calculated and, if possible, normalized to the control.

### 2.5.3 Clonogenicity Assay

To check for their clone formation capacity, cells were seeded at low density. For this purpose,  $1 \times 10^3$  (AGS and NUGC-4) or  $1 \times 10^3$  (NCI-N87) cells were seeded in a 2.5 cm plate. Cells were incubated for two weeks (AGS) or 2.5 weeks (NUGC-4 and NCI-N87) at  $37^\circ\text{C}$  and five percent (v/v)  $\text{CO}_2$ . Next, formed clones were fixated and stained with five percent glutaraldehyde/trypan blue solution for 30 to 60 minutes, washed with tap water, and air-dried. Images were taken by scanning plates, and formed clones were counted manually.

### 2.5.4 Soft agar Assay

Anchorage-independent growth was assessed by performing a soft agar assay. For this purpose, a bottom agar was prepared in appropriate concentration in IMDM/0 percent (v/v) of FCS (IMDM 0) (0.4 percent (v/v) for AGS and NUGC-4; 0.5 percent (v/v) for NCI-N87) and 50  $\mu\text{L}$  of bottom agar was seeded in 96-well plate and solidified at RT. For each treatment, four wells were prepared. Meanwhile, cells were trypsinized, counted, and  $1.5 \times 10^3$  cells (AGS, NUGC-4) or  $2 \times 10^3$  cells (NCI-N87) per well were prepared in 25  $\mu\text{L}$  pre-warmed IMDM supplemented with 20 percent (v/v) of FCS (IMDM 20). 0.2 (v/v) or 0.25 percent (v/v) of top agar was prepared double concentrated (0.4 or 0.5) in IMDM 0 and stored in a thermomixer at  $42^\circ\text{C}$ . 25  $\mu\text{L}$  of top agar were mixed with 25  $\mu\text{L}$  of cell suspension, and 50  $\mu\text{L}$  were plated on bottom agar with pre-warmed tips, avoiding the formation of air bubbles. The agar was solidified at RT. Next, IMDM 10 (IMDM with ten percent (v/v) of FCS) was added as a feeding layer. Empty wells were filled with PBS, and the plate was sealed with parafilm to avoid dehydration. The plate was incubated for one week. On day eight, pictures of formed colonies were taken, and viability/proliferation was measured by adding 40  $\mu\text{L}$  of MTT (five mg/mL) dissolved in autoclaved  $\text{dH}_2\text{O}$ . The plate was incubated for three hours at  $37^\circ\text{C}$ , and absorbance was measured at 570 nm with a plate reader.

## 2.6 *Helicobacter pylori*

### 2.6.1 *H. pylori* strains

Table 27: *H. pylori* strains used and antibiotic resistance for selection.

<i>H. PYLORI</i> STRAINS	ANTIBIOTIC SELECTION	REFERENCE
G27 wild type	WC-Dent	(Xiang et al. 1995)
G27 $\Delta$ hopQ	WC-Dent chlor	(Javaheri et al. 2016)
G27 $\Delta$ cagE	WC-Dent kana	Censini et al. 1996
P12 wild type	WC-Dent	(Haas et al. 1993)
P12 $\Delta$ hopQ	WC-Dent strep	(Königer et al. 2016)
P12 $\Delta$ cagA	WC-Dent chlor	(Backert et al. 2001)
P12 $\Delta$ cagE	WC-Dent chlor	(Shariq et al. 2015)
PMSS1	WC-Dent	(Arnold et al. 2011)

### 2.6.2 *H. pylori* cultivation and propagation

*H. pylori* wild type strains (P12, G27, SS1 or PMSS1) were cultivated on Wilkins-Chalgren (WC) blood agar plates complemented with Dent (OXOID) at 37°C and ten percent (v/v) of CO<sub>2</sub>. P12/G27/SS1 mutant strains (G27 $\Delta$ hopQ, G27 $\Delta$ cagE, G27 $\Delta$ hopQ+hopQ, P12 $\Delta$ hopQ, P12 $\Delta$ cagA, P12 $\Delta$ cagE, and SS1 $\Delta$ hopQ) were grown on WC-Dent blood agar plates supplemented with antibiotics (50 µg/mL kanamycin, 15 µg/mL of chloramphenicol or 50 µg/mL streptomycin; see Table 27) under the same conditions. For splitting, *H. pylori* was collected with an inoculation loop and resuspended in a 1.5 mL tube containing one mL BHI supplemented with ten percent FCS (v/v) (BHI/FCS). 100 µL of bacteria suspension was put on a new WC-Dent blood agar plate and distributed with an L-shaped spreader. *H. pylori* was cultivated for 48 hours before usage.

### 2.6.3 Cell infection experiments

Cells were either seeded in a six-well plate for harvesting RNA (see 2.4.1) or in a 24-well plate for harvesting proteins/ELISA (see 2.4.2) and incubated for 48 hours before infection. Twenty-four hours after seeding, the medium from cells was changed to remove antibiotics. Cells were washed once with PBS, and a medium containing only FCS was added. On the day of infection, one well was counted to estimate the appropriate multiplicity of infection (MOI). The cell media was exchanged to the infection media containing DMEM/FCS supplemented with ten percent (v/v) of BHI/FCS. Bacteria were grown for 48 hours, collected, and resuspended in one mL of BHI/FCS media. The bacterial density was determined by measuring the optical density (OD 600). OD 600 = 1 corresponds to 2 x 10<sup>8</sup> bacteria per mL. To do so, 100 µL of bacterial suspension was mixed with 900 µL of BHI/FCS in a cuvette, as blank BHI/FCS only was used. The appropriate MOI (10, 20, or 50) was

calculated, bacteria were added to the cells, and plates were incubated for indicated periods (three, six, or eight hours). After incubation, the supernatant was collected for ELISA, and RNA or proteins were isolated for further expression analysis.

#### **2.6.4 Enzyme-linked immunosorbent Assay**

An enzyme-linked immunosorbent assay (ELISA) was conducted to determine cytokine secretion by gastric epithelial cells after *H. pylori* infection. A Ready-Set Go ELISA Kit to detect human IL-8 was used according to the manufacturer's instruction. Briefly, a 96-well flat-bottom plate was coated with a capture antibody o/n at four°C. The next day, the plate was washed with washing buffer (PBS + 0.05 percent (v/v) Tween20) and blocked for one hour at RT. Samples (supernatant: MKN45 1:40, NUGC-4 1:20, SNU1 1:1) and standard were diluted, added, and incubated o/n at four°C. Next, plates were washed and incubated with a biotin-conjugated detection antibody for one hour at RT. Subsequently, an avidin-coupled HRP (horse radish peroxidase) antibody was added for 30 minutes. The plates were washed and incubated with TMB (tetramethylbenzidine) substrate. The reaction was stopped by adding one M H<sub>3</sub>PO<sub>4</sub> and absorbance was measured at 450 nm. The cytokine levels were calculated by using a standard curve with known concentration.

#### **2.6.5 *H. pylori* binding assay by flow cytometry**

*H. pylori* was grown on WC-Dent blood agar plates for 48 hours, the optical density was measured and adjusted to  $2 \times 10^8$  bacteria in one mL BHI/FCS media and stained for 30 minutes with ten  $\mu\text{M}$  carboxyfluorescein succinimidyl ester (CFSE, eBioscience). Next, labelled bacteria were washed twice with PBS, counted again, and added at an MOI of 10 or 20 to  $1 \times 10^5$  cells which were previously seeded in a 96-well V bottom plate. After 30 minutes of incubation under constant shaking, the supernatant was discarded, and cells were washed with PBS four times. After fixing cells with 0.5 percent (v/v) PFA/PBS, fluorescent intensity of the cells was acquired on a CytoFLEX S flow cytometer (Beckman Coulter). Binding was evaluated after pre-gating on single cells, based on a fluorescent signal using FlowJo software (v. 10.7.2). Percentage of binding indicates whether a gastric epithelial cell was bound by a CFSE labelled bacteria. If every cell was bound by a labelled bacterium, this would represent 100 percent of binding. As a negative control, cells without labelled bacteria were used.

### **2.7 Generation of a novel ATP4b-LT<sup>TG</sup> mouse model**

We generated a new transgenic mouse model to investigate the impact of stomach-specific lymphotoxin (LT) expression on gastric carcinogenesis in vivo. For this purpose, a plasmid construct

was generated (see section 2.7.1) and introduced in oocytes of C57BL/6 mice via pronuclear injections (PNI) performed in-house by Karin Mink. Injected eggs were then transferred to pseudo pregnant C57BL/6 female mice. Born offspring were screened by PCR using screening primer 1-3 (Table 28) as described in section 2.7.2. We generated one ATP4b-LT<sup>TG</sup> (LT $\alpha$  $\beta$ <sup>TG</sup>) founder line.

### 2.7.1 Generation of plasmid construct and mouse line

For generating the DNA construct of our new mouse model, the pEX-K4-plasmid substituted with an ATP4 $\beta$  promoter, and a minigene was used. This construct was produced by Eurofins Genomics. The ATP4 $\beta$  promoter ensures a stomach-specific expression of our construct; in more detail, it will be expressed by parietal cells, the acid-producing cells of the stomach (Lorenz and Gordon 1993; Li et al. 1995). A small exon-intron sequence after the promoter is used to increase the expression levels of the construct, as it seems to have positive effects such as mRNA stabilization and efficient translocation of mRNA to the cytoplasm (Haruyama et al. 2009). Moreover, the construct contains a BFP fluorophore bound to H<sub>2</sub>B to stain the nucleus of cells positive for the construct.



Figure 9: DNA construct scheme of transgenic mouse model

LT $\alpha$ -T2A-LT $\beta$ , H<sub>2</sub>B-BFP, and bovine growth hormone (BGH)-polyA were amplified from single plasmids using primers with overlapping ends to adjacent regions of the end-construct to perform Gibson assembly (Gibson et al. 2009). The different parts of the construct are fused by 2A sequences, ensuring that the proteins are expressed separately and in equal amounts (Ryan et al. 1991; Szymczak and Vignali 2005). The pEX-K4 vector was linearized by *Xba*I digestion. Next, the vector and single inserts with overlapping ends were cleaned up from an agarose gel with Promega wizard SV gel & PCR clean-up kit and incubated at 50°C for one hour with Gibson assembly master mix (Figure 10).

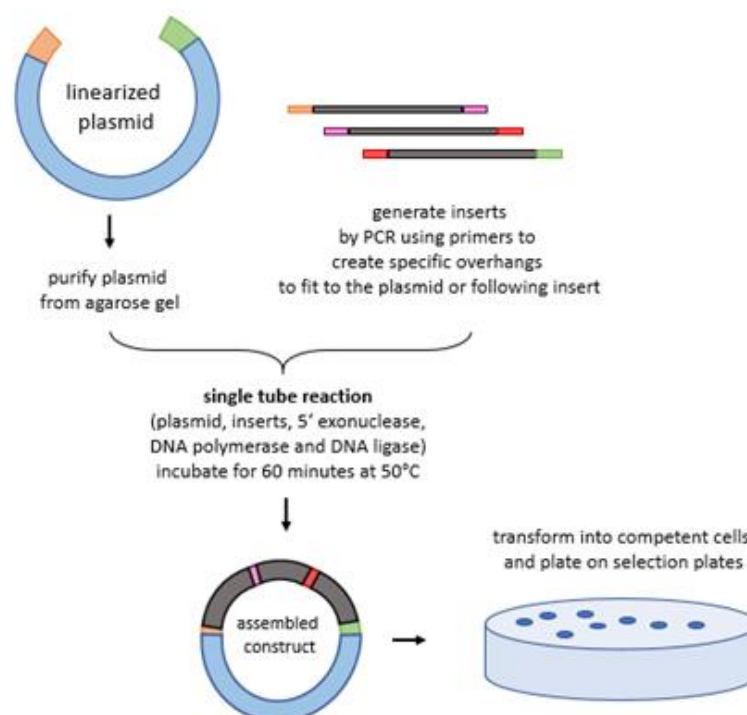


**Figure 10: Workflow of Gibson Assembly.**

Linearize and purify the plasmid. Meanwhile, used inserts are amplified by PCR using specific primers to generate overhangs that fit adjacent regions of the end construct. A single tube reaction is performed to create the assembled construct. The construct is transformed into competent cells and plated on selection plates before picking clones for screening.

Transformation of plasmid was performed in Stab13 *E. coli* as described in section 2.8.1. Single colonies were picked and screened for correct/complete insertion by PCR using specific screening primers (Table 28).

**Table 28: List of screening primers for DNA construct.**

PRIMER	FORWARD	REVERSE	PRODUCT SIZE
<b>Screening 1 (565+566)</b>	CAA GCT TGA GGT GTG GCA GG	CCT CAA GAG GTG GAG ACG G	182 bp
<b>Screening 2 (567+568)</b>	ACA TCA GTC ACC CCG ACA TG	CAT GGC CTT GGA CGA AAT GC	323 bp
<b>Screening 3 (569+570)</b>	GGA TCA CTC TCG GCA TGG AC	TCC GGC TCG TAT GTT GTG TG	334 bp

The correct clone was amplified using a midiprep kit described in section 2.8.3 and sent for sequencing to exclude any point mutations in the end construct. The DNA construct was cut out from the vector backbone by digesting with restriction enzyme *ApaI* (#R0507, NEB) and *PciI* (#R0655, NEB). The linearized and cleaned-up DNA construct was injected into the pronuclei of a fertilized egg of a C57BL/6 mouse, which was implanted into a pseudo pregnant C57BL/6 female mouse. Thereby, the DNA construct was integrated randomly into the mouse genome.

## 2.7.2 Genotyping of mice

From newborn mice, DNA was collected from ear punching. Ear punches were incubated o/n or for three hours in 250  $\mu$ L of tail lysis buffer supplemented with seven  $\mu$ L proteinase K at 56°C. Next, digested ear punches were centrifuged for three minutes at full speed to remove hairs. The supernatant was transferred into a fresh 1.5 mL micro tube, and DNA was precipitated by isopropanol-ethanol clean-up. The pellet was dried for about 30 minutes to one hour to remove EtOH and resuspended in 150  $\mu$ L of nuclease-free water. For genotyping, 1.5  $\mu$ L of isolated DNA was added to the PCR master mix (Table 29) using genotyping primers (Table 30). The founder line was tested for all inserts by using all three screening primers (Table 28).

Table 29: Master mix for genotyping PCR.

MASTERMIX GENOTYPING PCR	VOLUME [ $\mu$ L]
Primer mix (fwd. + rev.)	1
nuclease-free water	10
GreenTaq Master mix	12.5
<b>Total</b>	<b>23.5</b>

Table 30: Primer sequences for genotyping PCR.

PRIMER NAME	SEQUENCE	PRODUCT SIZE
577 fwd. (vector backbone-polyA)	GCC ATG CCC GAA GGC TAC	693 bp
576 rev. (middle H <sub>2</sub> B-BFP)	AGT CCC CAG CAT GCC TGC	

Table 31: Thermal cycle program for genotyping.

STAGES	TEMP [°C]	TIME [mm:ss]	
Enzyme activation	95	02:00	
Denaturation	95	00:45	30 x
Annealing and elongation	58	00:30	
Elongation	72	1:30	
Final Hold	12	$\infty$	

A sample without DNA (only master mix with water) served as a negative control. After establishing the genotyping PCR, a previously positive tested mouse sample served as a positive control. 12  $\mu$ L of each PCR sample was loaded on a one percent agarose gel. The estimated product size for a positive transgenic mouse was 182 bp by using screening 1 primers, 323 bp by screening 2 primers, and 334 bp by using screening3 primers. For the genotyping PCR, the estimated product size of a positive transgenic mouse was around 700 bp.

## 2.7.3 Mouse infection experiments

### 2.7.3.1 Mouse strains and housing

C57BL/6 (in-house breed or purchased from Envigo) or LT $\alpha$  $\beta$ <sup>TG</sup> (in-house generated) C57BL/6 or

---

C57BL/6<sup>-hCEACAM1+/mouse CEACAM1-</sup> mice at the age of six to eight weeks were co-housed in individually ventilated cages (Tecniplast) under specific pathogen-free conditions. Mice were fed standard rodent chow (Envigo) and water ad libitum.

### **2.7.3.2 Experimental infection with *H. pylori* PMSS1**

Mice were orogastrically inoculated twice with  $2 \times 10^8$  bacteria diluted in 200  $\mu$ L BHI/FCS suspension and infected for 24 and 48 weeks to investigate the combined impact of specific LT expression in the stomach with *H. pylori* infection on GC.

### **2.7.3.3 Analysis of infected mice**

After 24 or 48 weeks of infection, mice were sacrificed, and organs (stomach, spleen, liver, kidney, intestine, and colon) were harvested for further experimental analysis.

#### **2.7.3.3.1 Harvesting of organs**

The foregut was removed, and the stomach was opened following the longer curvature, washed with PBS, and segmented longitudinally in several pieces for colony-forming unit determination (CFU), DNA isolation, histology, RNA extraction, and cryo sections. RNA/DNA samples were put in a 1.5 mL safe lock tube, snap-frozen in liquid nitrogen, and stored at  $-80^{\circ}\text{C}$  until usage. Stomach tissue for histology was stretched over a wood piece, placed in a pink histology cassette, and put in formaldehyde for at least 48 hours before being processed in the pathology department of the Klinikum Rechts der Isar for embedding in paraffin. The stomach tissue was placed in OCT media for cryosections, slowly frozen in liquid nitrogen, and stored at  $-80^{\circ}\text{C}$ . Other organs were collected for RNA and histology only.

#### **2.7.3.3.2 Determination of colony-forming units after *H. pylori* infection**

To determine that the mice were successfully infected, a stomach piece was weighted and placed in one mL of BHI/FCS media. Next, the tissue was homogenized, diluted at 1:10, 1:100, and 1:1000 in BHI/FCS, and 100  $\mu$ L of each dilution was plated on WC-DENT special blood agar plates to select specifically for *H. pylori*. The plates were kept at microaerophilic conditions at  $37^{\circ}\text{C}$  and ten percent (v/v)  $\text{CO}_2$  for five to six days. Finally, the number of CFUs was counted and calculated per mg stomach tissue used.

## 2.8 Molecular Cloning Techniques

### 2.8.1 Transformation of plasmid DNA in competent cells

To amplify plasmid DNA, a transformation in *E. coli* was performed. Therefore, an aliquot of competent cells (*E. coli* DH5 $\alpha$  or Stab13) was thawed on ice for three to five minutes. 2-5  $\mu$ L of plasmid DNA was added to competent cells by pipetting up and down and incubated on ice for 20 minutes. Next, *E. coli* was heat shocked by incubating at 42 °C for 42 seconds. Afterward, 1 mL of pre-warmed LB media was added and incubated at 37°C for one hour on a shaking thermomixer (300 rpm). 100  $\mu$ L of bacteria/plasmid DNA mixture was spread on pre-warmed LB-selection plates (containing antibiotics for selection). Plates were incubated overnight at 37 C. On the other day, a colony was picked and resuspended in nuclease-free water for a screening PCR or put in LB medium containing antibiotics for a bacterial overnight culture see 2.8.3 (miniprep, midiprep). LB plates, sealed with parafilm, could be stored at 4°C until further processing.

### 2.8.2 Bacterial o/n culture

For the bacterial o/n culture, a colony of a transformation (see 2.8.1) was picked and resuspended in 5 mL LB medium supplemented with an antibiotic to select for the bacteria that had taken up the plasmid. The culture was incubated o/n at 37°C on a shaker (200 rpm) for no longer than sixteen hours. The following day, plasmid DNA was isolated from a miniprep (see 2.8.3), or to obtain a higher amount of plasmid DNA, a midiprep was set up. To do so, one mL of the bacteria/plasmid culture is added to 100 mL of LB medium supplemented with antibiotics. The culture was incubated o/n at 37°C on a shaker (200 rpm), and the next day, a midiprep clean-up was performed (see section 2.8.3).

### 2.8.3 Plasmid Miniprep and Midiprep System

To purify plasmid DNA from 5 mL bacterial o/n culture, a miniprep kit or for isolation of high amount of plasmid DNA (100 mL bacterial o/n culture) a midiprep kit according to manufacturer's instructions was used.

Both systems allow high-quality plasmid DNA isolation from bacterial cultures. In brief, the bacterial culture was centrifuged, and the pellet was lysed by adding cell lysis buffer. Next, lysis was stopped by adding neutralization solution and mixing it by inverting the tube. After lysis, the suspension was transferred on a silica-membrane column and cleared by a few washing steps, including endotoxin removal to remove contaminations (proteins, RNA, or endotoxins). Plasmid

DNA was eluted by adding 30  $\mu$ L (miniprep) or 500  $\mu$ L (midiprep) of nuclease-free water or elution buffer. The concentration of the isolated plasmid DNA was determined with a spectrophotometer, nanodrop, and plasmid DNA was stored at  $-20^{\circ}\text{C}$  for the long term or at  $4^{\circ}\text{C}$  when used immediately.

## 2.9 Gastric organoids

### 2.9.1 Preparation and cultivation of gastric organoids

#### Murine gastric organoids

For organoid preparation, the whole stomach without the foregut was used and processed according to the protocol described by Sina Bartfeld (Bartfeld and Clevers 2015). Briefly, the tissue was cut into one to two  $\text{mm}^2$  cubes and transferred into a 50 mL tube containing ten mL of chelation buffer. Pieces were washed by pipetting ten times up and down using a 25 mL pre-wetted pipette (using chelation buffer). It is crucial to pre-wet the pipette before use since stomach tissues are very sticky and can clot the pipette or stick to the plastic wall of the pipette. When the pieces settled, the supernatant was removed, and fresh ten mL of chelation buffer were added. Stomach pieces were washed at least up to ten times until the supernatant was clear. After washing, the supernatant was removed, the pieces were resuspended in 20 mL chelation buffer supplemented with ten mM EDTA and incubated for 30 minutes on a rolling shaker at  $4^{\circ}\text{C}$ . Next, the pieces were pipetted up and down ten times to disintegrate the tissue structure. Once the pieces settled, the supernatant was removed until only one to two mL were left. The stomach pieces were poured into a ten cm petri dish, placed in the centre, and covered with a glass slide. By putting pressure on the glass slide, the glands were released from the tissue. Glands were collected with five mL of basal medium (Table 32) and transferred into a 15 mL tube. The tissue pieces settled, and the supernatant containing isolated glands was transferred into a fresh 15 mL tube and centrifuged for five minutes at 200 G at  $4^{\circ}\text{C}$  to form a pellet. The pellet was resuspended in two mL basal medium, and the number of glands in 20  $\mu$ L of suspension was determined under the microscope. An appropriate number of glands for seeding (about 400 glands/well) was transferred into a fresh 15 mL tube, centrifuged (200 G, five minutes at  $4^{\circ}\text{C}$ ), and the pellet was resuspended carefully in matrigel avoiding bubbles. 40  $\mu$ L of the matrigel-gland mixture was placed per well in a pre-warmed 24-well plate and kept for ten minutes at  $37^{\circ}\text{C}$  to allow the matrigel to polymerize. Next, 400  $\mu$ L organoid medium (Table 33) supplemented with ten  $\mu$ M RHOKi were added to matrigel droplets, and the medium was changed every two to three days. Organoids were split every six to seven days in a ratio of 1:2-4 or higher, depending on their growth. To do so, the medium was removed, ice-cold PBS was added to matrigel

droplets and pipetted up and down to break up the matrigel. The organoid-PBS mixture was collected in a 15 mL tube. This washing step was repeated several times until the well was clean and no matrigel or organoids were visible in the plate anymore. To break up organoids, a fire-narrowed glass pipette (pre-wet with FCS or PBS) was used, and organoids were vigorously pipetted up and down (ten times or more). Next, organoids were centrifuged (400 G, five minutes at four°C), the supernatant was removed, and the pellet was resuspended in an appropriate amount of matrigel, distributed in a pre-warmed 24-well plate, polymerized for ten minutes at 37°C and covered with organoid medium supplemented with ten  $\mu$ M RHOKi.

### Human gastric organoids

For human gastric organoid preparation, the same protocol (Bartfeld and Clevers 2015) was applied, and organoids were isolated from stomach biopsies with only a few modifications:

- After washing the human stomach tissue with chelation buffer, the supernatant was removed. The pieces were resuspended in ten mL chelation buffer supplemented with ten mM EDTA and incubated for ten minutes on a rolling shaker at RT.
- Organoids were split, depending on their growth, 10-14 days after seeding in a ratio of 1:2-3.

### Cultivation of gastric organoids with CERO 3D incubator

Organoids cultivated in the CERO 3D incubator (OLS) were processed as described before (see section 2.9.1). The organoids were incubated in Levi tubes containing either complete organoid medium or reduced organoid medium supplemented with three percent matrigel, 1:30 cero solution, and ten  $\mu$ M RHOKi. For splitting, organoids were transferred in a 15 mL tube by a pre-wet 20 mL glass pipette, centrifuged (400 G, five minutes, four°C), and the supernatant was removed as much as possible. Organoids were resuspended in cold PBS and pipetted up and down vigorously by a fire-narrowed glass pipette (pre-wet with FCS). The organoids were centrifuged (400 G, five minutes, four°C), the organoid pellet was taken up into new media and placed into Levi tube for further cultivation. The cultivation program was 80 rpm, one second left and right rotation continuously.

**Table 32: Components of the basal medium.**

COMPONENTS	FINAL VOLUME [mL]
Adv. DMEM/F12	97
Pen/Strep	1
Glutamax (100x)	1
Hepes (1M)	1
<b>Total</b>	<b>100</b>

**Table 33: Components of the complete organoid medium.**

COMPONENTS	STOCK CONC.	FINAL CONCENTRATION/VOLUME	
Advanced DMEM/F12	NA	NA	x
Pen/Strep	100 x	1 percent	1 mL
L-WRN medium (filtered; 22 µm filter)	NA	50 percent	50 mL
B27 supplement	50 x	1x	2 mL
N2 supplement	100 x	1x	1 mL
Hepes	1 M	10 mM	1 mL
Glutamax	100 x	1 percent	1 mL
N-acetyl – L – cysteine	500 mM	1 mM	200 µL
Amphotericin B	250 µg/mL		320 µL
Nicotinamide	1 M	10 mM	1 mL
Gastrin	100 µM	1 nM [h]/10 nM [m]	5/50 µL
TGFβ inhibitor	25 mM	2 µM [h]/0.5 mM [m]	8 µL/2 mL
FGF-10	100 µg/mL	200 ng/mL [h]/100 ng/mL [m]	200/100 µL
EGF	500 µg/mL	50 ng/mL	10 µL
p38 inhibitor	30 mM	10 µM	33,4 µL
Total			100 mL

h = human; m = mouse

## 2.9.2 Stimulation of human gastric organoids with ligands of the non-canonical NF-κB pathway

To explore whether the activation of the non-canonical NF-κB pathway impacts the growth or proliferation of organoids, freshly isolated human gastric stomach glands were stimulated with ligands specifically activating this pathway. Every second day, the organoid medium, supplemented with LIGHT or LTα<sub>1</sub>β<sub>2</sub>, was refreshed. The growth of organoids was monitored by taking images one, two, three, and six days after seeding. The organoid size of stimulated/treated organoids was compared to unstimulated organoids.

## 2.9.3 Generation of a two-dimensional culture of organoids

To infect organoids, the luminal side of the organoid must be approached during *H. pylori* infection, and therefore, two-dimensional (2D) cultures are generated using gastric organoids. Initially, organoids had to be generated, and hence, glands were isolated from stomachs of seven to eleven-week-old C57BL/6 or C57BL/6<sup>-hCEACAM1+/mouse CEACAM1-</sup> mice as described in section 2.9.1. About 25.000 glands were cultivated in 14 mL organoid growth medium for three to four days in the CERO 3D cell incubator. To perform infection experiments, organoids had to be broken up and grown in a 2D culture. Therefore, plates were precoated with matrigel, diluted at 1:15 with cold advanced DMEM/F12. For protein expression analysis, 24-well plates were precoated using 300 µL

matrigel/media mixture per well. For RNA expression analysis, 12-well plates were precoated using 600  $\mu\text{L}$  of matrigel/media mixture per well. Next, plates were incubated for at least 30 minutes at 37°C. Before seeding, the excess of matrigel/media mixture had to be removed to avoid the growth of organoids out of single cells. After the cultivation of organoids in CERO, organoids/media mixture was collected in two 15 mL tubes and filled with cold PBS to dilute the viscous solution. Next, the suspension was centrifuged, and the supernatant was removed. The pellet was incubated in 500  $\mu\text{L}$  recovery solution to remove the excess of matrigel and incubated for 20 minutes on ice. Next, the mixture was centrifuged, and again the supernatant was removed. The pellet was incubated with 500  $\mu\text{L}$  trypLE trypsin for three to five minutes at 37°C. After incubation, FCS was added to stop the enzymatic activity of trypsin and to further disrupt the organoids into single cells, a fire-narrowed glass pipette was used for pipetting the solution vigorously up and down. Cell number was estimated using a counting chamber, and in a 24-well plate,  $1\text{-}2 \times 10^5$  cells were seeded. In a 12-well plate, about  $4\text{-}5.5 \times 10^5$  cells were seeded per well. An appropriate cell number was resuspended in the appropriate volume of media (24-well: 400  $\mu\text{L}$ ; 12-well: 700  $\mu\text{L}$ ). The 2D culture was grown for five to six days to allow the growth of a monolayer. On the day of infection, one well was counted to estimate the number of cells/well. Cells were infected at an MOI of 20 for 20 hours. After infection, the supernatant was removed, cells were washed off by applying cold PBS (two to three times repeated) and collected in a 1.5 mL tube. The tube was centrifuged, and the pellet was resuspended in lysis puffer and processed as described in section 2.4.1 (for mRNA) or 2.4.2 (for protein).

## **2.10 Immunohistochemistry**

Tissue samples were fixated with 3.7 percent of paraformaldehyde for 48 hours at RT, changed to PBS afterward until embedding. Stomach tissue was placed on a piece of wood before fixation to ensure that the tissue will keep its shape. The paraffin inclusion was performed at the Pathology department in the Klinikum Rechts der Isar. Paraffin blocks were cut using the microtome into 3.5  $\mu\text{m}$  thick sections, and sections were dried for 24-48 hours until staining was performed.

Tissue sections were put in a stainless-steel staining tray and incubated for about 20 to 30 minutes at 60°C in a hybridization oven until the paraffin was melted. Next, rehydration was performed by incubated the slides three times for ten minutes in xylene, two times for ten minutes in absolute EtOH, once for five minutes in 90 percent EtOH, once for five minutes in 70 percent EtOH, once five minutes in 50 percent EtOH and finally placed in  $\text{dH}_2\text{O}$ . Antigen retrieval was performed by boiling the slides for ten minutes in 0.01 M sodium citrate buffer (pH 6). Afterward, the pressure cooker was cooled down for 30 minutes without opening the lid. Next, the slides were

immersed in dH<sub>2</sub>O and placed onto cover plates (Thermo scientific) facing the flat part with the tissue section and put into the racks. Correct assembly was tested by washing with distilled water. Subsequently, endogenous peroxidase activity was blocked by applying 150 µL of three percent H<sub>2</sub>O<sub>2</sub> for ten minutes and washed once with distilled water and once with 1x TBS/0.01 percent of Tween-20. Then, slides were blocked with 150 µL of five percent goat serum (#ab156046, Abcam) diluted in washing buffer (TBS/0.1 percent of Tween-20) for one hour at RT. After blocking, the slides were incubated with 130 µL of primary antibody diluted in SignalStain Antibody diluent at four°C o/n. Primary antibodies were diluted following the manufacture's instructions (Table 34).

**Table 34: List of primary antibodies for IHC**

PRIMARY ANTIBODY	DILUTION	COMPANY
<b>Ki67 (D3B5) #9129</b>	1:400	Cell signaling
<b>CD3 (SP7) #RM-9107-S1</b>	1:150/1:500	Thermo Fisher/NeoMarkers Lab Vision Corp
<b>B220 (RA3-6B2) #553084</b>	1:200/1:3000	BD Biosciences/BD Bioscience
<b>F4/80</b>	1:50/1:250	BMA/BMA (BM8)
<b>NF-κB2 (p100/p52)</b>	1:250	LS Bio

The next day, the slides were washed by rinsing five times with washing buffer (TBS-T). Slides were incubated with 150 µL of HRP-conjugated secondary antibody anti-rabbit (1:200) or anti-mouse (1:100) antibody diluted in SignalStain antibody diluent and incubated for one hour at RT. Next, the slides were washed five times with washing buffer (TBS-T). Meanwhile, hematoxylin was filtered (folded filter, 185 mm, #FF18, Hartenstein). The slides were developed by mixing one drop of chromogen per mL of substrate (SignalStain DAB substrate Kit, #8059, Cell Signaling), incubated for seven minutes, and washed off immediately with distilled water. The slides were removed from the rack and placed on a stainless-steel staining tray. Next, counterstaining was performed using hematoxylin by immersing the slides for three minutes and washed with tap water. The slides were dehydrated by incubating once for five minutes in 50 percent EtOH, once for five minutes in 70 percent EtOH, once for five minutes in 90 percent EtOH, two times for five minutes in absolute EtOH each, three times for ten minutes in xylene. Finally, the slides were mounted with DPX Mountant mounting media (Sigma Aldrich). Mounted slides were dried under a fume hood for at least 24 hours or until scanning with microscopy was performed. Slides were scanned (Zeiss microscopy, 20x magnification), and five high power fields (HPF) of the stained tissue were assessed at a 20 fold magnification.

## 2.11 Hematoxylin-eosin staining

For hematoxylin-eosin staining, the protocol as described in section 2.10 was used until rehydration. After placing the slides in dH<sub>2</sub>O, they were first stained with hematoxylin for six minutes

and washed with tap water, and then stained with eosin for six minutes and washed with tap water again. Slides were dehydrated by incubating as follows: once for one minute in 70 percent EtOH, once for one minute in 90 percent EtOH, two times for five minutes in absolute EtOH each, and finally three times five minutes in xylene. The slides were mounted with DPX Mountant (Sigma Aldrich) and dried under a fume hood for at least 24 hours or until scanning with microscopy was performed (see section 2.10).

## 2.12 Immunofluorescence

To assess the binding of *H. pylori* to the gastric epithelium,  $1 \times 10^5$  MKN45 or NUGC-4 cells were seeded on a coverslip in a 12-well plate and grown for 24 hours. The coverslips were soaked in ethanol for ten minutes and washed twice with PBS before usage. CFSE-labelled wild type *H. pylori* or isogenic mutant strains were added at an MOI of 10 and co-incubated with the cells for 3 hours at 37°C. Infected cells were fixated with methanol/acetone for 30 minutes, washed with PBS, stained with phalloidin (#ab176759, 1:1000, phalloidin-iFluor<sup>647</sup>, Abcam) for 60 minutes, and washed three times with PBS to remove excess phalloidin conjugate. The slides were mounted with Vector shield mounting containing DAPI stain (Vector Labs) and sealed with a glass coverslip. Next, confocal microscopy was done (SP5 confocal microscope, Leica).

## 2.13 Statistics

Statistical significances were calculated using GraphPad 9.0. Data are shown as mean  $\pm$  standard deviation (SD). All experiments were performed at least in triplicates. A one-way analysis of variance (ANOVA) with Dunnett's or Bonferroni's correction for multiple comparisons was applied for normally distributed data. Mann–Whitney test or ANOVA Kruskal–Wallis with Dunn's multiple comparisons test were used for not normally distributed data. Statistical significance was defined as: \*  $p \leq 0.05$ , \*\*  $p \leq 0.01$ , \*\*\*  $p \leq 0.001$ , \*\*\*\*  $p \leq 0.0001$

## 3 Results

### 3.1 HopQ–CEACAM interaction influences the activation of the non-canonical NF- $\kappa$ B pathway

Previous work had shown that a functional type IV secretion system (T4SS) was essential to activate the non-canonical NF- $\kappa$ B pathway via LT $\beta$ R signaling (Mejías-Luque et al. 2017). In more detail, this activation is occurring in a secondary loop that initially induces the canonical NF- $\kappa$ B pathway stimulating the expression of ligands which then activate non-canonical NF- $\kappa$ B signaling (Mejías-Luque et al. 2017). Different virulence factors of *H. pylori* were tested for the involvement in the activation of this pathway, but no differences were observed (Mejías-Luque et al. 2017). However, experiments with HopQ-deficient bacteria which are unable to translocate CagA or having a defect in T4SS functionality were not tested. To do so, GC cells were infected with *H. pylori* wild type or isogenic mutant strains at an MOI of 10/20/50 for eight hours. To investigate the activation of the pathway, the processing of p100 to p52 was evaluated by western blot. Increased processing after wild type *H. pylori* infection was observed, as expected. In contrast, reduced activation of the non-canonical NF- $\kappa$ B pathway was seen when HopQ or CagE were missing (Figure 11 a and b). Bacteria lacking CagA had no impact on the processing of p100 to p52 (Figure 11 a and b), as already published previously (Mejías-Luque et al. 2017). As a control for successful infection, IL-8 secretion was analysed by ELISA. Lack of HopQ or CagE led to a significantly reduced IL-8 secretion (Figure 11 c and d). To analyse the activation of the canonical NF- $\kappa$ B pathway, *A20* mRNA levels were evaluated by qPCR. *A20* mRNA was induced upon infection. CagE deficient *H. pylori* strains induced *A20* expression levels to a lesser extent. Bacteria strains lacking HopQ seemed to induce lower *A20* mRNA expression levels at an MOI of 10 (Figure 11e). At a higher MOI (20 or 50), *A20* mRNA expression levels were not influenced by the lack of HopQ (Figure 11f). Next, the expression of ligands (LT $\beta$ ) activating the non-canonical NF- $\kappa$ B pathway was examined by qPCR. *LT $\beta$*  mRNA expression levels were highly increased upon *H. pylori* infection. In contrast, lower levels were detected when HopQ was absent, which was independent of the MOI used (Figure 11 g and h). Furthermore, CagE mutant *H. pylori* strains induced significantly lower *LT $\beta$*  mRNA expression levels upon infection, confirming previously published data (Mejías-Luque et al. 2017) (Figure 11 g and h). Bacteria lacking CagA had no impact on IL-8 secretion, *A20* or *LT $\beta$*  mRNA expression levels independent of applied MOI (Figure 11).

Similar results were detected when using different *H. pylori* strains, indicating that these effects

are strain-independent. These observations suggest that HopQ is involved in activating the non-canonical NF- $\kappa$ B pathway by modulating the *LT $\beta$*  expression.

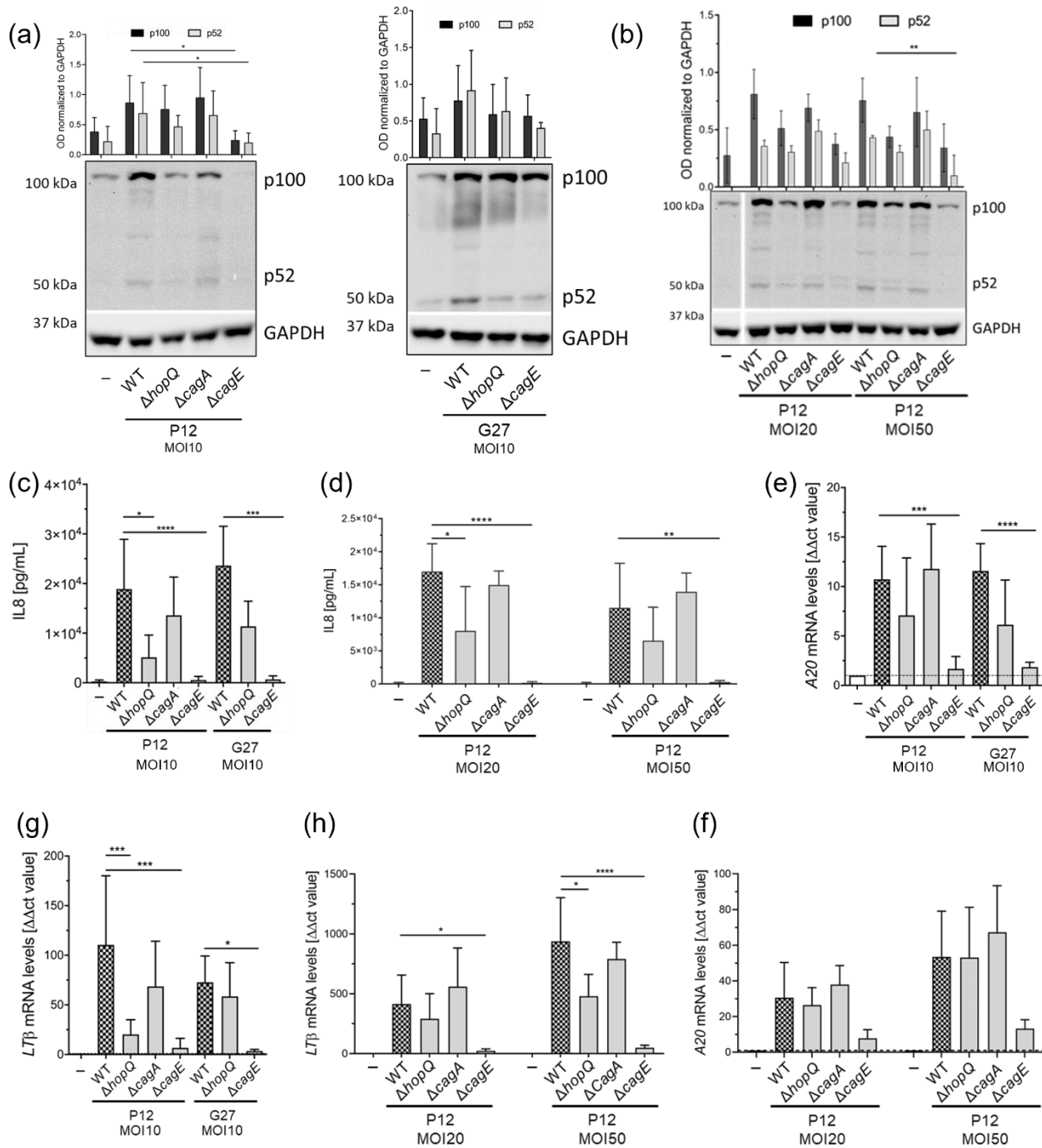


**Figure 11: Activation of the non-canonical NF- $\kappa$ B pathway upon *H. pylori* infection.**

MKN45 cells were infected with *H. pylori* G27/P12 wild type strains or isogenic mutant strains for HopQ, CagA, or CagE at an MOI of 10/20/50 for eight hours. (a, b) p100 to p52 processing was checked by western blot. (c, d) IL-8 secretion was checked by ELISA. (e, f) A20 mRNA and (g, h) *LT $\beta$*  expression levels were analysed by qPCR. As a housekeeping gene, *GAPDH* was used. All values were normalized to *GAPDH* and the negative control/uninfected cells ( $\Delta\Delta$ ct value). All graphs show mean  $\pm$  SD of at least three independent experiments. One-way ANOVA with Bonferroni's multiple comparisons test. \*  $p \leq 0.05$ , \*\*  $p \leq 0.01$ , \*\*\*  $p \leq 0.001$ , \*\*\*\*  $p \leq 0.0001$

To further substantiate the involvement of HopQ in the activation of the non-canonical NF- $\kappa$ B pathway, the mRNA expression levels of NF- $\kappa$ B target genes upon *H. pylori* infection were analysed. Bacteria strains lacking HopQ tended to induce lower *CXCL10* mRNA expression levels than wild type

bacteria at an MOI of 10. At a higher MOI, HopQ deficient *H. pylori* strains had no impact on the *CXCL10* mRNA expression levels (Figure 12b). CagE mutant *H. pylori* strains led to lower expression of *CXCL10* independent of the applied MOI (Figure 12 a and b). *CCL2* mRNA expression levels were increased upon infection with wild type *H. pylori* strains. The absence of HopQ led to a significantly lower *CCL2* mRNA expression at an MOI of 10 (Figure 12c). At a higher MOI, HopQ-deficient *H. pylori* strains induced similar *CCL2* mRNA expression levels compared to wild type bacteria (Figure 12d). Lack of CagA had no impact at all on the expression levels of *CXCL10* or *CCL2* (Figure 12).

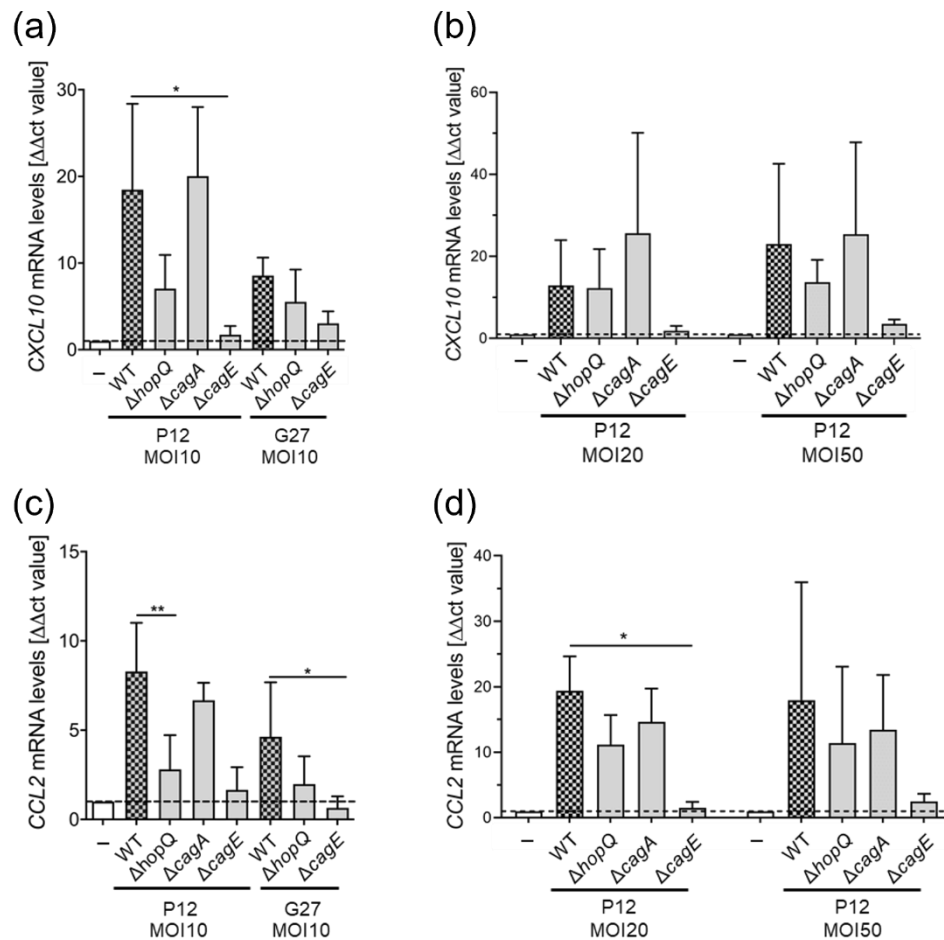


**Figure 12: Chemokine expression upon *H. pylori* infection.**

MKN45 cells were infected with *H. pylori* G27/P12 wild type strains or isogenic mutant strains for HopQ, CagA, or CagE at an MOI of 10/20/50 for eight hours. (a, b) *CXCL10* and (c, d) *CCL2* mRNA expression levels were analysed by qPCR. As a housekeeping gene, *GAPDH* was used. All values were normalized to *GAPDH* and the negative control/uninfected cells ( $\Delta\Delta$ ct value). All graphs show mean  $\pm$  SD of at least three independent experiments. Ordinary one-way ANOVA with Bonferroni's multiple comparisons test. \*  $p \leq 0.05$ , \*\*  $p \leq 0.01$

Previous data had shown that a functional T4SS was needed to activate the non-canonical NF- $\kappa$ B pathway and translocate CagA into the host cell (Mejías-Luque et al. 2017; Fischer 2011). CagA is phosphorylated in the host cell and was identified as the first bacterial oncogene, as it utilises numerous cellular processes linked to carcinogenesis (Fischer 2011; Takahashi-Kanemitsu et al. 2020). We tested whether the lack of HopQ influences the translocation of CagA into the host cell

by western blot (Figure 13). Indeed, we could observe that lack of HopQ drastically impaired CagA translocation as seen by reduced pCagA levels compared to wild type bacteria (Figure 13). This observation is in line with a study by Javaheri et al. (Javaheri et al. 2016). Lack of CagE, which is essential for T4SS formation, also decreased CagA translocation significantly (Figure 13). These findings were MOI and strain independent (Figure 13).

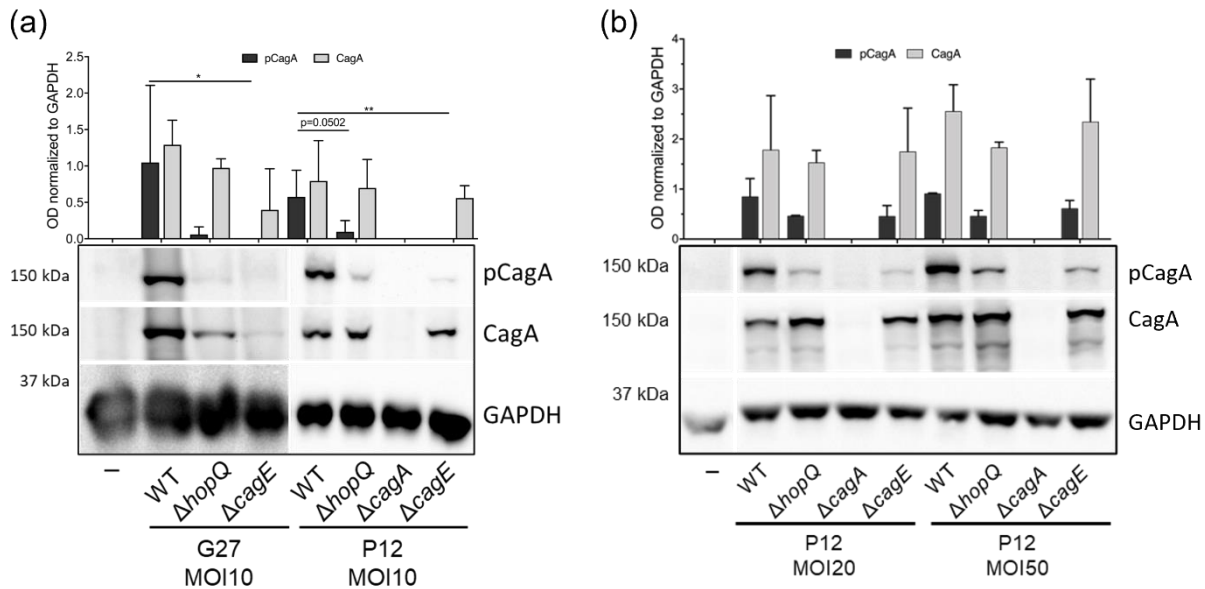


**Figure 13: CagA translocation after *H. pylori* infection.**

MKN45 cells were infected with *H. pylori* G27/P12 wild type strains or isogenic mutant strains for HopQ, CagA, or CagE at an MOI of 10/20/50 for eight hours. (a, b) pCagA and CagA were detected by western blot. GAPDH was used as a loading control. Data were normalized to GAPDH. Levels of pCagA (black bars) and CagA (light grey bars) are depicted. All graphs show mean  $\pm$  SD of at least 2 $\geq$  independent experiments. Kruskal–Wallis with Dunn's multiple comparisons test. \*  $p \leq 0.05$ , \*\*  $p \leq 0.01$

HopQ interacts with CEACAMs, expressed on gastric epithelial cells (Javaheri et al. 2016). We checked *CEACAM* mRNA expression levels upon *H. pylori* infection in MKN45 cells (Figure 14). MKN45 cells showed *CEACAM 1*, *5*, and *6* expression on mRNA and protein level at basal conditions. Upon infection, *CEACAM 1*, *5*, and *6* mRNA expression levels were elevated. However, lack of HopQ or CagE induced slightly lower *CEACAM* expression levels compared to wild type or CagA deficient bacteria, although this was not significant (Figure 14).

To confirm that HopQ-CEACAM interaction is essential for activating the non-canonical NF- $\kappa$ B pathway, we used NUGC-4 and SNU1 cells for further experiments. These two cell lines were selected as they showed intermediate or low/no expression of CEACAMs and hence are a suitable model to explore the importance of HopQ-CEACAM interaction on the activation of the non-canonical NF- $\kappa$ B pathway (Figure 14 a and b).

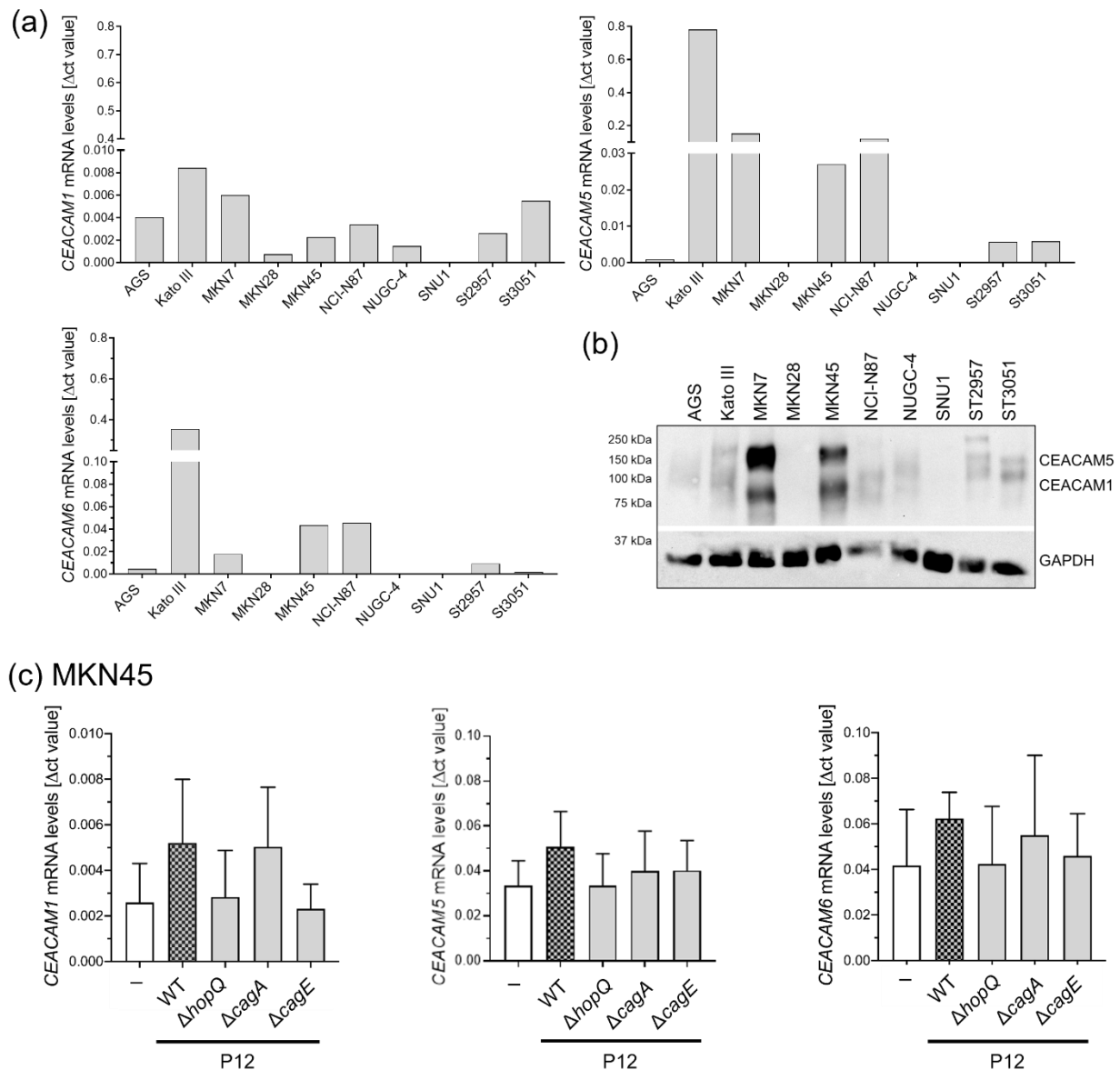


**Figure 14: CEACAM expression in various GC cells and upon *H. pylori* infection in MKN45 cells.**

A panel of GC cells was screened for CEACAM 1, 5, and 6 levels at basal conditions by qPCR for mRNA levels (a) or by western blot for protein levels (b). (c) MKN45 cells were infected with P12 wild type *H. pylori* strain or isogenic mutant strains for HopQ, CagA, or CagE for eight hours at an MOI of 10. Cells were tested for CEACAM 1, 5, and 6 mRNA expression levels by qPCR. GAPDH was used as a housekeeping gene. All qPCR values were normalized to GAPDH ( $\Delta$ ct value). All graphs show mean  $\pm$  SD of at least three independent experiments. Ordinary one-way ANOVA with Bonferroni's multiple comparisons test.

NUGC-4 and SNU1 cells were infected with *H. pylori* P12 wild type strain or isogenic mutant strains lacking HopQ, CagA, or CagE at an MOI of 10 for eight hours and tested for activation of non-canonical NF- $\kappa$ B pathway by qPCR and western blot. First, the processing of p100 to p52 was tested, but no difference in NUGC-4 and SNU1 cells compared to uninfected controls could be seen (Figure 15a). As a control for successful infection, IL-8 secretion was analysed by ELISA. NUGC-4 cells showed a slight upregulation of IL-8 secretion upon infection compared to infected MKN45 cells; however, SNU1 cells did not show any IL-8 secretion (Figure 15b). SNU1 cells showed no CEACAM expression at basal condition (Figure 14 a and b). Thus, the interaction partner of HopQ is missing, which may explain the absence of IL-8 secretion, and p100 to p52 processing seen upon infection.

*A20* and *LTβ* mRNA expression levels were checked upon infection. SNU1 cells did not show a difference in *A20* or *LTβ* expression levels after infection. In contrast, NUGC-4 cells showed an upregulation of *A20* as well as *LTβ* mRNA levels upon infection but independent of HopQ, while CagE deficiency induced a significantly lower *A20*, or *LTβ* mRNA expression levels (Figure 15 c and d).

These results indicate that HopQ-CEACAM interaction is important for activating the non-canonical NF- $\kappa$ B pathway since GC cells with low CEACAM expression levels show no activation of the signaling pathway upon bacterial infection.

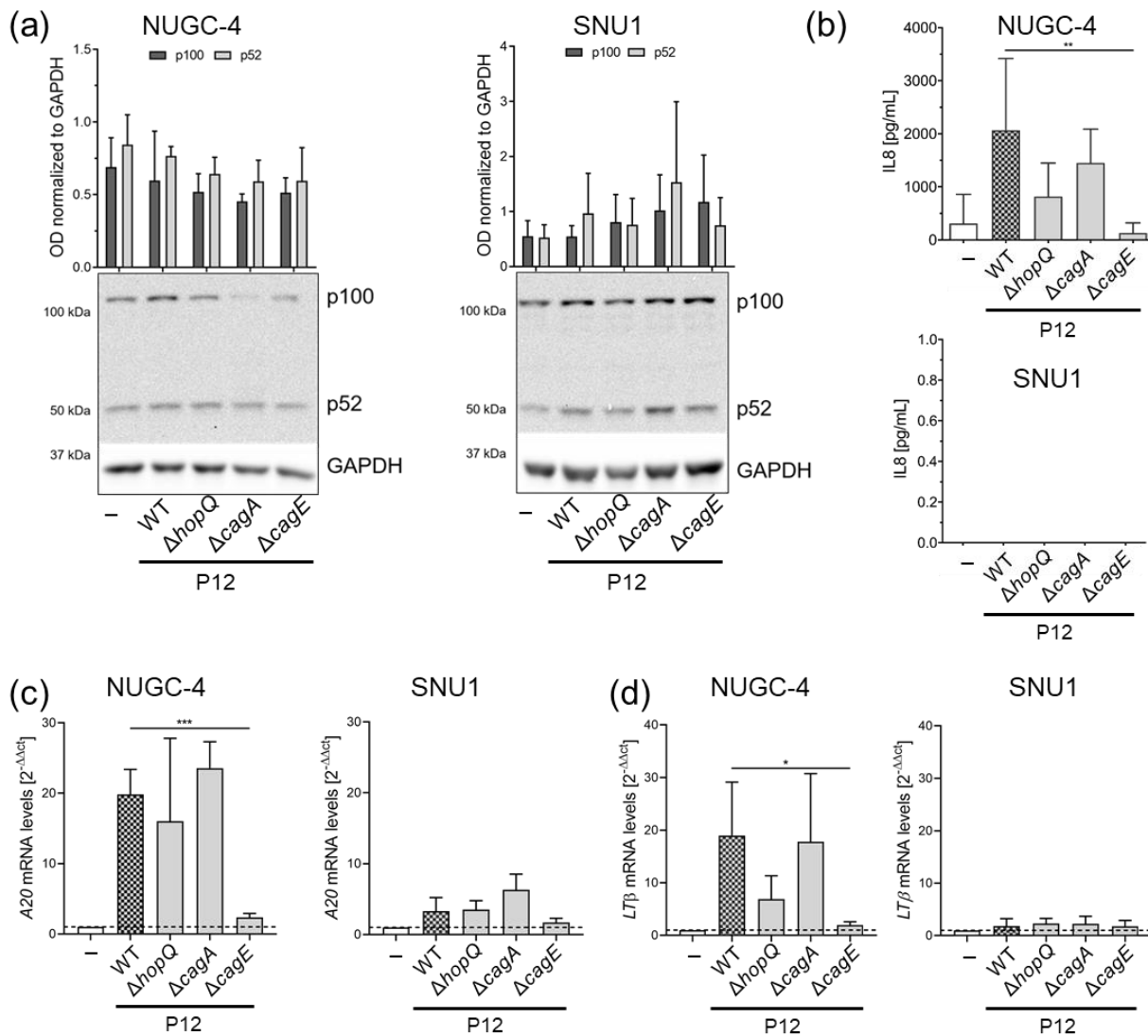


**Figure 15: Activation of non-canonical NF- $\kappa$ B pathway upon *H. pylori* infection in SNU1 and NUGC-4 cells.**

NUGC-4 and SNU1 cells were infected with *H. pylori* P12 wild type strain or isogenic mutant strains lacking HopQ, CagA, or CagE at an MOI of 10 for eight hours. (a) p100 to p52 processing was checked by western blot. (b) IL-8 secretion was analysed by ELISA. (c) *A20* and (d) *LTβ* mRNA expression levels were assessed by qPCR. As a housekeeping gene, *GAPDH* was used. All qPCR values were normalized to *GAPDH* and the negative control/uninfected cells ( $\Delta\Delta Ct$  value). All graphs show mean  $\pm$  SD of at least three independent experiments. Ordinary one-way ANOVA with Bonferroni's multiple comparisons test. \*  $p \leq 0.05$ , \*\*  $p \leq 0.01$ , \*\*\*  $p \leq 0.001$

SNU1 and NUGC-4 cells were tested for *CEACAM 1*, *5*, and *6* mRNA expression levels upon *H. pylori* infection. SNU1 cells, which showed no expression of CEACAM at baseline (Figure 14 a and b), did not show upregulation of CEACAM mRNA expression upon *H. pylori* infection. NUGC-4 cells

showed induction of CEACAM expression levels upon *H. pylori* infection, which was induced to a lower extent compared to MKN45 cells upon infection (Figure 14 c and Figure 16).

### NUGC-4

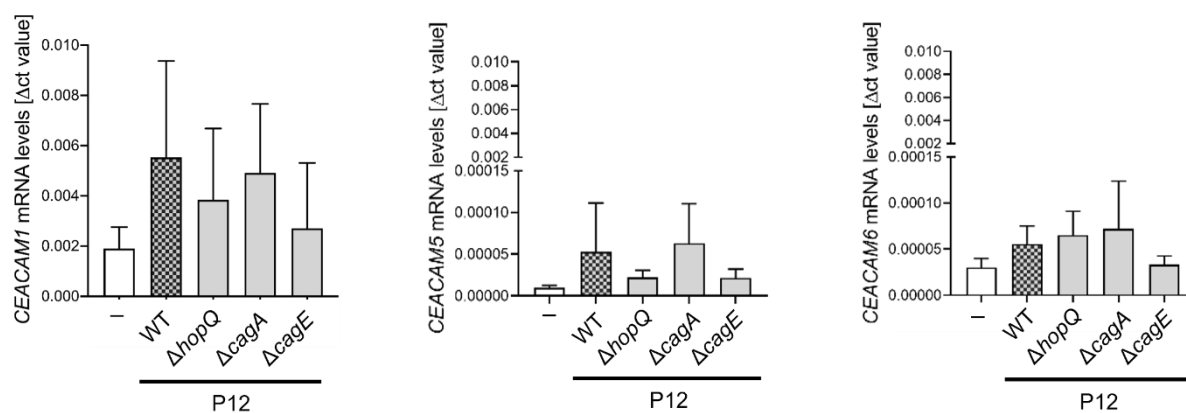


**Figure 16: CEACAM expression in NUGC-4 cells upon infection.**

NUGC-4 cells were infected with wild type P12 *H. pylori* strains or isogenic mutant strains for HopQ, CagA, or CagE at an MOI of 10 for eight hours. Cells were tested for CEACAM 1, 5, and 6 mRNA expression levels by qPCR. GAPDH was used as a housekeeping gene. All qPCR values were normalized to GAPDH ( $\Delta$ ct value). All graphs show mean  $\pm$  SD of at least three independent experiments. Ordinary one-way ANOVA with Bonferroni's multiple comparisons test. \*  $p \leq 0.05$ , \*\*  $p \leq 0.01$ , \*\*\*  $p \leq 0.001$

So far, we have observed that the lack of HopQ reduces the activity of the non-canonical NF- $\kappa$ B pathway by lowering *LT $\beta$*  mRNA expression, processing of p100 to p52, expression of NF- $\kappa$ B target gene, phosphorylation of CagA, and secretion of IL8 in GC cells. A previous study showed that HopQ-CEACAM interaction is involved in the binding of *H. pylori* to gastric epithelial cells (Javaheri et al. 2016). Thus, we examined the binding capacity of *H. pylori* to cells to determine whether decreased NF- $\kappa$ B pathway activation originates from the reduced binding of *H. pylori* to gastric epithelial cells. To do so, a binding assay was performed using CFSE-labelled bacteria which were incubated with gastric cells shaking for 30 minutes, washed, fixed and sorted for GFP signaling by CytoFLEX. *H. pylori* wild type and CagA or CagE deficient strains showed the highest binding capacity to MKN45 cells. At the same time, lack of HopQ reduced the binding capacity by almost 50 percent (Figure 17a). The binding of *H. pylori* to NUGC-4 cells was not influenced by the lack of CagA, CagE, or HopQ, since a similar binding capacity was observed compared to the wild type *H. pylori* strain. *H. pylori* showed a very low binding capacity to SNU1 cells compared to MKN45 or NUGC-4 cells. SNU1 cells showed no CEACAM expression, which could explain the low binding capacity of the gastric pathogen. The highest binding capacity of *H. pylori* was observed in MKN45 cells, which have higher CEACAM1, 5, and 6 expression levels compared to NUGC-4 or SNU1 cells.

Similar results were observed by confocal imaging using CFSE-labelled bacteria which were incubated with gastric cells for 3 hours and subsequently, fixated, stained and imaged. Lack of CagA or CagE did not influence the binding of *H. pylori* to gastric epithelial cells (Figure 17b). More bacteria

were binding to MKN45 cells compared to NUGC-4 cells, confirming previous data of the binding assay (Figure 17).

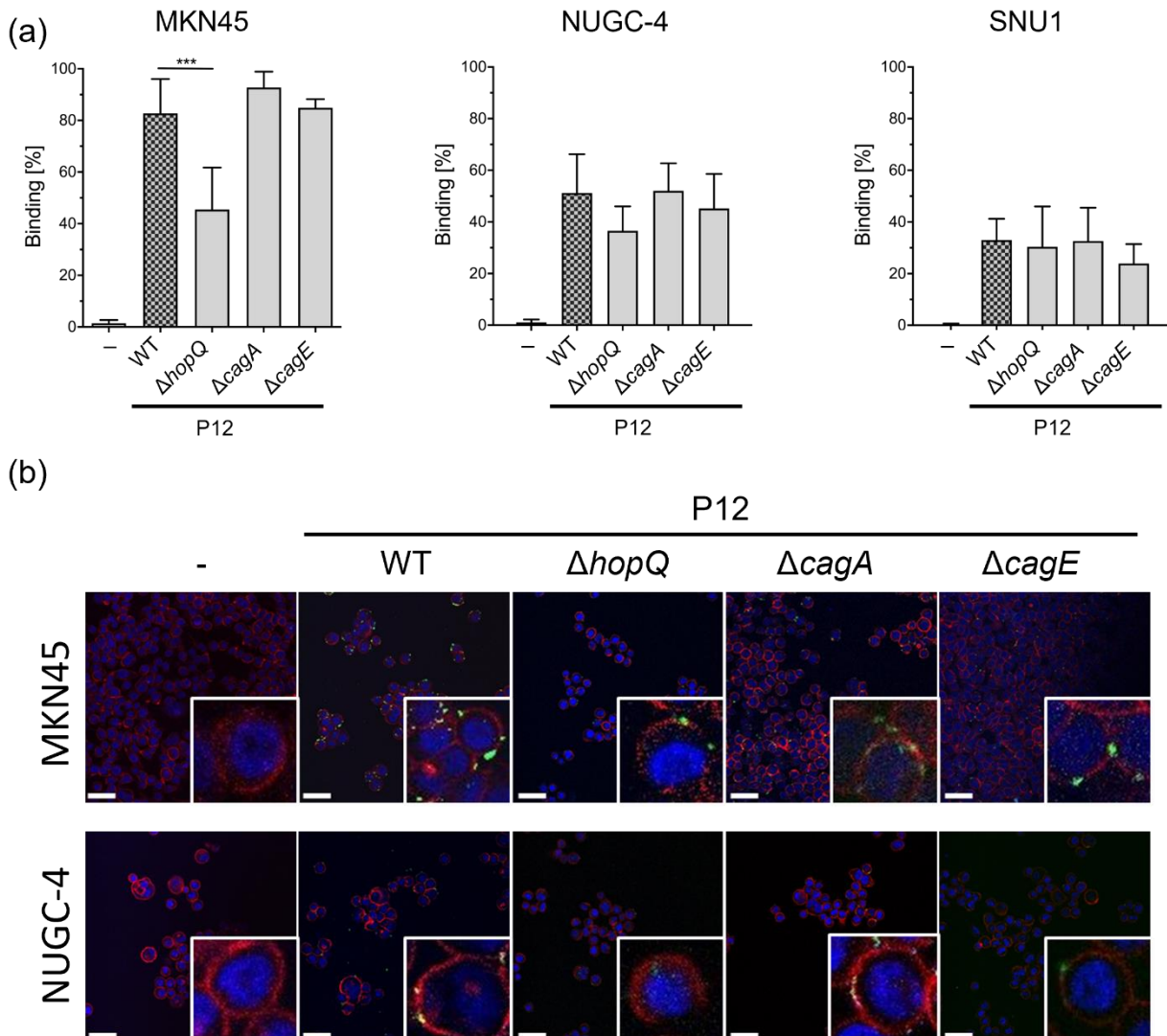


**Figure 17: Binding of *H. pylori* to gastric epithelial cells.**

(a) CFSE labelled bacteria were incubated with MKN45, NUGC-4, or SNU1 GC cells at an MOI of 10 for 30 minutes shaking. Next, infected cells were washed, fixed, and sorted for GFP signal by CytoFLEX. As a negative control, cells without labelled bacteria were used. (b) Representative confocal images of MKN45 and NUGC-4 GC cells infected with *H. pylori* P12 wild type strain or isogenic mutant strains for HopQ, CagA or CagE for 3 hours. Cell membranes were stained with phalloidin (red), and nuclei were stained with DAPI (blue). Scale bar: 50  $\mu$ m. All graphs show mean  $\pm$  SD of at least three independent experiments. Ordinary one-way ANOVA with Bonferroni's multiple comparisons test. \*  $p \leq 0.05$ , \*\*  $p \leq 0.01$ , \*\*\*  $p \leq 0.001$

To further confirm the *in vitro* data, we used primary gastric cells to generate organoids and bring them into a 2D culture to perform infection experiments. The CERO 3D cell incubator (OLS) was very useful to expand murine gastric organoids quickly to increase the yield needed to prepare a 2D culture. A comparison of the conventional seeding procedure of murine gastric organoids in matrigel droplets compared to cultivating organoids in the CERO is shown in Figure 18. With the help of the CERO 3D cell incubator, more glands in less medium could be cultivated, and organoids grew bigger compared to murine gastric organoids grown in matrigel droplets.

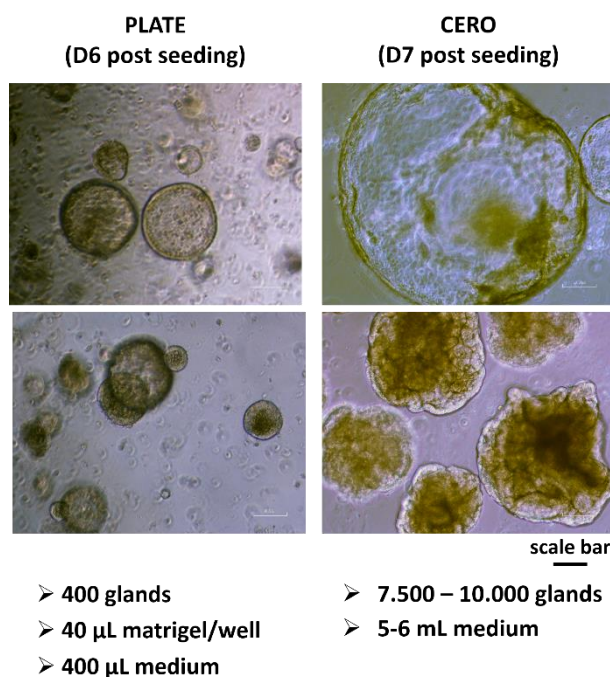


**Figure 18: Representative images of organoids cultured in two different setups.**

Representative images of murine gastric organoids cultivated in matrigel droplets in a plate after six days of seeding (left column) or in the 3D CERO incubator in solution after seven days of seeding (right column) are shown. Scale bar: 50  $\mu$ m.

Using these conditions, organoids were generated from isolated glands of C57BL/6 or C57BL/6<sup>hCEACAM1+/mouse CEACAM1-</sup> mice and grown for three to four days in the CERO 3D cell incubator. C57BL/6<sup>hCEACAM1+/mouse CEACAM1-</sup> mice have no murine CEACAM1 but express human CEACAM1 (Klaile et al. 2019). This model allows us to investigate specifically whether the species-specific interaction of HopQ and CEACAM1 (Javaheri et al. 2016) is responsible for activating the non-canonical NF- $\kappa$ B pathway. Once generated, organoids were broken up into single cells and grown into a monolayer, which was infected at an MOI of 20 for 20 hours with the *H. pylori* P12 wild type strain or HopQ-deficient strain. The *H. pylori* P12 strain has not been adapted to mice and hence cannot colonize the murine epithelium. A representative image of the generated monolayer upon infection or without bacteria is shown in Figure 19a. C57BL/6<sup>hCEACAM1+/mouse CEACAM1-</sup> mice induced *CEACAM1* expression independent of infection (Figure 19). We could not see differences in the *CEACAM1* expression levels of C57BL/6<sup>hCEACAM1+/mouse CEACAM1-</sup> mice upon infection of the 2D monolayer or if left uninfected (Figure 19). Finally, we checked whether *CEACAM1* expression is correlating with *Ltb* expression upon infection. We could observe a positive correlation of *CEACAM1* and *Ltb* expression when C57BL/6<sup>hCEACAM1+/mouse CEACAM1-</sup> primary gastric cells were infected with *H. pylori* P12 wild type strain (Figure 20b). HopQ-deficient P12 *H. pylori* strain did not show a correlation of *CEACAM1* and *Ltb* (Figure 19c).

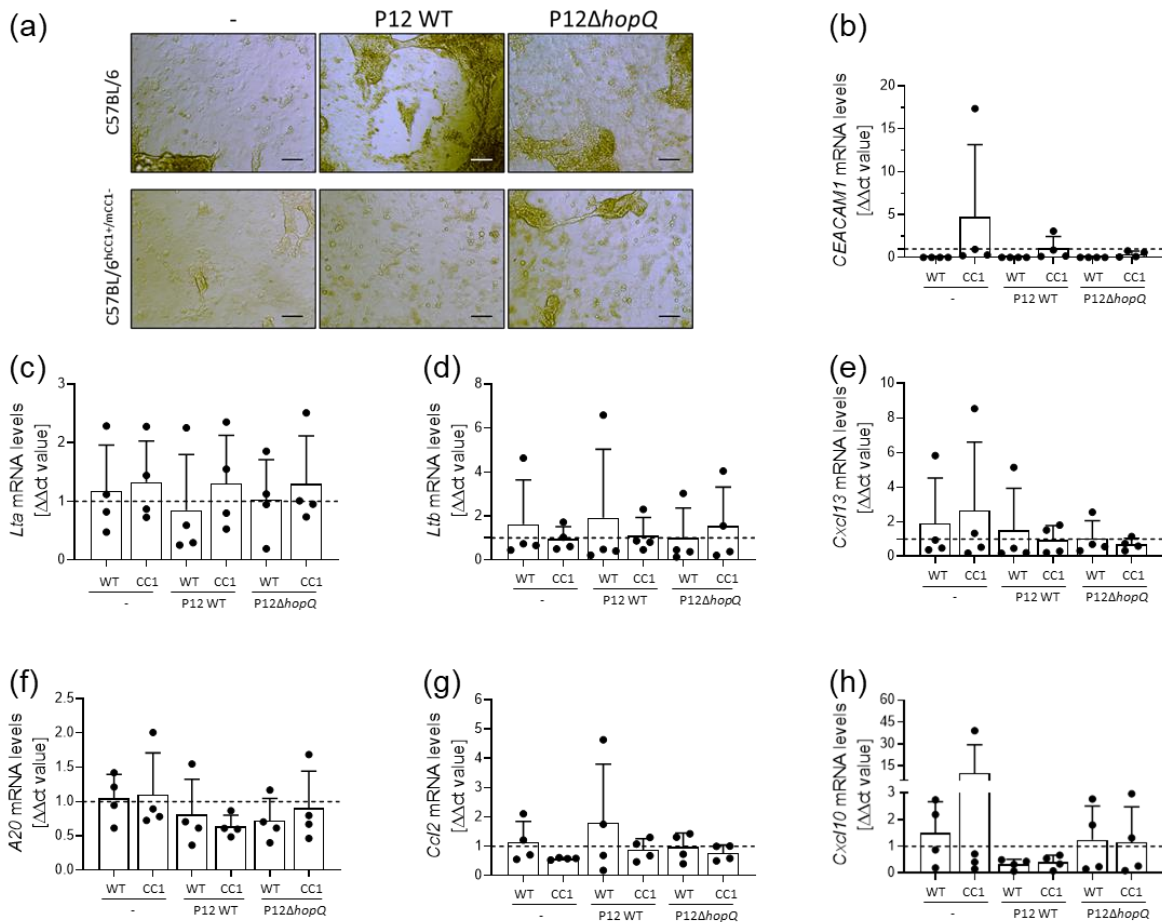


**Figure 19: Gene expression levels upon *H. pylori* infection in murine primary gastric cells.**

Organoids were grown from C57BL/6 (WT) or C57BL/6<sup>hCEACAM1+/mouse CEACAM1-</sup> (CC1) mice and broken up into single cells to grow in a monolayer. 2D cultures were infected with *H. pylori* P12 wild type or P12 $\Delta$ hopQ at an MOI of 20 for 20 hours. (a) Representative images of 2D culture uninfected or infected with *H. pylori* P12 strain or P12 $\Delta$ hopQ. Scale bar: 50  $\mu$ m. RNA was isolated from the cells and assessed by qPCR to check for expression levels of *CEACAM1* (b), *Lta* (c), *Ltb* (d), *Cxcl13* (e), *A20* (f), *Ccl2* (g), and *Cxcl10* (h) *Gapdh* served as a housekeeping gene. All qPCR values were normalized to GAPDH and the uninfected WT cells ( $\Delta\Delta$ ct value). All graphs show mean  $\pm$  SD of at least three independent experiments.

The influence of HopQ-CEACAM interaction upon infection may be different between murine or human gastric cells despite having murine *Ceacam1* replaced by human *CEACAM1* in the applied mouse model. In human GC cells, showing expression of CEACAM, infection with HopQ-deficient *H. pylori* strains reduced binding of the bacteria resulting in decreased activation of the non-canonical NF- $\kappa$ B pathway and lowered expression of NF- $\kappa$ B target genes.

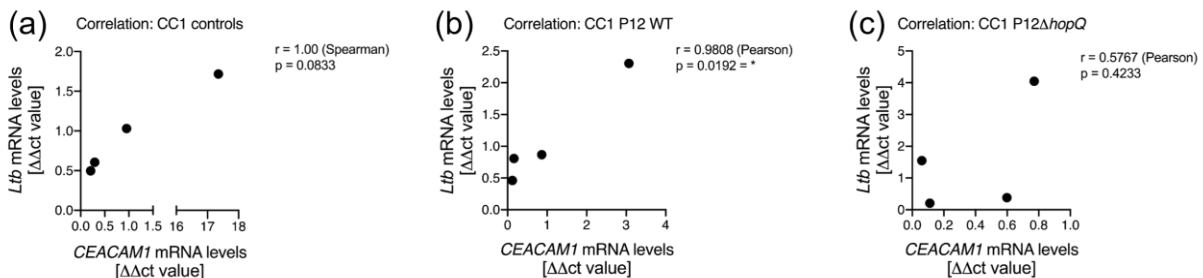


**Figure 20: Correlation of *Ltb* expression and *CEACAM1* expression in murine primary gastric cells.**

Organoids were grown from C57BL/6 (WT) or C57BL/6<sup>hCEACAM1+/mouse CEACAM1-</sup> mice (CC1) and broken up into single cells to grow in a monolayer. 2D cultures were infected with *H. pylori* P12 wild type or P12 $\Delta$ hopQ at an MOI of 20 for 20 hours. RNA was isolated from

the cells and assessed by qPCR to check for expression levels of CEACAM1 and *Ltb*. *Gapdh* served as a housekeeping gene. All qPCR values were normalized to GAPDH and the uninfected WT cells ( $\Delta\Delta\text{ct}$  value). All experiments were performed at least three times. Correlation of *Ltb* and *CEACAM1* mRNA expression levels of CC1 negative control (a), of CC1 infected with *H. pylori* P12 strain (b), and of CC1 infected with HopQ-deficient *H. pylori* P12 strain. For (a) Spearman correlation was used. For (b) and (c), Pearson correlation was used.

### 3.2 NIK depletion decreases the tumorigenic potential of GC cells

To investigate the impact of the non-canonical NF- $\kappa$ B pathway on gastric carcinogenesis, different approaches were selected to down-modulate the key protein NIK (Sun 2011). First, a panel of GC cells was investigated for basal activation of the pathway by screening p100 to p52 processing by western blot. Some of the GC cells tested showed processing of p100 to p52 at basal conditions, indicating a constitutive activation of the non-canonical NF- $\kappa$ B pathway (Figure 21).

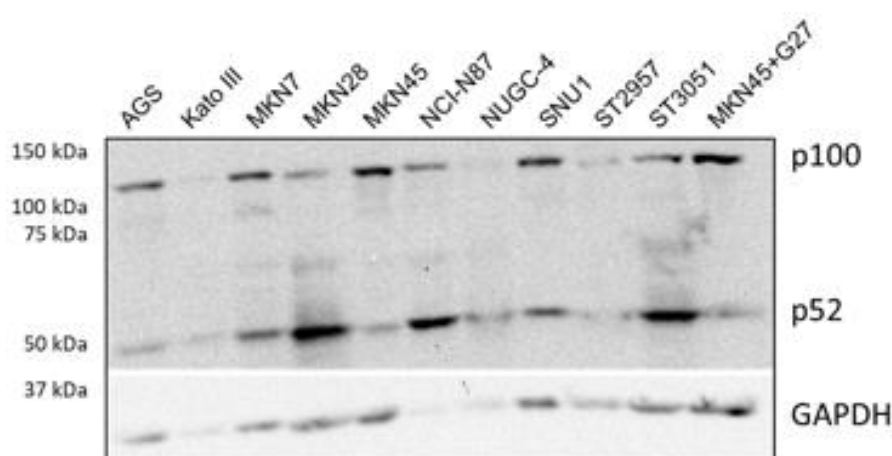


**Figure 21: p100 to p52 processing in different GC cells.**

A panel of GC cells was grown for 48 hours, and protein lysates were screened for p100 to p52 processing by western blot. GAPDH served as a loading control. A representative western blot is shown.

Next, NIK expression was assessed by qPCR and western blot at basal conditions. GC cells showed various levels of NIK mRNA and protein expression (Figure 22). For further *in vitro* experiments, GC cells with constitutive activation of the non-canonical NF- $\kappa$ B pathway and intermediate/high NIK protein expression levels were selected. As controls, cells with NIK expression but low or no constitutive activation of the non-canonical NF- $\kappa$ B pathway were used.

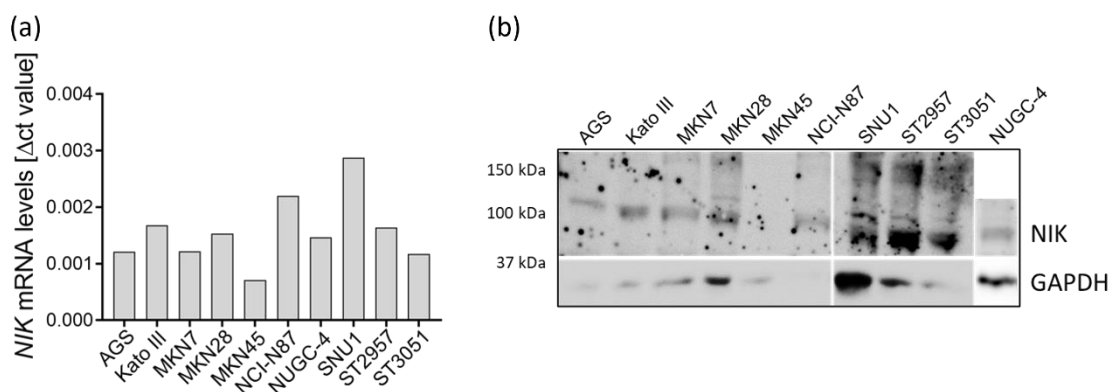


**Figure 22: NIK expression in different GC cells.**

GC cells were grown for 48 hours, and RNA and protein lysates were prepared. (a) *NIK* mRNA expression levels were measured by qPCR. *GAPDH* served as a housekeeping gene. All qPCR values were normalized to *GAPDH* ( $\Delta ct$  value). Experiments were performed twice. (b) NIK protein levels were investigated by western blot. *GAPDH* was used as a loading control. A representative blot is displayed.

### 3.2.1 NIK knock out by CRISPR/Cas9n technology was not effective

To knock out NIK, we used the CRISPR/Cas9n approach. First, guide RNAs (gRNAs) targeting the functional region of NIK in exon 7 were generated. As we used the pX335 (D10A mutant Cas9n) plasmid, two gRNAs had to be synthesized, targeting the same sequence from each side. Three pairs of gRNAs were produced and introduced into the pX335 plasmid (Figure 23a). Next, a U6 screening was performed, and the PCR product was checked on an agarose gel (Figure 23b).

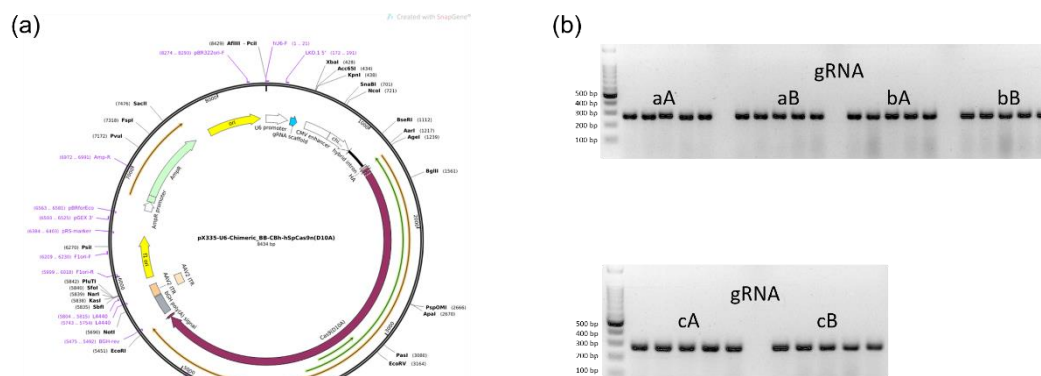


**Figure 23: Illustration of the pX335 plasmid and U6 screening.**

(a) Schematic illustration of pX335 plasmid from Addgene (Addgene plasmid #42335; <http://n2t.net/addgene:42335>; RRID:Addgene\_42335) (Le Cong et al. 2013). (b) After ligation of gRNAs (a/b/c) into pX335 plasmid, single colonies were picked, a U6 screening was performed, and PCR products were controlled on a two percent agarose gel. Expected size: 250 bp.

GC cells showing high (MKN28), intermediate (NCI-N87), or low (AGS) pathway activation and having NIK expression were selected for transfection with the generated CRISPR/Cas9n plasmids. Forty-eight hours later, cells were sorted for a positive GFP signal. As a negative control, untransfected wild type cells were used. The GFP positive cells were put in culture and expanded, single-cell colonies were picked and screened for NIK mutations. Unfortunately, it was impossible

---

to identify any NIK mutant cell colonies or NIK down modulated cell clones. The sequenced clones were also checked for NIK expression on protein level; however, no differences could be observed.

GC cells with constitutive activation of the non-canonical NF- $\kappa$ B pathway may be addicted to the pathway, and hence it is not possible to generate knock out cells. Consequently, we changed the strategy and continued using siRNA technology.

### **3.2.2 NIK down regulation by siRNA reduced proliferation of GC cells**

To down-regulate NIK *in vitro*, small interfering RNA (siRNA) was used. Therefore, AGS, MKN7, MKN28, MKN45, NUGC-4, and NCI-N87 cells were transfected with 10 nm of control siRNA (siSCR) or siNIK. Forty-eight hours post-transfection, cells were seeded for a proliferation assay and in parallel for protein lysates to check for NIK levels. A declined proliferation was observed in NCI-N87 siNIK cells (Figure 24). MKN28 siNIK cells showed a slight decrease in proliferation after NIK down-modulation without significance (Figure 24). AGS, MKN7, and NUGC-4 siNIK cells did not change their proliferative capacity. MKN45 cells were used as a negative control since these cells showed low NIK levels and no constitutive activity of the non-canonical NF- $\kappa$ B pathway (Figure 21 and Figure 22). As expected, NIK manipulation did not affect the proliferative capacity of these cells.

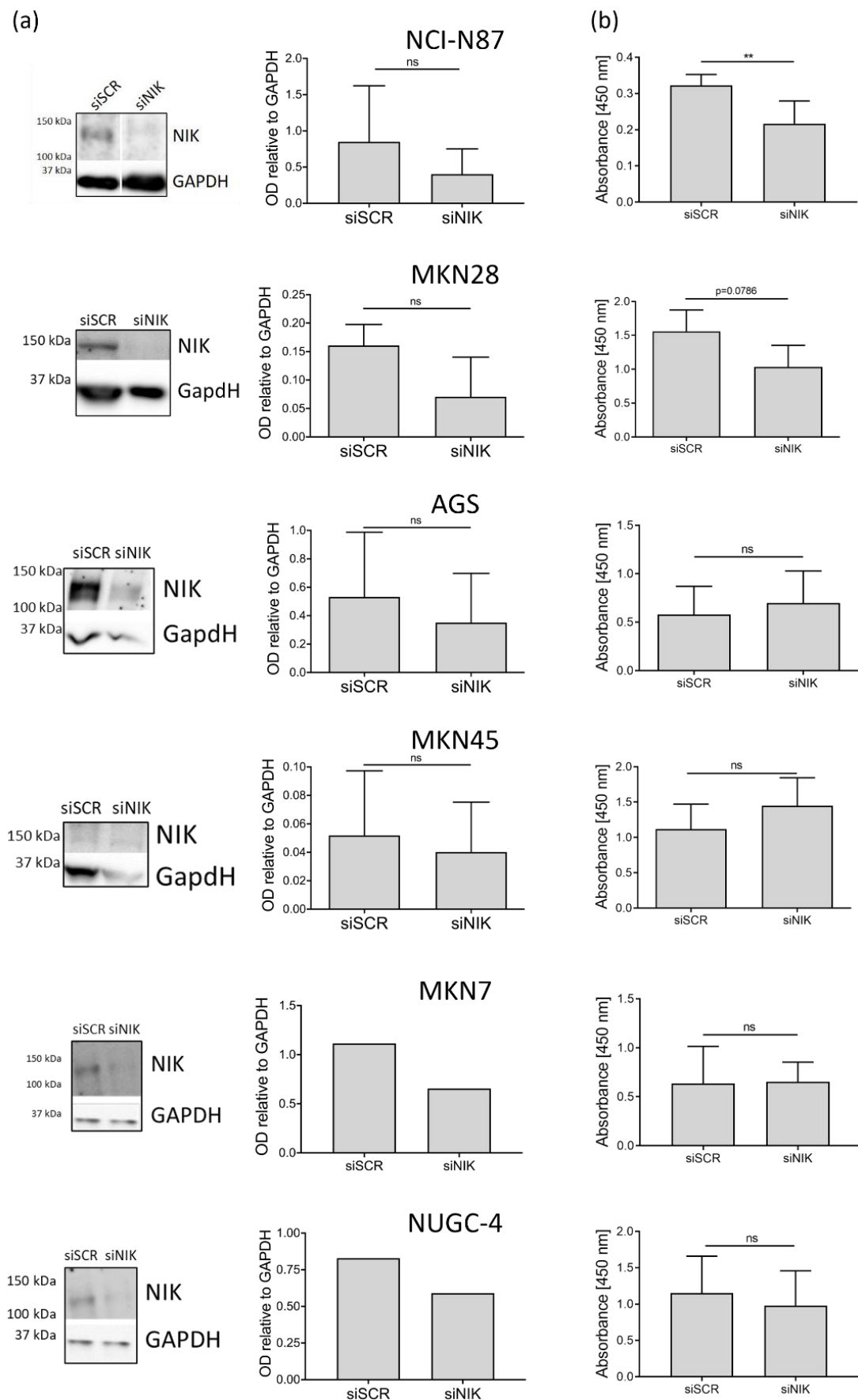


**Figure 24: Impact of NIK down regulation by siRNA on cell proliferation of GC cells.**

Various GC cells were transfected with siSCR or siNIK (10 nM) for 48 hours. Transfected cells were seeded and grown for 48 hours, and cells were lysed for protein samples (a) and measured for their proliferative capacity using the CCK8 kit (b). (a) All protein values were normalized to GAPDH, which was used as a loading control. All graphs show mean  $\pm$  SD of at least three independent experiments, except for MKN7 and NUGC-4, examined only twice. Unpaired t-test. \*  $p \leq 0.05$ , \*\*  $p \leq 0.01$

### 3.2.3 Down regulation of NIK by shRNA resulted in reduced proliferation, and fewer formed clones in AGS shNIK cells

To generate stable NIK knockdown cells, an shRNA approach was applied. The Web Portal of the Broad Institute was used to select different shRNA sequences targeting NIK (shNIK), which were inserted into the pLKO.1 plasmid. The plasmid was tested by transfecting MKN28 cells and isolating mRNA to check for NIK levels by qPCR. With this, a knockdown of NIK mRNA levels by shNIK1 and shNIK3 by about 60 percent compared to shcontrol could be observed (Figure 25).

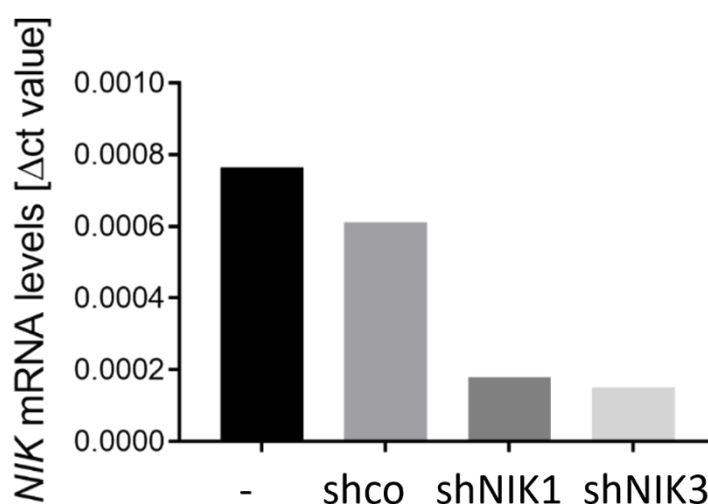


**Figure 25: NIK mRNA levels after shRNA transfection in MKN28 cells.**

MKN28 cells were transfected with the pLKO.1 plasmid containing shRNA control (shco), shNIK1, or shNIK3. Cells were seeded and grown for 48 hours. RNA was isolated to perform a qPCR detecting *NIK* mRNA expression levels. *GAPDH* was used as a housekeeping gene.

In collaboration with Prof.<sup>in</sup> Martina Anton, the packaging of lentiviruses and production of viral supernatants was performed. As the transduced cells were selected by puromycin addition, a killing assay was performed to determine the amount of puromycin needed to kill all wild type cells. To do so,  $1.5 \times 10^5$  cells/well were seeded, and 24 hours later, puromycin was added at different concentrations. Living cells were counted every other day. For AGS and NUGC-4 cells, 75  $\mu\text{g}/\text{mL}$  puromycin was needed. For NCI-N87 cells, 35  $\mu\text{g}/\text{mL}$  puromycin was needed to kill all wild type cells (Figure 26).

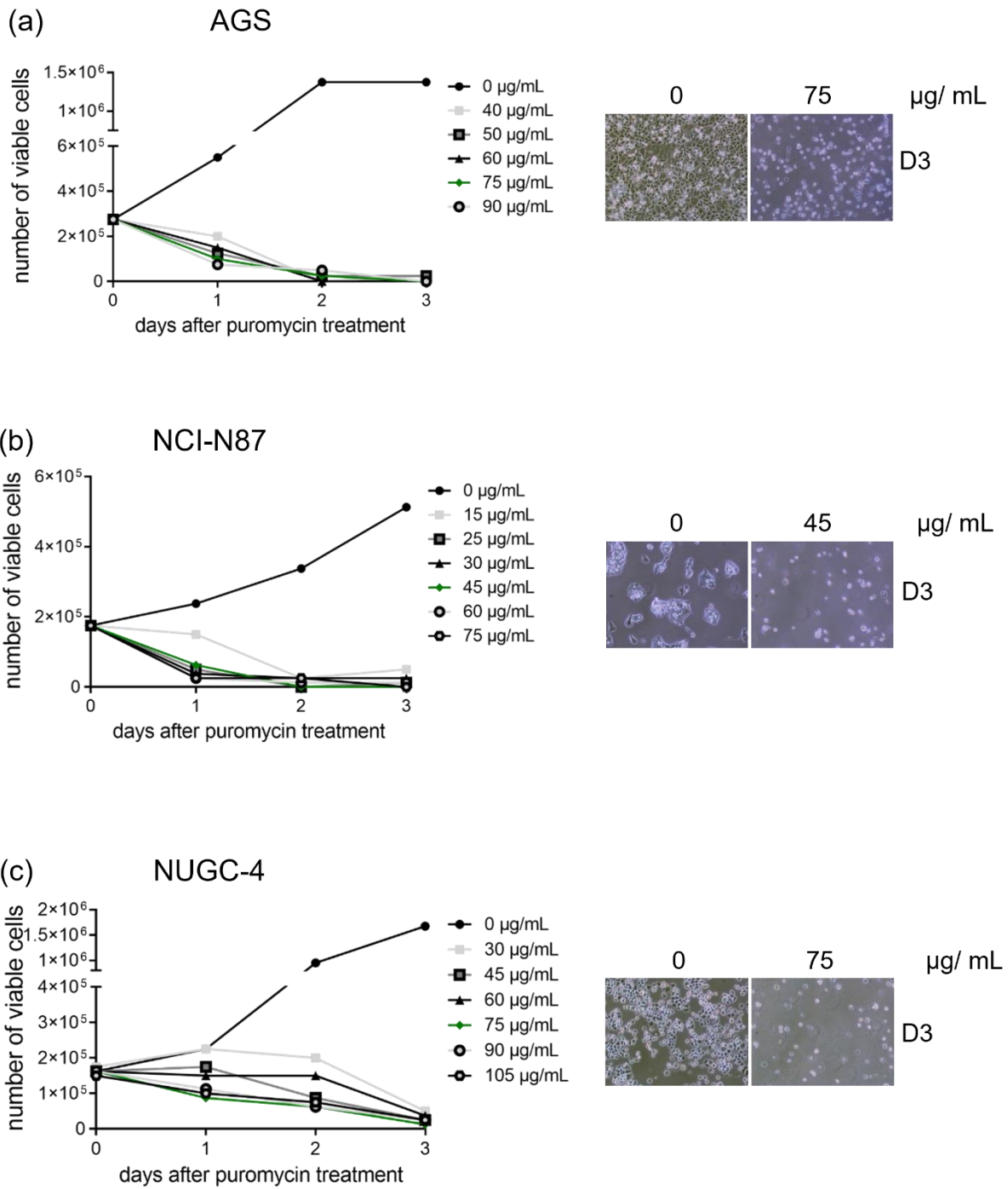


**Figure 26: Titration of puromycin concentration to kill GC cells.**

GS cells were seeded at a density of  $1.5 \times 10^5$  cells/well in quadruplicates, and 24 hours later, different concentrations of puromycin were added. As starting count, one well was counted before treatment. Every other day, the cells untreated or treated with puromycin were counted. The number of viable cells was plotted over days of treatment. Killing assays were run twice.

Next, AGS, NUGC-4, and NCI-N87 cells were transduced with the viral supernatant and expanded. The transduced cells were seeded in a low density to allow single-cell colony growth and selection by adding puromycin. Clones were picked and screened by qPCR and western blot for NIK levels (Figure 27). NIK could be successfully down-modulated on mRNA level by about 60-20 percent in the screened cells. The highest NIK knockdown was achieved in AGS shNIK cells (Figure 27).

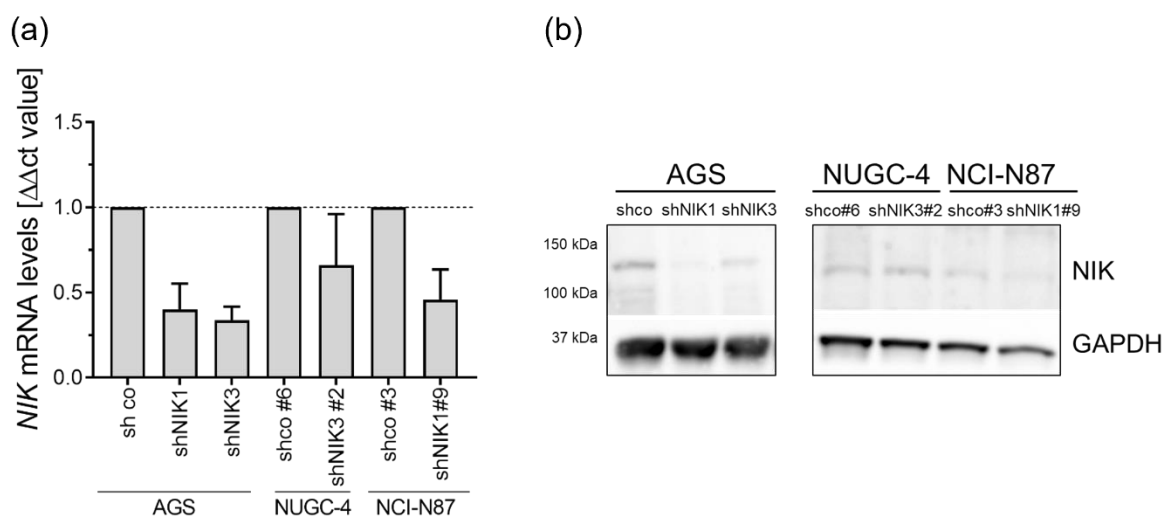


**Figure 27: Down modulation of NIK levels by lentiviral transduction of GC cells.**

AGS, NUGC-4, and NCI-N87 cells were lentiviral transduced, grown, and single colonies were selected. To determine the NIK levels after successful down-modulation, a qPCR and a western blot were performed. (a) *NIK* mRNA expression levels were normalized to *GAPDH* and sh control (shco) cells. *GAPDH* served as a housekeeping gene. qPCR values were normalized to *GAPDH* and shco cells ( $\Delta\Delta\text{ct}$  value). (b) A representative western blot of the NIK protein levels after transduction is shown.

To investigate the impact of NIK knockdown on proliferation, anchorage-dependent, and – independent growth, *in vitro* assays were performed. Initially, the impact on their proliferative capacity was tested in a proliferation assay. AGS shNIK cells showed lower proliferation compared to control cells (shco) (Figure 28a). No significant effect could be observed in NCI-N87 and NUGC-4 shNIK cells (Figure 28 b and c).

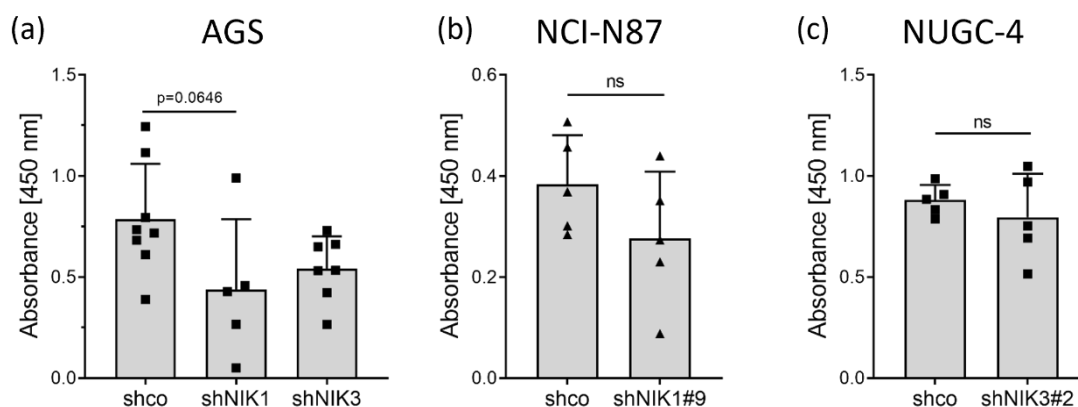


**Figure 28: Impact of NIK knockdown on cell proliferation of GC cells.**

AGS, NCI-N87, and NUGC-4 cells were seeded, grown for 48 hours, and cell proliferation was measured using the CCK8 kit. All measurements were performed in triplets. All graphs show mean  $\pm$  SD of at least three independent experiments. Ordinary one-way ANOVA with Bonferroni's multiple comparisons test for AGS and unpaired t-test for NCI-N87 and NUGC-4 cells. \*  $p < 0.05$ , \*\*  $p < 0.01$ , \*\*\*  $p < 0.001$

To check for anchorage-dependent growth, a clonogenicity assay was conducted. Therefore, GC cells were seeded at low density to allow colony growth for 2-2.5 weeks. Again, AGS shNIK cells showed a slight reduction in the number of formed colonies compared to AGS shco cells (Figure 29a). NCI-N87 and NUGC-4 shNIK cells showed no impairment in the anchorage-dependent growth

(Figure 29 b and c).

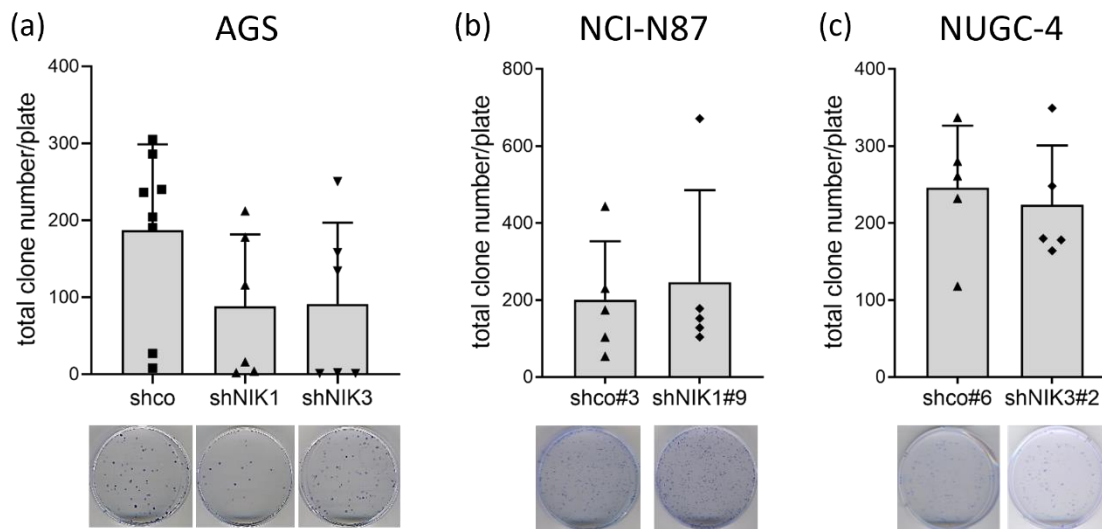


**Figure 29: Influence of NIK knockdown on anchorage-dependent growth of GC cells.**

AGS, NCI-N87, and NUGC-4 cells were seeded at low density and grown for two (AGS) or 2.5 (NCI-N87, NUGC-4) weeks. Formed colonies were stained with crystal violet and counted manually. All graphs show mean  $\pm$  SD of at least three independent experiments. Ordinary one-way ANOVA with Bonferroni's multiple comparisons test for AGS, Mann-Whitney test for NCI-N87, and unpaired t-test for NUGC-4 cells. \*  $p \leq 0.05$ , \*\*  $p \leq 0.01$ , \*\*\*  $p \leq 0.001$

To test for anchorage-independent growth, a soft agar assay was carried out. This assay shows whether cancer cells can grow without attachment, representing a hallmark of carcinogenesis (Borowicz et al. 2014). A slightly lower number of formed colonies could be observed in AGS shNIK and NUGC-4 shNIK cells but without significance (Figure 30 a and b). NCI-N87 shNIK cells did not have an impact on anchorage-independent growth (Figure 30c).

AGS shNIK had the lowest NIK levels left after transduction which could be linked to the strongest influence of NIK on proliferation. In NUGC-4 shNIK or NCI-N87 shNIK, the down-modulation was not that high compared to AGS shNIK cells (Figure 27). AGS GC cells seem to depend on the NF- $\kappa$ B pathway since NIK knockdown lowers the proliferative capacity, resulting in fewer formed clones in an anchorage-dependent and independent manner.

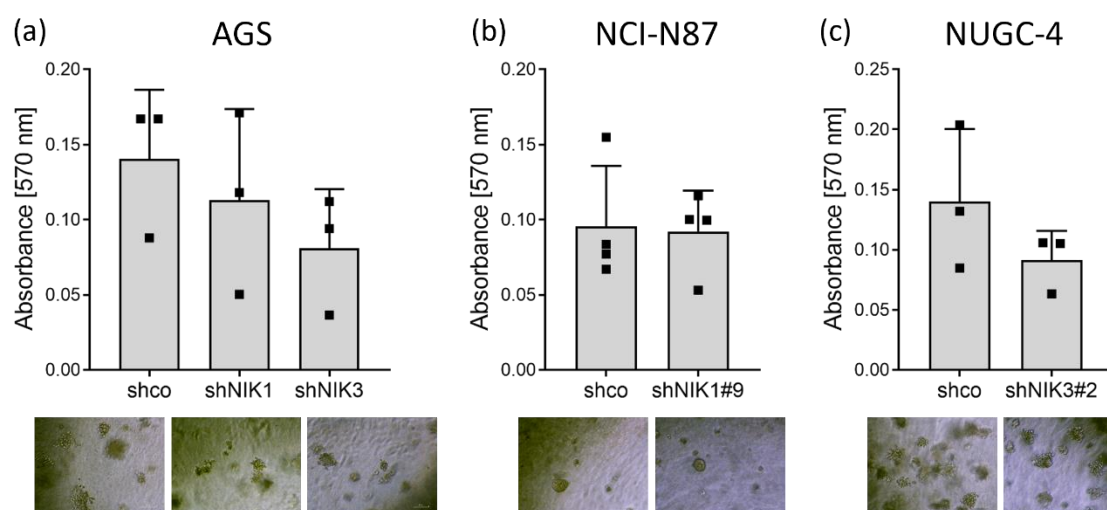


**Figure 30: Effect of NIK knockdown on anchorage-independent growth of GC cells.**

AGS, NCI-N87, and NUGC-4 cells were grown in agar for one week, and their proliferation was measured by an MTT assay. Absorbance was measured at 570 nm. As a reference, 650 nm was used and subtracted from the values measured. As a blank, agar only was used to correct for background signal. All measurements were performed in quadruplicates. All graphs show mean  $\pm$  SD of at least three independent experiments. Ordinary one-way ANOVA with Bonferroni's multiple comparisons test for AGS, Unpaired t-test for NCI-N87, and Mann-Whitney test for NUGC-4 cells. \*  $p < 0.05$ , \*\*  $p < 0.01$ , \*\*\*  $p < 0.001$

### 3.3 $LT\alpha\beta^{TG}$ transgenic mice showed activation of the non-canonical NF- $\kappa$ B pathway in the stomach of mice older than one year

To analyse the influence of a stomach-specific overexpression of lymphotoxin (LT) on gastric carcinogenesis, a transgenic mouse model was generated. All the required inserts were amplified with specific primers that had additional nucleotides (overhangs) fitting to the insert before or after to perform Gibson assembly (see section 2.7.1). The construct for the new transgenic mouse model makes use of a specific promoter, the  $H^+K^+ATPase$  promoter (Figure 31). This promoter has a stomach-specific expression, more precisely it is only expressed in parietal cells in the stomach (Canfield and Levenson 1991).

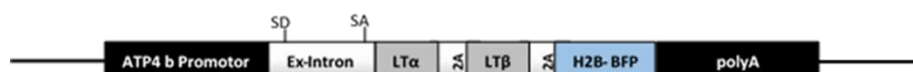


**Figure 31: Schematic illustration of the used transgene construct.**

After successful generation of the plasmid, the final construct was cut out of the vector and ligated into an overexpression plasmid to test its functionality *in vitro*. Therefore, AGS, MKN45 and CMT-93 (murine) cells were transfected with 500 and 1000 ng of plasmid DNA and screened for the expression of *BFP*, *Lta* and *Ltb* by qPCR. The expression of *Lta*, *Ltb* and BFP could be successfully demonstrated in equal levels (Figure 32).

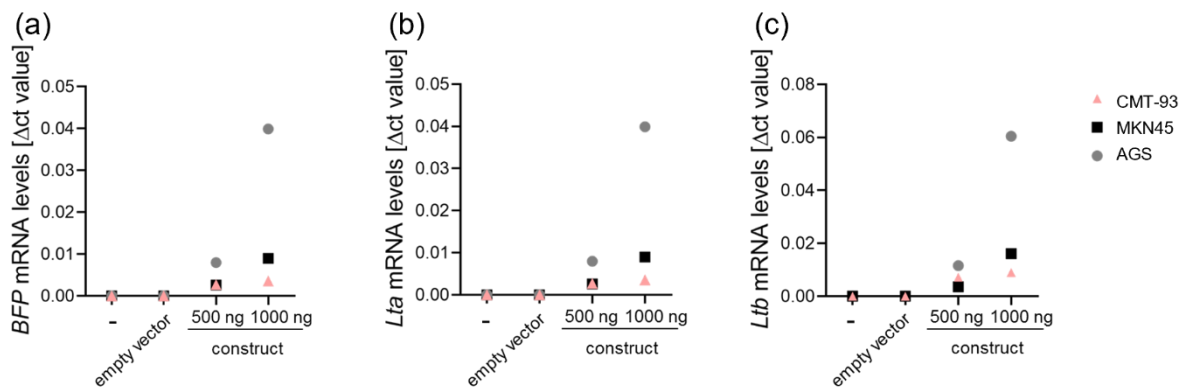


**Figure 32: In vitro testing of the generated construct for the transgenic mouse model.**

CMT-93, MKN45 and AGS cells were transfected with the empty vector, 500 or 1000 ng of plasmid DNA. mRNA expression levels of *BFP*, *Lta* and *Ltb* were screened by qPCR. *Gapdh* served as housekeeping gene. All values were normalized to *Gapdh* ( $\Delta\text{Act}$  value).

The construct was sequenced to ensure that every base was correct. Finally, the transgenic mouse was generated by inserting the construct via pronuclear injection (PNI) into fertilized eggs (performed in-house by Karin Mink) and transferred into a pseudo pregnant female C57BL/6 mouse. The offspring was tested by screening for the different inserts using specific screening primers. We could successfully generate one founder line.

### 3.3.1 Characterization of $\text{LT}\alpha\beta^{\text{TG}}$ transgenic mouse model at basal conditions

To characterize the new transgenic mouse line, organoids were generated from stomachs of wild type or  $\text{LT}\alpha\beta^{\text{TG}}$  mice and their growth was monitored over six days by taking images. The organoid size was measured by using ImageJ software after one, two, three, four and six days of seeding. The mean size of ten organoids is depicted (Figure 33). No significant difference in organoid size between wild type or  $\text{LT}\alpha\beta^{\text{TG}}$  gastric organoids could be observed.

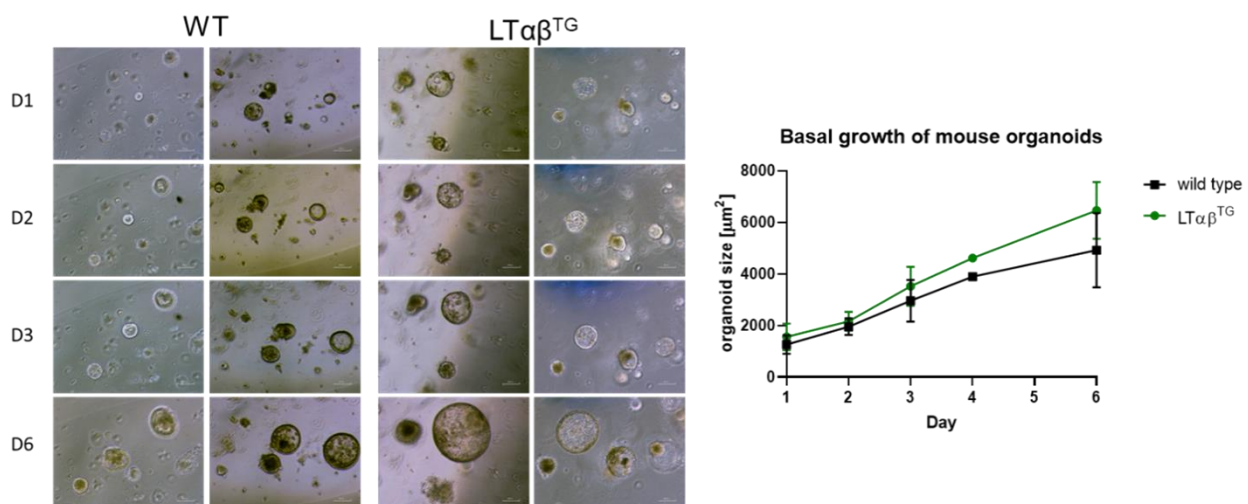


**Figure 33: Murine gastric organoids of wild type and  $\text{LT}\alpha\beta^{\text{TG}}$  transgenic mice.**

Murine gastric organoids were generated from stomachs of wild type or transgenic ( $\text{LT}\alpha\beta^{\text{TG}}$ ) mice. Images of exact the same organoids were taken one, two, three, four and six days after seeding. The organoid size was measured with the help of ImageJ software and displayed as black line wild type mice or green line indicating  $\text{LT}\alpha\beta^{\text{TG}}$  mice. Each experiment was repeated three times. Representative images of organoids generated from wild type or  $\text{LT}\alpha\beta^{\text{TG}}$  mice on day (D) one, two, three and six after seeding are shown.

Stomach specific expression of *Lta* and *Ltb* mRNA levels was tested by qPCR. Various organs of a nine week old  $LT\alpha\beta^{TG}$  mouse were checked for *Lta* and *Ltb* mRNA levels and compared to an age-matched wild type mouse. In fact, a higher *Lta* expression and a slight increase in *Ltb* mRNA expression levels could be observed in the stomach of  $LT\alpha\beta^{TG}$  mice compared to wild type mice. The other organs, except for colon, did not show differences in *Lta* and *Ltb* mRNA expression levels in the  $LT\alpha\beta^{TG}$  mouse compared to the age-matched wild type mouse (Figure 34). The higher *Lta* and *Ltb* mRNA expression levels in the colon could originate from a peyer's patch, which have very high *Lt* expression levels. The higher *Lt* expression in the colon is not due to expression of the construct since the used promoter is stomach specific and should not be active in the colon.

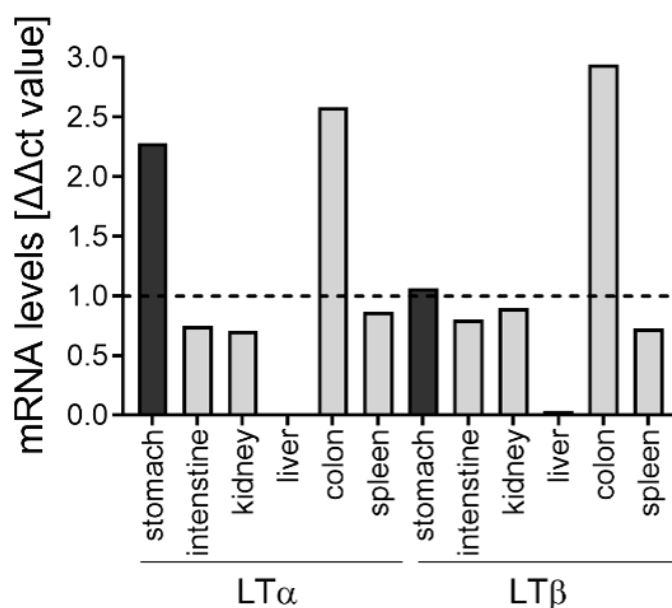


**Figure 34: Expression of *Lta* and *Ltb* in the new  $LT\alpha\beta^{TG}$  mouse model in various organs.**

RNA of stomach, intestine, kidney, liver, colon, and spleen from a nine week old transgenic and a wild type mouse were checked for *Lta* and *Ltb* mRNA expression levels. *Gapdh* was used as housekeeping gene. Values were normalized to *Gapdh* and to wild type mice ( $\Delta\Delta ct$  value).

To further characterise the transgenic mouse model, mice were sacrificed at 9, 13, 16, 20, 24, 28, 32 and 54 weeks of age. Initially, the BFP mRNA expression was tested to check for the expression levels of the construct, since the BFP is only present in the generated construct. The  $LT\alpha\beta^{TG}$  mice showed induction of BFP mRNA levels at low levels which differed over time. The highest expression of BFP mRNA levels in  $LT\alpha\beta^{TG}$  mice were observed at an age of 54 weeks (Figure 35).

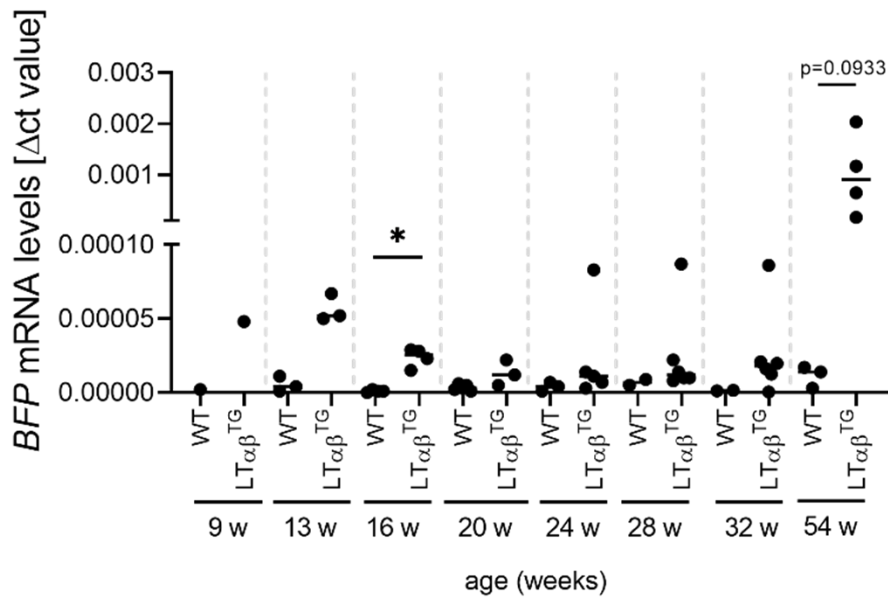


**Figure 35: BFP mRNA expression levels in stomachs of wild type (WT) or LTαβ<sup>TG</sup> mice.**

C57BL/6 wild type and LTαβ<sup>TG</sup> mice were sacrificed at different ages and RNA was isolated from stomach tissue. *BFP* mRNA levels were checked by qPCR. *Gapdh* served as housekeeping gene and was used for normalization (Δct value). Each dot represents an individual mouse. Black horizontal lines indicate median. Mann-Whitney test. \* p≤0.05, \*\* p≤0.01, \*\*\*p≤0.001

Next, *Lta* and *Ltb* mRNA expression levels were checked by qPCR. *Lta* mRNA levels were higher in LTαβ<sup>TG</sup> mice compared to wild type mice. A significant difference was detected at an age of 13 and 32 weeks (Figure 36c). In contrast, *Ltb* mRNA expression levels did not show a clear pattern. *Ltb* expression seemed to be slightly enhanced after 32 weeks but without significance. However, at an age of 54 weeks a significant increase was observed in LTαβ<sup>TG</sup> mice compared to age-matched wild type mice (Figure 36d).

To further prove the stomach specific expression of *Lta* and *Ltb*, an *in-situ* hybridization was performed in collaboration with group of Prof. Dr. Mathias Heikenwalder (DKFZ, Heidelberg) (Figure 36 a and b). Here, it could be observed that *Lta* and *Ltb* mRNA expression is slightly more seen in the stomach tissue of LTαβ<sup>TG</sup> mice compared to age-matched wild type mice as seen in Figure 36 (a and b).

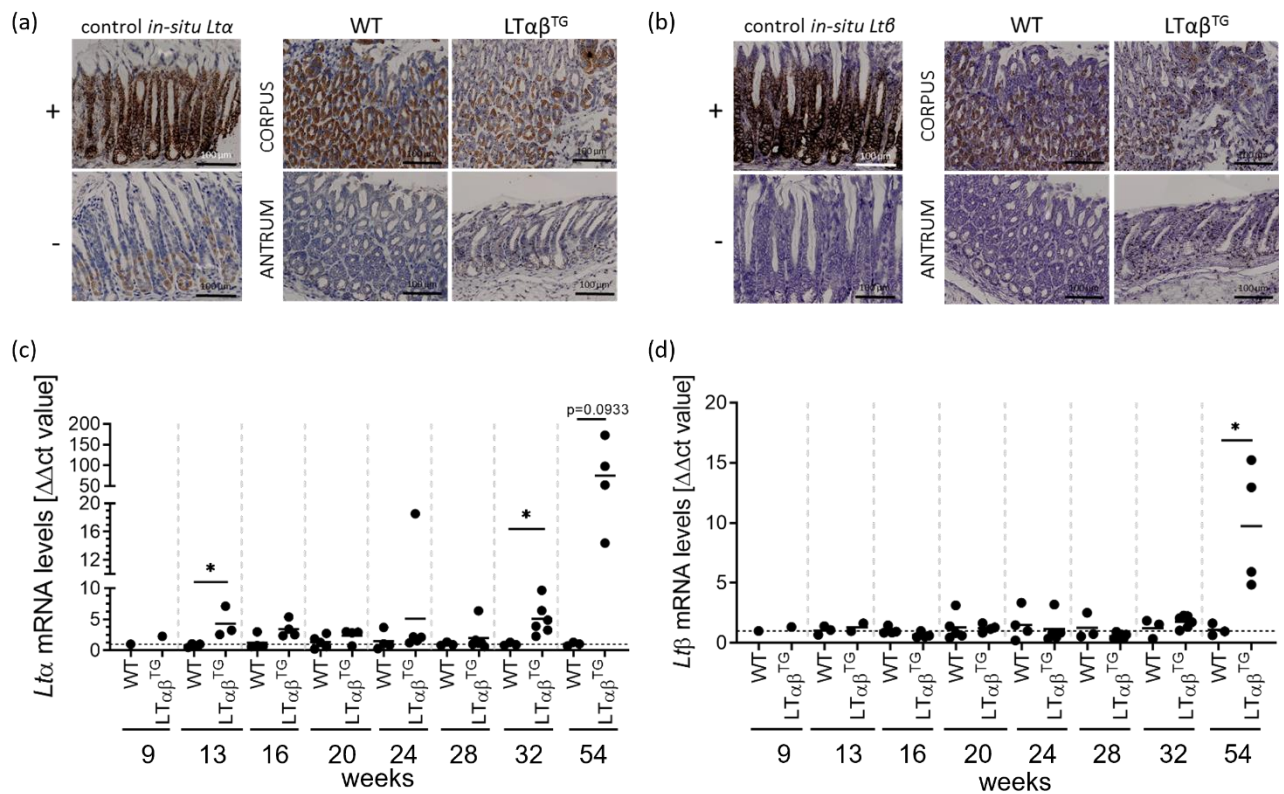


**Figure 36: *Lta* and *Ltb* expression levels in stomachs of wild type or *LTαβ<sup>TG</sup>* mice.**

(a, b) Representative images of an *in-situ* hybridization to detect *Lta* and *Ltb* in the stomach tissue of 13-week old wild type or *LTαβ<sup>TG</sup>* mice. (c, d) C57BL/6 wild type and *LTαβ<sup>TG</sup>* mice were sacrificed at different ages and RNA was isolated from stomach tissue to check for *Lta* (c) or *Ltb* (d) mRNA levels by qPCR. *Gapdh* served as housekeeping gene. All values were normalized to *Gapdh* and to wild type mice (ΔΔct value). Each dot represents an individual mouse. Black horizontal lines indicate median. Mann-Whitney test. \*  $p \leq 0.05$ , \*\*  $p \leq 0.01$ , \*\*\*  $p \leq 0.001$

As a next step, *Cxcl13* and *cmyc* mRNA levels were tested by qPCR. CXCL13 is a target gene of non-canonical NF- $\kappa$ B pathway important for organization of secondary lymphoid organs playing a role in the formation and maintenance of T/B cell zones (Sun 2012). CMYC is involved in regulating cell proliferation (Dang et al. 1999). No significant differences in *Cxcl13* mRNA expression were observed between wild type and *LTαβ<sup>TG</sup>* mice up to 32 weeks of age. Interestingly, induction of *Cxcl13* mRNA levels were observed in *LTαβ<sup>TG</sup>* compared to age-matched wild type mice after 54 weeks (Figure 37a). No differences in *cmyc* expression were detected in the stomach of *LTαβ<sup>TG</sup>* mice compared to age-matched wild type mice (Figure 37b).

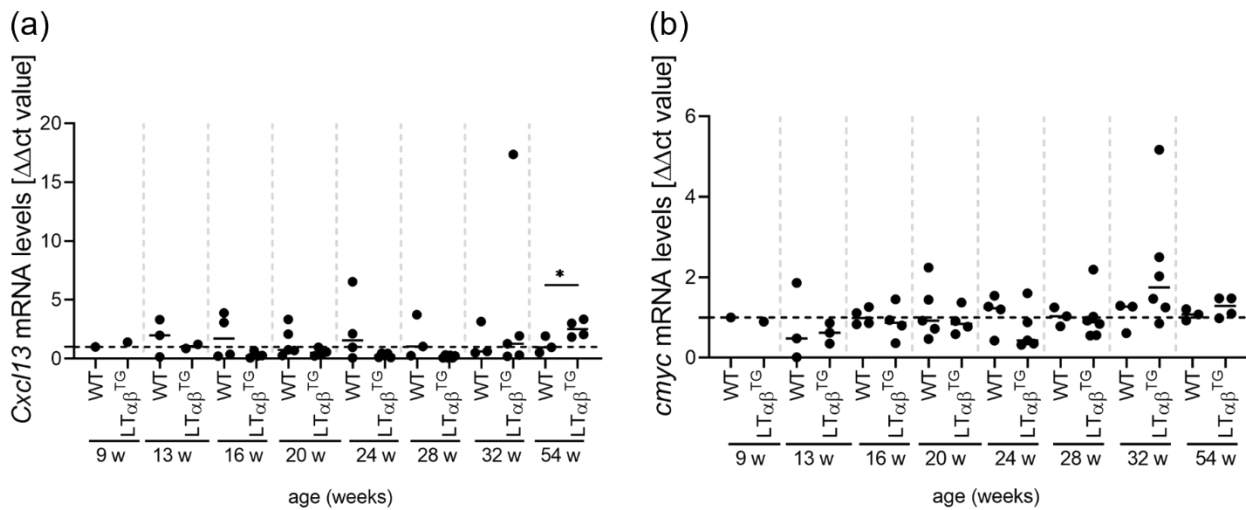


**Figure 37: *Cxcl13* and *cmyc* mRNA expression levels in stomachs of wild type or  $LT\alpha\beta^{TG}$  mice.**

C57BL/6 wild type and  $LT\alpha\beta^{TG}$  mice were sacrificed at different ages and RNA was isolated from stomach tissue to check for (a) *Cxcl13* or (b) *cmyc* mRNA levels by qPCR. *Gapdh* served as housekeeping gene. All values were normalized to *Gapdh* and to wild type mice ( $\Delta\Delta ct$  value). Each dot represents an individual mouse. Black horizontal lines indicate median. Mann-Whitney test. \*  $p \leq 0.05$ , \*\*  $p \leq 0.01$ , \*\*\*  $p \leq 0.001$

To confirm activation of the non-canonical NF- $\kappa B$  pathway in 54-week old  $LT\alpha\beta^{TG}$  mice, stomach tissue sections were stained for NF- $\kappa B2$  and nuclear  $p52^+$  cells were counted. No difference in number of  $p52^+$  cells was seen in 54-week old  $LT\alpha\beta^{TG}$  mice compared to age-matched wild type mice (Figure 38).

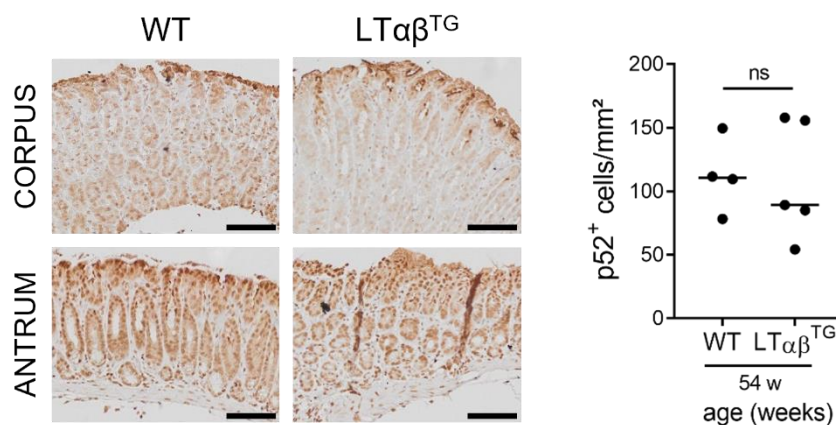


**Figure 38: NF- $\kappa B2$  staining and quantification of  $p52^+$  cells in stomachs of 54-week old wild type or  $LT\alpha\beta^{TG}$  mice.**

C57BL/6 wild type and  $LT\alpha\beta^{TG}$  mice were sacrificed at an age of 54 weeks and stomach tissue was stained for NF- $\kappa B2$  to check for activation of the non-canonical NF- $\kappa B$  by immunohistochemistry. Quantification was performed by counting five individual areas of the stomach section. Each dot represents an individual mouse. Black horizontal lines indicate median. Mann-Whitney test. \*  $p \leq 0.05$ , \*\*  $p \leq 0.01$ , \*\*\*  $p \leq 0.001$

Next, the general structure of the stomach tissue of  $LT\alpha\beta^{TG}$  mice was analysed on HE sections. No differences in the stomach tissue architecture or length of gastric glands of  $LT\alpha\beta^{TG}$  mice compared to age-matched wild type mice could be seen (Figure 40). Gastric epithelial proliferation was investigated by staining stomach tissue for Ki67 of  $LT\alpha\beta^{TG}$  mice or age-matched wild type mice (Figure 40).

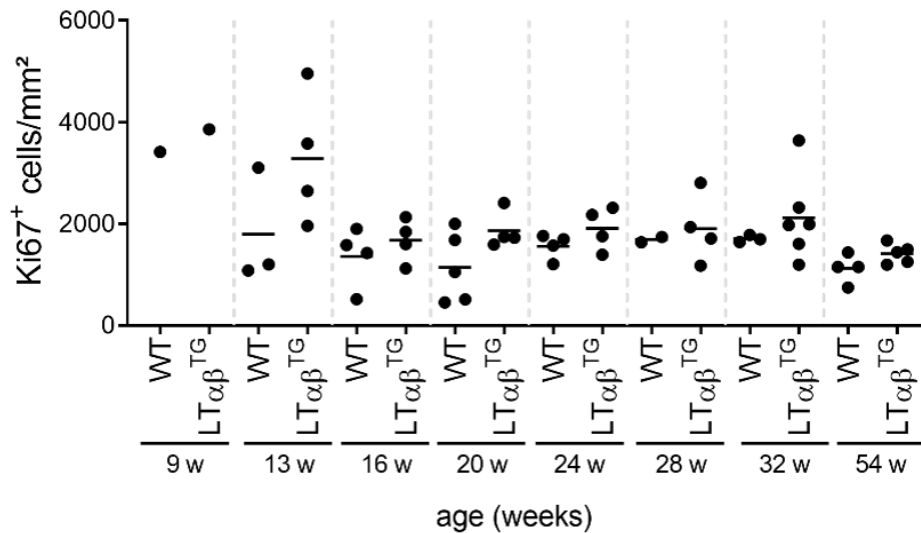


**Figure 39: Quantification of Ki67 positive cells in the stomachs of wild type or LTαβTG mice.**

C57BL/6 wild type and LTαβTG mice were sacrificed at different ages and stomach tissue was stained for Ki67 to check for proliferating cells by immunohistochemistry. Quantification was performed by counting five individual areas of the stomach section. Each dot represents an individual mouse. Black horizontal lines indicate median. Mann-Whitney test. \*  $p \leq 0.05$ , \*\*  $p \leq 0.01$ , \*\*\*  $p \leq 0.001$

A slight trend towards increased proliferation could be observed at an age of 13 and 32 weeks but without significance (Figure 39). Representative images of stomach sections stained for HE and Ki67 of wild type or LTαβTG mice at all time points are shown in Figure 40.

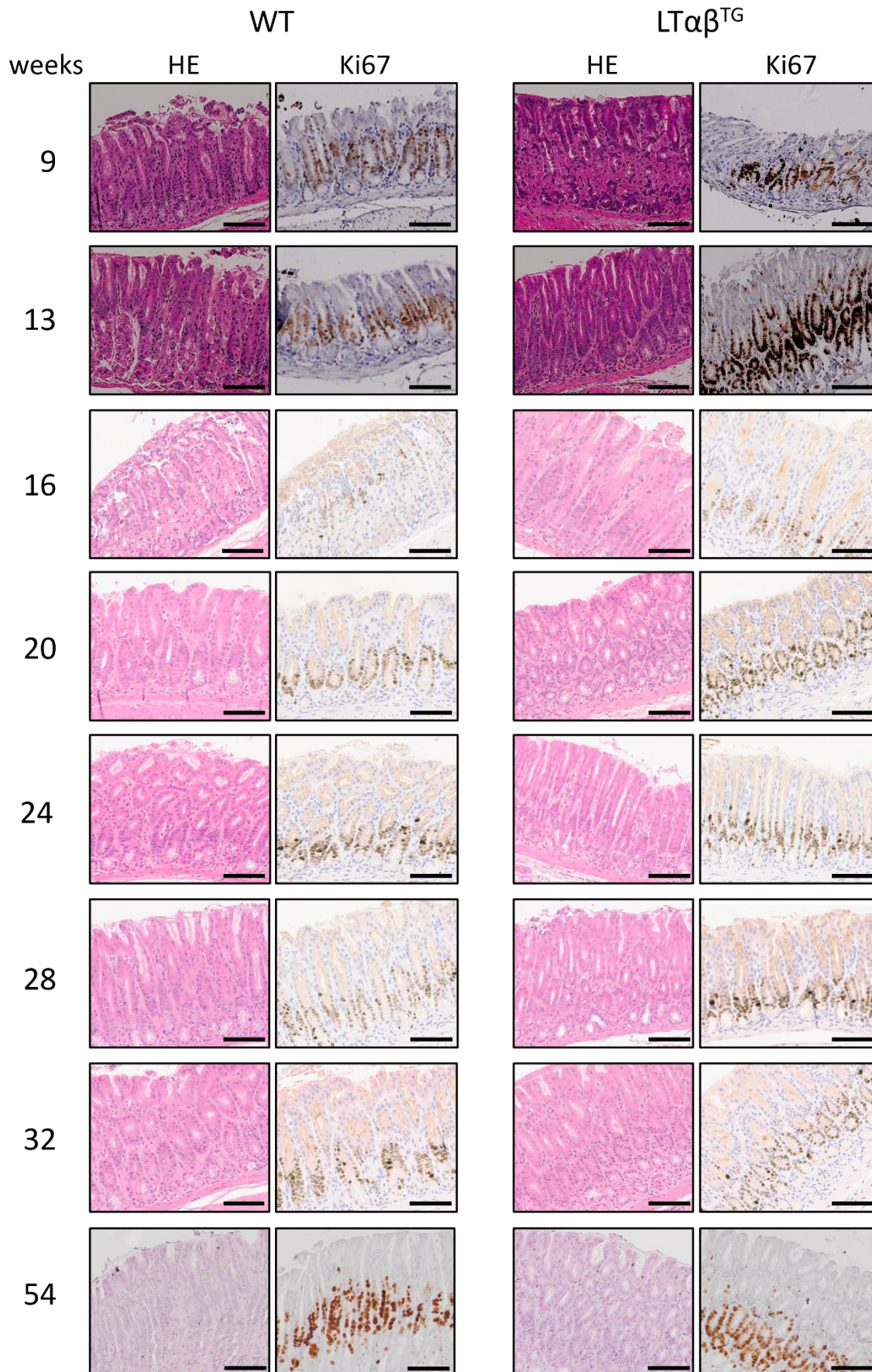


**Figure 40: Stomach samples of wild type or LT $\alpha\beta$ <sup>TG</sup> mice stained for HE and proliferating cells (Ki67).**

C57BL/6 wild type and LT $\alpha\beta$ <sup>TG</sup> mice were sacrificed at different ages and stomach tissue was stained for HE and Ki67 to check for proliferating cells by immunohistochemistry. Representative images of stomach tissue stained for HE and Ki67 of each time point are shown. Scale bar: 100  $\mu$ m.

As mentioned before, the non-canonical NF- $\kappa$ B pathway is a key player in T and B cell development as well as in inflammatory responses or maintenance (Sun 2012; Taniguchi and Karin 2018). Consequently, we examined whether the stomach specific LT expression in  $LT\alpha\beta^{TG}$  mice influenced the recruitment of immune cells to the stomach. The stomach tissue of  $LT\alpha\beta^{TG}$  mice and age-matched wild type mice was stained for macrophages (F4/80), B cells (B220) and T cells (CD3) by immunohistochemistry (in collaboration with Prof. Dr. Mathias Heikenwalder (DKFZ, Heidelberg)). No difference on infiltrating immune cells between  $LT\alpha\beta^{TG}$  and age-matched wild type mice could be observed at any time point investigated (Figure 41). Overall, the generated  $LT\alpha\beta^{TG}$  mouse line seems to be a low expresser of the construct, since the *BFP* levels were varying over time, and only at older age significantly elevated expression levels of *Lt $\alpha$*  and *Lt $\beta$*  mRNA could be observed.

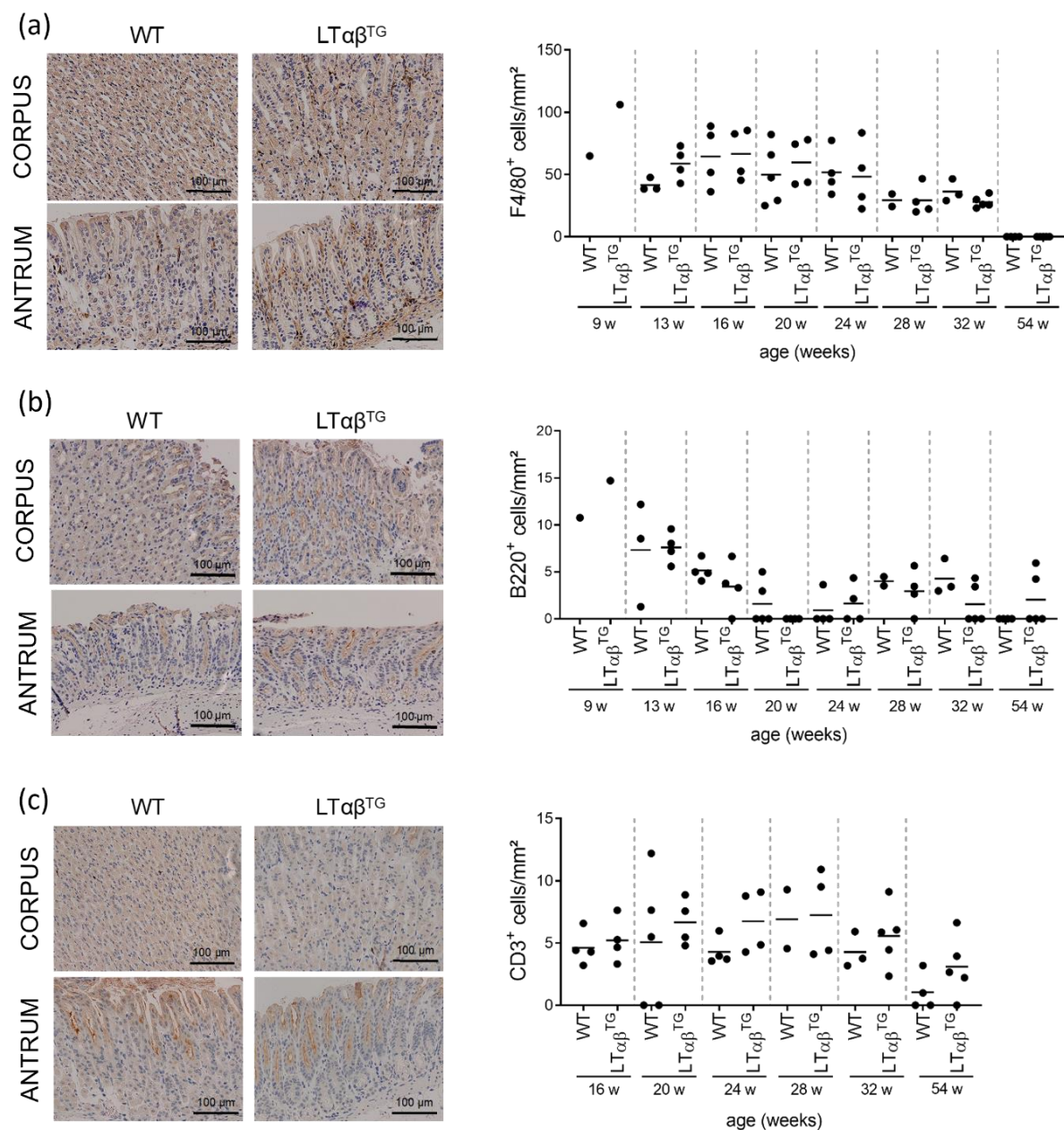


**Figure 41: Staining and quantification of infiltrating immune cells in the stomach of wild type or  $LT\alpha\beta^{TG}$  mice.**

C57BL/6 wild type and  $LT\alpha\beta^{TG}$  mice were sacrificed at different ages and stomach tissue was stained for macrophages (F4/80), B cells

(B220) and T cells (CD3) by immunohistochemistry. Representative images of stomach tissue stained for (a) macrophages, (b) B cells and (c) T cells are shown on the left side. Scale bar: 100  $\mu$ m. Right side represents the quantification of five areas per tissue. Each dot represents an individual mouse. Black horizontal lines indicate median. Mann-Whitney test. \*  $p \leq 0.05$ , \*\*  $p \leq 0.01$ , \*\*\*  $p \leq 0.001$

### 3.3.2 Constitutive activation of non-canonical NF- $\kappa$ B pathway in combination with *H. pylori* infection results in an increased T cell infiltration in the stomach.

To examine the joint contribution of stomach-specific lymphotoxin expression and *H. pylori* infection, six-week old  $LT\alpha\beta^{TG}$  mice and C57BL/6 wild type mice were infected with PMSS1 *H. pylori* strain for 24 weeks. First, colony forming units (CFUs) were assessed to confirm that the mice were successfully infected (Figure 42a). As the spleen is an important organ for B and T cell maturation, which is influenced by NF- $\kappa$ B signaling and infection (Hayden and Ghosh 2011), the spleen weight was determined (not normalized to body weight); however, no difference could be observed between transgenic mice or wild type mice.

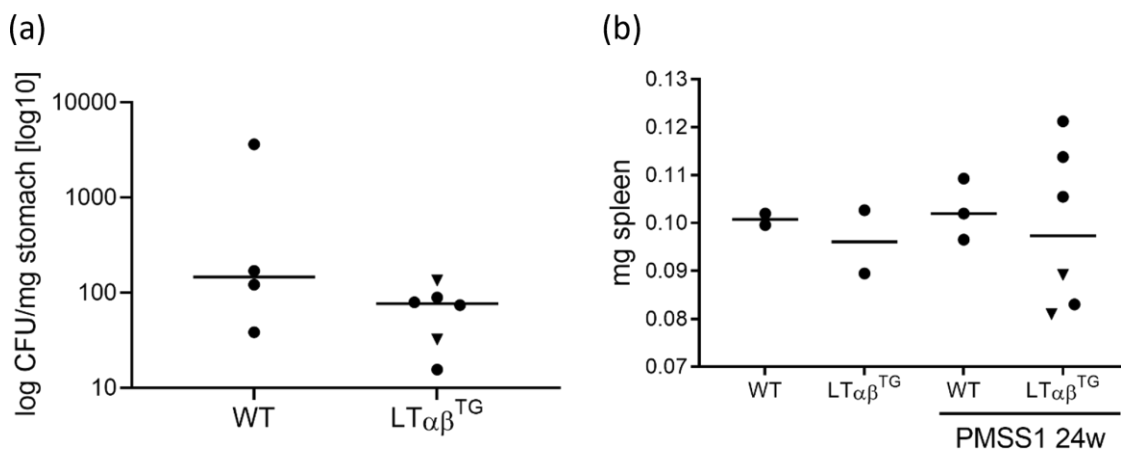


**Figure 42: CFU and spleen weight of uninfected as well as infected  $LT\alpha\beta^{TG}$  and age-matched wild type mice.**

C57BL/6 wild type and  $LT\alpha\beta^{TG}$  mice were infected with PMSS1 *H. pylori* strain for 24 weeks. (a) CFU/mg stomach was estimated of infected C57BL/6 wild type and  $LT\alpha\beta^{TG}$  mice. (b) Spleen weight of control as well as infected mice was checked. Each dot (male)/triangle (female) represents an individual mouse. Black horizontal lines indicate median. Mann-Whitney test. \*  $p \leq 0.05$ , \*\*  $p \leq 0.01$ , \*\*\*  $p \leq 0.001$

No marked pathologies resulting from the combined effect of lymphotoxin expression and *H. pylori* infection in the stomach tissue of infected  $LT\alpha\beta^{TG}$  mice compared to infected wild type mice were observed (Figure 43). All infected  $LT\alpha\beta^{TG}$  mice showed a very mild intraepithelial lymphocytosis, while this was only observed in two out of four infected wild type mice.

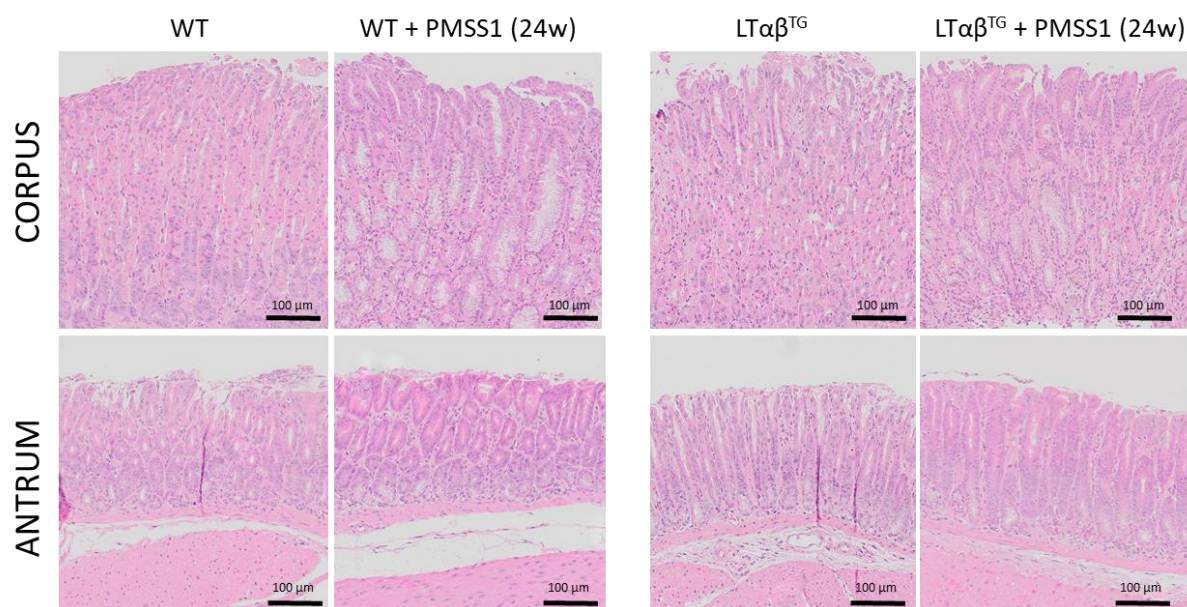


**Figure 43: Hematoxylin and eosin stained stomach tissue of uninfected and infected mice.**

C57BL/6 wild type and  $LT\alpha\beta^{TG}$  mice were infected with PMSS1 *H. pylori* strain for 24 weeks. Hematoxylin and eosin staining was performed as described in section 2.11.

Next, mRNA expression of *Lta*, *Ltb* and target genes of the canonical as well as non-canonical NF- $\kappa$ B pathway were investigated. *Lta* mRNA expression was highly induced in infected  $LT\alpha\beta^{TG}$  mice compared to infected wild type mice (Figure 44a). Similar effects were seen when checking *Ltb* mRNA expression (Figure 44b). *A20* mRNA levels were induced upon infection, however, no difference between the two different mouse models could be observed (Figure 44c). No difference in *Cxcl13* and *Ccl2* mRNA expression levels could be observed independent of infection status or mouse background (Figure 44 d and f). *Cxcl10* mRNA expression was enhanced upon *H. pylori* infection and even more elevated in infected  $LT\alpha\beta^{TG}$  mice (Figure 44e). The higher *Lta*, *Ltb*, *A20* and *Cxcl10* expression seemed to be gender specific, as infected female  $LT\alpha\beta^{TG}$  mice (black triangle) showed higher mRNA expression levels compared to infected male  $LT\alpha\beta^{TG}$  mice (black dots).

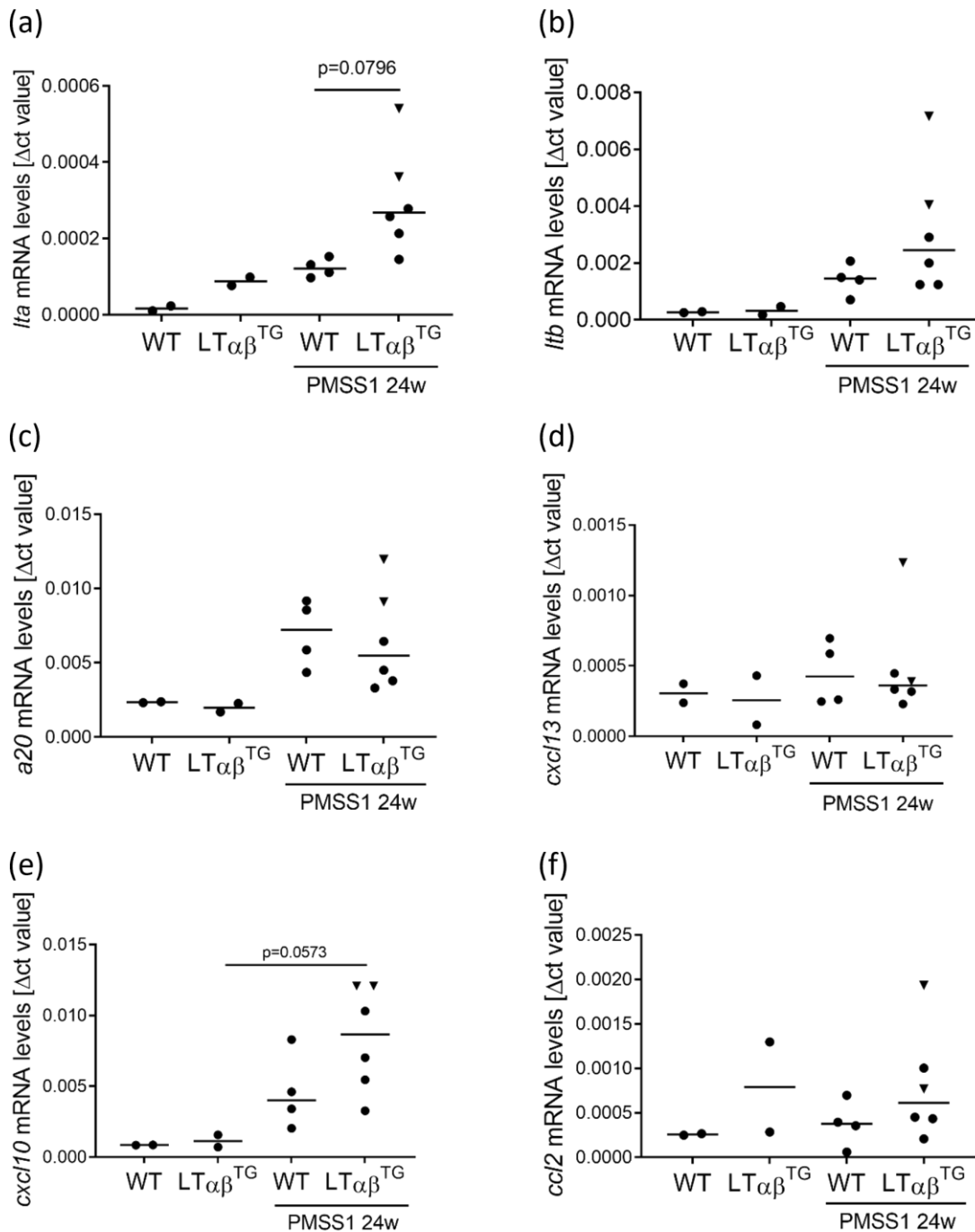


**Figure 44: mRNA expression levels of *Lta*, *Ltb* and NF- $\kappa$ B target genes upon *H. pylori* infection of  $LT\alpha\beta^{TG}$  and wild type mice.**

C57BL/6 wild type and  $LT\alpha\beta^{TG}$  mice were infected with PMSS1 *H. pylori* strain for 24 weeks. (a) *Lta*, (b) *Ltb*, (c) *A20*, (d) *Cxcl13*, (e) *Cxcl10* and (f) *Ccl2* mRNA levels were investigated in the stomach tissue by qPCR. *Gapdh* was used as housekeeping gene and for normalization ( $\Delta\text{ct}$  value). Each dot (male)/triangle (female) represents an individual mouse. Black horizontal lines indicate median. Mann-Whitney test. \*  $p \leq 0.05$ , \*\*  $p \leq 0.01$ , \*\*\*  $p \leq 0.001$

To check for successful infection, the mRNA levels of the murine IL-8 homolog *Kc* were screened. *Kc* mRNA levels were increased but independent of the genetic background of the mice used for infection (Figure 45a). Gastric proliferation was investigated by examining the *cmyc* mRNA levels via qPCR and staining stomach tissue for Ki67 positive cells. Gastric proliferation seemed to be slightly higher in infected  $LT\alpha\beta^{TG}$  mice compared to wild type mice but without significance (Figure 45 b and c).

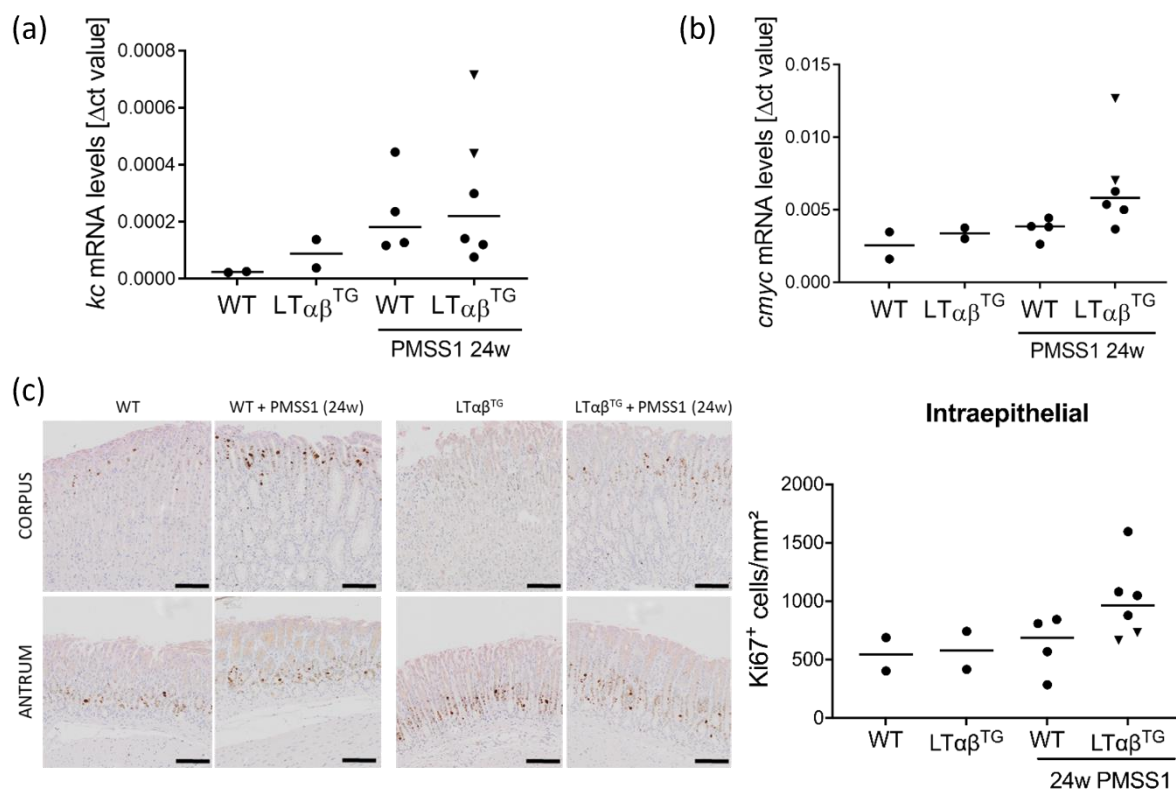


**Figure 45: *Kc* mRNA expression and gastric proliferation upon *H. pylori* infection.**

C57BL/6 wild type and  $LT\alpha\beta^{TG}$  mice were infected with PMSS1 *H. pylori* strain for 24 weeks. (a) *Kc* and (b) *cmyc* mRNA levels were examined in the stomach tissue by qPCR. *Gapdh* was used as housekeeping gene and values were normalized to *Gapdh* ( $\Delta$ ct value). (c) Stomach tissue was stained for Ki67 positive cells. Representative images of stomach tissue stained for proliferating cells (Ki67+) are shown on the left side. Scale bar: 100  $\mu$ m. Right side represents the quantification of five areas per tissue. Each dot (male)/triangle (female) represents an individual mouse. Black horizontal lines indicate median. Mann-Whitney test. \*  $p \leq 0.05$ , \*\*  $p \leq 0.01$ , \*\*\*  $p \leq 0.001$

Finally, stomach tissue was stained to analyse infiltrating immune cells. A trend towards a higher number of macrophages and B cells could be observed upon *H. pylori* infection independent of the genetic background of mice used (Figure 46 a and b). However, a significant higher number of infiltrating CD3<sup>+</sup> T cells was observed in infected  $LT\alpha\beta^{TG}$  mice compared to infected wild type mice (Figure 46c). *H. pylori* is known to induce a mixed T helper (Th)<sub>17</sub>/Th<sub>1</sub> T cell response in infected individuals by inducing the expression of cytokines such as IL17a (Th<sub>17</sub>) and *Ifng* (Th<sub>1</sub>) (Shi et al. 2010; Bhuiyan et al. 2014). Therefore, we checked *Ifng* and *Il17a* mRNA levels which seemed to be elevated upon infection but independent of the genetic background of the mice (Figure 46 d and e). *Ifng* seemed to be more prominent in female infected  $LT\alpha\beta^{TG}$  mice compared to male infected  $LT\alpha\beta^{TG}$  mice (Figure 46d). Regulatory T cell induction was unchanged upon infection, or the genetic background as seen by *Foxp3* mRNA levels (Figure 46f).

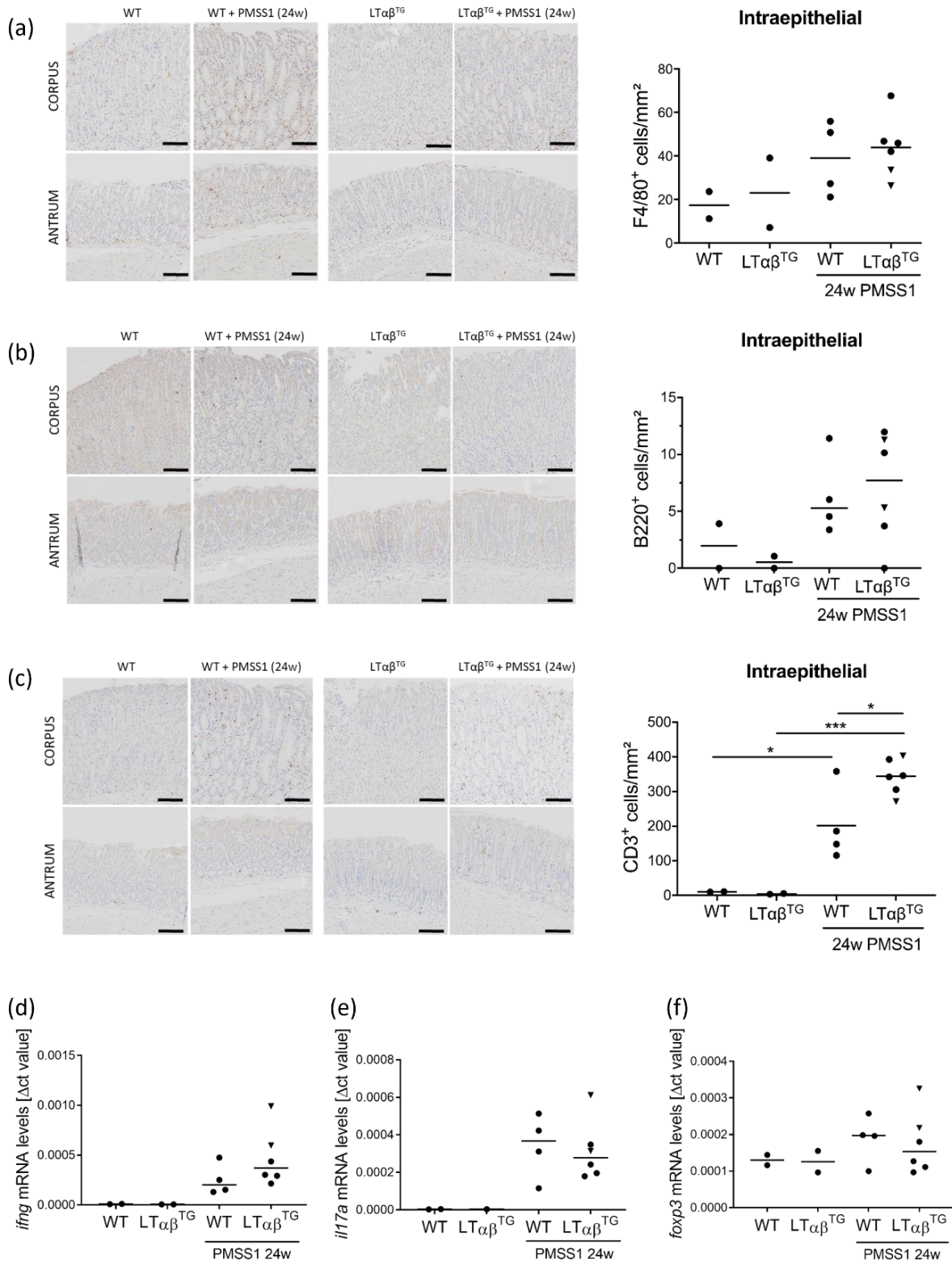


**Figure 46: Immune cell infiltration upon *H. pylori* infection of  $LT\alpha\beta^{TG}$  and age-matched wild type mice.**

C57BL/6 wild type and  $LT\alpha\beta^{TG}$  mice were infected with PMSS1 *H. pylori* strain for 24 weeks and stomach tissue was stained for (a) macrophages (F4/80), (b) B cells (B220) and (c) T cells (CD3) by immunohistochemistry. Representative images of stomach tissue are shown on the left side. Scale bar: 100  $\mu$ m. Right side represents the quantification of five areas per tissue. (d) *Ifng*, (e) *Il17a* and (f) *Foxp3* mRNA levels were examined in the stomach tissue by qPCR. *Gapdh* was used as housekeeping gene and values were normalized to *Gapdh* ( $\Delta$ ct value). Each dot (male)/triangle (female) represents an individual mouse. Black horizontal lines indicate median. Mann-Whitney test. \*  $p \leq 0.05$ , \*\*  $p \leq 0.01$ , \*\*\*  $p \leq 0.001$

The joint effect of stomach-specific LT expression and *H. pylori* infection elevates *Lta* mRNA expression, induces higher *Cxcl10* mRNA levels resulting in higher number of infiltrating CD3<sup>+</sup> T cells,

although, without leading to pathologies.

### **3.4 Stimulation of human gastric organoids with ligands activating the non-canonical NF- $\kappa$ B pathway results in enhanced growth of corpus as well as antrum organoids.**

The NF- $\kappa$ B pathway is essential for inflammatory responses, and chronic inflammation is tightly linked to the development as well as progression of cancer (Taniguchi and Karin 2018). LT $\beta$ R signaling axis is known to be involved in development and maintenance of lymphoid organs, regulation of innate and adaptive immunity, inflammation, and tissue homeostasis (Fernandes et al. 2016). Activity of LT $\beta$ R has been seen in various solid tumors with pro- and anti-tumorigenic effect resulting in tumor growth, angiogenesis, metastasis or led to anti-tumor immune response (Wolf et al. 2010).

To explore whether stimulation of primary cells with ligands (LIGHT or LT $\alpha_1\beta_2$ ) activating the non-canonical NF- $\kappa$ B pathway via the LT $\beta$ R induces changes in the cellular behaviour, we generated human gastric organoids from fresh human stomach biopsies. Organoid growth was monitored by taking pictures every other day and the size of the organoids was measured by using ImageJ. From each patient a biopsy from the corpus as well as the antrum of the stomach was taken. A representative image of antral and corpus organoids is shown in Figure 47a. Some of the antral organoids stimulated with LIGHT (blue line) or LT $\alpha_1\beta_2$  (orange line) showed a significant increase in growth upon day six of treatment compared to unstimulated organoids (Figure 47b). A subgroup of corpus organoids showed a slightly enhanced growth on day six after stimulation but without significance (Figure 47c). In total, a significant increase of organoid size in a subset of patients could be observed compared to the unstimulated organoids (Figure 47 d and e). *H. pylori* negative patients are indicated with grey dots and *H. pylori* positive patients are indicated in black dots (Figure 47 d and e). However, the *H. pylori* status showed no correlation to the treatment response.

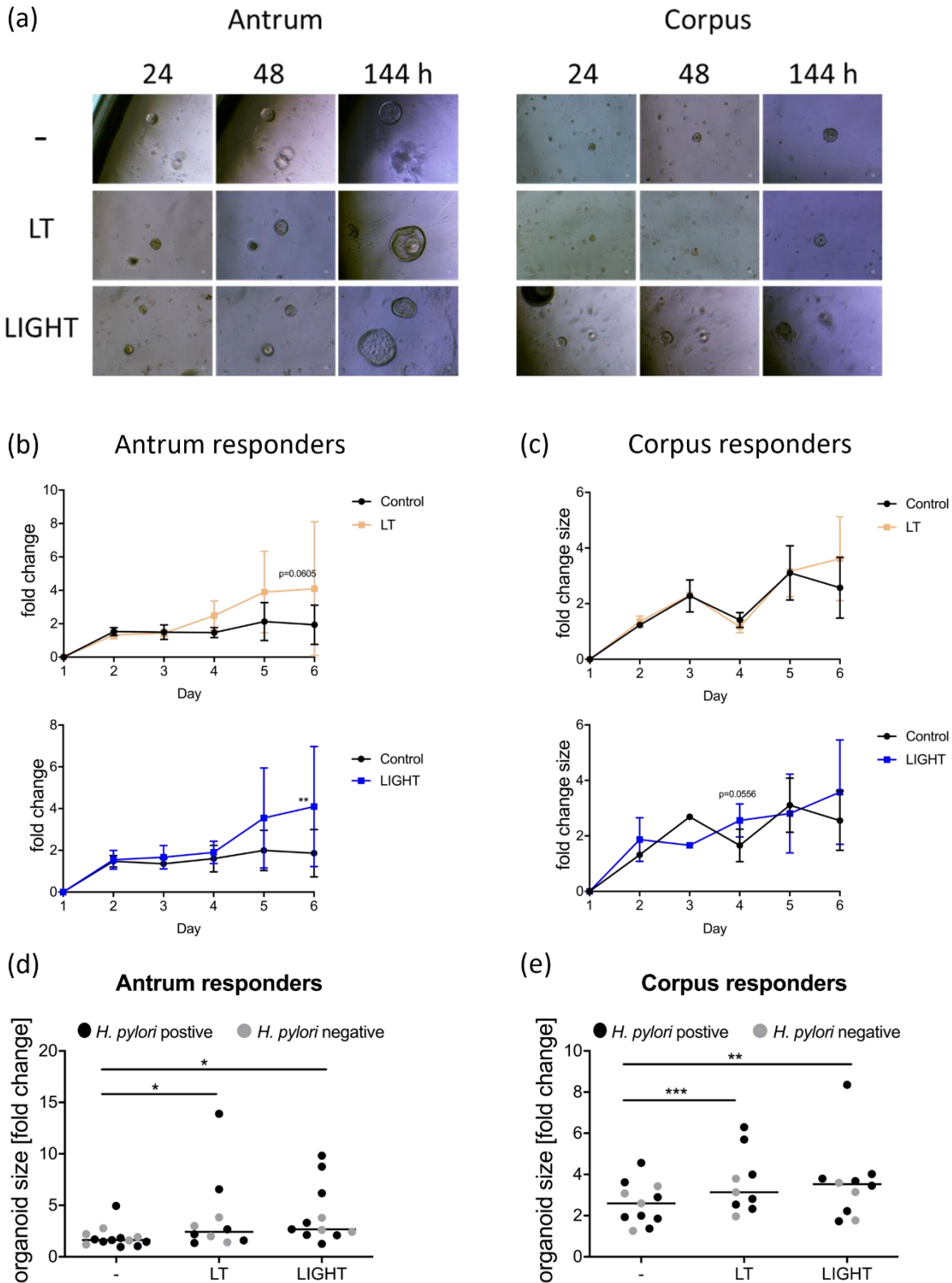


**Figure 47: Responsive human gastric organoids stimulated with LT or LIGHT.**

Gastric organoids were generated from antrum or corpus tissue and stimulated with LT or LIGHT for six days. Everyday images of the same organoids were taken, and organoid size was measured by using ImageJ. (b, c) Timeline of organoid growth is depicted and size was normalized to organoid size of day one post seeding. Orange line indicates LT treated samples and blue line indicates LIGHT stimulated organoids. (d, e) Organoid size of day six is normalized to size on day one post seeding. Grey dots indicated *H. pylori* negative samples and black dots indicated *H. pylori* positive samples. Mann-Whitney test for b and c. \*  $p \leq 0.05$ , \*\*  $p \leq 0.01$ . One sample t test for d and e. \*  $p \leq 0.05$ , \*\*  $p \leq 0.01$ , \*\*\*  $p \leq 0.001$

In a subset of patient samples, no enhanced growth through the ligand stimulation could be

observed. A representative image of antral and corpus organoids over time is shown in Figure 48a. In a subset of patients, corpus organoids stimulated with LT seemed to grow smaller compared to unstimulated organoids (Figure 48e). Again, the *H. pylori* status of the samples was not influencing the treatment outcome (Figure 48 d and e).

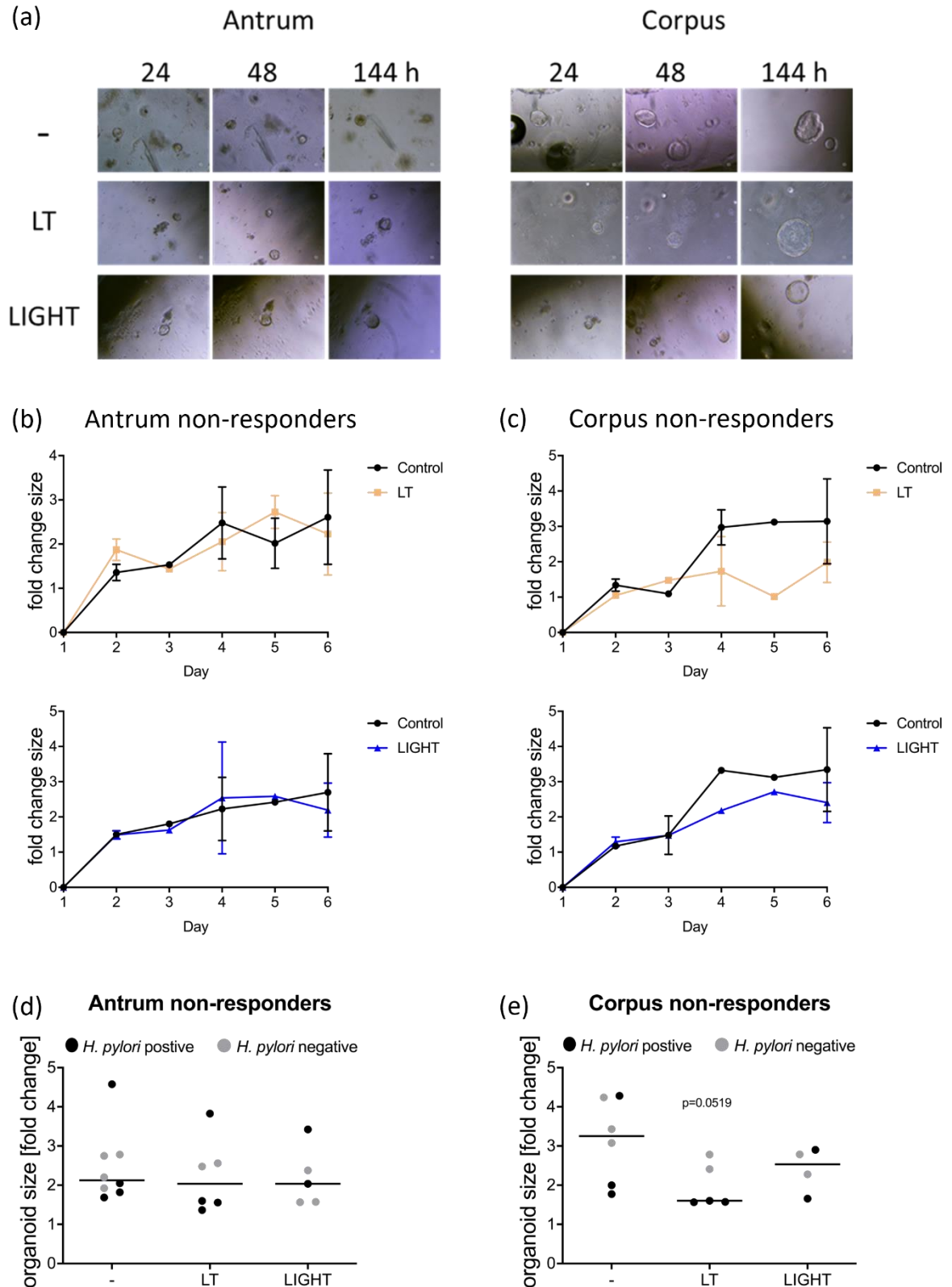


**Figure 48: Non-responsive human gastric organoids stimulated with LT or LIGHT.**

Gastric organoids were generated from antrum or corpus tissue and stimulated with LT or LIGHT for six days. Everyday images of the same organoids were taken, and organoid size was measured by using ImageJ. (b, c) Timeline of organoid growth is depicted and size

was normalized to organoid size of day one post seeding. Orange line indicates LT treated samples and blue line indicates LIGHT stimulated organoids. (d, e) Organoid size of day 6 is normalized to size on day one post seeding. Grey dots indicated *H. pylori* negative samples and black dots indicated *H. pylori* positive samples. Mann-Whitney test for b and c. \*  $p \leq 0.05$ , \*\*  $p \leq 0.01$ , \*\*\*  $p \leq 0.001$ . One sample t test for d and e: \*  $p \leq 0.05$ ; \*\*  $p \leq 0.01$ ; \*\*\*  $p \leq 0.001$ .

Further characterization is needed to examine the differences between responders and non-responders and determine whether different levels of pathway activation or receptor expression are affecting the treatment outcome.

## 4 Discussion and Conclusion

The  $LT\alpha_1\beta_2$ /LIGHT- $LT\beta R$  signaling plays an essential role in the innate/adaptive immunity by controlling the development, homeostasis, and organization of lymphoid organs and tissues (Fernandes et al. 2016). Hence, its deregulation results in autoimmunity, inflammatory diseases, and inflammation-induced cancers (Bauer et al. 2012; Fernandes et al. 2016). Little data addressing the specific influence of the  $LT\alpha_1\beta_2$ /LIGHT- $LT\beta R$  signaling axis in gastric carcinogenesis are available. Previous work showed that during *H. pylori*-induced inflammation, the non-canonical NF- $\kappa B$  pathway is activated in a secondary loop after initial T4SS-induced activation of the canonical NF- $\kappa B$  signaling (Mejías-Luque et al. 2017). Activation of the non-canonical NF- $\kappa B$  via  $LT\beta R$  worsened the *H. pylori*-induced gastric inflammation (Mejías-Luque et al. 2017). The link of non-canonical NF- $\kappa B$  favouring gastric diseases was further supported by a study in MyD88-deficient mice showing aberrant activation of the pathway accompanied by an increased expression of *Cxcl9* and *Icam1* which led to a strong T cell infiltration in the stomach upon *H. felis* infection (Mejías-Luque et al. 2019). The increased gastric pathologies observed in MyD88-deficient mice upon infection were induced via increased levels of LIGHT activating the non-canonical NF- $\kappa B$  pathway (Mejías-Luque et al. 2019).

The current study further analysed whether the non-canonical NF- $\kappa B$  pathway is involved in gastric carcinogenesis. The non-canonical NF- $\kappa B$  pathway is involved in gastric homeostasis since enhanced activity influenced cell proliferation, a requirement for tumor development, and in combination with infection, a stronger immune response was induced.

GC represents a global health burden favoured by *H. pylori* infection, host genetics, nutrition, and environmental factors (Petryszyn et al. 2020). During *H. pylori*-induced inflammation, various signaling pathways are activated, such as the NF- $\kappa B$  pathway (Mejías-Luque et al. 2017). *H. pylori* expresses different adhesion molecules and virulence factors that were already tested for their impact on activating the non-canonical NF- $\kappa B$  pathway (Mejías-Luque et al. 2017). A functional cagPAI was found to be necessary since bacteria lacking CagE, CagF, CagI, or a functional T4SS (SS1) induced less processing of p100 to p52 in gastric epithelial cells (Mejías-Luque et al. 2017). Moreover, peptidoglycan was suggested to activate the non-canonical NF- $\kappa B$  pathway (Mejías-Luque et al. 2017). However, the involvement of HopQ was not assessed. Here, it was observed that HopQ-CEACAM interaction is not only essential for adhesion, IL8 secretion, and CagA translocation as described before (Königer et al. 2016; Javaheri et al. 2016), but it also plays an important role in

activating the non-canonical NF- $\kappa$ B pathway. In addition, HopQ engagement to CEACAM receptors induced the expression of ligands activating the non-canonical NF- $\kappa$ B pathway as well as pro-inflammatory chemokines (CXCL10, CCL2). These observations are in line with a recent study showing that lack of HopQ induces less activation of the non-canonical NF- $\kappa$ B pathway by reduced expression of NIK and p-p100 (Maubach et al. 2020). In the same study, a single knockdown of CEACAM1, 5, or 6 by siRNA to about 20 percent endogenous expression was not efficient in interrupting the activation of the signaling pathway (Maubach et al. 2020). This may indicate that other CEACAMs are compensating for the loss of a single knockdown, as shown by Tegtmeyer et al.. In this study, the restoration of CEACAM1 or 5 in AZ-521 GC cells, which lack endogenous CEACAMs, was sufficient to induce injection and phosphorylation of *H. pylori's* CagA (Tegtmeyer et al. 2019). In the present study, different cell lines with varying levels of CEACAM were used to confirm that the interaction of HopQ-CEACAM is essential for the activation of the non-canonical NF- $\kappa$ B pathway and NF- $\kappa$ B target gene expression in GC cells. Here, it must be emphasized that cancer cells are transformed cells showing altered signaling compared to healthy or normal tissue. For this reason, primary cells derived from the stomach of C57BL/6<sup>hCEACAM1+/mouse CEACAM1-</sup> were used to explore the interaction *in vivo*. In these primary murine gastric cells, a positive correlation of *CEACAM1* and *Ltb* expression upon infection with wild type bacteria was observed, supporting the importance of HopQ-CEACAM interaction for the pathway activation.

In healthy human gastric tissue, no *CEACAM1* expression is observed (Shi et al. 2014). In contrast, in gastric adenocarcinoma, *CEACAM1* upregulation was observed, which might influence tumor angiogenesis (Shi et al. 2014; Guo et al. 2012). *CEACAM1* is involved in various physiological processes such as cell-cell adhesion, apoptosis, morphogenesis, angiogenesis, proliferation, cell motility, fibrosis, and immune T cell tolerance (Kim et al. 2019; Gray-Owen and Blumberg 2006; Pavlopoulou and Scorilas 2014). In humans, 11 different splice variants of *CEACAM1* have been detected, varying in their number of extracellular Ig-like domains, membrane anchor and/or length of C terminal tail (Gray-Owen and Blumberg 2006). The different cytoplasmic and transmembrane domains generated via exon splicing in *CEACAM1* have specific effects on the cellular response upon binding (Gray-Owen and Blumberg 2006). While some isoforms, including those with a long cytoplasmic tail that have two immunoreceptor tyrosine-based inhibitory motifs (ITIMs), transmit an inhibitory signal, isoforms with a short C terminal tail lack ITIMs but contain sequences that interact with the cytoskeleton such as calmodulin, tropomyosin, and actin (Gray-Owen and Blumberg 2006). Voges et al. showed that several bacterial pathogens are selectively associated with human *CEACAM1*, but not other mammalian *CEACAM1* orthologues, and have co-evolved with

their host to adhere to the epithelium for colonization (Voges et al. 2010). For instance, *Neisseria gonorrhoeae* and *N. meningitidis* engage via colony opacity-associated (Opa) proteins or *Haemophilus influenzae* interact with its outer membrane protein P5 or P1 to human CEACAM1 promoting its colonization (Voges et al. 2010; Tchoupa et al. 2015). These pathogens utilise CEACAM1's immunosuppressive abilities to evade the immune system (Gray-Owen and Blumberg 2006). For example, the interaction of *Neisseria species* with CEACAMs abolished cell exfoliation response via inducing *de novo* expression of a TGF- $\beta$ 1 receptor, CD105 (Muenzner et al. 2005). The interaction with CEACAMs blunted the innate defense mechanism while blocking CD105 upregulation with an antisense oligonucleotide treatment abrogated increased cell adhesion to ECM proteins upon bacterial infection (Muenzner et al. 2005). In the case of *H. pylori*, the interaction of HopQ to CEACAM1 expressed on activated T and NK cells hinders the innate/adaptive immunity inducing immunosuppressive functions (Gur et al. 2019). However, it is not the colonization of *H. pylori* that drives gastric cancer development per se; it is the inflammation-induced upon gastritis favoring cancer development (Dhar et al. 2016). A further example of host-pathogen interaction associated with carcinogenesis is *Fusobacterium nucleatum* linked to colon adenocarcinoma (Gur et al. 2015; Gur et al. 2019). This gram-negative bacterium interacts via its Fap2 protein with the human TIGIT receptor, an inhibitory receptor present on all human natural killer (NK) cells and several T cells (Gur et al. 2015). The protein-receptor interactions result in immune evasion by inhibiting NK cell toxicity and tumor-infiltrating lymphocytes blocking anti-tumor immunity (Gur et al. 2015; Gur et al. 2019). Moreover, this interaction is human-specific since murine TIGIT could not be bound by *F. nucleatum* strains (Gur et al. 2015). The species-specificity in binding is also observed in *H. pylori*'s interaction of HopQ to CEACAM, as murine CEACAMs can not bind to HopQ, which only interacts with human or rat CEACAMs (Javaheri et al. 2016). These reports highlight the importance of hampering the interaction of the pathogen and host, preventing adhesion and colonization.

Alterations in the NF- $\kappa$ B pathway affect cancer hallmarks such as cell proliferation, angiogenesis, metastasis, inhibition of apoptosis, induction of limitless replicative potential, and inflammation (Baud and Karin 2009; Hanahan and Weinberg 2011). Different studies showed that deregulation of the IKK/NF- $\kappa$ B pathway signaling network is often observed in solid cancers and hematopoietic malignancies (Baud and Karin 2009). According to the cBioPortal database, 1.4 percent of 370 GC cases tested showed amplification of NIK, and about 4 percent of GC cases showed a genetic alteration of TRAF3, a negative regulator of NIK (Cerami et al. 2012; Gao et al. 2013; Zhu et al. 2018). In the current study, a panel of GC cell lines was screened for basal processing of p100 to p52 and NIK expression levels. Some GC cell lines showed constitutive activation of the non-canonical NF- $\kappa$ B

pathway by increased NIK expression levels and p100 to p52 processing. To investigate the impact of the non-canonical NF- $\kappa$ B pathway on gastric carcinogenesis, different approaches were conducted to knock down the endogenous levels of NIK, a key protein of the pathway. First, CRISPR/Cas9n technology was used to generate NIK knockout cells. However, this strategy failed since we could only obtain wild type NIK clones. This could be due to the fact that the GC cells, used for the NIK knock out approach, might be addicted to the pathway and died after selecting positively modified cells. Hence, only wild type cells were present when the screening was performed. In a second approach, siRNAs and shRNAs were used to deplete NIK expression in GC cells. The present data indicated that the non-canonical NF- $\kappa$ B pathway in GC cells is involved in cancer cell proliferation. At the same time, depletion of NIK decreases the proliferative capacity and tumorigenic potential of GC cells. Interestingly, a down-modulation of about 50 percent of the endogenous NIK levels was sufficient to reduce proliferation and tumorigenic potential in GC cells. To analyse this under more physiological conditions, the non-canonical NF- $\kappa$ B pathway was stimulated in human gastric organoids by applying ligands that bind to the LT $\beta$ R in order to test whether this induces alterations in the cellular behaviour of organoids. A subset of human gastric organoids showed an increased growth after stimulation with LT $\alpha_1\beta_2$  or LIGHT. This effect was not influenced by the *H. pylori* infection status of the patients. However, further analysis is required to understand the molecular mechanism that influences gastric epithelial proliferation upon stimulation of the non-canonical NF- $\kappa$ B signaling, such as LT $\beta$ R levels, NIK expression, or constitutive activity of the non-canonical NF- $\kappa$ B pathway.

A study on human gastritis patient samples showed elevated NIK expression compared to healthy donors (Feige et al. 2018), further supporting that this pathway may be involved in gastric inflammation favouring carcinogenesis. Teng et al. showed in GC samples a positive correlation of NIK expression to GC stage and tumor infiltration, independent of patient age at diagnosis, proposing NIK as a potential diagnostic marker for GC (Teng et al. 2020). In a study on GC, Liu et al. showed that a direct target of miR-17-92 is TRAF3, and miR-17-92 was found to be upregulated in GC (Liu et al. 2018). Overexpression of miR-17-92 in MGC-803 GC cells increased the invasive and migratory phenotype (Liu et al. 2018). Since TRAF3 is a negative regulator of NIK (Morgan et al. 2020), these findings support the importance of NIK as a driver of carcinogenesis by activating the non-canonical NF- $\kappa$ B pathway in a subset of GC patients and suggest its blocking as an attractive therapeutic strategy.

Different strategies could be used to block the activation of the non-canonical NF- $\kappa$ B pathway. The most simple approach would be to target the interaction of bacteria or viruses to host receptors

to prevent infection. Different studies already used peptides to block the binding of pathogens that were demonstrated, for instance, in targeting viruses, such as Hepatitis B virus (Ye et al. 2016), human cytomegalovirus (Melnik et al. 2011), avian influenza viruses (Rajik et al. 2009), or others (Krepstakies et al. 2012). An alternative approach to prevent pathogen-host interaction is using antibodies (Javaheri et al. 2016) or nanobodies (Siontorou 2013). A study by Javaheri et al. showed that incubation of cells with  $\alpha$ -CEACAM1 antibody, an  $\alpha$ -HopQ antiserum or using a peptide derived from HopQ which corresponds to the HopQ-interaction domain (aa 189-220) led to a reduced CagA translocation in a dose-dependent manner upon *H. pylori* infection (Javaheri et al. 2016). Hence, decreased pTyr levels and a diminished percentage of cells showing the hummingbird phenotype were observed (Javaheri et al. 2016). This study indicated that blocking the HopQ-CEACAM interaction is a promising approach to reduce the inflammatory response induced by the oncoprotein CagA (Javaheri et al. 2016). Moreover, it might also decrease the activation of the non-canonical NF- $\kappa$ B signaling, as observed in the present study, that the interaction of HopQ to CEACAM is important for the activation of the pathway. Another concept to inhibit the non-canonical NF- $\kappa$ B signaling pathway would be applying an antagonist for LT $\beta$ R to block the ligand-receptor interaction. A study in mice challenged with *H. pylori* showed that the treatment with a systemic antagonist mLT $\beta$ R-mIgG1 (LT $\beta$ R-Ig) resulted in a higher bacterial load but a lower gastric inflammation via a decreased number of infiltrating B cells and lower nuclear translocation of RelB in the gastric mucosa (Mejías-Luque et al. 2017). While activating the LT $\beta$ R signaling with an agonist (ACH6 ab) resulted in enhanced gastric pathologies aggravated during the *H. pylori* challenge (Mejías-Luque et al. 2017). This is in line with the present study, as LT $\alpha\beta$ <sup>TG</sup> mice showed an increased inflammatory response upon infection, further supporting the essential status of the non-canonical NF- $\kappa$ B pathway in gastric carcinogenesis. These observations are further supported by a study in a colorectal and cervical cancer mouse model, where blockage of LT $\beta$ R by applying an anti-LT $\beta$ R mAb (CBE11) resulted in reduced tumor growth (Lukashev et al. 2006). However, the long-term application of LT $\beta$ R-Ig in clinical trials has to be investigated since it can have side effects on lymphoid tissue microarchitecture or NK cell compartment, to name a few (Wolf et al. 2010; Gommerman et al. 2002). The *H. pylori*-induced chronic inflammation in GC is one of the main driving forces for carcinogenesis (Smith et al. 2006; Petryszyn et al. 2020). A further example of inflammation-induced diseases is inflammatory bowel disease (IBD), shaped by chronic inflammation (McDaniel et al. 2016). Therefore, targeting inflammatory signaling pathways using biologics has proven to be a promising approach (McDaniel et al. 2016). In IBD, a functional interplay between the canonical and non-canonical NF- $\kappa$ B pathways is seen (McDaniel et al. 2016). TNF is a major causative factor for IBD, which is associated with the canonical NF- $\kappa$ B via binding to TNFR1 that can induce the

degradation of TRAF2, resulting in NIK stabilization and activation of the non-canonical NF- $\kappa$ B pathway (McDaniel et al. 2016). Additionally, CD40 expressed on B cells and APC cells is also involved in IBD pathogenesis, activating the non-canonical NF- $\kappa$ B pathway (McDaniel et al. 2016). CD40 is activated through ligand binding, CD40L, primarily expressed by activated CD4<sup>+</sup> T cell and platelets (McDaniel et al. 2016). The interaction of CD40-CD40L is essential for the proliferation and differentiation of B cells leading to the production of IL12 and TNF, enhancing the inflammation in the gut (McDaniel et al. 2016). Blocking CD40-CD40L interaction using mABS M90 or 5D12 in lamina propria T cell and monocyte co-culture reduced the production of IL12 and TNF (McDaniel et al. 2016). Regarding GC, higher CD40 expression levels were observed in GC tissue correlating with lymphatic metastasis, invasion, and augmented tumor TNM stage in tumor patients (Li et al. 2009; Guo et al. 2015). CD40 expression could be applied as a prognostic factor for GC (Li et al. 2009) and represents an interesting target for cancer therapy. Currently, several ongoing clinical trials address the interaction of CD40-CD40L in cancer as well as autoimmune diseases (Morgan et al. 2020). However, the CD40-CD40L signaling axis is used by many different immune cells such as T cells, B cells, natural killer cells, or others, and targeting this signaling route might lead to various side effects (Morgan et al. 2020). In a study on breast or pancreatic cancer, the inhibition of the ligand-receptor interaction by using anti-RANKL monoclonal antibodies (mAb) was used to prevent bone metastases (Morgan et al. 2020). Hindering the ligand-receptor interaction of the non-canonical NF- $\kappa$ B pathway seems to be a promising approach as reported by these studies. However, it is context-dependent due to its involvement in immunity, the blockage of the non-canonical NF- $\kappa$ B pathway could also induce adverse effects as seen in DSS-induced intestinal inflammation, where LT $\beta$ R blockage worsens inflammation (Bauer et al. 2012). Therefore, intensive research on the signaling network is necessary (Sokolova and Naumann 2017). A further strategy to block abnormal non-canonical NF- $\kappa$ B signaling could be the inactivation of NIK. In GC cells, depletion of NIK influenced the cell proliferation and reduced the anchorage-dependent growth of cell clones. Besides its involvement in GC, NIK has been found to play a crucial role in the carcinogenesis of several other cancer types, such as glioma, breast cancer, ovarian cancer, or pancreatic cancer (Maubach et al. 2019; Uno et al. 2014). Cherry et al. showed that in gliomas, activation of the non-canonical NF- $\kappa$ B pathway via TWEAK increased NIK expression, leading to matrix metalloproteinase 9 (MMP9) expression promoting tumor cell invasion in a 3D collagen assay (Cherry et al. 2015; Maubach et al. 2019). In breast cancer cells, NIK expression led to increased expression of stem cell markers (aldehyde dehydrogenase-1A1, NANOG, SOX2, and OCT4) while silencing NIK via shRNA application reduced the expression levels of cancer stem cell markers (Vazquez-Santillan et al. 2016). Additionally, NIK depletion weakened the ability of breast cancer cells to grow tumors in a xenograft

model *in vivo* (Vazquez-Santillan et al. 2016). In contrast, NIK overexpression elevated breast cancer stem cells population supporting the tumorigenic potential of the cancer cells (Vazquez-Santillan et al. 2016). Microarray data showed that NIK acts via the ERK signaling pathway on the cancer stem cells (Vazquez-Santillan et al. 2016). Relating to GC, it would be fascinating to explore if NIK depletion in GC cells impact cancer stemness or invasiveness of GC cells since depletion of NIK reduced the tumorigenic potential of GC cells. Similar results were observed in a study in the pancreas (Döppler et al. 2013). They showed that due to the reduction of TRAF2 levels, NIK gets stabilized, activating non-canonical NF- $\kappa$ B signaling (Döppler et al. 2013). This resulted in enhanced proliferation and anchorage-independent growth of pancreatic ductal adenocarcinoma cells, while NIK depletion reduced cell proliferation (Döppler et al. 2013). These observations were confirmed in human pancreatic cancer samples, where decreased TRAF2 levels and elevated levels of NIK or pT559-NIK were observed that were more frequent in high proliferating tumors (grade 2 or 3) (Döppler et al. 2013). NF- $\kappa$ B pathway activation via NIK stabilization is also seen in multiple myeloma cancer cells (Annunziata et al. 2007; Keats et al. 2007). In this sense, about 20 percent of 155 human multiple myeloma (MM) samples tested showed a malfunction of the NF- $\kappa$ B pathway (Keats et al. 2007). A high-resolution array-based comparative genomic hybridization and gene expression profiling identified mutations leading to the inactivation of *TRAF2*, *TRAF3*, *CYLD*, *CIAP1/2*, and activation of *NFKB1*, *NFKB2*, *LTBR*, *CD40*, *NIK*, and *TAC1*, resulting in constitutive non-canonical NF- $\kappa$ B pathway activation (Keats et al. 2007). TRAF3 inactivation was most commonly found as a single alteration in MM (Keats et al. 2007). The restoration of wild type TRAF3 in human myeloma cell lines (HMCLs) induced a significant delay in growth and enhanced apoptosis (Keats et al. 2007). Targeting the constitutive non-canonical NF- $\kappa$ B pathway activity in MM patients (with inactive TRAF3) with the proteasome inhibitor, bortezomib, could be a promising application as seen in clinical trials showing increased survival of patients (Keats et al. 2007; Mulligan et al. 2007; Baud and Karin 2009). Therefore, the use of NIK inhibitors represents an attractive strategy to treat tumors. For instance, head and neck cancer cells treated with 1,3[2H,4H]-Isoquinolinedione, a NIK inhibitor, showed reduced expression of NIK and p52/RelB proteins (Das et al. 2018). This resulted in impaired cell migration and invasion in *in vitro* assays (Das et al. 2018). A similar picture is found in GC patients. A subset of patients shows reduced TRAF3 levels according to the cBioPortal database (Cerami et al. 2012; Gao et al. 2013; Zhu et al. 2018) that might result in enhanced non-canonical NF- $\kappa$ B pathway activity. In *in vivo* assays, manipulation of NIK lowered the proliferation and tumorigenicity in GC cells. While stimulation of the non-canonical NF- $\kappa$ B pathway in human primary gastric cells by treating these cells with ligands (LT $\alpha_1\beta_2$  or LIGHT), activating the pathway, enhanced their proliferative capacity, stressing its importance in gastric epithelial proliferation. Thus, the

application of a NIK inhibitor, as stated above, could be an attractive treatment option for a subset of GC patients and should be further addressed in *in vitro* assays. Another concept would be to target the inhibitor of apoptosis (IAP) proteins with the second mitochondria-derived activator of caspases (SMAC) mimetics, which are currently tested for their chemotherapeutic potential to induce apoptosis (Pflug and Sitcheran 2020). In recent years, the constitutive activation of IKK $\alpha$ -signaling, by modulating the expression of TRAF and cIAP or mutations in these genes, has been reported in solid tumors and haematological cancers (Paul et al. 2018). A truncated p45 version of IKK $\alpha$  has been observed in colorectal cancer with B-Raf<sup>V600E</sup> mutations that signal in a TNFSF-independent manner (Paul et al. 2018). In prostate cancer, nuclear translocation of RelB is linked with higher-grade tumors and androgen treatment of prostate cancer cells, leading to enhanced nuclear p52 (Paul et al. 2018). In contrast, IKK $\alpha$  silencing lowered the androgen receptor activity and gene expression, supporting the value of IKK $\alpha$  in cancer growth, as the androgen receptor is the main driver of prostate cancer (Paul et al. 2018). A final approach to reduce the activity of the signaling pathway would be to prevent the translocation of p52/RelB into the nucleus by applying the peptide SN52 (Morgan et al. 2020), as shown in a study on prostate cancer cells where SN52 selectively inhibited the non-canonical NF- $\kappa$ B pathway and hence elevated tumor radiosensitivity (Xu et al. 2008). Together, these studies show that the non-canonical NF- $\kappa$ B pathway may be a promising target for cancer therapy (Döppler et al. 2013; Maubach et al. 2019). However, more research is needed to unravel the molecular regulation of NIK, particularly in GC.

To further explore the role of the non-canonical NF- $\kappa$ B pathway in gastric carcinogenesis *in vivo*, a mouse model was generated. The newly generated transgenic LT $\alpha\beta$ <sup>TG</sup> mice showed increased *Lt $\alpha$*  over time, while *Lt $\beta$*  was barely induced. Only after 54-weeks, an increase in *Lt $\beta$*  levels accompanied by increased *Cxcl13* expression levels were observed in LT $\alpha\beta$ <sup>TG</sup> mice compared to wild type mice. To induce the expression of two genes (*Lt $\alpha$* , *Lt $\beta$* ), we used a polycistronic cDNA linked via 2A to ensure equal expression (Szymczak and Vignali 2005; Müntjes et al. 2020). However, the LT $\alpha\beta$ <sup>TG</sup> mice showed very low *Lt $\beta$*  expression levels compared to *Lt $\alpha$*  mRNA expression, which could be due to the insertion site, since transcriptionally inactive regions in the mouse genome could result in transgene silencing (Haruyama et al. 2009; Lampreht Tratar et al. 2018). Moreover, the introduced DNA construct could also be integrated into a critical locus resulting in an unexpected genetic mutation or is silenced due to the insertion of multiple tandem copies leading to non-physiological phenotypic effects (Lampreht Tratar et al. 2018). Still, the generation of further founder lines would be helpful, as the transgene is randomly integrated into a small percentage of injected oocytes (Lampreht Tratar et al. 2018).

Upon *H. pylori* infection,  $LT\alpha\beta^{TG}$  mice showed a stronger T cell response related to elevated *Lta* and *Cxcl10* expression levels in the stomach but without pathologies compared to infected wild type mice. Female infected  $LT\alpha\beta^{TG}$  mice presented a stronger chemokine expression and inflammatory response compared to infected male  $LT\alpha\beta^{TG}$  mice. This gender difference was already stated in the literature, as female C57BL/6 mice infected with the *H. felis* strain showed more severe changes in gastric epithelial cells leading to chronic inflammation and epithelial hyperplasia at an earlier time point than infected male mice (Court et al. 2003). In general, the  $LT\alpha\beta^{TG}$  mice show a very late onset of low non-canonical NF- $\kappa$ B activation and are no ideal model to investigate gastric carcinogenesis. Therefore, a critical requirement for a transgenic mouse model is to select an appropriate promoter for tissue-specific expression (Haruyama et al. 2009). Different studies have already used the  $H^+/K^+$  ATPase  $\beta$  promoter to introduce genes of interest in the stomach (Tu et al. 2008; Syu et al. 2012). For instance, the  $H^+/K^+$  ATPase  $\beta$  promoter was used to express the soluble form of human IL-1 $\beta$  or murine *Infy* in the stomach; both cytokines are soluble and secreted by parietal cells in the stomach (Tu et al. 2008; Syu et al. 2012). In contrast, in our model, the promoter was used to induce the expression of a ligand formed of a soluble molecule (*Lt $\alpha$* ) and a membrane-anchored molecule (*Lt $\beta$* ) (Wolf et al. 2010). The ligand activating the non-canonical NF- $\kappa$ B pathway has to form a heterotrimer consisting of one *Lt $\alpha$*  molecule and two *Lt $\beta$*  molecules (Wolf et al. 2010). However, *LT $\alpha$*  can form *Lt $\alpha_3$*  homotrimer binding to TNFR1, thereby activating the canonical NF- $\kappa$ B pathway (Wolf et al. 2010). This could explain the high *CXCL10* levels upon *H. pylori* infection compared to the only low induced *CXCL13* in  $LT\alpha\beta^{TG}$  mice. hIL-1 $\beta$  transgenic mice older than one year showed severe hyperplasia, chronic inflammation, atrophy, metaplasia, and dysplasia in 70 percent of the transgenic mice compared to age-matched wild type mice (Tu et al. 2008). Additionally, *H. felis* infection boosted the risk for GC development by elevating TNF $\alpha$  and IL6 levels in hIL-1 $\beta$  transgenic mice compared to wild type infected mice (Tu et al. 2008). In *Infy* transgenic mice, 46 to 50 percent of the transgenic mice exhibited areas of dysplasia at the age of three to five months depending on the *Infy* expression levels induced by the construct (Syu et al. 2012). At the age of 12 months, a higher percentage of transgenic mice developed dysplasia (Syu et al. 2012). About 10 percent of *Infy* transgenic mice older than one year established polyps or more advanced lesions in the antrum, which was unexpected since the transgene expression is located in the corpus of the stomach (Syu et al. 2012). These two mouse models showed that stomach specific expression using the  $H^+/K^+$  ATPase  $\beta$  promoter of single cytokines such as *Infy* or hIL-1 $\beta$  is sufficient to induce changes in inflammatory, epithelial and mesenchymal cells resulting in pre-neoplastic changes in the stomach (Tu et al. 2008; Syu et al. 2012). However, further alterations are necessary to drive gastric carcinogenesis since *Infy* upregulation boosted the inflammatory response but only in a low number

of mice aged to one year or older led to tumor development (Syu et al. 2012).

A study by Ishikawa using p100<sup>-/-</sup> knock out mice is in line with the present study showing that activation of the non-canonical NF-κB pathway via increased levels of p52 is involved in growth control of the gastric mucosa and mature peripheral lymphocytes (Gerondakis et al. 1999; Ishikawa et al. 1997). These mice lack the COOH terminal domain of p100 and only have the mature p52 form present leading to gastric hyperplasia and enlarged lymph nodes that might reveal the involvement of activated Rel/NF-κB signaling in gastric epithelial proliferation (Ishikawa et al. 1997). The activation of the pathway was accompanied by upregulation of *TNFα*, *ICAM1*, and *ELAM1* levels (Ishikawa et al. 1997). The impact of canonical and non-canonical NF-κB pathway on gastric carcinogenesis was investigated by challenging mice with germline deletion in *Nfkb1* or *Nfkb2* with *H. felis* (Burkitt et al. 2013). Deletion of NF-κB1 or NF-κB2 proteins had different consequences on the inflammation-induced processes in the stomach (Burkitt et al. 2013). *Nfkb1*<sup>-/-</sup> mice showed the increased pathology, such as gastritis and gastric atrophy, at the age of 12 months without infection, accompanied with enhanced gastric mucosal proliferation and increased processing of p100 to p52 (Burkitt et al. 2013). In contrast, *H. felis* challenged *Nfkb2*<sup>-/-</sup> mice showed a higher bacterial load, while inflammation and mucosal cytokine production was reduced (Burkitt et al. 2013). Thus, NF-κB1 seems to protect against gastric inflammation and delays atrophy progression, while NF-κB2 might be needed to develop *H. felis*-induced stomach pathologies (Burkitt et al. 2013). Stomach-specific deletion of IKKβ induced higher apoptosis and necrosis rate along with higher infiltration of macrophages in the stomach mucosa upon *H. felis* infection resulting in a more rapid progression to dysplasia (Shibata et al. 2009). IKKβ deletion decreased the expression levels of anti-apoptotic genes such as c-FLIP or cIAP2 (Shibata et al. 2009). Shibata demonstrated that the IKKβ/NF-κB pathway might prevent progression to gastric dysplasia by inhibiting apoptosis or necrosis (Shibata et al. 2009).

Numerous mouse models are available to study gastric carcinogenesis, but no suitable stomach-specific Cre recombinase was available until lately (Yu et al. 2014; Kim et al. 2018; Seidlitz et al. 2019; Poh et al. 2016). Recently, new mouse models were established to investigate human GC subtypes by using the inducible Anxa10-CreER<sup>T2</sup> recombinase to induce alterations in the stomach (Seidlitz et al. 2019). Several mutations were induced in one mouse model such as TP53 (Tp53<sup>R172H</sup>)/RTK-RAS (Kras<sup>G12D</sup>)/Tgfβ (Smad4<sup>fl/fl</sup>) to mimic the CIN subtype, Cdh1<sup>fl/fl</sup>/RTK-Ras (Kras<sup>G12D</sup>)/Tgfβ (Smad4<sup>fl/fl</sup>) to generate the diffuse GS subtype or Cdh1<sup>fl/fl</sup>/RTK-RAS (Kras<sup>G12D</sup>)/WNT (APC<sup>fl/fl</sup>) to induce the serrated adenomatous GS subtype of GC (Seidlitz et al. 2019). These mouse models allow studying different human GC subtypes and the response to treatment agents (Seidlitz et al. 2019). This newly identified stomach-specific promotor (Anxa10-CreER<sup>T2</sup>) could be useful for our mouse model to induce the

construct expression in all gastric epithelial cell types increasing the overall expression levels of *Ltα* and *Ltβ* and do not restrict the expression to parietal cells.

To conclude, the current study shows that HopQ-CEACAM interaction is involved in activating the non-canonical NF-κB pathway in GC cells. This pathway may be a promising target for GC therapy, as it influences cell proliferation and worsens the inflammatory response to *H. pylori* infection. Also, the inhibition of host-pathogen interaction itself could be a favorable treatment option preventing the colonization of *H. pylori* and thereby dampening the non-canonical NF-κB pathway signaling. Consequently, the risk for GC development could be reduced since activation of the non-canonical NF-κB signaling is a force in gastric inflammation.

## 5 Summary

*Helicobacter pylori* (*H. pylori*) is a gram-negative bacterium that inhabits the stomach of every second human being globally. This bacterium is classified as a class I carcinogen, as it is a major risk factor for gastric cancer (GC) development, besides environmental or genetic host factors. *H. pylori* has been described to activate the non-canonical NF- $\kappa$ B pathway in a secondary loop. Although activation of the non-canonical NF- $\kappa$ B pathway was linked to *H. pylori*-induced inflammation, the role of this signaling pathway in gastric carcinogenesis and tumor growth remains unknown. Therefore, the main objective was to decipher the role of lymphotoxin (LT)/non-canonical NF- $\kappa$ B pathway axis in GC development and progression. Moreover, I examined the impact of *H. pylori*'s adhesion molecule HopQ, interacting with carcinoembryonic antigen-related cell adhesion molecules (CEACAMs), on the pathway activity. Here, HopQ-CEACAM interaction was essential for *H. pylori*-mediated activation of the non-canonical NF- $\kappa$ B pathway. *H. pylori* lacking HopQ or GC cells with low CEACAM expression showed reduced binding of *H. pylori* to the gastric epithelium, and hence, decreased activation of the non-canonical NF- $\kappa$ B as seen by reduced ligand expression levels (*LT $\beta$* ) and decreased p100 to p52 processing. Moreover, NIK depletion reduced the tumorigenicity in GC cells dependent on the signaling pathway. AGS shNIK cells showed reduced proliferation lowered anchorage-dependent and -independent growth compared to AGS control cells. Stimulation of human gastric organoids with ligands activating the non-canonical NF- $\kappa$ B pathway led to an increased organoid growth in a subset of patient samples (responders). However, further analysis is necessary to decipher the differences in signaling concerning responders vs. non-responders. A new mouse model (*LT $\alpha\beta$ <sup>TGstom</sup>*) with stomach-specific LT induction showed a very late onset of *LT $\alpha$*  and *LT $\beta$*  expression as well as target gene expression (*Cxcl13*). The combined effect of stomach-specific LT overexpression plus *H. pylori* infection led to increased *LT $\alpha$*  and *Cxcl10* levels inducing a more robust immune response as seen by a higher number of infiltrating CD3<sup>+</sup> T cells in *LT $\alpha\beta$ <sup>TGstom</sup>* infected mice compared to infected C57BL/6 mice.

Blocking the host-pathogen interaction might be a promising approach to hinder *H. pylori* from binding to the gastric epithelium. Hence, it reduces the host's inflammatory response elicited by the bacterium. The non-canonical NF- $\kappa$ B pathway seems to be a promising target in GC therapy; however, further research is necessary to unravel the underlying mechanism by which NIK deregulation or activation of the non-canonical NF- $\kappa$ B pathway influences gastric proliferation.

## 6 Zusammenfassung

*Helicobacter pylori* (*H. pylori*) ist ein gramnegatives Bakterium, das im Magen jedes zweiten Menschen weltweit vorkommt. Dieses Bakterium wird als Karzinogen der Klasse I eingestuft, da es neben umweltbedingten oder genetischen Wirtsfaktoren, ein Hauptrisikofaktor für die Entstehung von Magenkrebs ist. Es wurde beschrieben, dass *H. pylori* den nicht-kanonischen NF- $\kappa$ B-Signalweg in einer sekundären Schleife aktiviert. Obwohl die Aktivierung des nicht-kanonischen NF- $\kappa$ B-Signalwegs mit der durch *H. pylori* ausgelösten Entzündung in Verbindung gebracht wurde, ist die Rolle dieses Signalwegs bei der Entstehung von Magenkrebs und des Tumorwachstums noch unbekannt. Daher bestand das Hauptziel darin, die Rolle von Lymphotoxin (LT)/nicht-kanonischen NF- $\kappa$ B-Signalweg bei der Entstehung und Progression von Magenkrebs zu entschlüsseln. Darüber hinaus wollte ich untersuchen, welchen Einfluss das Adhäsionsmolekül HopQ von *H. pylori*, das mit den Zelladhäsionsmolekülen des Carcinoembryonalen Antigens (CEACAMs) interagiert, auf die Aktivität des Signalweges hat. In diesem Fall war die HopQ-CEACAM-Interaktion für die von *H. pylori* vermittelte Aktivierung des nicht-kanonischen NF- $\kappa$ B Signalweges wesentlich. *H. pylori* mit fehlendem HopQ, oder Magenkrebszelllinien mit geringer CEACAM-Expression zeigten eine verringerte Bindung von *H. pylori* an das Magenepithel und somit war eine reduzierte Aktivierung des nicht-kanonischen NF- $\kappa$ B ersichtlich, was sich in einer verringerten Ligandenexpression (*LT $\beta$* ) und einer verringerten Prozessierung von p100 zu p52 zeigte. Darüber hinaus reduzierte die NIK Verminderung die Tumorigenität von Magenkrebszelllinien, die von diesem Signalweg abhängig sind. AGS shNIK Zellen zeigten im Vergleich zu AGS Kontrollzellen eine geringere Proliferation und ein geringeres verankerungsabhängiges und -unabhängiges Wachstum. Die Stimulierung menschlicher Magenorganoide mit Liganden, die den nicht-kanonischen NF- $\kappa$ B-Signalweg aktivieren, führte bei einer Untergruppe von Patientenproben (Respondern) zu einem erhöhten Organoidwachstum. Es sind jedoch weitere Analysen erforderlich, um die Unterschiede in der Signalübertragung zwischen Respondern und Non-Respondern zu entschlüsseln. Ein neues Mausmodell (*LT $\alpha\beta$ <sup>TGstom</sup>*) mit magenspezifischer LT-Induktion zeigte einen sehr späten Beginn der *LT $\alpha$* - und *LT $\beta$* -Expression sowie der Expression des Zielgenes (*Cxcl13*). Die kombinierte Wirkung von magenspezifischer LT-Überexpression und *H. pylori*-Infektion führte zu erhöhten *LT $\alpha$* - und *Cxcl10*-Expressionsleveln, die eine robustere Immunantwort auslösten, was sich in einer höheren Anzahl von infiltrierenden CD3<sup>+</sup> T-Zellen in *LT $\alpha\beta$ <sup>TGstom</sup>* infizierten Mäusen im Vergleich zu infizierten C57BL/6 Mäusen zeigte.

Die Blockierung der Wirt-Pathogen-Interaktion könnte ein vielversprechender Ansatz sein, um *H.*

*pylori* an der Bindung an das Magenepithel zu hindern. Dadurch wird die durch das Bakterium ausgelöste Entzündungsreaktion des Wirts reduziert. Der nicht-kanonische NF-κB-Signalweg scheint ein vielversprechendes Ziel für die Therapie von Magenkrebs zu sein. Es sind jedoch weitere Forschungsarbeiten erforderlich, um den zugrundeliegenden Mechanismus zu entschlüsseln, durch den die Deregulierung von NIK oder die Aktivierung des nicht-kanonischen NF-κB Signalweges die Magenproliferation beeinflusst.

## 7 Publication bibliography

Alberts, Bruce (2008): *Molecular biology of the cell*. 5th ed. New York: Garland Science.

Alzeeb, George; Metges, Jean-Philippe; Corcos, Laurent; Le Jossic-Corcos, Catherine (2020): Three-Dimensional Culture Systems in Gastric Cancer Research. In *Cancers* 12 (10). DOI: 10.3390/cancers12102800.

American Type Culture Collection (Ed.): *Cell Lines*. Available online at <https://www.lgcstandards-atcc.org>, checked on 3/19/2020.

Amieva, Manuel; Peek, Richard M. (2016): Pathobiology of *Helicobacter pylori*-Induced Gastric Cancer. In *Gastroenterology* 150 (1), pp. 64–78. DOI: 10.1053/j.gastro.2015.09.004.

Annunziata, Christina M.; Davis, R. Eric; Demchenko, Yulia; Bellamy, William; Gabrea, Ana; Zhan, Fenghuang et al. (2007): Frequent engagement of the classical and alternative NF- $\kappa$ B pathways by diverse genetic abnormalities in multiple myeloma. In *Cancer cell* 12 (2), pp. 115–130. DOI: 10.1016/j.ccr.2007.07.004.

Ansari, Shamshul; Yamaoka, Yoshio (2019): *Helicobacter pylori* Virulence Factors Exploiting Gastric Colonization and its Pathogenicity. In *Toxins* 11 (11). DOI: 10.3390/toxins11110677.

Arnold, Isabelle C.; Lee, Josephine Y.; Amieva, Manuel R.; Roers, Axel; Flavell, Richard A.; Sparwasser, Tim; Müller, Anne (2011): Tolerance rather than immunity protects from *Helicobacter pylori*-induced gastric preneoplasia. In *Gastroenterology* 140 (1), pp. 199–209. DOI: 10.1053/j.gastro.2010.06.047.

Backert, S.; Müller, E. C.; Jungblut, P. R.; Meyer, T. F. (2001): Tyrosine phosphorylation patterns and size modification of the *Helicobacter pylori* CagA protein after translocation into gastric epithelial cells. In *Proteomics* 1 (4), pp. 608–617. DOI: 10.1002/1615-9861(200104)1:4<608::AID-PROT608>3.0.CO;2-G.

Backert, Steffen; Meyer, Thomas F. (2006): Type IV secretion systems and their effectors in bacterial pathogenesis. In *Current opinion in microbiology* 9 (2), pp. 207–217. DOI: 10.1016/j.mib.2006.02.008.

Backert, Steffen; Tegtmeyer, Nicole (2017): Type IV Secretion and Signal Transduction of *Helicobacter pylori* CagA through Interactions with Host Cell Receptors. In *Toxins* 9 (4). DOI: 10.3390/toxins9040115.

Balakrishnan, Maya; George, Rollin; Sharma, Ashish; Graham, David Y. (2017): Changing Trends in

- Stomach Cancer Throughout the World. In *Current gastroenterology reports* 19 (8), p. 36. DOI: 10.1007/s11894-017-0575-8.
- Banatvala, N.; Mayo, K.; Megraud, F.; Jennings, R.; Deeks, J. J.; Feldman, R. A. (1993): The cohort effect and *Helicobacter pylori*. In *The Journal of infectious diseases* 168 (1), pp. 219–221. DOI: 10.1093/infdis/168.1.219.
- Banerjee, Anirban; Thamphiwatana, Soracha; Carmona, Ellese M.; Rickman, Barry; Doran, Kelly S.; Obonyo, Marygorret (2014): Deficiency of the myeloid differentiation primary response molecule MyD88 leads to an early and rapid development of *Helicobacter*-induced gastric malignancy. In *Infection and immunity* 82 (1), pp. 356–363. DOI: 10.1128/IAI.01344-13.
- Bartfeld, Sina (2016): Modeling infectious diseases and host-microbe interactions in gastrointestinal organoids. In *Developmental biology* 420 (2), pp. 262–270. DOI: 10.1016/j.ydbio.2016.09.014.
- Bartfeld, Sina; Clevers, Hans (2015): Organoids as Model for Infectious Diseases: Culture of Human and Murine Stomach Organoids and Microinjection of *Helicobacter Pylori*. In *Journal of visualized experiments : JoVE* (105). DOI: 10.3791/53359.
- Basak, Soumen; Hoffmann, Alexander (2008): Crosstalk via the NF-kappaB signaling system. In *Cytokine & growth factor reviews* 19 (3-4), pp. 187–197. DOI: 10.1016/j.cytogfr.2008.04.005.
- Baud, Véronique; Karin, Michael (2009): Is NF-kappaB a good target for cancer therapy? Hopes and pitfalls. In *Nature reviews. Drug discovery* 8 (1), pp. 33–40. DOI: 10.1038/nrd2781.
- Bauer, Judith; Namineni, Sukumar; Reisinger, Florian; Zöller, Jessica; Yuan, Detian; Heikenwälder, Mathias (2012): Lymphotoxin, NF-κB, and cancer: the dark side of cytokines. In *Digestive diseases (Basel, Switzerland)* 30 (5), pp. 453–468. DOI: 10.1159/000341690.
- Bednarek, Kinga; Kostrzewska-Poczekaj, Magdalena; Szaumkessel, Marcin; Kiwerska, Katarzyna; Paczkowska, Julia; Byzia, Ewa et al. (2018): Downregulation of CEACAM6 gene expression in laryngeal squamous cell carcinoma is an effect of DNA hypermethylation and correlates with disease progression. In *American journal of cancer research* 8 (7), pp. 1249–1261.
- Belogolova, Elena; Bauer, Bianca; Pombaiah, Malvika; Asakura, Hiroshi; Brinkman, Volker; Ertl, Claudia et al. (2013): *Helicobacter pylori* outer membrane protein HopQ identified as a novel T4SS-associated virulence factor. In *Cellular microbiology* 15 (11), pp. 1896–1912. DOI: 10.1111/cmi.12158.

- Bhuiyan, Taufiqur R.; Islam, M. M. Towhidul; Uddin, Taher; Chowdhury, Mohiul I.; Janzon, Anders; Adamsson, Jenni et al. (2014): Th1 and Th17 responses to *Helicobacter pylori* in Bangladeshi infants, children and adults. In *PloS one* 9 (4), e93943. DOI: 10.1371/journal.pone.0093943.
- Bollschweiler, Elfriede; Boettcher, Knut; Hoelscher, Arnulf H.; Siewert, Joerg R.; Sasako, Mitsuro; Kinoshita, Taira; Maruyama, Keichi (1993): Is the prognosis for Japanese and German patients with gastric cancer really different? In *Cancer* 71 (10), pp. 2918–2925. DOI: 10.1002/1097-0142(19930515)71:10%3C2918::AID-CNCR2820711006%3E3.0.CO;2-V.
- Borowicz, Stanley; van Scoyk, Michelle; Avasarala, Sreedevi; Karuppusamy Rathinam, Manoj Kumar; Tauler, Jordi; Bikkavilli, Rama Kamesh; Winn, Robert A. (2014): The soft agar colony formation assay. In *Journal of visualized experiments : JoVE* (92), e51998. DOI: 10.3791/51998.
- Brown, L. M. (2000): *Helicobacter pylori*: epidemiology and routes of transmission. In *Epidemiologic reviews* 22 (2), pp. 283–297. DOI: 10.1093/oxfordjournals.epirev.a018040.
- Brücher, Björn L.D.M.; Lang, Florian; Jamall, Ijaz S. (2019): NF- $\kappa$ B signaling and crosstalk during carcinogenesis. In *4open* 2, p. 13. DOI: 10.1051/fopen/2019010.
- Burkitt, M. D.; Williams, J. M.; Duckworth, C. A.; O'Hara, A.; Hanedi, A.; Varro, A. et al. (2013): Signaling mediated by the NF- $\kappa$ B sub-units NF- $\kappa$ B1, NF- $\kappa$ B2 and c-Rel differentially regulate *Helicobacter felis*-induced gastric carcinogenesis in C57BL/6 mice. In *Oncogene* 32 (50), pp. 5563–5573. DOI: 10.1038/onc.2013.334.
- Cancer Genome Atlas Research Network (2014): Comprehensive molecular characterization of gastric adenocarcinoma. In *Nature* 513 (7517), pp. 202–209. DOI: 10.1038/nature13480.
- Canfield, V. A.; Levenson, R. (1991): Structural organization and transcription of the mouse gastric H<sup>+</sup>, K<sup>(+)</sup>-ATPase beta subunit gene. In *Proceedings of the National Academy of Sciences of the United States of America* 88 (18), pp. 8247–8251.
- Censini, S.; Lange, C.; Xiang, Z.; Crabtree, J. E.; Ghiara, P.; Borodovsky, M. et al. (1996): *cag*, a pathogenicity island of *Helicobacter pylori*, encodes type I-specific and disease-associated virulence factors. In *Proceedings of the National Academy of Sciences of the United States of America* 93 (25), pp. 14648–14653. DOI: 10.1073/pnas.93.25.14648.
- Cerami, Ethan; Gao, Jianjiong; Dogrusoz, Ugur; Gross, Benjamin E.; Sumer, Selcuk Onur; Aksoy, Bülent Arman et al. (2012): The cBio cancer genomics portal: an open platform for exploring multidimensional cancer genomics data. In *Cancer discovery* 2 (5), pp. 401–404. DOI: 10.1158/2159-8290.CD-12-0095.

- Cherry, Evan M.; Lee, Dong W.; Jung, Ji-Ung; Sitcheran, Raquel (2015): Tumor necrosis factor-like weak inducer of apoptosis (TWEAK) promotes glioma cell invasion through induction of NF- $\kappa$ B-inducing kinase (NIK) and noncanonical NF- $\kappa$ B signaling. In *Molecular cancer* 14, p. 9. DOI: 10.1186/s12943-014-0273-1.
- Cildir, Gökhan; Low, Kee Chung; Tergaonkar, Vinay (2016): Noncanonical NF- $\kappa$ B Signaling in Health and Disease. In *Trends in molecular medicine* 22 (5), pp. 414–429. DOI: 10.1016/j.molmed.2016.03.002.
- Correa, P. (1992): Human gastric carcinogenesis: a multistep and multifactorial process--First American Cancer Society Award Lecture on Cancer Epidemiology and Prevention. In *Cancer research* 52 (24), pp. 6735–6740.
- Correa, Pelayo (2003): Bacterial infections as a cause of cancer. In *Journal of the National Cancer Institute* 95 (7), E3. DOI: 10.1093/jnci/95.7.E3.
- Correa, Pelayo (2013): Gastric cancer: overview. In *Gastroenterology clinics of North America* 42 (2), pp. 211–217. DOI: 10.1016/j.gtc.2013.01.002.
- Court, M.; Robinson, P. A.; Dixon, M. F.; Jeremy, A. H. T.; Crabtree, J. E. (2003): The effect of gender on Helicobacter felis-mediated gastritis, epithelial cell proliferation, and apoptosis in the mouse model. In *The Journal of pathology* 201 (2), pp. 303–311. DOI: 10.1002/path.1422.
- Dang, C. V.; Resar, L. M.; Emison, E.; Kim, S.; Li, Q.; Prescott, J. E. et al. (1999): Function of the c-Myc oncogenic transcription factor. In *Experimental cell research* 253 (1), pp. 63–77. DOI: 10.1006/excr.1999.4686.
- Das, Rita; Coupar, Jamie; Clavijo, Paul E.; Saleh, Anthony; Cheng, Tsu-Fan; Yang, Xinpeng et al. (2018): Lymphotoxin- $\beta$  receptor-NIK signaling induces alternative RELB/NF- $\kappa$ B2 activation to promote metastatic gene expression and cell migration in head and neck cancer. In *Molecular carcinogenesis* 58 (3), pp. 411–425. DOI: 10.1002/mc.22938.
- Dhar, Poshmaal; Ng, Garrett Z.; Sutton, Philip (2016): How host regulation of Helicobacter pylori - induced gastritis protects against peptic ulcer disease and gastric cancer. In *American Journal of Physiology-Gastrointestinal and Liver Physiology* 311 (3), G514-G520. DOI: 10.1152/ajpgi.00146.2016.
- Döppler, Heike; Liou, Geou-Yarh; Storz, Peter (2013): Downregulation of TRAF2 mediates NIK-induced pancreatic cancer cell proliferation and tumorigenicity. In *PloS one* 8 (1), e53676. DOI: 10.1371/journal.pone.0053676.

- Falush, Daniel; Wirth, Thierry; Linz, Bodo; Pritchard, Jonathan K.; Stephens, Matthew; Kidd, Mark et al. (2003): Traces of human migrations in *Helicobacter pylori* populations. In *Science (New York, N.Y.)* 299 (5612), pp. 1582–1585. DOI: 10.1126/science.1080857.
- Feige, Michael Hartmut; Vieth, Michael; Sokolova, Olga; Täger, Christian; Naumann, Michael (2018): *Helicobacter pylori* induces direct activation of the lymphotoxin beta receptor and non-canonical nuclear factor-kappa B signaling. In *Biochimica et biophysica acta. Molecular cell research* 1865 (4), pp. 545–550. DOI: 10.1016/j.bbamcr.2018.01.006.
- Ferlay, J.; Colombet, M.; Soerjomataram, I.; Mathers, C.; Parkin, D. M.; Piñeros, M. et al. (2019): Estimating the global cancer incidence and mortality in 2018: GLOBOCAN sources and methods. In *International journal of cancer* 144 (8), pp. 1941–1953. DOI: 10.1002/ijc.31937.
- Fernandes, Mónica T.; Dejardin, Emmanuel; dos Santos, Nuno R. (2016): Context-dependent roles for lymphotoxin- $\beta$  receptor signaling in cancer development. In *Biochimica et biophysica acta* 1865 (2), pp. 204–219. DOI: 10.1016/j.bbcan.2016.02.005.
- Fischer, W.; Püls, J.; Buhrdorf, R.; Gebert, B.; Odenbreit, S.; Haas, R. (2001): Systematic mutagenesis of the *Helicobacter pylori* cag pathogenicity island: essential genes for CagA translocation in host cells and induction of interleukin-8. In *Molecular microbiology* 42 (5), pp. 1337–1348. DOI: 10.1046/j.1365-2958.2001.02714.x.
- Fischer, Wolfgang (2011): Assembly and molecular mode of action of the *Helicobacter pylori* Cag type IV secretion apparatus. In *The FEBS journal* 278 (8), pp. 1203–1212. DOI: 10.1111/j.1742-4658.2011.08036.x.
- Gao, Jianjiong; Aksoy, Bülent Arman; Dogrusoz, Ugur; Dresdner, Gideon; Gross, Benjamin; Sumer, S. Onur et al. (2013): Integrative analysis of complex cancer genomics and clinical profiles using the cBioPortal. In *Science signaling* 6 (269), pl1. DOI: 10.1126/scisignal.2004088.
- Gerondakis, S.; Grossmann, M.; Nakamura, Y.; Pohl, T.; Grumont, R. (1999): Genetic approaches in mice to understand Rel/NF-kappaB and IkappaB function: transgenics and knockouts. In *Oncogene* 18 (49), pp. 6888–6895. DOI: 10.1038/sj.onc.1203236.
- Gibson, Daniel G.; Young, Lei; Chuang, Ray-Yuan; Venter, J. Craig; Hutchison, Clyde A.; Smith, Hamilton O. (2009): Enzymatic assembly of DNA molecules up to several hundred kilobases. In *Nature methods* 6 (5), pp. 343–345. DOI: 10.1038/nmeth.1318.
- Gilmore, T. D. (2006): Introduction to NF-kappaB: players, pathways, perspectives. In *Oncogene* 25 (51), pp. 6680–6684. DOI: 10.1038/sj.onc.1209954.

GLOBOCAN (2018): Cancer Today - IARC. Edited by World Health Organization. International Agency for Research on Cancer. Available online at <https://gco.iarc.fr/today/online-analysis-map>, checked on 4/6/2020.

Gokcezade, Joseph; Sienski, Grzegorz; Duchek, Peter (2014): Efficient CRISPR/Cas9 plasmids for rapid and versatile genome editing in *Drosophila*. In *G3 (Bethesda, Md.)* 4 (11), pp. 2279–2282. DOI: 10.1534/g3.114.014126.

Gommerman, Jennifer L.; Mackay, Fabienne; Donskoy, Elina; Meier, Werner; Martin, Pauline; Browning, Jeffrey L. (2002): Manipulation of lymphoid microenvironments in nonhuman primates by an inhibitor of the lymphotoxin pathway. In *The Journal of Clinical Investigation* 110 (9), pp. 1359–1369. DOI: 10.1172/JCI15975.

Gray-Owen, Scott D.; Blumberg, Richard S. (2006): CEACAM1: contact-dependent control of immunity. In *Nature reviews. Immunology* 6 (6), pp. 433–446. DOI: 10.1038/nri1864.

Guo, Jian-Qiang; Yu, Wei-Hua; Wang, Hong-Juan; Liu, Bin; Zhu, Kong-Xi; Zhang, Qing-Hui et al. (2012): Different expression patterns of CEACAM1 and its impacts on angiogenesis in gastric nonneoplastic and neoplastic lesions. In *Annals of surgical oncology* 19 Suppl 3, S365-74. DOI: 10.1245/s10434-011-1811-3.

Guo, Jing; Xiao, Jia-Jia; Zhang, Xiaoli; Fan, Kai-Xi (2015): CD40 expression and its prognostic significance in human gastric carcinoma. In *Med Oncol* 32 (3). DOI: 10.1007/s12032-014-0463-0.

Gur, Chamutal; Ibrahim, Yara; Isaacson, Batya; Yamin, Rachel; Abed, Jawad; Gamliel, Moriya et al. (2015): Binding of the Fap2 Protein of *Fusobacterium nucleatum* to Human Inhibitory Receptor TIGIT Protects Tumors from Immune Cell Attack. In *Immunity* 42 (2), pp. 344–355. DOI: 10.1016/j.immuni.2015.01.010.

Gur, Chamutal; Maalouf, Naseem; Gerhard, Markus; Singer, Bernhard B.; Emgård, Johanna; Temper, Violeta et al. (2019): The *Helicobacter pylori* HopQ outermembrane protein inhibits immune cell activities. In *Oncoimmunology* 8 (4). DOI: 10.1080/2162402X.2018.1553487.

Haas, R.; Meyer, T. F.; van Putten, J. P. (1993): Aflagellated mutants of *Helicobacter pylori* generated by genetic transformation of naturally competent strains using transposon shuttle mutagenesis. In *Molecular microbiology* 8 (4), pp. 753–760. DOI: 10.1111/j.1365-2958.1993.tb01618.x.

Hanahan, Douglas; Weinberg, Robert A. (2011): Hallmarks of cancer: the next generation. In *Cell* 144 (5), pp. 646–674. DOI: 10.1016/j.cell.2011.02.013.

- Haruyama, Naoto; Cho, Andrew; Kulkarni, Ashok B. (2009): Overview: engineering transgenic constructs and mice. In *Current protocols in cell biology* Chapter 19, Unit 19.10. DOI: 10.1002/0471143030.cb1910s42.
- Hatakeyama, Masanori (2009): Helicobacter pylori and gastric carcinogenesis. In *Journal of gastroenterology* 44 (4), pp. 239–248. DOI: 10.1007/s00535-009-0014-1.
- Hayden, Matthew S.; Ghosh, Sankar (2011): NF- $\kappa$ B in immunobiology. In *Cell research* 21 (2), pp. 223–244. DOI: 10.1038/cr.2011.13.
- Hoesel, Bastian; Schmid, Johannes A. (2013): The complexity of NF- $\kappa$ B signaling in inflammation and cancer. In *Molecular cancer* 12, p. 86. DOI: 10.1186/1476-4598-12-86.
- Huang, Tingting; Kang, Wei; Zhang, Bin; Wu, Feng; Dong, Yujuan; Tong, Joanna H. M. et al. (2016): miR-508-3p concordantly silences NFKB1 and RELA to inactivate canonical NF- $\kappa$ B signaling in gastric carcinogenesis. In *Molecular cancer* 15, p. 9. DOI: 10.1186/s12943-016-0493-7.
- International Agency for Research on Cancer; International Agency for Research on Cancer (1994): Schistosomes, liver flukes and Helicobacter pylori. ... views and expert opinions of an IARC Working Group on the Evaluation of Carcinogenesis Risks to Humans, which met in Lyon, 7 - 14 June 1994. Lyon (IARC monographs on the evaluation of carcinogenic risks to humans, 61).
- Ishikawa, H.; Carrasco, D.; Claudio, E.; Ryseck, R. P.; Bravo, R. (1997): Gastric hyperplasia and increased proliferative responses of lymphocytes in mice lacking the COOH-terminal ankyrin domain of NF- $\kappa$ B2. In *The Journal of experimental medicine* 186 (7), pp. 999–1014. DOI: 10.1084/jem.186.7.999.
- Isobe, Yoh; Nashimoto, Atsushi; Akazawa, Kohei; Oda, Ichiro; Hayashi, Kenichi; Miyashiro, Isao et al. (2011): Gastric cancer treatment in Japan: 2008 annual report of the JGCA nationwide registry. In *Gastric cancer : official journal of the International Gastric Cancer Association and the Japanese Gastric Cancer Association* 14 (4), pp. 301–316. DOI: 10.1007/s10120-011-0085-6.
- Ito, Nozomi; Tsujimoto, Hironori; Ueno, Hideki; Xie, Qian; Shinomiya, Nariyoshi (2020): Helicobacter pylori-Mediated Immunity and Signaling Transduction in Gastric Cancer. In *Journal of clinical medicine* 9 (11). DOI: 10.3390/jcm9113699.
- Javaheri, Anahita; Kruse, Tobias; Moonens, Kristof; Mejías-Luque, Raquel; Debraekeleer, Ayla; Asche, Carmen I. et al. (2016): Helicobacter pylori adhesin HopQ engages in a virulence-enhancing interaction with human CEACAMs. In *Nature microbiology* 2, p. 16189. DOI: 10.1038/nmicrobiol.2016.189.

Jost, Philipp J.; Ruland, Jürgen (2007): Aberrant NF-kappaB signaling in lymphoma: mechanisms, consequences, and therapeutic implications. In *Blood* 109 (7), pp. 2700–2707. DOI: 10.1182/blood-2006-07-025809.

Kalali, Behnam; Mejías-Luque, Raquel; Javaheri, Anahita; Gerhard, Markus (2014): H. pylori virulence factors: influence on immune system and pathology. In *Mediators of inflammation* 2014, p. 426309. DOI: 10.1155/2014/426309.

Karimi, Parisa; Islami, Farhad; Anandasabapathy, Sharmila; Freedman, Neal D.; Kamangar, Farin (2014): Gastric cancer: descriptive epidemiology, risk factors, screening, and prevention. In *Cancer epidemiology, biomarkers & prevention : a publication of the American Association for Cancer Research, cosponsored by the American Society of Preventive Oncology* 23 (5), pp. 700–713. DOI: 10.1158/1055-9965.EPI-13-1057.

Keats, Jonathan J.; Fonseca, Rafael; Chesi, Marta; Schop, Roelandt; Baker, Angela; Chng, Wee-Joo et al. (2007): Promiscuous Mutations Activate the Non-Canonical NF-kB Pathway in Multiple Myeloma. In *Cancer cell* 12 (2), pp. 131–144. DOI: 10.1016/j.ccr.2007.07.003.

Kidd, M.; Modlin, I. M. (1998): A century of Helicobacter pylori: paradigms lost-paradigms regained. In *Digestion* 59 (1), pp. 1–15. DOI: 10.1159/000007461.

Kim, Hyeonhui; Kim, Minki; Im, Sun-Kyoung; Fang, Sungsoon (2018): Mouse Cre-LoxP system: general principles to determine tissue-specific roles of target genes. In *Laboratory animal research* 34 (4), pp. 147–159. DOI: 10.5625/lar.2018.34.4.147.

Kim, Walter M.; Huang, Yu-Hwa; Gandhi, Amit; Blumberg, Richard S. (2019): CEACAM1 structure and function in immunity and its therapeutic implications. In *Seminars in immunology* 42, p. 101296. DOI: 10.1016/j.smim.2019.101296.

Klaile, Esther; Klassert, Tilman E.; Scheffrahn, Inka; Müller, Mario M.; Heinrich, Annina; Heyl, Kerstin A. et al. (2013): Carcinoembryonic antigen (CEA)-related cell adhesion molecules are co-expressed in the human lung and their expression can be modulated in bronchial epithelial cells by non-typable Haemophilus influenzae, Moraxella catarrhalis, TLR3, and type I and II interferons. In *Respiratory research* 14, p. 85. DOI: 10.1186/1465-9921-14-85.

Klaile, Esther; Müller, Mario M.; Zubiría-Barrera, Cristina; Brehme, Saskia; Klassert, Tilman E.; Stock, Magdalena et al. (2019): Unaltered Fungal Burden and Lethality in Human CEACAM1-Transgenic Mice During Candida albicans Dissemination and Systemic Infection. In *Frontiers in Microbiology* 10. DOI: 10.3389/fmicb.2019.02703.

- Königer, Verena; Holsten, Lea; Harrison, Ute; Busch, Benjamin; Loell, Eva; Zhao, Qing et al. (2016): *Helicobacter pylori* exploits human CEACAMs via HopQ for adherence and translocation of CagA. In *Nature microbiology* 2, p. 16188. DOI: 10.1038/nmicrobiol.2016.188.
- Koroleva, Ekaterina P.; Fu, Yang-Xin; Tumanov, Alexei V. (2018): Lymphotoxin in physiology of lymphoid tissues - Implication for antiviral defense. In *Cytokine* 101, pp. 39–47. DOI: 10.1016/j.cyto.2016.08.018.
- Krepstakies, Marcel; Lucifora, Julie; Nagel, Claus-Henning; Zeisel, Mirjam B.; Holstermann, Barbara; Hohenberg, Heinrich et al. (2012): A new class of synthetic peptide inhibitors blocks attachment and entry of human pathogenic viruses. In *The Journal of infectious diseases* 205 (11), pp. 1654–1664. DOI: 10.1093/infdis/jis273.
- Kuipers, E. J.; Pérez-Pérez, G. I.; Meuwissen, S. G.; Blaser, M. J. (1995): *Helicobacter pylori* and atrophic gastritis: importance of the *cagA* status. In *Journal of the National Cancer Institute* 87 (23), pp. 1777–1780. DOI: 10.1093/jnci/87.23.1777.
- Lamprecht Tratar, Ursa; Horvat, Simon; Cemazar, Maja (2018): Transgenic Mouse Models in Cancer Research. In *Frontiers in oncology* 8, p. 268. DOI: 10.3389/fonc.2018.00268.
- Lauren, P. (1965): The two histological main types of gastric carcinoma: diffuse and so-called intestinal-type carcinoma. An attempt at a histo-clinical classification. In *Acta pathologica et microbiologica Scandinavica* 64, pp. 31–49. DOI: 10.1111/apm.1965.64.1.31.
- Le Cong; Ran, F. Ann; Cox, David; Lin, Shuailiang; Barretto, Robert; Habib, Naomi et al. (2013): Multiplex genome engineering using CRISPR/Cas systems. In *Science (New York, N.Y.)* 339 (6121), pp. 819–823. DOI: 10.1126/science.1231143.
- Lee, Byung Lan; Lee, Hye Seung; Jung, Jieun; Cho, Sung Jin; Chung, Hee-Yong; Kim, Woo Ho et al. (2005): Nuclear factor-kappaB activation correlates with better prognosis and Akt activation in human gastric cancer. In *Clinical cancer research : an official journal of the American Association for Cancer Research* 11 (7), pp. 2518–2525. DOI: 10.1158/1078-0432.CCR-04-1282.
- Li, Dan; Wu, Chuancheng; Cai, Yuanhua; Liu, Baoying (2017): Association of NFKB1 and NFKBIA gene polymorphisms with susceptibility of gastric cancer. In *Tumour biology : the journal of the International Society for Oncodevelopmental Biology and Medicine* 39 (7), 1010428317717107. DOI: 10.1177/1010428317717107.
- Li, Q.; Karam, S. M.; Gordon, J. I. (1995): Simian virus 40 T antigen-induced amplification of pre-parietal cells in transgenic mice. Effects on other gastric epithelial cell lineages and evidence for a

p53-independent apoptotic mechanism that operates in a committed progenitor. In *The Journal of biological chemistry* 270 (26), pp. 15777–15788. DOI: 10.1074/jbc.270.26.15777.

Li, Rui; Chen, Wei-Chang; Pang, Xue-Qin; Hua, Chen; Li, Ling; Zhang, Xue-Guang (2009): Expression of CD40 and CD40L in Gastric Cancer Tissue and Its Clinical Significance. In *IJMS* 10 (9), pp. 3900–3917. DOI: 10.3390/ijms10093900.

Linz, Bodo; Balloux, François; Moodley, Yoshan; Manica, Andrea; Liu, Hua; Roumagnac, Philippe et al. (2007): An African origin for the intimate association between humans and *Helicobacter pylori*. In *Nature* 445 (7130), pp. 915–918. DOI: 10.1038/nature05562.

Liu, Fei; Cheng, Li; Xu, Jingjing; Guo, Feng; Chen, Weichang (2018): miR-17-92 functions as an oncogene and modulates NF- $\kappa$ B signaling by targeting TRAF3 in MGC-803 human gastric cancer cells. In *International journal of oncology* 53 (5), pp. 2241–2257. DOI: 10.3892/ijo.2018.4543.

Liu, Ting; Zhang, Lingyun; Joo, Donghyun; Sun, Shao-Cong (2017): NF- $\kappa$ B signaling in inflammation. In *Signal transduction and targeted therapy* 2. DOI: 10.1038/sigtrans.2017.23.

Lodish, Harvey F. (2008): *Molecular cell biology*. 6th ed. New York: W.H. Freeman.

Lorenz, R. G.; Gordon, J. I. (1993): Use of transgenic mice to study regulation of gene expression in the parietal cell lineage of gastric units. In *The Journal of biological chemistry* 268 (35), pp. 26559–26570.

Loureiro, Alexandre; da Silva, Gabriela Jorge (2019): CRISPR-Cas: Converting A Bacterial Defence Mechanism into A State-of-the-Art Genetic Manipulation Tool. In *Antibiotics (Basel, Switzerland)* 8 (1). DOI: 10.3390/antibiotics8010018.

Lukashev, Matvey; LePage, Doreen; Wilson, Cheryl; Bailly, Véronique; Garber, Ellen; Lukashin, Alex et al. (2006): Targeting the lymphotoxin-beta receptor with agonist antibodies as a potential cancer therapy. In *Cancer research* 66 (19), pp. 9617–9624. DOI: 10.1158/0008-5472.CAN-06-0217.

Maeda, S.; Yoshida, H.; Ogura, K.; Mitsuno, Y.; Hirata, Y.; Yamaji, Y. et al. (2000): *H. pylori* activates NF-kappaB through a signaling pathway involving IkappaB kinases, NF-kappaB-inducing kinase, TRAF2, and TRAF6 in gastric cancer cells. In *Gastroenterology* 119 (1), pp. 97–108. DOI: 10.1053/gast.2000.8540.

Marshall, B. J.; Armstrong, J. A.; McGeachie, D. B.; Glancy, R. J. (1985): Attempt to fulfil Koch's postulates for pyloric *Campylobacter*. In *The Medical journal of Australia* 142 (8), pp. 436–439.

DOI: 10.5694/j.1326-5377.1985.tb113443.x.

Marshall, Barry J.; Warren, J. Robin (1984): UNIDENTIFIED CURVED BACILLI IN THE STOMACH OF PATIENTS WITH GASTRITIS AND PEPTIC ULCERATION. In *The Lancet* 323 (8390), pp. 1311–1315.

DOI: 10.1016/S0140-6736(84)91816-6.

Maubach, Gunter; Feige, Michael H.; Lim, Michelle C. C.; Naumann, Michael (2019): NF- $\kappa$ B-inducing kinase in cancer. In *Biochimica et biophysica acta. Reviews on cancer* 1871 (1), pp. 40–49.

DOI: 10.1016/j.bbcan.2018.10.002.

Maubach, Gunter; Sokolova, Olga; Täger, Christian; Naumann, Michael (2020): CEACAMs interaction with *Helicobacter pylori* HopQ supports the type 4 secretion system-dependent activation of non-canonical NF- $\kappa$ B. In *International journal of medical microbiology : IJMM* 310 (6), p. 151444. DOI: 10.1016/j.ijmm.2020.151444.

McDaniel, Dylan K.; Eden, Kristin; Ringel, Veronica M.; Allen, Irving C. (2016): Emerging Roles for Non-canonical NF- $\kappa$ B Signaling in the Modulation of Inflammatory Bowel Disease Pathobiology. In *Inflammatory bowel diseases* 22 (9), pp. 2265–2279. DOI: 10.1097/MIB.0000000000000858.

Mejías-Luque, Raquel; Lozano-Pope, Ivonne; Wanisch, Andreas; Heikenwälder, Matthias; Gerhard, Markus; Obonyo, Marygorret (2019): Increased LIGHT expression and activation of non-canonical NF- $\kappa$ B are observed in gastric lesions of MyD88-deficient mice upon *Helicobacter felis* infection. In *Scientific reports* 9 (1), p. 7030. DOI: 10.1038/s41598-019-43417-x.

Mejías-Luque, Raquel; Zöllner, Jessica; Anderl, Florian; Loew-Gil, Elena; Vieth, Michael; Adler, Thure et al. (2017): Lymphotoxin  $\beta$  receptor signalling executes *Helicobacter pylori*-driven gastric inflammation in a T4SS-dependent manner. In *Gut* 66 (8), pp. 1369–1381. DOI: 10.1136/gutjnl-2015-310783.

Melnik, Lilia I.; Garry, Robert F.; Morris, Cindy A. (2011): Peptide inhibition of human cytomegalovirus infection. In *Virology journal* 8, p. 76. DOI: 10.1186/1743-422X-8-76.

Merga, Yvette J.; O'Hara, Adrian; Burkitt, Michael D.; Duckworth, Carrie A.; Probert, Christopher S.; Campbell, Barry J.; Pritchard, D. Mark (2016): Importance of the alternative NF- $\kappa$ B activation pathway in inflammation-associated gastrointestinal carcinogenesis. In *American journal of physiology. Gastrointestinal and liver physiology* 310 (11), G1081-90. DOI:

10.1152/ajpgi.00026.2016.

Moodley, Yohan; Linz, Bodo; Bond, Robert P.; Nieuwoudt, Martin; Soodyall, Himla; Schlegel, Carina M. et al. (2012): Age of the Association between *Helicobacter pylori* and Man. In *PLoS*

*Pathogens* 8 (5). DOI: 10.1371/journal.ppat.1002693.

Morgan, Dhakshayini; Garg, Manoj; Tergaonkar, Vinay; Tan, Soo Yong; Sethi, Gautam (2020): Pharmacological significance of the non-canonical NF- $\kappa$ B pathway in tumorigenesis. In *Biochimica et biophysica acta. Reviews on cancer* 1874 (2), p. 188449. DOI: 10.1016/j.bbcan.2020.188449.

Morris, A.; Nicholson, G. (1987): Ingestion of *Campylobacter pyloridis* causes gastritis and raised fasting gastric pH. In *The American journal of gastroenterology* 82 (3), pp. 192–199.

Morris, A. J.; Ali, M. R.; Nicholson, G. I.; Perez-Perez, G. I.; Blaser, M. J. (1991): Long-term follow-up of voluntary ingestion of *Helicobacter pylori*. In *Annals of internal medicine* 114 (8), pp. 662–663. DOI: 10.7326/0003-4819-114-8-662.

Muenzner, Petra; Rohde, Manfred; Kneitz, Susanne; Hauck, Christof R. (2005): CEACAM engagement by human pathogens enhances cell adhesion and counteracts bacteria-induced detachment of epithelial cells. In *The Journal of Cell Biology* 170 (5), pp. 825–836. DOI: 10.1083/jcb.200412151.

Mulligan, George; Mitsiades, Constantine; Bryant, Barb; Zhan, Fenghuang; Chng, Wee J.; Roels, Steven et al. (2007): Gene expression profiling and correlation with outcome in clinical trials of the proteasome inhibitor bortezomib. In *Blood* 109 (8), pp. 3177–3188. DOI: 10.1182/blood-2006-09-044974.

Müntjes, Kira; Philipp, Magnus; Hüsemann, Lisa; Heucken, Nicole; Weidtkamp-Peters, Stefanie; Schipper, Kerstin et al. (2020): Establishing Polycistronic Expression in the Model Microorganism *Ustilago maydis*. In *Frontiers in Microbiology* 11, p. 1384. DOI: 10.3389/fmicb.2020.01384.

Oeckinghaus, Andrea; Ghosh, Sankar (2009): The NF- $\kappa$ B family of transcription factors and its regulation. In *Cold Spring Harbor perspectives in biology* 1 (4), a000034. DOI: 10.1101/cshperspect.a000034.

O'Reilly, Lorraine A.; Putoczki, Tracy L.; Mielke, Lisa A.; Low, Jun T.; Lin, Ann; Preaudet, Adele et al. (2018): Loss of NF- $\kappa$ B1 Causes Gastric Cancer with Aberrant Inflammation and Expression of Immune Checkpoint Regulators in a STAT-1-Dependent Manner. In *Immunity* 48 (3), 570-583.e8. DOI: 10.1016/j.immuni.2018.03.003.

Panse, J.; Friedrichs, K.; Marx, A.; Hildebrandt, Y.; Luetkens, T.; Barrels, K. et al. (2008): Chemokine CXCL13 is overexpressed in the tumour tissue and in the peripheral blood of breast cancer patients. In *British journal of cancer* 99 (6), pp. 930–938. DOI: 10.1038/sj.bjc.6604621.

- Paul, Andrew; Edwards, Joanne; Pepper, Christopher; Mackay, Simon (2018): Inhibitory- $\kappa$ B Kinase (IKK)  $\alpha$  and Nuclear Factor- $\kappa$ B (NF $\kappa$ B)-Inducing Kinase (NIK) as Anti-Cancer Drug Targets. In *Cells* 7 (10). DOI: 10.3390/cells7100176.
- Pavlopoulou, Athanasia; Scorilas, Andreas (2014): A comprehensive phylogenetic and structural analysis of the carcinoembryonic antigen (CEA) gene family. In *Genome biology and evolution* 6 (6), pp. 1314–1326. DOI: 10.1093/gbe/evu103.
- Peek, Richard M.; Crabtree, Jean E. (2006): Helicobacter infection and gastric neoplasia. In *The Journal of pathology* 208 (2), pp. 233–248. DOI: 10.1002/path.1868.
- Peng, Chao; Ouyang, Yaobin; Lu, Nonghua; Li, Nianshuang (2020): The NF- $\kappa$ B Signaling Pathway, the Microbiota, and Gastrointestinal Tumorigenesis: Recent Advances. In *Frontiers in Immunology* 11, p. 1387. DOI: 10.3389/fimmu.2020.01387.
- Petryszyn, Pawel; Chapelle, Nicolas; Matysiak-Budnik, Tamara (2020): Gastric Cancer: Where Are We Heading? In *Digestive diseases (Basel, Switzerland)* 38 (4), pp. 280–285. DOI: 10.1159/000506509.
- Pflug, Kathryn M.; Sitcheran, Raquel (2020): Targeting NF- $\kappa$ B-Inducing Kinase (NIK) in Immunity, Inflammation, and Cancer. In *International journal of molecular sciences* 21 (22). DOI: 10.3390/ijms21228470.
- Pincock, Stephen (2005): Nobel Prize winners Robin Warren and Barry Marshall. In *The Lancet* 366 (9495), p. 1429. DOI: 10.1016/S0140-6736(05)67587-3.
- Poh, Ashleigh R.; O'Donoghue, Robert J. J.; Ernst, Matthias; Putoczki, Tracy L. (2016): Mouse models for gastric cancer: Matching models to biological questions. In *Journal of gastroenterology and hepatology* 31 (7), pp. 1257–1272. DOI: 10.1111/jgh.13297.
- Rajik, Mohamed; Omar, Abdul Rahman; Ideris, Aini; Hassan, Sharifah Syed; Yusoff, Khatijah (2009): A novel peptide inhibits the influenza virus replication by preventing the viral attachment to the host cells. In *International journal of biological sciences* 5 (6), pp. 543–548. DOI: 10.7150/ijbs.5.543.
- Ran, F. Ann; Hsu, Patrick D.; Lin, Chie-Yu; Gootenberg, Jonathan S.; Konermann, Silvana; Trevino, Alexandro E. et al. (2013): Double nicking by RNA-guided CRISPR Cas9 for enhanced genome editing specificity. In *Cell* 154 (6), pp. 1380–1389. DOI: 10.1016/j.cell.2013.08.021.
- Rao, Donald D.; Vorhies, John S.; Senzer, Neil; Nemunaitis, John (2009): siRNA vs. shRNA:

- similarities and differences. In *Advanced drug delivery reviews* 61 (9), pp. 746–759. DOI: 10.1016/j.addr.2009.04.004.
- Rawla, Prashanth; Barsouk, Adam (2019): Epidemiology of gastric cancer: global trends, risk factors and prevention. In *Przegląd gastroenterologiczny* 14 (1), pp. 26–38. DOI: 10.5114/pg.2018.80001.
- Roder, David M. (2002): The epidemiology of gastric cancer. In *Gastric cancer : official journal of the International Gastric Cancer Association and the Japanese Gastric Cancer Association* 5 Suppl 1, pp. 5–11. DOI: 10.1007/s10120-002-0203-6.
- Ruddle, Nancy H. (2014): Lymphotoxin and TNF: how it all began-a tribute to the travelers. In *Cytokine & growth factor reviews* 25 (2), pp. 83–89. DOI: 10.1016/j.cytogfr.2014.02.001.
- Ryan, M. D.; King, A. M.; Thomas, G. P. (1991): Cleavage of foot-and-mouth disease virus polyprotein is mediated by residues located within a 19 amino acid sequence. In *The Journal of general virology* 72 (Pt 11), pp. 2727–2732. DOI: 10.1099/0022-1317-72-11-2727.
- Sasaki, N.; Morisaki, T.; Hashizume, K.; Yao, T.; Tsuneyoshi, M.; Noshiro, H. et al. (2001): Nuclear factor-kappaB p65 (RelA) transcription factor is constitutively activated in human gastric carcinoma tissue. In *Clinical cancer research : an official journal of the American Association for Cancer Research* 7 (12), pp. 4136–4142.
- Seidlitz, Therese; Chen, Yi-Ting; Uhlemann, Heike; Schölch, Sebastian; Kochall, Susan; Merker, Sebastian R. et al. (2019): Mouse Models of Human Gastric Cancer Subtypes With Stomach-Specific CreERT2-Mediated Pathway Alterations. In *Gastroenterology* 157 (6), 1599-1614.e2. DOI: 10.1053/j.gastro.2019.09.026.
- Selbach, Matthias; Moese, Stefan; Hauck, Christof R.; Meyer, Thomas F.; Backert, Steffen (2002): Src is the kinase of the Helicobacter pylori CagA protein in vitro and in vivo. In *The Journal of biological chemistry* 277 (9), pp. 6775–6778. DOI: 10.1074/jbc.C100754200.
- Sen, Ranjan; Baltimore, David (1986): Multiple nuclear factors interact with the immunoglobulin enhancer sequences. In *Cell* 46 (5), pp. 705–716. DOI: 10.1016/0092-8674(86)90346-6.
- Shariq, Mohd; Kumar, Navin; Kumari, Rajesh; Kumar, Amarjeet; Subbarao, Naidu; Mukhopadhyay, Gauranga (2015): Biochemical Analysis of CagE: A VirB4 Homologue of Helicobacter pylori Cag-T4SS. In *PloS one* 10 (11), e0142606. DOI: 10.1371/journal.pone.0142606.
- Shi, Jun-Feng; Xu, Shi-Xin; He, Ping; Xi, Zhi-Hui (2014): Expression of carcinoembryonic antigen-related cell adhesion molecule 1(CEACAM1) and its correlation with angiogenesis in gastric cancer.

- In *Pathology, research and practice* 210 (8), pp. 473–476. DOI: 10.1016/j.prp.2014.03.014.
- Shi, Yun; Liu, Xiao-Fei; Zhuang, Yuan; Zhang, Jin-Yu; Liu, Tao; Yin, Zhinan et al. (2010): Helicobacter pylori-induced Th17 responses modulate Th1 cell responses, benefit bacterial growth, and contribute to pathology in mice. In *Journal of immunology (Baltimore, Md. : 1950)* 184 (9), pp. 5121–5129. DOI: 10.4049/jimmunol.0901115.
- Shibata, Wataru; Takaishi, Shigeo; Muthupalani, Sureshkumar; Pritchard, D. Mark; Whary, Mark T.; Rogers, Arlin B. et al. (2009): Conditional deletion of IkappaB-kinase beta (IKK $\beta$ ) accelerates Helicobacter-dependent gastric apoptosis, proliferation and preneoplasia. In *Gastroenterology* 138 (3), 1022-1034.e10. DOI: 10.1053/j.gastro.2009.11.054.
- Shinkura, R.; Kitada, K.; Matsuda, F.; Tashiro, K.; Ikuta, K.; Suzuki, M. et al. (1999): A lymphoplasia is caused by a point mutation in the mouse gene encoding Nf-kappa b-inducing kinase. In *Nature genetics* 22 (1), pp. 74–77. DOI: 10.1038/8780.
- Shishodia, Shishir; Aggarwal, Bharat B. (2004): Nuclear factor-kappaB: a friend or a foe in cancer? In *Biochemical pharmacology* 68 (6), pp. 1071–1080. DOI: 10.1016/j.bcp.2004.04.026.
- Siegel, Rebecca L.; Miller, Kimberly D.; Jemal, Ahmedin (2018): Cancer statistics, 2018. In *CA: a cancer journal for clinicians* 68 (1), pp. 7–30. DOI: 10.3322/caac.21442.
- Siontorou, Christina G. (2013): Nanobodies as novel agents for disease diagnosis and therapy. In *International Journal of Nanomedicine* 8, pp. 4215–4227. DOI: 10.2147/IJN.S39428.
- Smith, Malcolm G.; Hold, Georgina L.; Tahara, Eiichi; El-Omar, Emad M. (2006): Cellular and molecular aspects of gastric cancer. In *World Journal of Gastroenterology : WJG* 12 (19), pp. 2979–2990. DOI: 10.3748/wjg.v12.i19.2979.
- Sokolova, Olga; Naumann, Michael (2017): NF- $\kappa$ B Signaling in Gastric Cancer. In *Toxins* 9 (4). DOI: 10.3390/toxins9040119.
- Stein, Saskia C.; Faber, Eugenia; Bats, Simon H.; Murillo, Tatiana; Speidel, Yvonne; Coombs, Nina; Josenhans, Christine (2017): Helicobacter pylori modulates host cell responses by CagT4SS-dependent translocation of an intermediate metabolite of LPS inner core heptose biosynthesis. In *PLoS Pathogens* 13 (7), e1006514. DOI: 10.1371/journal.ppat.1006514.
- Stewart, Sheila A.; Dykxhoorn, Derek M.; Palliser, Deborah; Mizuno, Hana; Yu, Evan Y.; An, Dong Sung et al. (2003): Lentivirus-delivered stable gene silencing by RNAi in primary cells. In *RNA (New York, N.Y.)* 9 (4), pp. 493–501. DOI: 10.1261/rna.2192803.

- Suerbaum, Sebastian; Josenhans, Christine (2007): *Helicobacter pylori* evolution and phenotypic diversification in a changing host. In *Nature reviews. Microbiology* 5 (6), pp. 441–452. DOI: 10.1038/nrmicro1658.
- Sun, Shao-Cong (2011): Non-canonical NF- $\kappa$ B signaling pathway. In *Cell research* 21 (1), pp. 71–85. DOI: 10.1038/cr.2010.177.
- Sun, Shao-Cong (2012): The noncanonical NF- $\kappa$ B pathway. In *Immunological reviews* 246 (1), pp. 125–140. DOI: 10.1111/j.1600-065X.2011.01088.x.
- Sung, Hyuna; Ferlay, Jacques; Siegel, Rebecca L.; Laversanne, Mathieu; Soerjomataram, Isabelle; Jemal, Ahmedin; Bray, Freddie (2021): Global Cancer Statistics 2020: GLOBOCAN Estimates of Incidence and Mortality Worldwide for 36 Cancers in 185 Countries. In *CA: a cancer journal for clinicians* 71 (3), pp. 209–249. DOI: 10.3322/caac.21660.
- Swiss Institute of Bioinformatics (Ed.): Cell Lines. Available online at <https://web.expasy.org>, checked on 3/19/2020.
- Syu, Li-Jyun; El-Zaatari, Mohamad; Eaton, Kathryn A.; Liu, Zhiping; Tetarbe, Manas; Keeley, Theresa M. et al. (2012): Transgenic expression of interferon- $\gamma$  in mouse stomach leads to inflammation, metaplasia, and dysplasia. In *The American journal of pathology* 181 (6), pp. 2114–2125. DOI: 10.1016/j.ajpath.2012.08.017.
- Szymczak, Andrea L.; Vignali, Dario A. A. (2005): Development of 2A peptide-based strategies in the design of multicistronic vectors. In *Expert opinion on biological therapy* 5 (5), pp. 627–638. DOI: 10.1517/14712598.5.5.627.
- Takahashi-Kanemitsu, Atsushi; Knight, Christopher T.; Hatakeyama, Masanori (2020): Molecular anatomy and pathogenic actions of *Helicobacter pylori* CagA that underpin gastric carcinogenesis. In *Cellular & molecular immunology* 17 (1), pp. 50–63. DOI: 10.1038/s41423-019-0339-5.
- Tan, Patrick; Yeoh, Khay-Guan (2015): Genetics and Molecular Pathogenesis of Gastric Adenocarcinoma. In *Gastroenterology* 149 (5), 1153-1162.e3. DOI: 10.1053/j.gastro.2015.05.059.
- Taniguchi, Koji; Karin, Michael (2018): NF- $\kappa$ B, inflammation, immunity and cancer: coming of age. In *Nature reviews. Immunology* 18 (5), pp. 309–324. DOI: 10.1038/nri.2017.142.
- Tchoupa, Arnaud Kengmo; Lichtenegger, Sabine; Reidl, Joachim; Hauck, Christof R. (2015): Outer membrane protein P1 is the CEACAM-binding adhesin of *Haemophilus influenzae*. In *Molecular microbiology* 98 (3), pp. 440–455. DOI: 10.1111/mmi.13134.

- Tegowski, Matthew; Baldwin, Albert (2018): Noncanonical NF- $\kappa$ B in Cancer. In *Biomedicines* 6 (2). DOI: 10.3390/biomedicines6020066.
- Tegtmeyer, Nicole; Backert, Steffen (2017): Molecular Pathogenesis and Signal Transduction by *Helicobacter pylori*. Cham: Springer International Publishing (Current Topics in Microbiology and Immunology, v.400). Available online at <https://ebookcentral.proquest.com/lib/gbv/detail.action?docID=4791252>.
- Tegtmeyer, Nicole; Harrer, Aileen; Schmitt, Verena; Singer, Bernhard B.; Backert, Steffen (2019): Expression of CEACAM1 or CEACAM5 in AZ-521 cells restores the type IV secretion deficiency for translocation of CagA by *Helicobacter pylori*. In *Cellular microbiology* 21 (1), e12965. DOI: 10.1111/cmi.12965.
- Tegtmeyer, Nicole; Moodley, Yoshan; Yamaoka, Yoshio; Pernitzsch, Sandy Ramona; Schmidt, Vanessa; Traverso, Francisco Rivas et al. (2016): Characterisation of worldwide *Helicobacter pylori* strains reveals genetic conservation and essentiality of serine protease HtrA. In *Molecular microbiology* 99 (5), pp. 925–944. DOI: 10.1111/mmi.13276.
- Teng, Hairong; Xue, Liang; Wang, Yuexia; Ding, Xian; Li, Jiabin (2020): Nuclear factor  $\kappa$ B -inducing kinase is a diagnostic marker of gastric cancer. In *Medicine* 99 (5), e18864. DOI: 10.1097/MD.00000000000018864.
- Tu, Shuiping; Bhagat, Govind; Cui, Guanglin; Takaishi, Shigeo; Kurt-Jones, Evelyn A.; Rickman, Barry et al. (2008): Overexpression of interleukin-1 $\beta$  induces gastric inflammation and cancer and mobilizes myeloid-derived suppressor cells in mice. In *Cancer cell* 14 (5), pp. 408–419. DOI: 10.1016/j.ccr.2008.10.011.
- Uno, Masaya; Saitoh, Yasunori; Mochida, Kanako; Tsuruyama, Eri; Kiyono, Tohru; Imoto, Issei et al. (2014): NF- $\kappa$ B inducing kinase, a central signaling component of the non-canonical pathway of NF- $\kappa$ B, contributes to ovarian cancer progression. In *PloS one* 9 (2), e88347. DOI: 10.1371/journal.pone.0088347.
- Valenti, Maria Teresa; Serena, Michela; Carbonare, Luca Dalle; Zipeto, Donato (2019): CRISPR/Cas system: An emerging technology in stem cell research. In *World journal of stem cells* 11 (11), pp. 937–956. DOI: 10.4252/wjsc.v11.i11.937.
- Vazquez-Santillan, Karla; Melendez-Zajgla, Jorge; Jimenez-Hernandez, Luis Enrique; Gaytan-Cervantes, Javier; Muñoz-Galindo, Laura; Piña-Sanchez, Patricia et al. (2016): NF- $\kappa$ B-inducing kinase regulates stem cell phenotype in breast cancer. In *Scientific reports* 6. DOI:

10.1038/srep37340.

Voges, Maike; Bachmann, Verena; Kammerer, Robert; Gophna, Uri; Hauck, Christof R. (2010): CEACAM1 recognition by bacterial pathogens is species-specific. In *BMC Microbiology* 10, p. 117. DOI: 10.1186/1471-2180-10-117.

Ware, Carl F. (2009): Targeting the LIGHT-HVEM pathway. In *Advances in experimental medicine and biology* 647, pp. 146–155. DOI: 10.1007/978-0-387-89520-8\_10.

Weih, Falk; Caamaño, Jorge (2003): Regulation of secondary lymphoid organ development by the nuclear factor-kappaB signal transduction pathway. In *Immunological reviews* 195, pp. 91–105. DOI: 10.1034/j.1600-065X.2003.00064.x.

Wharry, Catherine E.; Haines, Kathleen M.; Carroll, Richard G.; May, Michael J. (2009): Constitutive non-canonical NFkappaB signaling in pancreatic cancer cells. In *Cancer biology & therapy* 8 (16), pp. 1567–1576. DOI: 10.4161/cbt.8.16.8961.

Wolf, M. J.; Seleznik, G. M.; Zeller, N.; Heikenwalder, M. (2010): The unexpected role of lymphotoxin beta receptor signaling in carcinogenesis: from lymphoid tissue formation to liver and prostate cancer development. In *Oncogene* 29 (36), pp. 5006–5018. DOI: 10.1038/onc.2010.260.

Wroblewski, Lydia E.; Peek, Richard M. (2013): Helicobacter pylori in gastric carcinogenesis: mechanisms. In *Gastroenterology clinics of North America* 42 (2), pp. 285–298. DOI: 10.1016/j.gtc.2013.01.006.

Wroblewski, Lydia E.; Peek, Richard M.; Wilson, Keith T. (2010): Helicobacter pylori and gastric cancer: factors that modulate disease risk. In *Clinical microbiology reviews* 23 (4), pp. 713–739. DOI: 10.1128/CMR.00011-10.

Wu, Cheng-Shyong; Chen, Miao-Fen; Lee, I-Lin; Tung, Shui-Yi (2007): Predictive role of nuclear factor-kappaB activity in gastric cancer: a promising adjuvant approach with caffeic acid phenethyl ester. In *Journal of clinical gastroenterology* 41 (10), pp. 894–900. DOI: 10.1097/MCG.0b013e31804c707c.

Xiang, Z.; Censini, S.; Bayeli, P. F.; Telford, J. L.; Figura, N.; Rappuoli, R.; Covacci, A. (1995): Analysis of expression of CagA and VacA virulence factors in 43 strains of Helicobacter pylori reveals that clinical isolates can be divided into two major types and that CagA is not necessary for expression of the vacuolating cytotoxin. In *Infection and immunity* 63 (1), pp. 94–98. DOI: 10.1128/IAI.63.1.94-98.1995.

- Xu, Yong; Fang, Fang; St. Clair, Daret K.; Sompol, Pradoldej; Josson, Sajni; St. Clair, William H. (2008): SN52, a novel nuclear factor- $\kappa$ B inhibitor, blocks nuclear import of RelB:p52 dimer and sensitizes prostate cancer cells to ionizing radiation. In *Molecular cancer therapeutics* 7 (8), pp. 2367–2376. DOI: 10.1158/1535-7163.MCT-08-0238.
- Yang, Jyh-Chin; Lu, Chien-Wei; Lin, Chun-Jung (2014): Treatment of Helicobacter pylori infection: current status and future concepts. In *World Journal of Gastroenterology : WJG* 20 (18), pp. 5283–5293. DOI: 10.3748/wjg.v20.i18.5283.
- Ye, Xiaoli; Zhou, Ming; He, Yonggang; Wan, Yanmin; Bai, Weiya; Tao, Shuai et al. (2016): Efficient Inhibition of Hepatitis B Virus Infection by a preS1-binding Peptide. In *Scientific reports* 6, p. 29391. DOI: 10.1038/srep29391.
- Yin, L.; Wu, L.; Wesche, H.; Arthur, C. D.; White, J. M.; Goeddel, D. V.; Schreiber, R. D. (2001): Defective lymphotoxin-beta receptor-induced NF-kappaB transcriptional activity in NIK-deficient mice. In *Science (New York, N.Y.)* 291 (5511), pp. 2162–2165. DOI: 10.1126/science.1058453.
- Yu, Sungsook; Yang, Mijeong; Nam, Ki Taek (2014): Mouse models of gastric carcinogenesis. In *Journal of gastric cancer* 14 (2), pp. 67–86. DOI: 10.5230/jgc.2014.14.2.67.
- Zarnegar, Brian J.; Wang, Yaya; Mahoney, Douglas J.; Dempsey, Paul W.; Cheung, Herman H.; He, Jeannie et al. (2008): Noncanonical NF-kappaB activation requires coordinated assembly of a regulatory complex of the adaptors cIAP1, cIAP2, TRAF2 and TRAF3 and the kinase NIK. In *Nature immunology* 9 (12), pp. 1371–1378. DOI: 10.1038/ni.1676.
- Zhu, Mingzhao; Fu, Yang-Xin (2011): The role of core TNF/LIGHT family members in lymph node homeostasis and remodeling. In *Immunological reviews* 244 (1), pp. 75–84. DOI: 10.1111/j.1600-065X.2011.01061.x.
- Zhu, Sining; Jin, Juan; Gokhale, Samantha; Lu, Angeli M.; Shan, Haiyan; Feng, Jianjun; Xie, Ping (2018): Genetic Alterations of TRAF Proteins in Human Cancers. In *Frontiers in Immunology* 9. DOI: 10.3389/fimmu.2018.02111.
- Zinatizadeh, Mohammad Reza; Schock, Bettina; Chalbatani, Ghanbar Mahmoodi; Zarandi, Peyman Kheirandish; Jalali, Seyed Amir; Miri, Seyed Rouhollah (2021): The Nuclear Factor Kappa B (NF- $\kappa$ B) signaling in cancer development and immune diseases. In *Genes & diseases* 8 (3), pp. 287–297. DOI: 10.1016/j.gendis.2020.06.005.

## 8 Publication

Parts of this doctoral thesis have been submitted:

Karin Taxauer, Youssef Hamway, Anna Ralser, Alisa Dietl, Karin Mink, Michael Vieth, Bernhard B. Singer, Markus Gerhard, and Raquel Mejías-Luque; Engagement of CEACAM1 by *Helicobacter pylori* HopQ is important for the activation of non-canonical NF- $\kappa$ B in gastric epithelial cells. **Microorganisms**. 2021 (submitted)

## 9 Appendix

### 9.1 List of figures

FIGURE 1: MAP OF AGE-STANDARDIZED INCIDENCE RATES (ASR) OF BOTH SEXES ON STOMACH CANCER CASES/100.000 CITIZENS IN 2018 (GLOBOCAN 2018). .....	17
FIGURE 2: ENVIRONMENTAL AND HOST FACTORS CONTRIBUTING TO THE DEVELOPMENT OF INTESTINAL-TYPE OF GC (TAN AND YEOH 2015). .....	19
FIGURE 3: KEY FEATURES OF THE DIFFERENT MOLECULAR SUBTYPES OF GC (CANCER GENOME ATLAS RESEARCH NETWORK 2014). .....	20
FIGURE 4: TARGET GENES OF THE NF- $\kappa$ B PATHWAY INDUCED UPON INFLAMMATION DEVELOPMENT AND PROGRESSION (LIU ET AL. 2017). .....	23
FIGURE 5: MEMBERS OF NF- $\kappa$ B/REL FAMILY, I $\kappa$ B FAMILY, AND THE IKK COMPLEX FAMILY (HAYDEN AND GHOSH 2011). .....	24
FIGURE 6: ACTIVATION OF CANONICAL/CLASSICAL NF- $\kappa$ B PATHWAY UPON STIMULATION (JOST AND RULAND 2007). .....	25
FIGURE 7: ACTIVATION OF NON-CANONICAL NF- $\kappa$ B PATHWAY AT BASAL CONDITIONS AND UPON STIMULATION (CILDIR ET AL. 2016). .....	26
FIGURE 8: CRISPR/Cas9N STRATEGY (RAN ET AL. 2013) .....	40
FIGURE 9: DNA CONSTRUCT SCHEME OF TRANSGENIC MOUSE MODEL .....	56
FIGURE 10: WORKFLOW OF GIBSON ASSEMBLY. ....	57
FIGURE 11: ACTIVATION OF THE NON-CANONICAL NF- $\kappa$ B PATHWAY UPON <i>H. PYLORI</i> INFECTION. ....	68
FIGURE 12: CHEMOKINE EXPRESSION UPON <i>H. PYLORI</i> INFECTION. ....	69
FIGURE 13: CAG $\Delta$ TRANSLOCATION AFTER <i>H. PYLORI</i> INFECTION. ....	70
FIGURE 14: CEACAM EXPRESSION IN VARIOUS GC CELLS AND UPON <i>H. PYLORI</i> INFECTION IN MKN45 CELLS. ....	71
FIGURE 15: ACTIVATION OF NON-CANONICAL NF- $\kappa$ B PATHWAY UPON <i>H. PYLORI</i> INFECTION IN SNU1 AND NUGC-4 CELLS. ....	72
FIGURE 16: CEACAM EXPRESSION IN NUGC-4 CELLS UPON INFECTION. ....	73
FIGURE 17: BINDING OF <i>H. PYLORI</i> TO GASTRIC EPITHELIAL CELLS. ....	74
FIGURE 18: REPRESENTATIVE IMAGES OF ORGANOIDS CULTURED IN TWO DIFFERENT SETUPS. ....	75
FIGURE 19: GENE EXPRESSION LEVELS UPON <i>H. PYLORI</i> INFECTION IN MURINE PRIMARY GASTRIC CELLS. ....	76
FIGURE 20: CORRELATION OF LTB EXPRESSION AND CEACAM1 EXPRESSION IN MURINE PRIMARY GASTRIC CELLS. ....	76
FIGURE 21: P100 TO P52 PROCESSING IN DIFFERENT GC CELLS. ....	77
FIGURE 22: NIK EXPRESSION IN DIFFERENT GC CELLS. ....	78

---

FIGURE 23: ILLUSTRATION OF THE PX335 PLASMID AND U6 SCREENING.....	78
FIGURE 24: IMPACT OF NIK DOWN REGULATION BY siRNA ON CELL PROLIFERATION OF GC CELLS.....	80
FIGURE 25: NIK MRNA LEVELS AFTER SHRNA TRANSFECTION IN MKN28 CELLS.....	81
FIGURE 26: TITRATION OF PUROMYCIN CONCENTRATION TO KILL GC CELLS. ....	82
FIGURE 27: DOWN MODULATION OF NIK LEVELS BY LENTIVIRAL TRANSDUCTION OF GC CELLS. ....	83
FIGURE 28: IMPACT OF NIK KNOCKDOWN ON CELL PROLIFERATION OF GC CELLS. ....	83
FIGURE 29: INFLUENCE OF NIK KNOCKDOWN ON ANCHORAGE-DEPENDENT GROWTH OF GC CELLS.....	84
FIGURE 30: EFFECT OF NIK KNOCKDOWN ON ANCHORAGE-INDEPENDENT GROWTH OF GC CELLS. ....	85
FIGURE 31: SCHEMATIC ILLUSTRATION OF THE USED TRANSGENE CONSTRUCT. ....	85
FIGURE 32: <i>IN VITRO</i> TESTING OF THE GENERATED CONSTRUCT FOR THE TRANSGENIC MOUSE MODEL. ....	86
FIGURE 33: MURINE GASTRIC ORGANOID OF WILD TYPE AND L <sup>TAB</sup> TRANSGENIC MICE.....	86
FIGURE 34: EXPRESSION OF <i>LTA</i> AND <i>LTB</i> IN THE NEW L <sup>TAB</sup> MOUSE MODEL IN VARIOUS ORGANS. ....	87
FIGURE 35: BFP MRNA EXPRESSION LEVELS IN STOMACHS OF WILD TYPE (WT) OR L <sup>TAB</sup> MICE. ....	88
FIGURE 36: <i>LTA</i> AND <i>LTB</i> EXPRESSION LEVELS IN STOMACHS OF WILD TYPE OR L <sup>TAB</sup> MICE. ....	89
FIGURE 37: <i>CXCL13</i> AND <i>CMYC</i> MRNA EXPRESSION LEVELS IN STOMACHS OF WILD TYPE OR L <sup>TAB</sup> MICE.....	90
FIGURE 38: NF-κB2 STAINING AND QUANTIFICATION OF p52 <sup>+</sup> CELLS IN STOMACHS OF 54-WEEK OLD WILD TYPE OR L <sup>TAB</sup> MICE.....	90
FIGURE 39: QUANTIFICATION OF Ki67 POSITIVE CELLS IN THE STOMACHS OF WILD TYPE OR L <sup>TAB</sup> MICE. ....	91
FIGURE 40: STOMACH SAMPLES OF WILD TYPE OR L <sup>TAB</sup> MICE STAINED FOR HE AND PROLIFERATING CELLS (Ki67)..	92
FIGURE 41: STAINING AND QUANTIFICATION OF INFILTRATING IMMUNE CELLS IN THE STOMACH OF WILD TYPE OR L <sup>TAB</sup> MICE.....	93
FIGURE 42: CFU AND SPLEEN WEIGHT OF UNINFECTED AS WELL AS INFECTED L <sup>TAB</sup> AND AGE-MATCHED WILD TYPE MICE.....	94
FIGURE 43: HEMATOXYLIN AND EOSIN STAINED STOMACH TISSUE OF UNINFECTED AND INFECTED MICE.....	95
FIGURE 44: MRNA EXPRESSION LEVELS OF <i>LTA</i> , <i>LTB</i> AND NF-κB TARGET GENES UPON <i>H. PYLORI</i> INFECTION OF L <sup>TAB</sup> AND WILD TYPE MICE. ....	96
FIGURE 45: <i>KC</i> MRNA EXPRESSION AND GASTRIC PROLIFERATION UPON <i>H. PYLORI</i> INFECTION. ....	97
FIGURE 46: IMMUNE CELL INFILTRATION UPON <i>H. PYLORI</i> INFECTION OF L <sup>TAB</sup> AND AGE-MATCHED WILD TYPE MICE.	98
FIGURE 47: RESPONSIVE HUMAN GASTRIC ORGANOID STIMULATED WITH LT OR LIGHT.....	100
FIGURE 48: NON-RESPONSIVE HUMAN GASTRIC ORGANOID STIMULATED WITH LT OR LIGHT. ....	101

## 9.2 List of tables

TABLE 1: LIST LABORATORY EQUIPMENT USED.	32
TABLE 2: LIST OF CONSUMABLES USED.	33
TABLE 3: LIST OF BUFFERS	34
TABLE 4: LIST OF USED SUBSTANCES.	36
TABLE 5: LIST OF APPLIED MEDIA AND SUPPLEMENTS.	37
TABLE 6: LIST OF BACTERIAL CULTURE MEDIA.	38
TABLE 7: LIST OF GC CELLS USED (AMERICAN TYPE CULTURE COLLECTION; SWISS INSTITUTE OF BIOINFORMATICS).	39
TABLE 8: LIST OF GUIDE RNAs AND SEQUENCING PRIMERS.	41
TABLE 9: OLIGO ANNEALING REACTION FOR gRNAs.	41
TABLE 10: VECTOR DIGESTION WITH <i>BbsI</i> .	42
TABLE 11: LIGATION REACTION FOR INSERTING ANNEALED gRNA IN DIGESTED PX335 VECTOR.	42
TABLE 12: MASTER MIX FOR SCREENING FOR PCR.	42
TABLE 13: THERMAL CYCLE PROGRAM FOR SCREENING PCR.	42
TABLE 14: LIST OF USED siRNAs.	44
TABLE 15: LIST OF PLASMIDS FOR shRNA-BASED DOWN-MODULATION.	44
TABLE 16: LIST OF SELECTED shRNA SEQUENCES.	45
TABLE 17: MASTER MIX FOR ANNEALING OLIGOS.	45
TABLE 18: MASTER MIX FOR LIGATION REACTION.	45
TABLE 19: MASTER MIX COMPONENTS FOR RT-PCR.	48
TABLE 20: MASTER MIX COMPONENTS FOR qPCR	48
TABLE 21: THERMAL CYCLE PROFILE FOR qPCR.	49
TABLE 22: LIST OF USED HUMAN PRIMERS.	49
TABLE 23: LIST OF USED MOUSE PRIMERS.	49
TABLE 24: REAGENTS FOR THE SEPARATING GEL.	51
TABLE 25: REAGENTS FOR THE STACKING GEL.	51
TABLE 26: LIST OF ANTIBODIES	52
TABLE 27: <i>H. PYLORI</i> STRAINS USED AND ANTIBIOTIC RESISTANCE FOR SELECTION.	54
TABLE 28: LIST OF SCREENING PRIMERS FOR DNA CONSTRUCT.	57
TABLE 29: MASTER MIX FOR GENOTYPING PCR.	58
TABLE 30: PRIMER SEQUENCES FOR GENOTYPING PCR.	58
TABLE 31: THERMAL CYCLE PROGRAM FOR GENOTYPING.	58
TABLE 32: COMPONENTS OF THE BASAL MEDIUM.	62

TABLE 33: COMPONENTS OF THE COMPLETE ORGANOID MEDIUM.	63
TABLE 34: LIST OF PRIMARY ANTIBODIES FOR IHC	65

## 10 Declaration

I, Karin Taxauer, hereby declare that I independently prepared the present doctoral thesis entiteled “Role of lymphotoxin/non-canonical NF- $\kappa$ B signaling in gastric carcinogenesis”, using only the references/sources stated under the supervision of Prof. Dr. Markus Gerhard. This work has not been submitted to any examination board yet. Parts of this doctoral thesis will be published in scientific journals.

Munich, July 2021

# 11 Acknowledgement

It is my pleasure to thank many people who were essential for completion of my doctoral thesis.

First of all, I would like to express my gratitude to my supervisor Prof. Dr. Markus Gerhard for giving me the opportunity to do my research in his lab on this interesting and great project. His critical advices and great support throughout my thesis.

Besides my supervisor, I would like to thank the rest of my thesis committee: Prof. Dietmar Zehn and PD Dr. Raquel Mejías-Luque for their critical minds, discussions, and support.

I would like to express my gratitude to PD Dr. Raquel Mejías-Luque for her great ideas, guidance, discussions, and tremendous support throughout my research. It was a pleasure for me to work with her and learn how to present the data as a story. She was very encouraging and had many ideas and suggestions which helped me to develop my scientific mind.

My sincere thanks also go to Prof. Dr. Mathias Heikenwälder and Danijela Heide for performing IHC stainings and *in-situ* hybridiazation of our LT $\alpha$  $\beta$ <sup>TG</sup> mice for us. Also I would like to thank Prof.<sup>in</sup> Martina Anton for her support in packaging of lentiviruses and producing viral supernatants for us. I would like to thank Prof. Michael Vieth for his expertise in pathology and Dr. Birkner for collecting human stomach biopsies and Ursula Kälberer for picking them up and taking care of organization. I would like to express my gratitude to the OLS team especially to Amir Keric and Noelle for their support in establishing the CERO 3D incubator in our lab.

I would like to thank Andreas Wanisch, Martin Skerhut, and our animal facility for supporting me with the mouse work. I would like to express my gratitude to my labmates who were introducing me various methods and helping me in my daily lab work. Therefore, I would like to especially thank to Victoria Neumeyer, Andreas Wanisch, Martin Skerhut, Karin Mink, Behnam Kalali, Anna Ralsler, Alisa Dietl, Youssef Hamway, Teresa Burrell, Mona Wang, Martina Grandl, Raphaela Semper, and Monika Schön. For the great working atmosphere, I would like to thank the whole team! I enjoyed a lot our social gatherings, coffee breaks, cooking nights and the fun at or after work.

For critical reviewing of my thesis, I would like to thank Raquel Mejías-Luque, Markus Gerhard and Rebecca.

Finally, I would like to express my gratitude to my friends and family. Most of all, I would like to thank Rebecca for her support in all those years and her encouraging words in struggling times of my research. I would like to express my gratitude to my family for their support and love. Especially, I am grateful to the support of my grandmother who was proud of me and had been excited seeing me graduating.